

THESIS

3

2004

This is to certify that the
thesis entitled

THE USE OF TRAJECTORIES TO STUDY THE RELATIONSHIP
BETWEEN ATMOSPHERIC TELECONNECTIONS AND THE
CLIMATE OF THE LOWER PENINSULA OF MICHIGAN

presented by

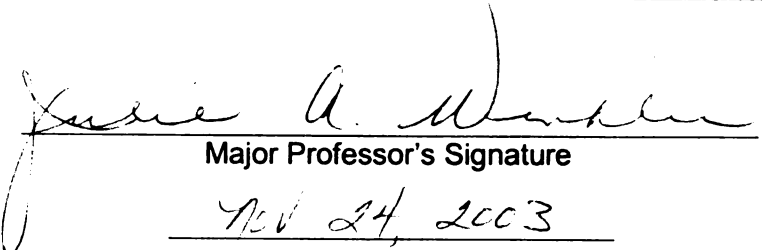
Ryan P. Shadbolt

has been accepted towards fulfillment
of the requirements for the

M.A.

degree in

Geography


Major Professor's Signature

Nov 24, 2003

Date

MSU is an Affirmative Action/Equal Opportunity Institution

LIBRARY
Michigan State
University

PLACE IN RETURN BOX to remove this checkout from your record.

TO AVOID FINES return on or before date due.

MAY BE RECALLED with earlier due date if requested.

[illegible]

**THE USE OF TRAJECTORIES TO STUDY THE RELATIONSHIP BETWEEN
ATMOSPHERIC TELECONNECTIONS AND THE CLIMATE OF THE LOWER
PENINSULA OF MICHIGAN**

By

Ryan P. Shadbolt

A THESIS

**Submitted to
Michigan State University
in partial fulfillment of the requirements
for the degree of**

MASTER OF ARTS

Department of Geography

2003

THE USE ATMOSPHERIC

The cir

on the climate

upper-level air

low-level air

and atmospheric

peninsula of N

monitoring ch

circulation. A

(constant-pres

Centers for En

Research (NCA

and temporal re

Information Sy

climatologies d

heat and/or moi

illustrate the pat

which are impor

ABSTRACT

THE USE OF TRAJECTORIES TO STUDY THE RELATIONSHIP BETWEEN ATMOSPHERIC TELECONNECTIONS AND THE CLIMATE OF THE LOWER PENINSULA OF MICHIGAN

By

Ryan P. Shadbolt

The circulation associated with atmospheric teleconnections has profound effects on the climate of the midwestern United States. Previous studies have investigated the low-level airflow associated with different teleconnection patterns, but the variation of high-level airflow has not been studied. Analyses of the association of low-level airflow with atmospheric teleconnections are presented for an example location in the lower peninsula of Michigan. Air-parcel trajectories, which provide an important approach to understanding changes in atmospheric circulation, are used to represent the low-level circulation. A five-day back-trajectory climatology was developed using an isobaric (constant-pressure) model, for the 925 hPa surface, from the four-times daily National Centers for Environmental Prediction (NCEP) and the National Center for Atmospheric Research (NCAR) reanalysis data. Methodological issues addressed include the spatial and temporal resolution of the trajectories, as well as the effective use of a Geographic Information System (GIS) to display and analyze the trajectory patterns. The methodologies developed here will help delineate potential regions where advection of heat and/or moisture can be expected during particular times of the year and will also help to understand the patterns in circulation associated with atmospheric teleconnections, both of which are important for medium to long-range weather forecasting.

"You don't

“You don’t need a weather man to know which way the wind blows.” -Bob Dylan

I would
been possible v
advisor, Dr. Ju
previous drafts
like to thank th
Messina, for th
the research an
teleconnection
of the study, to
assistance with
revisions. Mo
for their patien
support of the
all expectation

ACKNOWLEDGEMENTS

I would like to express that the completion of the following thesis would not have been possible without the help of some important people. First, I would like to thank my advisor, Dr. Julie Winkler, for her guidance, for her extensive amount of reviewing of previous drafts, and for her never-ending dedication to my research project. I would also like to thank the other members of my committee, Dr. Jeffrey Andresen and Dr. Joseph Messina, for their helpful and thought-provoking suggestions throughout the course of the research and analysis. Additional thanks to Dr. David McGinnis for his advice on the teleconnection analysis; to Dr. Bruce Pigozzi for his suggestions on the statistical portion of the study; to Eleanor Waller for the use of her software; to James Brown for his assistance with computer issues and data storage; and to Jennifer Lamb for her help with revisions. Most importantly, I wish to give my gratitude to my family and closest friends, for their patience, support, and understanding throughout the research project. With the support of these people, the project proceeded with much more efficiency and surpassed all expectations.

LIST OF T

LIST OF F

LIST OF E

CHAPTER

1. In

2. Li

3. Objec

4. Organ

CHAPTER 2. D

1. Overv

2. Wind L

3. Study L

TABLE OF CONTENTS

LIST OF TABLES	xi
LIST OF FIGURES	xii
LIST OF EQUATIONS	xxiv
CHAPTER 1. INTRODUCTION, LITERATURE REVIEW, AND OBJECTIVES	1
1. Introduction	1
2. Literature Review	3
<i>a. Air-parcel Trajectory Analysis</i>	3
1. Temporal and Spatial Resolution	6
2. Trajectory Models	8
3. Waller's Isobaric Airflow Climatology	12
<i>b. Atmospheric Teleconnections</i>	14
1. The North Atlantic Oscillation (NAO)	16
2. The Pacific/North American Pattern (PNA)	18
3. The Southern Oscillation (SO)	20
4. Teleconnection Association with the Midwest	22
3. Objectives and Research Questions	24
4. Organization of Thesis	26
CHAPTER 2. DATA AND METHODOLOGY	28
1. Overview	28
2. Wind Data from the NCEP/NCAR Reanalysis	29
3. Study Location	31

4. Algo

5. Geog

6. Isoba

7. Atmo

8. Ident

9. Temp

10. Sun

CHAPTER 3. C

1. Over

2. Annu

3. Janua

4. Febru

5. March

6. April

7. May..

8. June..

9. July...

10. Augu

11. Septe

12. Octob

4. Algorithm for the Trajectory Analysis	32
5. Geographic Information System Analysis	38
<i>a. Obtaining the Base Map</i>	38
<i>b. Converting the Back Trajectories to a Coverage Format</i>	38
<i>c. Projecting to the Lambert-Azimuthal Equal-Area Projection</i>	39
6. Isobaric Trajectories Compared to HY-SPLIT Trajectories	40
7. Atmospheric Teleconnection Data	48
8. Identifying Months of Strong Teleconnections	49
9. Temperature and Precipitation Data	51
10. Summary	53
CHAPTER 3. CLIMATOLOGY OF AIR-PARCEL TRAJECTORIES	54
1. Overview	54
2. Annual Climatology	55
3. January	56
4. February	61
5. March	62
6. April	65
7. May	67
8. June	69
9. July	71
10. August	73
11. September	75
12. October	77

13. Nov

14. Dec

15. Sum

CHAPTER 4. 1
AND LOWER-

1. Over

2. TC2

3. TC4

4. TC6

5. TC8

6. TC9

7. TC1

8. TC

9. TC

10. T

11. T

12. T

13. T

14. T

15.

16.

CHAPTER

1.

2.

13. November	79
14. December	81
15. Summary	83
CHAPTER 4. RELATIONSHIP BETWEEN ATMOSPHERIC TELECONNECTIONS AND LOWER-TROPOSPHERIC AIRFLOW TRAJECTORIES	84
1. Overview	84
2. TC2 (PNA+, NAO+, SOI).....	87
3. TC4 (PNA, NAO+, SOI+).....	89
4. TC6 (PNA-, NAO-, SOI)	91
5. TC8 (PNA, NAO-, SOI-)	93
6. TC9 (PNA+, NAO, SOI).....	96
7. TC10 (PNA, NAO+, SOI).....	100
8. TC11 (PNA, NAO, SOI+).....	103
9. TC12 (PNA-, NAO, SOI).....	107
10. TC13 (PNA, NAO-, SOI).....	110
11. TC14 (PNA, NAO, SOI-).....	113
12. TC21 (PNA, NAO+, SOI-)	117
13. TC23 (PNA+, NAO, SOI-)	121
14. TC25 (PNA+, NAO-, SOI)	123
15. TC27 (PNA, NAO, SOI)	125
16. Summary	128
CHAPTER 5. DISCUSSION AND CONCLUSION.....	129
1. Overview	129
2. Discussion of the Research Questions	129

3. Limit

4. Future

APPENDIX A: F

1. Readg

2. Merge

3. Getbk

4. Comb

5. Count

6. Reach

7. Bound

8. Hyspli

9. Anoma

10. Telex

11. Telec

12. Divide

13. Stand

14. Temp

APPENDIX B: G

1. Project

2. Project

3. Traject

APPENDIX C: T

1. TC2 (PN

3. Limitations of the Study	145
4. Future Work	147
APPENDIX A: FORTRAN PROGRAMS	149
1. Readgeneral.f.....	149
2. Merge.f	149
3. Getbktr.f	152
4. Combine.f.....	168
5. Count.f.....	170
6. Readhysplit.f	171
7. Boundary.f.....	173
8. Hysplitcheck.f	174
9. Anomaly.f.....	176
10. Teleextract.f.....	176
11. Teleconnections.f	181
12. Divide.f.....	182
13. Standardize.f.....	183
14. Temp_precip.f	184
APPENDIX B: GIS COMMANDS	187
1. Projecting the Back-Trajectory files.....	187
2. Projecting the Raster Grids	187
3. Trajectory Node Locations in Meters.....	188
APPENDIX C: T-TEST RESULTS.....	189
1. TC2 (PNA+, NAO+, SOI) Spring.....	189

2. TC

3. TC

4. TC

5. TC

6. TC

7. TC

8. TC

9. TC

10. T

11. T

12. T

13. T

14. T

15. T

16. T

17. T

18. T

19. T

20. T

21. T

22. T

23. T

24. T

2. TC4 (PNA, NAO+, SOI+) Winter	190
3. TC6 (PNA-, NAO-, SOI) Winter	191
4. TC6 (PNA-, NAO-, SOI) Spring.....	192
5. TC8 (PNA, NAO-, SOI-) Winter	193
6. TC8 (PNA, NAO-, SOI-) Spring.....	194
7. TC8 (PNA, NAO-, SOI-) Summer.....	195
8. TC9 (PNA+, NAO, SOI) Winter.....	196
9. TC9 (PNA+, NAO, SOI) Spring	197
10. TC9 (PNA+, NAO, SOI) Summer	198
11. TC9 (PNA+, NAO, SOI) Autumn.....	199
12. TC10 (PNA, NAO+, SOI) Winter.....	200
13. TC10 (PNA, NAO+, SOI) Spring	201
14. TC10 (PNA, NAO+, SOI) Summer	202
15. TC10 (PNA, NAO+, SOI) Autumn.....	203
16. TC11 (PNA, NAO, SOI+) Winter.....	204
17. TC11 (PNA, NAO, SOI+) Spring	205
18. TC11 (PNA, NAO, SOI+) Summer	206
19. TC11 (PNA, NAO, SOI+) Autumn.....	207
20. TC12 (PNA-, NAO, SOI) Winter.....	208
21. TC12 (PNA-, NAO, SOI) Spring	209
22. TC12 (PNA-, NAO, SOI) Autumn.....	210
23. TC13 (PNA, NAO-, SOI) Winter.....	211
24. TC13 (PNA, NAO-, SOI) Spring.....	212

25. TC13

26. TC13

27. TC14

28. TC14

29. TC14

30. TC14

31. TC21

32. TC21

33. TC21

34. TC21

35. TC23

36. TC23

37. TC25

38. TC25

39. TC27

40. TC27

41. TC27

42. TC27

BIBLIOGRAPHY

25. TC13 (PNA, NAO-, SOI) Summer	213
26. TC13 (PNA, NAO-, SOI) Autumn.....	214
27. TC14 (PNA, NAO, SOI-) Winter.....	215
28. TC14 (PNA, NAO, SOI-) Spring	216
29. TC14 (PNA, NAO, SOI-) Summer	217
30. TC14 (PNA, NAO, SOI-) Autumn.....	218
31. TC21 (PNA, NAO+, SOI-) Winter	219
32. TC21 (PNA, NAO+, SOI-) Spring.....	220
33. TC21 (PNA, NAO+, SOI-) Summer	221
34. TC21 (PNA, NAO+, SOI-) Autumn	222
35. TC23 (PNA+, NAO, SOI-) Winter	223
36. TC23 (PNA+, NAO, SOI-) Spring.....	224
37. TC25 (PNA+, NAO-, SOI) Winter	225
38. TC25 (PNA+, NAO-, SOI) Autumn	226
39. TC27 (PNA, NAO, SOI) Winter	227
40. TC27 (PNA, NAO, SOI) Spring	228
41. TC27 (PNA, NAO, SOI) Summer	229
42. TC27 (PNA, NAO, SOI) Autumn	230
BIBLIOGRAPHY	231

2.1 Steps to con

2.2 Steps to con

2.3 Average u, v
SPLIT mode

2.4 Average u, v
SPLIT mode
represent bias

2.5 The 27 possib
for each seas

4.1 Temperature o
combinations

5.1 Summary of a

5.2 Statistically st
teleconnection
05: ** is sign

5.3 Summary of a
precipitation a

LIST OF TABLES

2.1 Steps to convert the back trajectories to a coverage format	39
2.2 Steps to compute a HY-SPLIT trajectory	41
2.3 Average u, v, and hypotenuse distance in kilometers between the isobaric and HY-SPLIT model trajectory nodes at each of the 40 time steps	46
2.4 Average u, v, and hypotenuse distance in kilometers between the isobaric and HY-SPLIT model trajectory nodes at each of the 40 time steps. The sign is included to represent bias in direction	47
2.5 The 27 possible teleconnection combinations and the number of monthly occurrences for each seasonal grouping	50
4.1 Temperature (°C) and precipitation (mm) anomalies for the 27 teleconnection combinations by seasonal groupings	87
5.1 Summary of atmospheric teleconnection association with low-level airflow	134
5.2 Statistically significant temperature (°C) and precipitation (mm) anomalies for the 27 teleconnection combinations by seasonal groupings (where: *** is significant at $\alpha = .05$; ** is significant at $\alpha = .1$; and * is significant at $\alpha = .2$)	139
5.3 Summary of atmospheric teleconnection association with temperature and precipitation anomalies	141

1.1 Streamlines
horizontal p
streamlines d
1977; p. 381

1.2 Example of a
Darker colors
p. 74).....

1.3 Geopotential
Atlantic Osc

1.4 Geopotential
Pacific North

1.5 Typical Janu
moderate to s

2.1 Summary of

2.2 Summary of

2.3 Map of the d

2.4 The trajectory
hour node loc
location: and
1999; p. 55)

2.5 Results of th
comparison

2.6 Isobarc and

2.7 Isobarc and

2.8 Isobarc and

2.9 Climate divis

LIST OF FIGURES

1.1 Streamlines and trajectories in an eastward-moving wave. Heavy arrows denote horizontal projections of air trajectories, solid thin arrows denote earlier streamlines and dashed arrows denote later streamlines (from Wallace and Hobbs, 1977; p. 381)	5
1.2 Example of a raster-based display of five-day air-parcel trajectories for January. Darker colors depict regions where more trajectories originated (from Waller, 1999; p. 74).....	13
1.3 Geopotential height anomaly map in meters for the positive phase of the North Atlantic Oscillation (from the CPC, 2002a).....	17
1.4 Geopotential height anomaly map in meters for the positive phase of the Pacific/North American teleconnection (from the CPC, 2002b)	19
1.5 Typical January-March weather anomalies and atmospheric circulation during moderate to strong El Niño and La Niña (from the CPC, 2002c).....	21
2.1 Summary of steps to perform the trajectory climatology.....	28
2.2 Summary of steps to perform the atmospheric teleconnection analysis	29
2.3 Map of the data grid (10° to 85° N and 60° to 145° W)	32
2.4 The trajectory calculation, where point 1 is starting location; point 2' is the new three-hour node location after the calculation; point 2 is the revised three-hour node location; and points a, b, c, and d are the surrounding grid point values (from Waller, 1999; p. 55)	35
2.5 Results of the isobaric trajectory model and HY-SPLIT trajectory model comparison	43
2.6 Isobaric and HY-SPLIT comparison for 0000 UTC July 1, 1999	44
2.7 Isobaric and HY-SPLIT comparison for 0000 UTC August 1, 1999.....	44
2.8 Isobaric and HY-SPLIT comparison for 0000 UTC September 1, 1999	45
2.9 Climate division #9 within lower Michigan (from the CDC, 2003d)	53

3.1 Annual clim
for the period
hPa surface

3.2 January clim
trajectories.
nodes per grid
following each
(100-199), at
first difference
and then exp
details.) The
and >3) stand
(-1 to -2, -2 to

3.3 February clim
back trajectory

3.4 March climat
trajectories.

3.5 April climat
trajectories.

3.6 May climat
trajectories.

3.7 June climat
trajectories.

3.8 July climat
trajectories.

3.9 August clim
trajectories.

3.10 September
back trajectory

3.11 October cli
back trajectory

3.12 November
back trajectory

3.1 Annual climatology map. Number of trajectory nodes per 50 km by 50 km grid cell for the period 1960-1999. The trajectories are five-day back trajectories for the 925 hPa surface. Grid nodes were calculated at three-hour intervals	56
3.2 January climatology (top) and anomaly (bottom) maps for the 925 hPa, isobaric back trajectories. The climatology map shows the total number of three-hour trajectory nodes per grid cell for the 1960-1999 study period. The colors represent the following categories: clear (0-19), tan (20-34), green (35-59), purple (60-99), red (100-199), and cyan (200 or more) nodes per grid cell. Anomalies were calculated by first differencing the monthly totals and the average annual value for each grid cell, and then expressing the differences as standard deviations. (See text for further details.) The “warm” colors on the anomaly map represent positive (1 to 2, 2 to 3, and >3) standard deviations from the mean and the “cool” colors represent negative (-1 to -2, -2 to -3, <-3) standard deviations from the mean.....	60
3.3 February climatology (top) and anomaly (bottom) maps for the 925 hPa, isobaric back trajectories. See caption to Figure 3.2 for further details.....	62
3.4 March climatology (top) and anomaly (bottom) maps for the 925 hPa, isobaric back trajectories. See caption to Figure 3.2 for further details	64
3.5 April climatology (top) and anomaly (bottom) maps for the 925 hPa, isobaric back trajectories. See caption to Figure 3.2 for further details	66
3.6 May climatology (top) and anomaly (bottom) maps for the 925 hPa, isobaric back trajectories. See caption to Figure 3.2 for further details	68
3.7 June climatology (top) and anomaly (bottom) maps for the 925 hPa, isobaric back trajectories. See caption to Figure 3.2 for further details	70
3.8 July climatology (top) and anomaly (bottom) maps for the 925 hPa, isobaric back trajectories. See caption to Figure 3.2 for further details	72
3.9 August climatology (top) and anomaly (bottom) maps for the 925 hPa, isobaric back trajectories. See caption to Figure 3.2 for further details	74
3.10 September climatology (top) and anomaly (bottom) maps for the 925 hPa, isobaric back trajectories. See caption to Figure 3.2 for further details.....	76
3.11 October climatology (top) and anomaly (bottom) maps for the 925 hPa, isobaric back trajectories. See caption to Figure 3.2 for further details.....	78
3.12 November climatology (top) and anomaly (bottom) maps for the 925 hPa, isobaric back trajectories. See caption to Figure 3.2 for further details.....	80

3.13 December
back trajectory

4.1 Deviation of
the average
calculating
grid cells
springtime
the proportion
standard deviation
The "warm"
from the mean
deviations from

4.2 Deviation of
the average w
details

4.3 Deviation of
the average w
details

4.4 Deviation of
the average s
details

4.5 Deviation of
the average
details

4.6 Deviation of
the average
details

4.7 Deviation of
the average
details

4.8 Deviation of
the average
details

4.9 Deviation of
the average
details

3.13 December climatology (top) and anomaly (bottom) maps for the 925 hPa, isobaric back trajectories. See caption to Figure 3.2 for further details.....	82
4.1 Deviation of trajectory frequencies during TC2 (PNA+, NAO+, SOI) in spring from the average springtime trajectory frequencies. The anomalies were calculated by first calculating the proportion of the total number of trajectory nodes (summed across all grid cells) that fell within each grid cell and then differencing the proportions for the springtime (March-May) occurrences of Teleconnection Combination #2 (TC2) from the proportional values for all spring seasons. The differences are plotted in terms of standard deviations around a mean difference of zero (see text for further details). The “warm” colors on the map indicate positive (1 to 2, 2 to 3, and >3) deviations from the mean and the “cool” colors represent negative (-1 to -2, -2 to -3, <-3) deviations from the mean	89
4.2 Deviation of trajectory frequencies during TC4 (PNA, NAO+, SOI+) in winter from the average wintertime trajectory frequencies. See caption to Figure 4.1 for further details	90
4.3 Deviation of trajectory frequencies during TC6 (PNA-, NAO-, SOI) in winter from the average wintertime trajectory frequencies. See caption to Figure 4.1 for further details	92
4.4 Deviation of trajectory frequencies during TC6 (PNA-, NAO-, SOI) in spring from the average springtime trajectory frequencies. See caption to Figure 4.1 for further details	93
4.5 Deviation of trajectory frequencies during TC8 (PNA, NAO-, SOI-) in winter from the average wintertime trajectory frequencies. See caption to Figure 4.1 for further details	95
4.6 Deviation of trajectory frequencies during TC8 (PNA, NAO-, SOI-) in spring from the average springtime trajectory frequencies. See caption to Figure 4.1 for further details	95
4.7 Deviation of trajectory frequencies during TC8 (PNA, NAO-, SOI-) in summer from the average summertime trajectory frequencies. See caption to Figure 4.1 for further details	96
4.8 Deviation of trajectory frequencies during TC9 (PNA+, NAO, SOI) in winter from the average wintertime trajectory frequencies. See caption to Figure 4.1 for further details	98
4.9 Deviation of trajectory frequencies during TC9 (PNA+, NAO, SOI) in spring from the average springtime trajectory frequencies. See caption to Figure 4.1 for further details	98

4.10 Deviation of
the average
details

4.11 Deviation of
the average
details

4.12 Deviation of
the average
details

4.13 Deviation of
the average
details

4.14 Deviation of
from the ave
further detai

4.15 Deviation of
from the ave
details

4.16 Deviation of
the average
details

4.17 Deviation of
the average
details

4.18 Deviation of
from the ave
further detai

4.19 Deviation of
from the ave
details

4.20 Deviation of
the average
details

4.10 Deviation of trajectory frequencies during TC9 (PNA+, NAO, SOI) in summer from the average summertime trajectory frequencies. See caption to Figure 4.1 for further details	99
4.11 Deviation of trajectory frequencies during TC9 (PNA+, NAO, SOI) in autumn from the average autumn trajectory frequencies. See caption to Figure 4.1 for further details	99
4.12 Deviation of trajectory frequencies during TC10 (PNA, NAO+, SOI) in winter from the average wintertime trajectory frequencies. See caption to Figure 4.1 for further details	101
4.13 Deviation of trajectory frequencies during TC10 (PNA, NAO+, SOI) in spring from the average springtime trajectory frequencies. See caption to Figure 4.1 for further details	102
4.14 Deviation of trajectory frequencies during TC10 (PNA, NAO+, SOI) in summer from the average summertime trajectory frequencies. See caption to Figure 4.1 for further details.....	102
4.15 Deviation of trajectory frequencies during TC10 (PNA, NAO+, SOI) in autumn from the average autumn trajectory frequencies. See caption to Figure 4.1 for further details	103
4.16 Deviation of trajectory frequencies during TC11 (PNA, NAO, SOI+) in winter from the average wintertime trajectory frequencies. See caption to Figure 4.1 for further details	104
4.17 Deviation of trajectory frequencies during TC11 (PNA, NAO, SOI+) in spring from the average springtime trajectory frequencies. See caption to Figure 4.1 for further details	105
4.18 Deviation of trajectory frequencies during TC11 (PNA, NAO, SOI+) in summer from the average summertime trajectory frequencies. See caption to Figure 4.1 for further details.....	106
4.19 Deviation of trajectory frequencies during TC11 (PNA, NAO, SOI+) in autumn from the average autumn trajectory frequencies. See caption to Figure 4.1 for further details	107
4.20 Deviation of trajectory frequencies during TC12 (PNA-, NAO, SOI) in winter from the average wintertime trajectory frequencies. See caption to Figure 4.1 for further details	108

4.21 Deviation of
the average
details

4.22 Deviation of
the average
details

4.23 Deviation of
the average
details

4.24 Deviation of
the average
details

4.25 Deviation of
from the ave
further detail

4.26 Deviation of
the average a
details

4.27 Deviation of
the average v
details

4.28 Deviation of
the average s
details

4.29 Deviation of
from the ave
further detail

4.30 Deviation of
the average a
details

4.31 Deviation of
the average w
details

4.21 Deviation of trajectory frequencies during TC12 (PNA-, NAO, SOI) in spring from the average springtime trajectory frequencies. See caption to Figure 4.1 for further details	109
4.22 Deviation of trajectory frequencies during TC12 (PNA-, NAO, SOI) in autumn from the average autumn trajectory frequencies. See caption to Figure 4.1 for further details	109
4.23 Deviation of trajectory frequencies during TC13 (PNA, NAO-, SOI) in winter from the average wintertime trajectory frequencies. See caption to Figure 4.1 for further details	111
4.24 Deviation of trajectory frequencies during TC13 (PNA, NAO-, SOI) in spring from the average springtime trajectory frequencies. See caption to Figure 4.1 for further details	112
4.25 Deviation of trajectory frequencies during TC13 (PNA, NAO-, SOI) in summer from the average summertime trajectory frequencies. See caption to Figure 4.1 for further details.....	112
4.26 Deviation of trajectory frequencies during TC13 (PNA, NAO-, SOI) in autumn from the average autumn trajectory frequencies. See caption to Figure 4.1 for further details	113
4.27 Deviation of trajectory frequencies during TC14 (PNA, NAO, SOI-) in winter from the average winter trajectory frequencies. See caption to Figure 4.1 for further details	115
4.28 Deviation of trajectory frequencies during TC14 (PNA, NAO, SOI-) in spring from the average springtime trajectory frequencies. See caption to Figure 4.1 for further details	115
4.29 Deviation of trajectory frequencies during TC14 (PNA, NAO, SOI-) in summer from the average summertime trajectory frequencies. See caption to Figure 4.1 for further details.....	116
4.30 Deviation of trajectory frequencies during TC14 (PNA, NAO, SOI-) in autumn from the average autumn trajectory frequencies. See caption to Figure 4.1 for further details	116
4.31 Deviation of trajectory frequencies during TC21 (PNA, NAO+, SOI-) in winter from the average wintertime trajectory frequencies. See caption to Figure 4.1 for further details	118

4.32 Deviation of
the average
details

4.33 Deviation of
from the av
further det.

4.34 Deviation
from the a
details

4.35 Deviation
the average
details

4.36 Deviation
the average
details

4.37 Deviation of
the average
details

4.38 Deviation of
from the av
details

4.39 Deviation of
the average
details

4.40 Deviation of
the average
details

4.41 Deviation
the average
details

4.42 Deviation
the average
details

C.I. One-sampl
Prob = 0.0

Deviation of trajectory frequencies during TC21 (PNA, NAO+, SOI-) in spring from the average springtime trajectory frequencies. See caption to Figure 4.1 for further details	119
Deviation of trajectory frequencies during TC21 (PNA, NAO+, SOI-) in summer from the average summertime trajectory frequencies. See caption to Figure 4.1 for further details.....	120
Deviation of trajectory frequencies during TC21 (PNA, NAO+, SOI-) in autumn from the average autumn trajectory frequencies. See caption to Figure 4.1 for further details	121
Deviation of trajectory frequencies during TC23 (PNA+, NAO, SOI-) in winter from the average wintertime trajectory frequencies. See caption to Figure 4.1 for further details	122
Deviation of trajectory frequencies during TC23 (PNA+, NAO, SOI-) in spring from the average springtime trajectory frequencies. See caption to Figure 4.1 for further details	123
Deviation of trajectory frequencies during TC25 (PNA+, NAO-, SOI) in winter from the average wintertime trajectory frequencies. See caption to Figure 4.1 for further details	124
Deviation of trajectory frequencies during TC25 (PNA+, NAO-, SOI) in autumn from the average autumn trajectory frequencies. See caption to Figure 4.1 for further details	125
Deviation of trajectory frequencies during TC27 (PNA, NAO, SOI) in winter from the average wintertime trajectory frequencies. See caption to Figure 4.1 for further details	126
Deviation of trajectory frequencies during TC27 (PNA, NAO, SOI) in spring from the average springtime trajectory frequencies. See caption to Figure 4.1 for further details	127
Deviation of trajectory frequencies during TC27 (PNA, NAO, SOI) in summer from the average summertime trajectory frequencies. See caption to Figure 4.1 for further details	127
Deviation of trajectory frequencies during TC27 (PNA, NAO, SOI) in autumn from the average autumn trajectory frequencies. See caption to Figure 4.1 for further details	128
One-sample t test of temperature with 3 cases; Mean = 1.3, SD = 0.5, Prob = 0.0	189

one-sample t test of precipitation with 3 cases; Mean = -2.0, SD = 27.0, Prob = 0.9	189
one-sample t test of temperature with 7 cases; Mean = 1.7, SD = 2.2, Prob = 0.1	190
one-sample t test of precipitation with 7 cases; Mean = 18.0, SD = 31.0, Prob = 0.2	190
one-sample t test of temperature with 6 cases; Mean = -0.4, SD = 1.1, Prob = 0.4	191
one-sample t test of precipitation with 6 cases; Mean = 4.0, SD = 18.0, Prob = 0.6	191
one-sample t test of temperature with 4 cases; Mean = -2.4, SD = 1.3, Prob = 0.0	192
one-sample t test of precipitation with 4 cases; Mean = 3.0, SD = 22.0, Prob = 0.8	192
one-sample t test of temperature with 5 cases; Mean = -1.1, SD = 2.9, Prob = 0.2	193
one-sample t test of precipitation with 5 cases; Mean = -7.0, SD = 25.0, Prob = 0.6	193
one-sample t test of temperature with 3 cases; Mean = -1.0, SD = 1.7, Prob = 0.4	194
one-sample t test of precipitation with 3 cases; Mean = -4.0, SD = 36.0, Prob = 0.9	194
one-sample t test of temperature with 7 cases; Mean = -0.2, SD = 1.5, Prob = 0.8	195
one-sample t test of precipitation with 7 cases; Mean = -13.0, SD = 16.0, Prob = 0.1	195
one-sample t test of temperature with 5 cases; Mean = -1.8, SD = 1.1, Prob = 0.0	196
one-sample t test of precipitation with 5 cases; Mean = -28.0, SD = 13.0, Prob = 0.0	196

C.17. One-samp
Prob = 0

C.18. One-samp
Prob = 0

C.19. One-samp
Prob = 0

C.20. One-samp
Prob = 0

C.21. One-samp
Prob = 0

C.22. One-samp
Prob = 0.5

C.23. One-samp
Prob = 0.5

C.24. One-samp
Prob = 0.4

C.25. One-samp
Prob = 0.6

C.26. One-samp
Prob = 0.2

C.27. One-samp
Prob = 0.0

C.28. One-samp
Prob = 0.8

C.29. One-samp
Prob = 0.1

C.30. One-samp
Prob = 0.1

C.31. One-samp
Prob = 0.5

C.17. One-sample t test of temperature with 8 cases; Mean = -0.2, SD = 2.4, Prob = 0.8	197
C.18. One-sample t test of precipitation with 8 cases; Mean = -9.0, SD = 33.0, Prob = 0.5	197
C.19. One-sample t test of temperature with 3 cases; Mean = -0.1, SD = 1.5, Prob = 0.9	198
C.20. One-sample t test of precipitation with 3 cases; Mean = -29.0, SD = 44.0, Prob = 0.4	198
C.21. One-sample t test of temperature with 8 cases; Mean = -1.4, SD = 1.4, Prob = 0.0	199
C.22. One-sample t test of precipitation with 8 cases; Mean = -10.0, SD = 35.0, Prob = 0.5	199
C.23. One-sample t test of temperature with 14 cases; Mean = 0.5, SD = 3.0, Prob = 0.5	200
C.24. One-sample t test of precipitation with 14 cases; Mean = -4.0, SD = 17.0, Prob = 0.4	200
C.25. One-sample t test of temperature with 6 cases; Mean = 0.3, SD = 1.2, Prob = 0.6	201
C.26. One-sample t test of precipitation with 6 cases; Mean = -12.0, SD = 18.0, Prob = 0.2	201
C.27. One-sample t test of temperature with 11 cases; Mean = 0.9, SD = 1.0, Prob = 0.0	202
C.28. One-sample t test of precipitation with 11 cases; Mean = 2.0, SD = 31.0, Prob = 0.8	202
C.29. One-sample t test of temperature with 7 cases; Mean = -0.6, SD = 1.0, Prob = 0.1	203
C.30. One-sample t test of precipitation with 7 cases; Mean = -11.0, SD = 23.0, Prob = 0.2	203
C.31. One-sample t test of temperature with 12 cases; Mean = -0.4, SD = 2.2, Prob = 0.5	204

C.32. One-samp
Prob = 0

C.33. One-samp
Prob = 0

C.34. One-samp
Prob = 0

C.35. One-samp
Prob = 0

C.36. One-samp
Prob = 0.9

C.37. One-samp
Prob = 0.4

C.38. One-samp
Prob = 0.7

C.39. One-samp
Prob = 0.7

C.40. One-samp
Prob = 0.8

C.41. One-samp
Prob = 0.5

C.42. One-samp
Prob = 0.8

C.43. One-samp
Prob = 0.0

C.44. One-samp
Prob = 0.2

C.45. One-samp
Prob = 0.2

C.46. One-samp
Prob = 0.

C.32. One-sample t test of precipitation with 12 cases; Mean = 6.0, SD = 20.0, Prob = 0.3	204
C.33. One-sample t test of temperature with 9 cases; Mean = -0.2, SD = 1.8, Prob = 0.7	205
C.34. One-sample t test of precipitation with 9 cases; Mean = 3.0, SD = 40.0, Prob = 0.8	205
C.35. One-sample t test of temperature with 7 cases; Mean = 0.8, SD = 1.0, Prob = 0.1	206
C.36. One-sample t test of precipitation with 7 cases; Mean = -2.0, SD = 38.0, Prob = 0.9	206
C.37. One-sample t test of temperature with 14 cases; Mean = 0.5, SD = 1.8, Prob = 0.4	207
C.38. One-sample t test of precipitation with 14 cases; Mean = 3.0, SD = 34.0, Prob = 0.7	207
C.39. One-sample t test of temperature with 5 cases; Mean = -0.3, SD = 1.9, Prob = 0.7	208
C.40. One-sample t test of precipitation with 5 cases; Mean = 4.0, SD = 30.0, Prob = 0.8	208
C.41. One-sample t test of temperature with 9 cases; Mean = -0.4, SD = 1.7, Prob = 0.5	209
C.42. One-sample t test of precipitation with 9 cases; Mean = 3.0, SD = 29.0, Prob = 0.8	209
C.43. One-sample t test of temperature with 9 cases; Mean = 1.0, SD = 1.2, Prob = 0.0	210
C.44. One-sample t test of precipitation with 9 cases; Mean = 15.0, SD = 37.0, Prob = 0.3	210
C.45. One-sample t test of temperature with 4 cases; Mean = 0.8, SD = 1.0, Prob = 0.2	211
C.46. One-sample t test of precipitation with 4 cases; Mean = 13.0, SD = 26.0, Prob = 0.4	211

C.47. One-sa
Prob =

C.48. One-sa
Prob =

C.49. One-sa
Prob =

C.50. One-sa
Prob =

C.51. One-sa
Prob =

C.52. One-sa
Prob =

C.53. One-sa
Prob =

C.54. One-sa
Prob =

C.55. One-sa
Prob =

C.56. One-sa
Prob =

C.57. One-sa
Prob =

C.58. One-sa
Prob =

C.59. One-samp
Prob =

C.60. One-samp
Prob =

C.61. One-samp
Prob =

C.47. One-sample t test of temperature with 15 cases; Mean = -0.6, SD = 1.2, Prob = 0.1	212
C.48. One-sample t test of precipitation with 15 cases; Mean = -6.0, SD = 23.0, Prob = 0.3	212
C.49. One-sample t test of temperature with 8 cases; Mean = -0.2, SD = 1.4, Prob = 0.7	213
C.50. One-sample t test of precipitation with 8 cases; Mean = -11.0, SD = 25.0, Prob = 0.2	213
C.51. One-sample t test of temperature with 7 cases; Mean = -1.1, SD = 1.7, Prob = 0.1	214
C.52. One-sample t test of precipitation with 7 cases; Mean = 13.0, SD = 30.0, Prob = 0.3	214
C.53. One-sample t test of temperature with 6 cases; Mean = 1.6, SD = 2.1, Prob = 0.1	215
C.54. One-sample t test of precipitation with 6 cases; Mean = 10.0, SD = 33.0, Prob = 0.5	215
C.55. One-sample t test of temperature with 10 cases; Mean = 1.1, SD = 1.6, Prob = 0.1	216
C.56. One-sample t test of precipitation with 10 cases; Mean = 14.0, SD = 18.0, Prob = 0.0	216
C.57. One-sample t test of temperature with 10 cases; Mean = -0.2, SD = 1.1, Prob = 0.5	217
C.58. One-sample t test of precipitation with 10 cases; Mean = 7.0, SD = 31.0, Prob = 0.5	217
C.59. One-sample t test of temperature with 11 cases; Mean = 0.1, SD = 1.3, Prob = 0.8	218
C.60. One-sample t test of precipitation with 11 cases; Mean = -3.0, SD = 39.0, Prob = 0.8	218
C.61. One-sample t test of temperature with 5 cases; Mean = 1.7, SD = 2.3, Prob = 0.2	219

C.62. One-sam
Prob = 0

C.63. One-sam
Prob = 0

C.64. One-sam
Prob = 0

C.65. One-sam
Prob = 0

C.66. One-sam
Prob = 0

C.67. One-sam
Prob = 0

C.68. One-sam
Prob = 0

C.69. One-sam
Prob = 0

C.70. One-sam
Prob = 0

C.71. One-sam
Prob = 0

C.72. One-sam
Prob = 0

C.73. One-sam
Prob = 0

C.74. One-sam
Prob = 0

C.75. One-sam
Prob = 0

C.76. One-sam
Prob = 0

C.62. One-sample t test of precipitation with 5 cases; Mean = 6.0, SD = 27.0, Prob = 0.7	219
C.63. One-sample t test of temperature with 5 cases; Mean = 1.1, SD = 0.7, Prob = 0.0	220
C.64. One-sample t test of precipitation with 5 cases; Mean = -8.0, SD = 20.0, Prob = 0.4	220
C.65. One-sample t test of temperature with 6 cases; Mean = -1.0, SD = 0.8, Prob = 0.0	221
C.66. One-sample t test of precipitation with 6 cases; Mean = -7.0, SD = 32.0, Prob = 0.6	221
C.67. One-sample t test of temperature with 5 cases; Mean = 0.8, SD = 2.4, Prob = 0.5	222
C.68. One-sample t test of precipitation with 5 cases; Mean = -19.0, SD = 42.0, Prob = 0.4	222
C.69. One-sample t test of temperature with 7 cases; Mean = 2.9, SD = 1.7, Prob = 0.0	223
C.70. One-sample t test of precipitation with 7 cases; Mean = -15.0, SD = 16.0, Prob = 0.0	223
C.71. One-sample t test of temperature with 6 cases; Mean = 1.0, SD = 1.6, Prob = 0.2	224
C.72. One-sample t test of precipitation with 6 cases; Mean = -4.0, SD = 23.0, Prob = 0.7	224
C.73. One-sample t test of temperature with 5 cases; Mean = -4.0, SD = 2.1, Prob = 0.0	225
C.74. One-sample t test of precipitation with 5 cases; Mean = -20.0, SD = 20.0, Prob = 0.1	225
C.75. One-sample t test of temperature with 3 cases; Mean = 0.3, SD = 0.6, Prob = 0.4	226
C.76. One-sample t test of precipitation with 3 cases; Mean = 2.0, SD = 30.0, Prob = 0.9	226

C.77. One-sam
Prob = 0

C.78. One-sam
Prob = 1

C.79. One-sam
Prob = 0

C.80. One-sam
Prob = 0

C.81. One-sam
Prob = 0

C.82. One-sam
Prob = 0

C.83. One-sam
Prob = 0

C.84. One-sam
Prob =

C.77. One-sample t test of temperature with 25 cases; Mean = -0.2, SD = 2.6, Prob = 0.8	227
C.78. One-sample t test of precipitation with 25 cases; Mean = 0.0, SD = 2.1, Prob = 1.0	227
C.79. One-sample t test of temperature with 30 cases; Mean = 0.1, SD = 2.5, Prob = 0.8	228
C.80. One-sample t test of precipitation with 30 cases; Mean = -0.0, SD = 27.0, Prob = 0.9	228
C.81. One-sample t test of temperature with 52 cases; Mean = -0.0, SD = 1.1, Prob = 0.8	229
C.82. One-sample t test of precipitation with 52 cases; Mean = 1.0, SD = 33.0, Prob = 0.8	229
C.83. One-sample t test of temperature with 36 cases; Mean = -0.1, SD = 1.5, Prob = 0.8	230
C.84. One-sample t test of precipitation with 36 cases; Mean = -4.0, SD = 32.0, Prob = 0.4	230

$$(1.1) PNA = 1 + \dots + Z^*$$

$$(2.1) \text{new_latit}$$

$$(2.2) \text{temp_latit}$$

$$(2.3) \text{degrees_lo}$$

$$(2.4) \text{new_longi}$$

$$(2.5) x_i = ((-.4$$

$$(2.6) x_j = ((-.4$$

$$(2.7) p = x_i - \text{ain}$$

$$(2.8) q = x_j - \text{ain}$$

$$(2.9) u = u_a * p + u_b * (1 + u_c * (1 + u_d * p$$

$$(2.10) v = v_a * p + v_b * (+ v_c * (+ v_d * p$$

$$(2.11) \text{Standardi}$$

$$(2.12) \text{Standardi}$$

LIST OF EQUATIONS

PNA = 1/4 [z* (20° N, 160° W) – z* (45° N, 165° W) + z* (55° N, 115° W) – z* (30° N, 85° W)].....	14
new_latitude = original_latitude - (DISv / (111 km / degree)).....	35
temp_latitude = new_latitude * (0.01745329 radians / degree)	35
degrees_longitude = cos (temp_latitude) * (111 km / degree)	35
new_longitude = original_longitude + (DISu / degrees_longitude).....	35
xi = ((-.4) * new_latitude) + 37	36
xj = ((-.4) * new_longitude) + 145	36
p = xi - aint (xi).....	36
q = xj - aint (xj).....	36
u = ua * p * (1 - q) + ub * (1 - p) * (1 - q) + uc * (1 - p) * q + ud * p * q.....	37
v = va * p * (1 - q) + vb * (1 - p) * (1 - q) + vc * (1 - p) * q + vd * p * q.....	37
) Standardized Value = Number of nodes within grid cell (x _i , y _i) / Total number of nodes	51
) Standardized Value = Standardized Value * 100,000	51

INTRO

1. Introduction

The rela
important and p
fluctuations in g

temperature (SS

teleconnection p

1860's (Hildebr

Bjerknes, 1969

teleconnection

teleconnection

in meteorologi

1981; p. 784).

recent *Glossar*

Atmos

scale climate a

latitude, plane

in the western

Oscillation is p

to anomalous t

Extremes such

CHAPTER 1

INTRODUCTION, LITERATURE REVIEW, AND OBJECTIVES

1. Introduction

The relationship between atmospheric teleconnections and local climate is an important and popular area of research in climatology. Atmospheric teleconnections are fluctuations in geopotential height, sea-level pressure (SLP), and/or sea-surface temperature (SST) that span large areas over the globe. Early descriptions of teleconnection patterns have appeared in the meteorological literature since the late 1800's (Hildebrandsson, 1897; Walker, 1924; Walker and Bliss, 1932; Lorenz, 1951; Bjerknes, 1969). However, Ångström (1935) was the first to define the term “teleconnection” as an “atmospheric seesaw.” In 1981, Wallace and Gutzler defined a teleconnection as a “significant simultaneous correlation between temporal fluctuations in meteorological parameters at widely separated points on earth” (Wallace and Gutzler, 1981; p. 784). The teleconnection definition by Wallace and Gutzler is still used in the recent *Glossary of Meteorology* by the American Meteorological Society (AMS) (2000).

Atmospheric teleconnections have been associated with local-scale and regional-scale climate anomalies. For example, the Southern Oscillation is defined as “a low-latitude, planetary-scale seesaw in SLP, with one pole in the eastern Pacific and the other in the western Pacific-Indian Ocean region” (AMS, 2000; p. 706). The Southern Oscillation is perhaps the most studied of all teleconnection patterns and has been linked to anomalous temperature and precipitation around the globe (Barry and Carleton, 2001). Extremes such as the 1988 summer drought in the central United States (Bates et al.,

2001), the 1993

even hurricane

linked to the S

teleconnections

with anomalies

shortcomings in

responsible for

precipitation and

The stud

in the frequency

infinitesimally s

space tracing the

"particle" and "

trajectories were

selected termina

Michigan's low

chosen because

precipitation in a

this study summa

provide a long-te

study relates the

authors have sho

and central Unite

2001), the 1993 summer floods in the midwestern United States (Bates et al., 2001), and even hurricane frequency in the Atlantic Ocean (Barry and Carleton, 2001) have been linked to the Southern Oscillation. Most previous studies of the association between teleconnections and local and/or regional climate have correlated teleconnection patterns with anomalies of temperature and precipitation. However, this approach has inherent shortcomings in that it ignores the intervening synoptic and mesoscale circulations responsible for the advection of different air masses and the consequent temperature and precipitation anomalies.

The study presented here relates atmospheric teleconnection indices to variations in the frequency and direction of air-parcel trajectories. An air parcel is defined as an infinitesimally small puff of air (Austin and Tuck, 1985), and a trajectory as “a curve in space tracing the points successively occupied by a particle in motion,” where the terms “particle” and “parcel” are used interchangeably (AMS, 2000; p. 786). Five-day back trajectories were calculated four times per day for a 40-year period (1960-1999). The selected terminus point for the trajectories was 42.5° N and 85.0° W located in Michigan’s lower peninsula within the midwestern United States. The study area was chosen because it experiences large interannual variations in temperature and precipitation in association with airflow from multiple source regions. The first part of this study summarizes the trajectories using a Geographic Information System (GIS) to provide a long-term (40-year) climatology of airflow by month. The second part of the study relates the trajectories to three atmospheric teleconnection patterns that previous authors have shown to be associated with weather and climate variations in the eastern and central United States. The three teleconnection patterns are the North Atlantic

Oscillation (N.S.
northern and ce
pattern, defined
northwest of N
554), and the p
trajectories from
teleconnection
related to season
Analysis is prov
teleconnection p
month. The goe
mesoscale mech
temperature and

2. Literature Review

A review
review is separat
air-parcel traject
atmospheric tele
midwestern Unit

a. Air-parcel

As describ

Oscillation (NAO), defined as a fluctuation in pressure and temperature between the **n**orthern and central Atlantic Ocean (Walker, 1924), the Pacific North/American (PNA) **p**attern, defined as “a wave-train signal that spans from the equatorial Pacific through the **n**orthwest of North America to the southeastern part of North America” (AMS, 2000; p. **554**), and the previously defined Southern Oscillation (SO). The frequencies of **t**rajectories from different source regions for months with high, low, and neutral **t**eleconnection index values are compared to the climatological trajectory patterns and are **r**elated to seasonal anomalies in temperature and precipitation for the study area. **A**nalysis is provided for each single teleconnection pattern and for “co-existing” **t**eleconnection patterns, as frequently more than one teleconnection is present in the same **m**onth. The goal of the study is to provide a better understanding of the synoptic and **m**esoscale mechanisms by which teleconnections are related to local anomalies of **t**emperature and precipitation.

2. Literature Review

A review of previous research relevant to this study will now be presented. The **r**evue is separated into two sections. The first section explains the previous research on **a**ir-parcel trajectories and trajectory models. The second section reviews past research on **a**tmospheric teleconnections and the teleconnection association with the climate of the **m**idwestern United States.

a. Air-parcel Trajectory Analysis

As described above, a trajectory is defined as “a curve in space tracing the points

successively oc

capable of capt

(Wallace and H

approximating

of streamlines

tangent at any p

point" (AMS, 2)

streamlines. Str

not represent air

movement and d

midlatitude cycl

streamlines is ill

eastward-movin

it progresses to

trajectory AC w

trajectory AD w

a faster wind sp

do not account

the actual paths

suggests that lo

result from slo

successively occupied by a particle in motion” (AMS, 2000; p. 786). Trajectories are **c**apable of capturing all three dimensions (x, y, z) of an air parcel’s path through time (Wallace and Hobbs, 1977). Therefore, air-parcel trajectories are useful for **a**pproximating atmospheric circulation. Another method to depict circulation is the use **o**f streamlines (Wendland and Bryson, 1981). A streamline is defined as “a line with its **t**angent at any point in a fluid parallel to the instantaneous velocity of the fluid at that **p**oint” (AMS, 2000; p. 735). However, trajectories have important advantages over **s**tr streamlines. Streamlines only depict the airflow at a particular moment in time, but do **n**ot represent airflow like trajectories because streamlines do not take into account the **m**ovement and development of larger-scale systems such as upper-level waves or **m**idlatitude cyclones (Wallace and Hobbs, 1977). A comparison of trajectories and **s**tr streamlines is illustrated in Figure 1.1. The figure uses an example of point A within an **e**astward-moving wave. Assuming that point A remains at the same speed at time one as **i**t **p**rogresses to time two, point A will remain coincident with the streamline and **t**rajectory AC will result. However, if point A has a slower wind speed at time two, **t**rajectory AD will result. Likewise, trajectory AB will result in the case that point A has **a** **f**aster wind speed at time two (Wallace and Hobbs, 1977). The result is that streamlines **d**o **n**ot account for system movement, and therefore, trajectories more closely represent **t**he actual paths of air parcels (Wallace and Hobbs, 1977). Additionally, Figure 1.1 **s**uggests that longer trajectories result from faster wind speeds and shorter trajectories **r**esult from slower wind speeds.

Figure 1.1. S
denote hor
streamlines and

A number
the term "model"
dynamical system
dependent on w
require tempera
atmospheric lev
backward or for
model is used. A
locate the source
terminus point.
of air parcels in
Airflow predict
insects (Eliassen
trajectories can

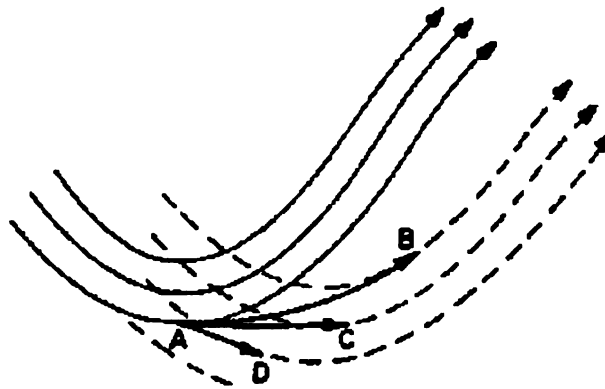


Figure 1.1. Streamlines and trajectories in an eastward-moving wave. Heavy arrows denote horizontal projections of air trajectories, solid thin arrows denote earlier streamlines and dashed arrows denote later streamlines (from Wallace and Hobbs, 1977; p. 381).

A number of different models can be used to calculate trajectories. In this case, the term “model” is defined as “a tool for simulating or predicting the behavior of a dynamical system like the atmosphere” (AMS, 2000; p. 501). Trajectory models are dependent on wind speed and direction. However, some trajectory models may also require temperature, height, and barometric pressure at the surface and at many atmospheric levels to calculate trajectories. Trajectories can be calculated either backward or forward in time from a selected location and time value. If a back-trajectory model is used, a terminus point is chosen and air parcels are traced backward in time to locate the source regions where the air parcels originated prior to propagating through the terminus point. Forward trajectories begin from a starting point and trace the future paths of air parcels in order to predict airflow of air parcels from selected source regions. Airflow prediction is commonly desired for studies such as the transport of pollution and insects (Eliassen, 1978; Scott and Achtemeier, 1987). Either backward or forward trajectories can be calculated for a trajectory climatology depending on what research

questions need

The pa

the meteorolog

al. (2001) state

crucial than the

has been diffic

high temporal a

Weather Service

approximately 4

et al. (1985) and

is too coarse for

velocities for th

values for vertic

trajectory error

model-derived

and the Nationa

al., 1996; Kistle

from the Europ

NCEP NCAR m

NCEP NCAR f

2.5° latitude an

questions need to be answered.

1. Temporal and Spatial Resolution

The path of a trajectory depends heavily on the temporal and spatial resolution of the meteorological data used to calculate the trajectory (Lee et al., 1997). In fact, Stohl et al. (2001) state that the spatial and temporal resolution of the input data is even more crucial than the choice of trajectory model. Increasing temporal and spatial resolution has been difficult in the past because wind observations have simply not been available at high temporal and spatial resolution. The traditional upper-air data from the National Weather Service (NWS) are only reported every 12 hours at a spatial resolution of approximately 400 km. Even though the data have been used in trajectory models, Kuo et al. (1985) and Kahl and Samson (1986) claim that this temporal and spatial resolution is too coarse for accurate trajectories. Additionally, the data only include horizontal wind velocities for the measured pressure levels. If three-dimensional trajectories are desired, values for vertical wind velocities must be interpolated, which leads to increased trajectory error (Doty and Perkey, 1993). Alternatives to the NWS upper-air data are model-derived data such as the National Centers for Environmental Prediction (NCEP) and the National Center for Atmospheric Research (NCAR) reanalysis data (Kalnay et al., 1996; Kistler et al., 2001). Other reanalysis data archives exist as well, such as those from the European Center for Medium Range Forecasting (ECMRF). However, the NCEP/NCAR reanalysis data have been the most widely used. Resulting data from the NCEP/NCAR fields have a temporal resolution of six hours and a spatial resolution of 2.5° latitude and longitude (approximately 277.5 km assuming 111 km per degree

latitude) (Robt

three-dimensio

derived fields a

within the NW

improvement in

observations.

Tempo

calculated from

error (Scott and

hours exhibit m

al., 2001). How

best results as l

interpolation ar

Doty and Perke

(Djuric, 1961; 1

1999). For exa

al. report that "

of 750 km" (19

Increasi

the resulting tra

atmosphere (Ka

spatial resolutio

hPa trajectories

latitude) (Robinson et al., 1978; Dent, 1999). Vertical velocity data are also available if three-dimensional trajectories are desired. Additionally, complete NCEP/NCAR model-derived fields are available for all time steps, whereas missing data are problematic within the NWS upper-air archive. Therefore, reanalysis data are a significant improvement in temporal and spatial resolution over the traditional upper-air observations.

Temporal resolution is important for minimizing trajectory error. Trajectories calculated from a coarse temporal resolution of greater than six hours have the largest error (Scott and Achtemeier, 1987). Calculations with time steps less than or equal to six hours exhibit much greater accuracy (Kuo et al., 1985; Doty and Perkey, 1993; Stohl et al., 2001). However, temporal resolutions of less than or equal to three hours display the best results as long as data are adequately available. If extreme amounts of temporal interpolation are required, additional trajectory error will be introduced (Kuo et al., 1985; Doty and Perkey, 1993). Errors in the observations also play a role in trajectory accuracy (Djurić, 1961; Kahl and Samson, 1988; Saxena et al., 1996; Lee et al., 1997; Waller, 1999). For example, wind direction is often reported to the nearest 10 degrees. Pack et al. report that “a five degree initial error gives rise to a 65 km error after a travel distance of 750 km” (1977; p. 426).

Increasing the spatial resolution of the input data also increases the accuracy of the resulting trajectories. Spatial resolution is most critical at lower heights in the atmosphere (Kahl and Samson, 1988; Lee et al., 1997). For example, an increase in spatial resolution from 320 km to 160 km resulted in greater accuracy of low-level, 925 hPa trajectories (Lee et al., 1997). Trajectories at 850 hPa and 700 hPa did not display as

much sensitive

mesoscale vari

finding (Lee et

Previous

resolution is m

(1986, 1988) fo

persistent cond

was more impo

different study

(1986, 1988) ps

result, Kuo et al

was necessary to

A variety

However, each t

possible to conc

One reason for t

tracer exactly ma

Many studies ha

what have been r

Clarke, 1983; Ba

trajectories becau

much sensitivity to increased spatial resolution (Lee et al., 1997). The decrease of mesoscale variability with height in the atmosphere is most likely the explanation for this finding (Lee et al., 1997).

Previous studies have found conflicting evidence on whether increasing spatial resolution is more important than increasing temporal resolution. Kahl and Samson (1986, 1988) found that an increase in spatial resolution was more important under persistent conditions, whereas Kuo et al. (1985) found that increasing temporal resolution was more important under cyclonic conditions. However, Kuo et al. (1985) used a different study period consisting of a single cyclone situation, whereas Kahl and Samson (1986, 1988) performed a two-month study of relatively undisturbed conditions. As a result, Kuo et al. (1985) stated that an increase in both temporal and spatial resolution was necessary to significantly improve trajectory accuracy.

2. Trajectory Models

A variety of trajectory models can be used for an airflow trajectory study. However, each trajectory model has advantages and disadvantages making it not always possible to conclude which model is most accurate for a particular atmospheric situation. One reason for this is that a “true” trajectory is impossible to obtain. No experimental tracer exactly matches the airflow (Austin and Tuck, 1985; Haagenson et al., 1987). Many studies have used special balloons, called “tetroons,” that can be tracked to display what have been referred to as “true” trajectories (Hoecker, 1977; Pack et al., 1977; Clarke, 1983; Baumann and Stohl, 1997). However, tetroons do not result in “true” trajectories because tetroons travel along isopycnic (constant-density) surfaces, which are

not true to atm

have compared

atmospheric tra

include the isob

trajectory mode

Isobaric

1978; Gisason &

propagate along

vertical motions

level. Any pres

atmospheric dis

models. Thus,

(Austin and Tu

conditions, or u

are required, is

and Seibert, 19

trajectory mod

fact that the pa

Haagenson et a

trajectories and

compared to hi

been widely us

Additionally, u

not true to atmospheric flow (Doty and Perkey, 1993). Therefore, these previous studies have compared the results of trajectory models to isopycnic trajectories rather than “true” atmospheric trajectories. The most popular trajectory models used in previous research include the isobaric, isentropic, isosigma, isoeta, isopycnic, and three-dimensional trajectory models. Each of these trajectory models will be introduced below.

Isobaric models are the most simplistic and have been widely used (Elliassen, 1978; Gisason and Prahm, 1983; Waller, 1999). Isobaric models assume that air parcels propagate along surfaces of constant pressure (Haagenson et al., 1987). Therefore, vertical motions of isobaric trajectories are limited to changes in the height of a pressure level. Any pressure level can be chosen if data are available. Trajectories within atmospheric disturbances, such as baroclinic zones, are highly underestimated by isobaric models. Thus, isobaric models are not the best choice for disturbed weather conditions (Austin and Tuck, 1985; Lee et al., 1997). However, under long-term, steady-state conditions, or under circumstances when only the horizontal positions of the air parcels are required, isobaric models perform as accurately as any other trajectory model (Stohl and Seibert, 1998). In fact, Stohl and Seibert (1998) state that compared to other trajectory models, isobaric models have smaller errors for longer trajectories due to the fact that the paths of isobaric trajectories fluctuate less over time. Additionally, Haagenson et al. (1987) conducted a comparison of tracer data versus calculated isobaric trajectories and found that trajectory error was minimized at the lower 950 hPa level compared to higher atmospheric levels. Another advantage is that isobaric models have been widely used, so trajectory results can be compared with previous studies. Additionally, upper-air meteorological data are readily available for pressure surfaces

from sources

Isobaric mod

making the is

If ver

is a good cho

1994). Isent

surfaces of c

isentropic m

However, is

adiabatic, s

unnoticed i

height (Wa

isentropic s

termination

Th

The vertic

or as the d

normalize

models ar

elevations

at low lev

Achtemen

ground an

sources such as the NWS observations or the NCEP/NCAR reanalysis data.

ic models only require wind speed and direction for a selected pressure surface, making the isobaric model much less data-intensive than other trajectory models.

If vertical motion is desired, such as in baroclinic conditions, an isentropic model is a good choice (Danielsen, 1961; Haagenson et al., 1985; Kuo et al., 1985; Merrill,

. Isentropic models assume that vertical movements of air parcels occur along surfaces of constant potential temperature (entropy). Compared to isobaric models, isentropic models are more accurate within disturbed conditions (Kuo et al., 1985).

However, isentropic models perform poorly for conditions when the lapse rate is near dry adiabatic, such as in the mixed layer (Kahl and Samson, 1988). Vertical motion goes unmodeled in dry adiabatic conditions because potential temperature is constant with height (Wallace and Hobbs, 1977). Another limitation of isentropic models is that isentropic surfaces at low levels often intersect the ground, which results in premature termination of the trajectories (Lee et al., 1997).

The isosigma, isoeta, and isopycnic trajectory models are less frequently used.

The vertical coordinate of sigma is defined as “pressure normalized by its surface value, divided by the difference in pressure and its value at the top of the model atmosphere

and normalized by the surface value of this difference” (AMS, 2000; p. 683). Isosigma

models are similar to isobaric models in the middle and upper troposphere above

altitudes of approximately 2,000 meters (Scott and Achtemeier, 1987). Sigma surfaces

at low levels closely resemble the terrain and are parallel to the ground (Scott and

Achtemeier, 1987). Due to the fact that sigma surfaces are terrain following near the

surface and constant pressure following above 2,000 meters, a linear function is applied

to blend the two

Scott and Ach

isosigma mode

have not been

coordinate is "

previously des

along surfaces

atmospheric fl

The last

and Hess (1996)

Integrated Traj

because it can

(Draxler, 1999)

approach is us

and Stein et al

the model per

model is comp

(north-south)

surface and at

vertical motio

downloading

Cohn (1996)

among the mo

and the two elements together within the middle atmosphere (Haagenson et al., 1987; and Achtemeier, 1987). Isoeta models are also terrain-following models much like sigma models (Stohl and Seibert, 1998; Stohl et al., 2001). However, isoeta models have not been as widely used as other trajectory models because the eta vertical coordinate is “step-like” in nature rather than smooth like other trajectory model surfaces previously described (AMS, 2000). Isopycnic models assume that trajectories propagate along surfaces of constant density, which as previously discussed, is not exactly true to spherical flow (Haagenson et al., 1987; Doty and Perkey, 1993).

The last trajectory models are the three-dimensional trajectory models. Draxler and Hess (1996, 1998a, 1998b, 1999) introduced the Hybrid Single-Particle Lagrangian Integrated Trajectory (HY-SPLIT) model. The HY-SPLIT model has been widely used because it can construct complex simulations from either a “puff” or “particle” approach (Draxler, 1999). The “puff” approach includes dispersion of a fluid and a “particle” approach is used for air-parcel trajectories. Rolph et al. (1992), Stein and Lamb (2000), and Stein et al. (2000) used the HY-SPLIT model in pollution transport studies because the model performs well for dispersion and deposition simulations. The HY-SPLIT model is complex since it requires, at minimum, the following data: u (east-west) and v (north-south) wind components, temperature, height, and barometric pressure at the start time and at all measured atmospheric levels in order to calculate the three-dimensional motion. However, the large amount of data required for HY-SPLIT can result in input loading time and storage space problems (Draxler and Hess, 1998a). Clark and Draxler (1990) compared HY-SPLIT to 10 other trajectory models and found it to perform among the most accurate in the study. Other known trajectory models include the

FLEXTRA (F)

and the TRA

1998; Stohl, 2

as the HY-SP

The pro

Waller (1999).

terminus poin

climatology w

in order to de

air-mass stud

used with dat

12-hour temp

1975). How

year period.

Wai

substantiall

west were r

trajectories

trajectories

trajectories

during sum

FLEXTRA (flexible trajectories) kinematic trajectory model, the LAGRANTO model, and the TRAJKS model (Stohl et al., 1995; Baumann and Stohl, 1997; Stohl and Seibert, 1998; Stohl, 2001; Stohl et al., 2001). However, these models are not as highly regarded as the HY-SPLIT model.

3. Waller's Isobaric Airflow Climatology

The previous research most relevant to this study is the trajectory climatology by Waller (1999). Waller prepared a 10-year, five-day, back-trajectory climatology for a terminus point in northwest Ohio (41.56° N, 84.09° W). The 10-year, trajectory climatology was compiled for 1976-1985. Waller performed the trajectory climatology in order to describe air-mass source regions as an alternative to the more conventional air-mass studies based on temperature and dewpoint. An 850 hPa isobaric model was used with data from the National Meteorological Center (NMC). The NMC data have a 12-hour temporal resolution and a spatial resolution of approximately 381 km (Jenne, 1975). However, the NMC data set does include some missing data throughout the 10-year period.

Waller (1999) found that the source regions for air-parcel trajectories changed substantially during the course of the year. In winter, trajectories originating from the west were most frequent. A shift to more frequent northwesterly and northerly trajectories was evident throughout the spring months with a large number of the trajectories originating near the Hudson Bay region. In summer, the lengths of the trajectories were shorter compared to the other months, suggesting weaker wind speeds during summer months. Additionally, Waller found that westerly and northwesterly

trajectories de
southwesterly
summer. How
did not occur
September and
trajectory map
short trajectory
organized and
northwesterly
strengthen as w
January as an e
reading black a

trajectories dominated during the summer. This result was surprising, as southerly and/or southwesterly trajectories would be expected given the warmer temperatures during the summer. However, an expected increase in southerly and/or southwesterly trajectories did not occur. These results may suggest a possible northerly bias of the NMC data. September and October were associated with a disorganized trajectory pattern. The trajectory maps for these months had a “bull’s-eye” appearance, indicating relatively short trajectories from multiple directions. By November, the trajectory pattern was more organized and northwesterly trajectories were once again most frequent. The northwesterly flow pattern continued through December when westerly airflow began to strengthen as well. Figure 1.2 illustrates Waller’s resulting trajectory climatology for January as an example of the output from her analysis. It should be noted to those reading black and white copies that many images in this thesis are presented in color.

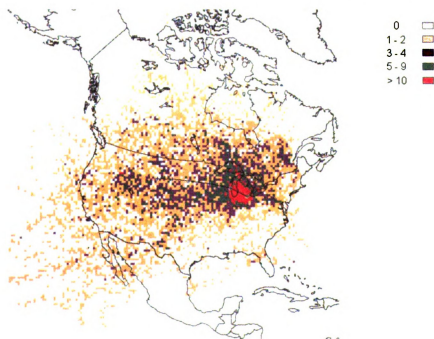


Figure 1.2. Example of a raster-based display of five-day air-parcel trajectories for January. Darker colors depict regions where more trajectories were originating (from Waller, 1999; p. 74).

b. *Atm*

A num

teleconnection

teleconnection

geopotential he

pressure (SLP)

teleconnection

is defined as th

prominent. B

be detected fo

correlation w

Gutzler, 1981

values at the

teleconnecti

teleconnecti

latitude long

(from Walla

(1.1) PN.

Re

b. Atmospheric Teleconnections

A number of methods have been developed to characterize atmospheric teleconnection patterns and the changes in these patterns with time. Most often, a teleconnection pattern is described using a simple numerical index, calculated from geopotential height values (most commonly for the 500 hPa or 700 hPa levels), sea-level pressure (SLP), or sea-surface temperature (SST). Barnston and Livezey (1987) state that teleconnections are named based on the location of a so-called “base point.” A base point is defined as the location where the presence of the particular teleconnection is most prominent. Barnston and Livezey (1987) also state that up to four strong base points can be detected for some teleconnections. Typically, a base point will have a strong negative correlation with another corresponding base point 2,500-6,000 km away (Wallace and Gutzler, 1981; Barnston and Livezey, 1987). The geopotential height, SLP, or SST values at the base points can then be combined into an overall index value for the teleconnection. Equation 1.1 is an example for the Pacific/North American (PNA) teleconnection where z^* is the normalized 500 hPa geopotential height anomalies and the latitude/longitude values correspond to the four base points for the teleconnection pattern (from Wallace and Gutzler, 1981; p. 798):

$$(1.1) \quad \text{PNA} = 1/4 [z^*(20^\circ \text{ N}, 160^\circ \text{ W}) - z^*(45^\circ \text{ N}, 165^\circ \text{ W}) \\ + z^*(55^\circ \text{ N}, 115^\circ \text{ W}) - z^*(30^\circ \text{ N}, 85^\circ \text{ W})]$$

Recent teleconnection studies have often abandoned this correlation method

because the va
teleconnection
not stationary,
realistically, a
turn, each spa
whereas the ab
(Trenberth and

A second

principle comp
hPa principle c
(1987). Other
Wallace and G
chosen for this
been standardi
and negative in

Three c

(NAO), the Pa
Each teleconn
interdecadal se
strong teleconn
possible comb
NAO and PNA
(Wallace and C

because the values are based on measurements at fixed base points for each teleconnection (Horel, 1981; Barnston and Livezey, 1987). However, teleconnections are not stationary, and indices calculated using fixed base points may be misleading. More realistically, a teleconnection influences spatial areas that contain each base point. In turn, each spatial area associated with a teleconnection may differ in size and strength, whereas the above equation assumes that each base point is of equal size and strength (Trenberth and Hurrell, 1994).

A second, more widely used method for measuring teleconnections is a rotated principle components analysis. The Climate Prediction Center (CPC) performed a 700 hPa principle component analysis similar to that conducted by Barnston and Livezey (1987). Other studies have performed the analysis at 500 hPa as well (Horel, 1981; Wallace and Gutzler, 1981). However, the methodology developed by the CPC was chosen for this study, because it was the most recent. The values in that data set have been standardized. Positive index values represent the positive phase of a teleconnection and negative index values represent the negative phase.

Three of the most studied teleconnections are the North Atlantic Oscillation (NAO), the Pacific North/American (PNA) pattern, and the Southern Oscillation (SO). Each teleconnection may fluctuate on intermonthly, interseasonal, interannual, interdecadal scales, or any combination of these. It is possible to have more than one strong teleconnection during a particular month, which results in a large number of possible combinations of teleconnections to analyze. Past research suggests that the NAO and PNA have a significant impact on the climate of the midwestern United States (Wallace and Gutzler, 1981; Rogers, 1984; Leathers et al., 1991; Assel, 1992; Rohli and

Rogers, 1993;

concerning the

Feng, 2001b).

components are

points. The S

difference in S

the NAO, PNA

The first

the oscillation

area" (AMS, 2

CPC that is ev

Portis et al., 2

between the N

strength of th

January and v

Greischar, 20

mostly negat

Based

of the Greenl

1981). Seco

because the p

Rogers, 1993; Serreze et al., 1998). The SO has also been an important area of interest concerning the climate of the Midwest (Rogers, 1984; Changnon et al., 2000; Hu and Feng, 2001b). However, the SO typically has not been described using a principal components analysis. Rather, index values for this teleconnection are based on fixed points. The Southern Oscillation index (SOI) has traditionally been measured by the difference in SLP between Tahiti and Darwin, Australia. A more detailed description of the NAO, PNA, and SO teleconnections is presented below.

1. The North Atlantic Oscillation (NAO)

The first discussion of the NAO was by Walker and Bliss (1932) who noted that the oscillation “represents the distribution of temperature and pressure over a wide ocean area” (AMS, 2000; p. 549). The NAO is one of three teleconnections monitored by the CPC that is evident in all months of the year (Barnston and Livezey, 1987; Rogers, 1990; Portis et al., 2001). Wallace and Gutzler (1981) describe strong negative correlations between the NAO’s base points located at 40° N and 65° N over the Atlantic Ocean. The strength of the NAO does vary throughout the year (Figure 1.3). The NAO is strongest in January and weakest during October and November (Rogers, 1984, 1985; Hastenrath and Greischar, 2001). Additionally, over the last three decades, the NAO has shifted from mostly negative index values to mostly positive index values (Visbeck et al., 2001).

Based on temperature, a negative correlation exists between the severity of winter of the Greenland region versus the northwestern European region (Wallace and Gutzler, 1981). Secondly, there is a negative correlation in SLP across the Atlantic Ocean because the positive phase of the NAO is associated with a strong Icelandic low-pressure

system arou

Gutzler, 198

correlations

normal temp

region while

and the east

true during

the Azores I

system around 65° N and the Azores high-pressure system along 40° N (Wallace and Gutzler, 1981). Therefore, a strong, westerly flow results across the Atlantic. Negative correlations in temperature also exist during the positive phase of the NAO. Below-normal temperatures are found in the Greenland-Labrador region and Middle Eastern region while warmer-than-normal temperatures exist throughout northwestern Europe and the eastern United States (Wallace and Gutzler, 1981; Rogers, 1984). The opposite is true during the negative phase of the NAO since the Icelandic low-pressure system and the Azores high-pressure system are both weaker than normal.

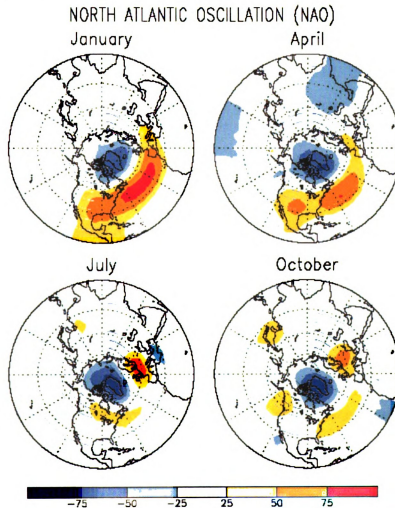


Figure 1.3. Geopotential height anomaly map in meters for the positive phase of the North Atlantic Oscillation (from the CPC, 2002a).

The PN
mid-Pacific to
Hawaii (20° N)
and the southeast
intermonthly and
the positive and
moderate values
phase. However
negative phase

The p
system. A s
results in wa
over the eas
The negativ
and a zonal
al. correlate
divisions fo
correlations
anomalies in
United State
correlations

2. The Pacific/North American Index (PNA)

The PNA teleconnection is associated with four base points spanning from the mid-Pacific to the eastern United States (Figure 1.4). The base points are located near Hawaii (20° N, 160° W), the north Pacific (45° N, 165° W), Alberta (55° N, 115° W), and the southeastern United States (30° N, 85° W). The PNA signal is evident on both intermonthly and interannual time scales (Esbensen, 1984). Dole (1986) describes that the positive and negative phases of the PNA are not symmetrical in occurrence. Low to moderate values of the positive phase occur more frequently than those for the negative phase. However, for large anomalies in the PNA values, the opposite is the case, with the negative phase occurring more frequently.

The positive phase of the PNA is associated with a strong Aleutian low-pressure system. A strong ridge over the western United States and Canada is also present, which results in warmer-than-normal temperatures in that region. Additionally, a strong trough over the eastern United States results in cooler-than-normal temperatures in that area. The negative phase of the PNA is associated with a weaker Aleutian low-pressure system and a zonal (west to east) 500 hPa height field (Wallace and Gutzler, 1981). Leathers et al. correlated “monthly mean temperature and precipitation values for all 344 climatic divisions for the period 1895 to 1983” with PNA index values (1991; p. 519). Strong correlations with temperature were discovered. In particular, during winter, warm anomalies in the Pacific Northwest and cold outbreaks throughout the southeastern United States were common during the positive phase of the PNA. The temperature correlations also agree with a study of citrus freezes within the southeastern United States

by Rohli and R
were also prese
(Leathers et al.
those for temp
States and sout
situation occur

by Rohli and Rogers (1993). Increases in precipitation across the eastern United States were also present during the negative phase of the PNA when zonal flow was evident (Leathers et al., 1991). However, the correlations with precipitation were not as strong as those for temperature. Increased precipitation was evident in the southwestern United States and southern plains during the positive phase of the PNA when a split-flow situation occurred (Leathers et al., 1991).

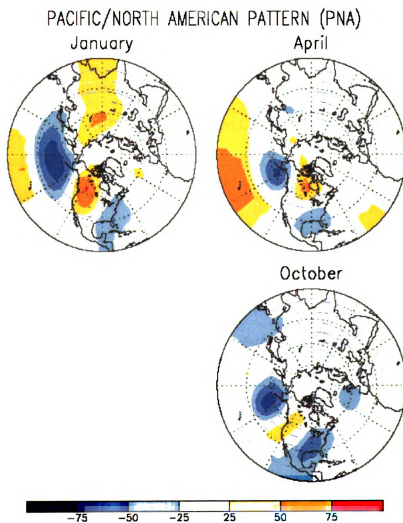


Figure 1.4. Geopotential height anomaly map in meters for the positive phase of the Pacific/North American teleconnection (from the CPC, 2002b).

The SO
Hildebrandsson
using a different
mentioned earl
Darwin, Austral
are commonly
spatial scale of
name may sugge
Pacific. Ocean
with the SO (B
SO is more evi

The SO
scale with an o
cold events of
tends to occur
2001). Addition
the PNA over t
negative SO ev
Janowiak, 1999,
and negative (E
March.

3. The Southern Oscillation (SO)

The SO has been one of the most studied teleconnections since its introduction by **Hildebrandsson** in 1897. The Southern Oscillation Index (SOI) is usually calculated **using** a different method other than the correlation or principle component methods **mentioned** earlier. Typically, the SOI is simply the difference in SLP between Tahiti and **Darwin**, Australia. The index values are then standardized. Positive values of the SOI **are** commonly referred to as “La Niña” and negative SOI values as “El Niño.” The **spatial** scale of the SO is very large and is not confined to the Southern Hemisphere as its **name** may suggest (Barry and Carleton, 2001). The SO is strongly related to SST in the **Pacific**. Ocean waters off the coast of Ecuador and Peru have the strongest relationship **with** the SO (Barry and Carleton, 2001). Mo and Livezey (1986) also discovered that the **SO is** more evident at the 700 hPa level than the 500 hPa level.

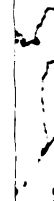
The SO is usually described as a fluctuation on an interannual to interdecadal **scale** with an oscillation of two to seven years (Trenberth and Hurrell, 1994). Warm and **cold events** of the SO tend to be in phase with the annual cycle since onset of these events **tends to** occur between March and June and lasts at least a year (Barry and Carleton, 2001). Additionally, since the SO is located over the Pacific region, the SO is linked to the **PNA** over time (Esbensen, 1984). Generally, the PNA is in a positive phase during **negative** SO events and in a negative phase during positive SO events (Bell and Janowiak, 1995; Barry and Carleton, 2001). Figure 1.5 illustrates the positive (La Niña) and **negative** (El Niño) phases associated with the SO cycle during January through **March**.

EL



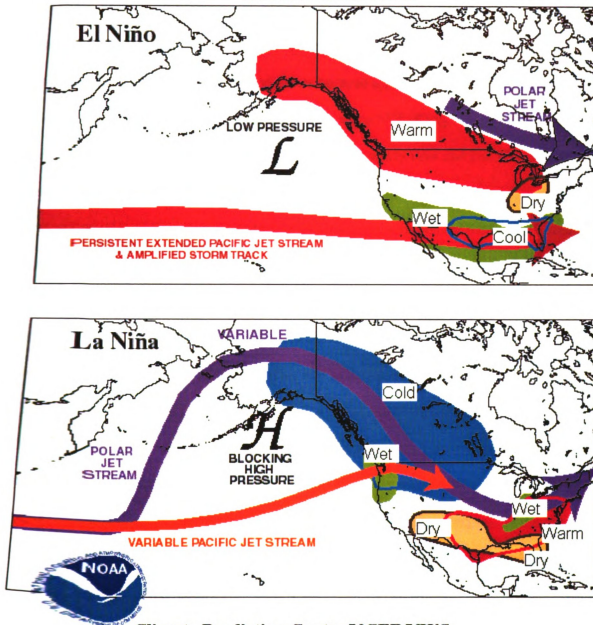
PET

L



Fig

**TYPICAL JANUARY-MARCH WEATHER ANOMALIES
AND ATMOSPHERIC CIRCULATION
DURING MODERATE TO STRONG
EL NIÑO & LA NIÑA**



Climate Prediction Center/NCEP/NWS

Figure 1.5. Typical January-March weather anomalies and atmospheric circulation during moderate to strong el Niño and la Niña (from the CPC, 2002c).

Over t

anomalous w

(2001a, 2001b)

years of 1871

anomalies with

for increased

Additionally,

present. An i

interannual va

States (Hu and

flow toward th

located over th

2000; Bradbu

Midwest (Kur

relationship b

the western N

negative SO y

tropical cyclon

(Barry and Car

The pos

normal tempera

Over the last 125 years, previous studies have attempted to link the SO to anomalous weather situations within the central United States. A study by Hu and Feng (2001a, 2001b) discovered a connection between precipitation and the SO during the years of 1871-1916 and 1948-1978. The study correlated SST anomalies with rainfall anomalies within the central United States because the convergence of moisture needed for increased precipitation tends to be dependent on SST (Barry and Carleton, 2001). Additionally, a relationship between low-level, southerly flow and the SO cycle is present. An increase in low-level, southerly flow from the Gulf of Mexico has significant interannual variations corresponding to increases in the rainfall of the central United States (Hu and Feng, 2001b). Dry years also correspond to strong anomalies of northerly flow toward the Gulf. During the positive phase of the SO (La Niña), lower pressure is located over the central section of the continent (Rogers, 1984; Trenberth and Caron, 2000; Bradbury et al., 2003), which can lead to increased precipitation throughout the Midwest (Kunkel and Angel, 1999; Bradbury et al., 2003). Past research has also noted a relationship between the negative phase of the SO (El Niño) and tropical cyclones within the western North Atlantic-Caribbean Sea region (Gray and Sheaffer, 1991). During negative SO years spanning 1900-1988, there was a significant decrease in the number of tropical cyclones at 5.4 events versus an average of 9.1 events in positive SO years (Barry and Carleton, 2001).

4. Teleconnection Association with the Midwest

The positive phase of the NAO teleconnection is associated with warmer-than-normal temperatures throughout the eastern United States, and the negative phase is

associated with

1984). However

NAO and prec

The po

United States a

resulting in coo

and Rogers, 19

negative phase

and precipitati

the positive ph

Serreze et al. (

general, posit

Valley in win

related to the

235).

The S

southerly flo

CPC, 2002c).

warmer temp

(Changnon et

are associated

Niña), the opp

spring, while

associated with cooler-than-normal temperatures (Wallace and Gutzler, 1981; Rogers, 1984). However, previous literature does not present a strong relationship between the NAO and precipitation in the Midwest (Wallace and Gutzler, 1981; Rogers, 1984).

The positive phase of the PNA is associated with a strong ridge over the western United States and Canada. A strong trough over the eastern United States is also present resulting in cooler-than-normal temperatures in the Midwest (Leathers et al., 1991; Rohli and Rogers, 1993). Zonal flow resulting in mild temperatures is associated with the negative phase of the PNA (Wallace and Gutzler, 1981). Relationships between the PNA and precipitation are not as strong. However, increases in precipitation can occur during the positive phase of the PNA when a split-flow pattern is present (Leathers et al., 1991). Serreze et al. (1998) also state that, “precipitation anomalies are less coherent, but, in general, positive PNA events tend to be associated with reduced precipitation in the Ohio Valley in winter. Assel (1992) supports that both air temperatures and ice cover are related to the PNA pattern but finds no association with snowfall” (Serreze et al., 1998; p. 235).

The SO cycle tends to be related to an increase in the amount of low-level, southerly flow into the Midwest (Barry and Carleton, 2001; Hu and Feng, 2001a, 2001b; CPC, 2002c). Negative values of the SO (El Niño) are associated with zonal flow, warmer temperatures, and drier conditions during the winter and spring seasons (Changnon et al., 2000). However, negative SO values during the summer and autumn are associated with cooler and drier conditions. During the positive phase of the SO (La Niña), the opposite is the case. Cooler and wetter conditions are present in the winter and spring, while warmer and wetter conditions are present in the summer and autumn.

However, the p

temperature an

Midwest than

Other r

Midwest. Ho

literature, wh

climate is not

when two or m

association of

some preliminar

literature.

3. Objectives

The th

developed by

years) and wi

climatology v

regions for th

Waller's earl

climatologies

study, the traj

teleconnection

temperature an

However, the primary SO association has more of a northwest to southeast opposition in temperature and precipitation over the continent. Therefore, the SO may less affect the Midwest than other sections of the United States (Rogers, 1984).

Other teleconnections exist that may be associated with the climate of the Midwest. However, those teleconnections have not been as largely discussed in past literature, which suggests that the association of those teleconnections with midwestern climate is not as strong. It is also possible that the association of a teleconnection differs when two or more teleconnections are simultaneously present. However, the combined association of teleconnection patterns with local climate has not been studied, except for some preliminary work by McGinnis (2001) that has not yet appeared in the refereed literature.

3. Objectives and Research Questions

The thesis has two parts. In the first part, the earlier trajectory climatology developed by Waller (1999) is updated using a longer time period (40 years versus 10 years) and wind data at higher spatial and temporal resolutions. The updated trajectory climatology will hopefully better represent the monthly variations in the air-mass source regions for the upper Midwest. Also, a comparison of the improved climatology with Waller's earlier climatology will provide some insights on the sensitivity of trajectory climatologies to differences in resolution and record length. In the second part of the study, the trajectory climatology is used to study the relationships between atmospheric teleconnection patterns, air-parcel trajectories, and local-scale climate anomalies of temperature and precipitation. Previous studies of the relationship between atmospheric

teleconne

temperatu

investiga

airflow tr

better un

and low-l

forecastin

(1) Based

what are

(2) How c

previousl

period, an

(3) Does t

circulatio

teleconne

(4) During

relationsh

local-scale

teleconnection patterns and local-scale and/or regional-scale climate have focused on temperature and precipitation anomalies. This study goes one step further, by investigating the low-level circulation associated with these anomalies. The focus on airflow trajectories contributes to the uniqueness and significance of the study. Also, a better understanding of the relationship between planetary-scale teleconnection patterns and low-level airflow trajectories can be an excellent tool for long-range weather forecasting. The following research questions will be addressed in this study:

(1) Based on an isobaric trajectory model using the NCEP/NCAR reanalysis wind data, what are the major airflow source regions and how do they vary by month?

(2) How does the trajectory climatology presented here differ from the climatology previously presented by Waller (1999), which used a different data source, a shorter time period, and a location in northwest Ohio (41.56° N, 84.09° W)?

(3) Does the low-level circulation, as depicted by back trajectories, differ from the mean circulation in the upper Midwest during months of strong, singly or co-existing teleconnection patterns?

(4) During months of anomalous circulation associated with teleconnections, can relationships be drawn between the trajectory patterns and trajectory frequencies with local-scale climate, as depicted by temperature and precipitation anomalies?

(5) Does the a

and local-scu

The ra

conducted on

considered po

United States

and the local-s

trajectories w

associated wit

Influences on t

teleconnection

air-parcel traje

moisture origin

medium-range

4. Organizatio

Chapte

calculating the

(3) preparing th

patterns, and (5

teleconnection

trajectories are

(5) Does the association of single or co-existing teleconnections with airflow trajectories and local-scale temperature and precipitation vary by season?

The rationale for the current project is relatively simple. Previous research conducted on atmospheric teleconnections has been incomplete. Many projects have considered possible relationships between teleconnections and anomalous climate of the United States. However, the link between the planetary-scale teleconnection phenomena and the local-scale climate has not been adequately described. The use of low-level trajectories will provide a better description of the synoptic and mesoscale circulations associated with teleconnection events that have been missing from previous studies. Influences on temperature and precipitation can be better explained by the dynamics of teleconnections. By gaining a better understanding of teleconnection association with air-parcel trajectories, source regions can be identified where advection of heat and moisture originate. As patterns of advection are linked to teleconnections, better medium-range and long-range climate forecasts can be performed for the upper Midwest.

4. Organization of Thesis

Chapter 2 describes the data used in the study and the methodologies for (1) calculating the air-parcel trajectories, (2) deriving the monthly trajectory climatologies, (3) preparing the GIS displays, (4) relating the airflow trajectories and teleconnection patterns, and (5) estimating the temperature and precipitation anomalies for different teleconnection conditions. In Chapter 3, the monthly climatological patterns of airflow trajectories are described and compared to the earlier climatology prepared by Waller

(1999). T

combinatio

the results

the study a

summarize

(1999). The differences in airflow trajectories and air-mass source regions for different combinations of teleconnection patterns are discussed in Chapter 4. Lastly, in Chapter 5, the results of the study are placed in the context of previous research; the limitations of the study and recommendations for further work are discussed; and the major findings are summarized.

1. Overview

As me
between atm
describes the
results. Figur
trajectory clim
teleconnection
follow each o

NMC data
1.1.a.3

NCEP NCA
2.2

Base map
2.5.a

CHAPTER 2

DATA AND METHODOLOGY

1. Overview

As mentioned in the previous sections, the project investigates the relationship between atmospheric teleconnections and low-level, air-parcel trajectories. Chapter 2 describes the data and methods used to perform the research project and display the results. Figure 2.1 is a flow chart that summarizes the steps needed to carry out the trajectory climatology and Figure 2.2 is a flow chart that summarizes the atmospheric teleconnection analysis of this study. The corresponding chapter and section numbers follow each of the steps of the flowcharts.

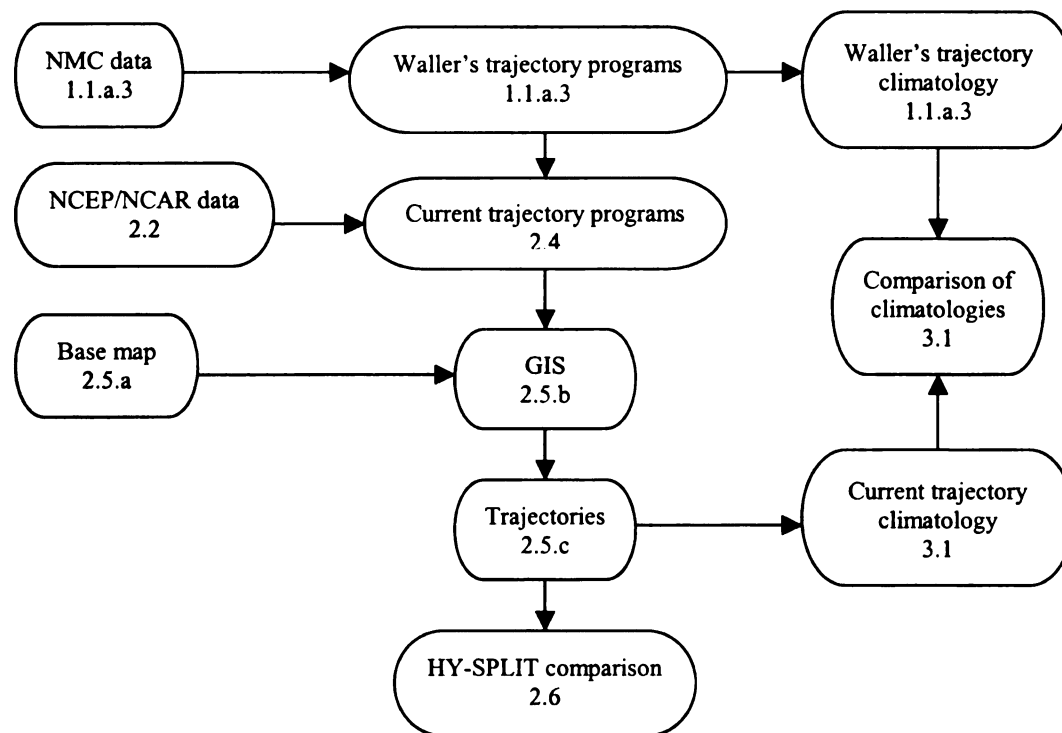


Figure 2.1. Summary of steps to perform the trajectory climatology.

CPC tel

CDC r
and pr

Figure

2. Wind

TI

Centers for

Research

reanalysis

data assim

The wind

Comprehe

synoptic d

wind speed

T62 28-le

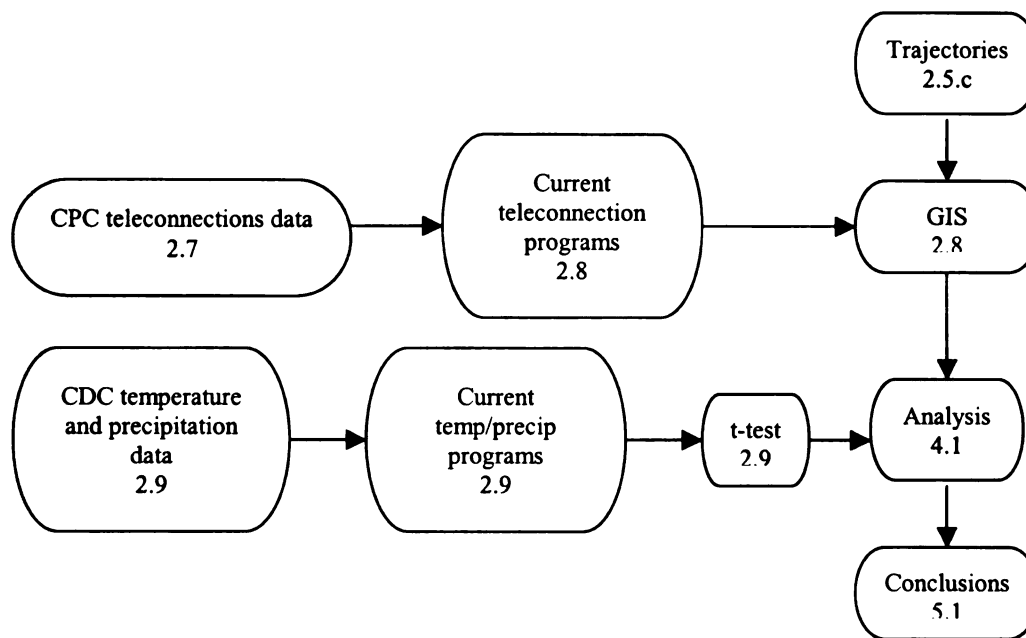


Figure 2.2. Summary of steps to perform the atmospheric teleconnection analysis.

2. Wind Data from the NCEP/NCAR Reanalysis

The data used to calculate air-parcel trajectories were obtained from the National Centers for Environmental Prediction (NCEP) and the National Center for Atmospheric Research (NCAR) reanalysis archive. According to Kalnay et al., “the basic idea of the reanalysis project is to use a frozen state-of-the-art analysis/forecast system and perform data assimilation using past data, from [1948] to the present (reanalysis)” (1996, p. 438). The wind data used in the reanalysis were obtained from global rawinsonde data, the Comprehensive Ocean-Atmosphere Data Set (COADS), aircraft data, surface land synoptic data, satellite sounder data, Special Sensing Microwave/Imager (SSM/I) surface wind speed data, and satellite cloud drift winds. The collected data were then put into a T62/28-level global spectral model, which initially computes data for 28 sigma levels at a

spatial re

following

50, 30, 2

90° S) an

An impo

Howeve

levels su

insertin

values a

variable

heavily

only tal

1800 ar

The u a

B varia

are not

T62 mo

model.

1996).

1200, a

collecte

spatial resolution of 208 km (Jenne, 2001). The data were then interpolated to the following 17 pressure levels: 1000, 925, 850, 700, 500, 400, 300, 250, 200, 150, 100, 70, 50, 30, 20, 10, and 3 hPa. The data are in a 2.5° by 2.5° grid format of 73 rows (90° N-90° S) and 144 columns (0° E-357.5° E) that span the entire globe (Kalnay et al., 1996). An important benefit of the NCEP/NCAR reanalysis is that no “missing” data exist. However, some pressure levels may intersect the topography. In mountainous regions, levels such as 1000, 925, and 850 hPa frequently intersect the surface. Rather than inserting “missing” values into the reanalysis, the convention is to substitute the wind values at the surface for the “missing” levels.

Output variables from the T62 model are categorized as Type A, B, C or D variables (Kalnay et al., 1996). Type A variables are the most reliable because they are heavily dependent upon observed data. However, upper-air observations are typically only taken twice a day at 0000 and 1200 UTC, so even Type A variables at the 0600 and 1800 are “model generated” since the reanalysis fields are provided four times per day. The u and v wind components used in this study are considered Type A variables. Type B variables are influenced by both the observations and the T62 model. Type C variables are not directly influenced by observational data and thus are primarily dependent on the T62 model. Lastly, Type D variables are not dependent on either observations or the T62 model. Rather, Type D variables are fixed from climatological values (Kalnay et al., 1996).

The reanalysis wind fields are provided for the six-hourly intervals of 0000, 0600, 1200, and 1800 UTC. However, upper-air data from January 1948 to June 1957 were collected three hours later at 0300 and 1500 UTC compared to the 0000 and 1200 UTC

observation

0000, 0600

this study

to use a c

files by y

Climate I

large at a

"readgen

2003b).

section 1

day, and

wind co

section

3. Stud

145° W

trajecto

Michiga

calculat

because

Figure 2

midwest

observation times used today (Kistler et al., 2001). Model simulations were run to obtain 0000, 0600, 1200, and 1800 UTC data for the time period prior to June 1957. However, this study used a 40-year time period of January 1, 1960 to December 31, 1999 in order to use a consistent study period. The u and v wind components are provided in separate files by year. These files, which are in netCDF format, were downloaded from the Climate Diagnostics Center (CDC) website (CDC, 2003a). The netCDF files were quite large at approximately 521 megabytes per file. A FORTRAN program titled “readgeneral.f” is available on the web to convert netCDF files to ASCII format (CDC, 2003b). Additional information needed to use the program is included in Appendix A, section 1. The grid point values for the u and v wind components, location, year, month, day, and hour were extracted for the study region using the program. Because the u and v wind components are in separate files, another FORTRAN program (see Appendix A, section 2) was used to merge the two files.

3. Study Location

The study used a subset of the reanalysis grid bounded by 10° to 85° N and 60° to 145° W, which spans North America (Figure 2.3). The terminus point for the back-trajectory calculation is the reanalysis grid point located in the central region of Michigan’s lower peninsula (42.5° N, 85.0° W). Even though trajectories can be calculated for any number of grid points, a single point was selected for this study because of the time-consuming analysis. The terminus point is highlighted in red on Figure 2.3, and is believed to be a good representation of the general airflow for the midwestern United States. This region experiences large interannual variations in

temperature and precipitation in association with airflow from multiple source regions.

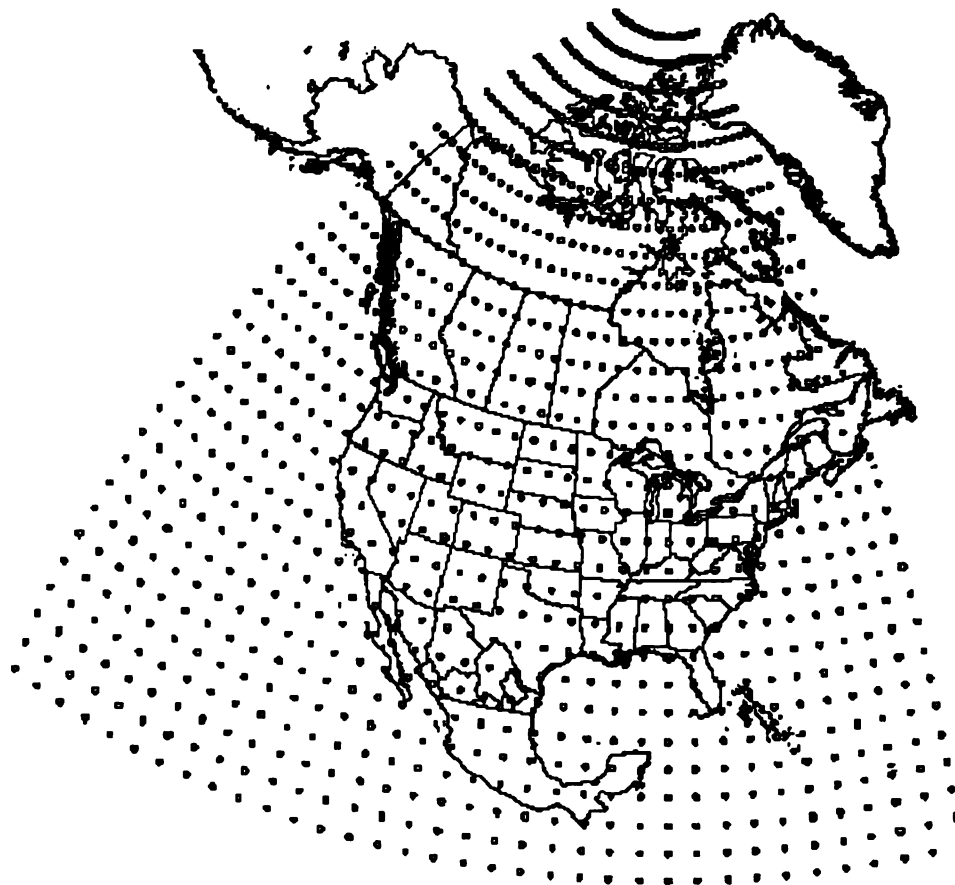


Figure 2.3. Map of the data grid (10° to 85° N and 60° to 145° W).

4. Algorithm for the Trajectory Analysis

An isobaric trajectory model similar to the one used by Scott and Achtemeier (1987) and Waller (1999) was implemented. As previously described, the isobaric model calculates trajectories along a surface of constant pressure (Haagenson et al., 1987). An isobaric model was selected because it is the least data-intensive of the trajectory models. Isobaric models only require data for the u and v wind components at the selected pressure level. Past research has shown isobaric models to perform well under long-term,

steady-s

and Seib

the goa

SO tele

minim

level i

Howe

regio

that c

the N

terra

track

five

85.0

resu

erro

day

time

ava

hour

perfo

steady-state conditions or in situations when only the horizontal position is desired (Stohl and Seibert, 1998).

Trajectories were calculated for the 925 hPa level. The level was chosen because the goal of this study is to relate variations in low-level airflow to the NAO, PNA, and SO teleconnections. Additionally, a previous study confirmed that trajectory error is minimized for isobaric models at lower levels (Haagenson et al., 1987). The 925 hPa level is close to the surface, but does not intersect the surface within the Midwest region. However, air parcels are tracked backwards in time. The parcel locations may fall within regions such as the Rocky Mountains, where the 925 hPa level intersects the ground. In that case, trajectories are terrain following because the surface wind values are used in the NCEP/NCAR reanalysis data for situations when the pressure level is below the terrain surface.

Back trajectories were calculated for five-day periods, so that air parcels could be tracked to their source region. With a westerly flow, an air parcel takes approximately five days to travel across the United States and pass through the terminus point (42.5° N, 85.0° W) (Waller, 1999). Using a shorter time period may limit the interpretation of results. Extending the time period beyond five days is not beneficial since trajectory error increases with increasing time. Back trajectories were calculated four times each day at 0000, 0600, 1200, and 1800 UTC. The trajectories were calculated in three-hour time steps in order to increase the temporal resolution. Since the reanalysis data are only available every six hours, simple interpolations were performed for the intervening three-hour positions (i.e. 0300, 0900, 1500, and 2100 UTC). The interpolations were performed by averaging the wind values from the previous times and the following times.

For examp

for 0900 U

maximum

A I

back-trajec

program ca

revisions v

determined

year, mont

atmospher

data, and ti

to see if th

example, i

program w

first backw

also consic

isobaric m

Step 1. Th

calculated

distance fr

east west d

of 111 km

For example, the 0600 and 1200 UTC wind values were averaged to achieve a wind value for 0900 UTC. The three-hour positions are referred to as “nodes.” Therefore, a maximum of 40 nodes were possible per five-day back trajectory.

A FORTRAN program for the isobaric model was used to perform the five-day back-trajectory calculations (see Appendix A, section 3). The template of code for this program came from software previously developed by Waller (1999). However, many revisions were required because different data sets were used. The program first determined the latitude/longitude values for each point. A prompt to input the desired year, month, terminus grid point, the number of three-hour time steps, and the desired atmospheric level was given. The program then searched to find the grid point, wind data, and time. Since the trajectories were calculated back in time, checks were included to see if the program should read from the previous time, day, month, or year. For example, if the starting time of the trajectory was 0000 UTC on January 1, 1999, the program would need to read data from 1800 UTC December 31, 1998 to calculate the first backward node at 2100 UTC. Whether or not the current year was a leap year was also considered. Steps one through seven describe further tasks carried out by the isobaric model.

Step 1. The first estimate of the previous three-hour location 2' (Figure 2.4) was calculated based on the u and v wind component data from the terminus grid point. The distance from point 1 to point 2' was found as DISu and DISv, where DISu is the east/west distance and DISv is the north/south distance in kilometers. An approximation of 111 km per degree latitude was used (Robinson et al., 1978; Dent, 1999). The number

of kilomet

(Waller, 1

(2.1) ne

(2.2) ter

(2.3) de

(2.4) ne

Step 2. Lo

and 60° to

grid points

FORTRA.

Figure 2.4
new three-
location;

of kilometers per degree longitude was determined from the cosine of the latitude (Waller, 1999).

$$(2.1) \quad \text{new_latitude} = \text{original_latitude} - (\text{DISv} / (111 \text{ km} / \text{degree}))$$

$$(2.2) \quad \text{temp_latitude} = \text{new_latitude} * (0.01745329 \text{ radians} / \text{degree})$$

$$(2.3) \quad \text{degrees_longitude} = \cos (\text{temp_latitude}) * (111 \text{ km} / \text{degree})$$

$$(2.4) \quad \text{new_longitude} = \text{original_longitude} + (\text{DISu} / \text{degrees_longitude})$$

Step 2. Location 2' was then checked to see if it fell outside the domain of 10° to 85° N and 60° to 145° W. If so, the remainder of the trajectory was terminated. If not, the four grid points (a, b, c, d) surrounding the current location 2' were identified using a FORTRAN subroutine (Waller, 1999).

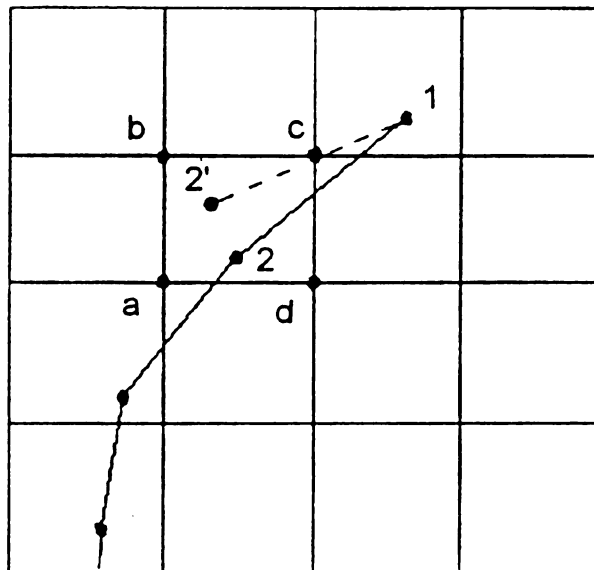


Figure 2.4. The trajectory calculation, where point 1 is starting location; point 2' is the new three-hour node location after the calculation; point 2 is the revised three-hour node location; and points a, b, c, and d are the surrounding grid point values (from Waller, 1999; p. 55).

Step 3. T

longitude

$$(2.5) \quad x$$

$$(2.6) \quad x$$

Step 4. T

(Figure 2

interpolat

from the

Step 5. T

Where p

$$(2.7) \quad p$$

$$(2.8) \quad q$$

and u_a, u_b

points a, b

right of the

Step 3. The grid location of point 2' (xi, xj) was defined in terms of its latitude and longitude using the following linear equations:

$$(2.5) \quad x_i = ((-.4) * \text{new_latitude}) + 37$$

$$(2.6) \quad x_j = ((-.4) * \text{new_longitude}) + 145$$

Step 4. The u and v wind component values were extracted for points a, b, c, and d (Figure 2.4) using another subroutine. After that, a bi-linear interpolation was used to interpolate the u and v wind component values for the new trajectory node location 2' from the four surrounding grid points.

Step 5. The equations used to compute u and v at point 2' are the following:

Where p and q are:

$$(2.7) \quad p = x_i - \text{aint} (x_i)$$

$$(2.8) \quad q = x_j - \text{aint} (x_j)$$

and ua, ub, uc, ud, va, vb, vc, and vd represent the u and v wind component values for points a, b, c, d (Figure 2.4). The use of “aint” in FORTRAN removes everything to the right of the decimal point.

(2.9)

(2.10) v

Step 6. .

trajectory

assumed

averaged

modified

through t

2.4. Poin

starting p

Step 7. O

back traje

trajectory

$$\begin{aligned}
 (2.9) \quad u = & ua * p * (1 - q) \\
 & + ub * (1 - p) * (1 - q) \\
 & + uc * (1 - p) * q \\
 & + ud * p * q
 \end{aligned}$$

$$\begin{aligned}
 (2.10) \quad v = & va * p * (1 - q) \\
 & + vb * (1 - p) * (1 - q) \\
 & + vc * (1 - p) * q \\
 & + vd * p * q
 \end{aligned}$$

Step 6. At this point, values of the u and v wind components exist for the current trajectory node 2' (Figure 2.4). However, it is debatable that the wind speed can be assumed to be constant over three hours. To account for this, the 2' wind values were averaged with the original wind values of the terminus grid point. The result is a modified u and v wind component value for the current trajectory node. Steps one through five were repeated to update location and wind values for point 2' from Figure 2.4. Point 2 was the resulting trajectory node after the update. Point 2 then became the starting point (or the new point 1) for the next back-trajectory calculation of the program.

Step 7. Once the back trajectory was complete, the time step incremented and a five-day back trajectory was calculated for the next six-hour time period. At this point, the back-trajectory nodes were in separate files by year and month. Another FORTRAN program

(see App

data sets

5. Geog

A

trajectory

ERDAS

describe

o

A

A

World w

shapefil

within A

Imagine

A

7

summar

(see Appendix A, section 4) was used to combine all of the years for each month (i.e. all data sets from January in the years 1960-1999), for a total of 12 back-trajectory files.

5. Geographic Information System Analysis

A geographic information system (GIS) was used to display the results of the trajectory climatology. The GIS and remote sensing tools ArcView, ArcInfo, and ERDAS Imagine were used to accomplish these tasks. The following sections will describe the steps of the GIS display and analysis.

a. Obtaining the Base Map

A base map of North America was downloaded from the Digital Chart of the World website (1992). Each state and country file was downloaded separately in shapefile format. The files were uncompressed and then converted to a coverage format within ArcInfo. The coverages were then combined into a single coverage using ERDAS Imagine.

b. Converting the Back Trajectories to a Coverage Format

The steps to convert the back-trajectory text files to a coverage format are summarized in Table 2.1.

Tab

Open ArcV
Select "tab
Select the
Go to "vie
The table v
Select this
Go to "the
The file ca
using the "

c. Pro

At thi

geographic (1

account wher

direction of tr

important. S

To make the t

dimension an

150 columns.

higher spatia

trajectory cal

Lambert-Azin

being true wi

(42.5° N, 85.0

grids were pro

point, the loca

Table 2.1. Steps to convert the back trajectories to a coverage format.

Open ArcView
Select “table” within ArcView and then add a desired trajectory text file
Select the view window
Go to “view” and select “add event theme”
The table will be plotted in the viewer window
Select this theme within the window
Go to “theme” and select “convert to shapefile” to change the format of the file
The file can then be imported in ERDAS Imagine and converted to a coverage by using the “import” option and then selecting “shapefile”

c. Projecting to the Lambert-Azimuthal Equal-Area Projection

At this point in the study, both the base map and the trajectory data were still in a geographic (i.e. latitude/longitude) map projection. Two considerations were taken into account when choosing the map projection for displaying the results. First, the true direction of trajectories with respect to the terminus point (42.5° N, 85.0° W) was very important. Second, a raster-grid format was chosen to display the trajectory densities. To make the trajectory display effective, it was important that the grid cells were of equal dimension after the projection. The chosen grid size was 50 km by 50 km (160 rows by 150 columns, which is less than 0.5° by 0.5° used by Waller (1999)), and has a much higher spatial resolution than the original 2.5° by 2.5° reanalysis grid used in the trajectory calculations. Both direction and grid size were conserved with the use of a Lambert-Azimuthal Equal-Area projection. Conservation of direction refers to direction being true with respect to the center point, which, in this case, was the terminus point (42.5° N, 85.0° W). The trajectory nodes were re-projected using ArcInfo, and the raster grids were projected using ERDAS Imagine (see Appendix B, sections 1 and 2). At this point, the locations of the trajectory nodes needed to be expressed in meters from the

terminus point (see Appendix B, section 3). A FORTRAN program was then used to count the number of trajectory nodes per grid cell (see Appendix A, section 5).

6. Isobaric Trajectories Compared to HY-SPLIT Trajectories

The isobaric trajectories were validated against trajectories calculated using the Hybrid Single-Particle Lagrangian Integrated Trajectory (HY-SPLIT) model (Draxler 1996, 1999; Draxler and Hess, 1998a, 1998b). As mentioned in Chapter 1, HY-SPLIT is one of the most widely used trajectory models (Clark and Cohn, 1990; Rolph et al., 1992; Saxena et al., 1996; Stein et al., 2000; Stein and Lamb, 2000). The intent of the validation was to estimate whether the back trajectories calculated using the simpler isobaric trajectory model differed substantially from those calculated using the more complex HY-SPLIT model. Back trajectories for the 0000 UTC time period for 1999 from the two models were compared using a GIS. The steps to obtain the comparison image were:

Step 1. Table 2.2 lists the steps that were performed to calculate HY-SPLIT trajectories.

Registered
Resources
Went to ht
Used the tr
Specified t
"REANAL
An archive
file needed
computed.
The next p
computation
The user w
A backwar
The desired
The total r
Height abo
trajectory r
Once the m
of the spec
"Trajectory
The text fil
The proces

Step 2. A FO
output text fil
data were ori
Only nodes f
step for the is
the 10° to 85°
program (see

Step 3. Steps
HY-SPLIT m

Table 2.2. Steps to compute a HY-SPLIT trajectory.

Registered with the National Oceanic and Atmospheric Administration (NOAA) Air Resources Laboratory to receive a username and password
Went to http://www.arl.noaa.gov/ready/hysplit4.html and logged on
Used the trajectory model and selected “compute trajectories”
Specified the correct data set under “ARCHIVED DATA,” in this case was “REANALYSIS 1996-Aug 2001”
An archive file list was displayed and the appropriate year (1999) and month (1-12) file needed to be selected one at a time until the entire time period had been computed.
The next page asked the user for the desired trajectory terminus point for the computation, which was 42.5° latitude and -85.0° longitude
The user was then prompted for all the desired criteria for the trajectory calculation.
A backward trajectory for the vertical velocity model was selected
The desired year, month, day, and hour were then selected
The total run time was chosen to be 120 hours, which is equal to five days.
Height above the ground was chosen to be 500 m to resemble the 925 hPa isobaric trajectory model (Committee on Extension to the Standard Atmosphere, 1962)
Once the model was run, the user selected “Your Trajectory Plot” to see the image of the specified trajectory
“Trajectory endpoints file” contained the trajectory data as hourly nodes
The text file was then saved in text format for later use in a UNIX environment
The process was repeated at 0000 UTC for all 365 days of the year 1999

Step 2. A FORTRAN program (see Appendix A, section 6) wrote out the HY-SPLIT output text files in the same format as the previously calculated isobaric trajectories. The data were originally in daily files and as noted in the table, had values for hourly nodes. Only nodes for every three hours were extracted in order to be consistent with the time step for the isobaric trajectories. HY-SPLIT trajectory nodes that were located outside of the 10° to 85° N and 60° to 145° W domain were also removed by another FORTRAN program (see Appendix A, section 7).

Step 3. Steps b and c, described under section 5 of this chapter, were repeated for the HY-SPLIT model data and the isobaric model data to obtain a comparison image.

Another l

the node

each grid

comparis

cases wer

used here

dimension

TH

how much

red grid c

trajectory

SPLIT tra

the image

a large nu

southerly

farther we

trajectory

continent.

which is e

Another FORTRAN program (see Appendix A, section 9) simply took the difference in the node total of the HY-SPLIT trajectory model and the isobaric trajectory model for each grid cell to arrive at a new value for each grid cell. The HY-SPLIT and isobaric comparison was then displayed on one image (Figure 2.5). Additionally, three single cases were also included to show the differences between the isobaric trajectory model used here, the HY-SPLIT isobaric trajectory model, and the HY-SPLIT three-dimensional model (Figures 2.6, 2.7, and 2.8).

The colors of the grid cells on Figure 2.5 represent standard deviations in terms of how much the isobaric model differs from the HY-SPLIT model. Yellow, orange, and red grid cells represent areas where the isobaric trajectory model calculated higher trajectory node densities. Areas of cyan, blue, and purple represent areas where the HY-SPLIT trajectory model calculated higher trajectory node densities. In order to interpret the image and draw conclusions, it is best to look for areas of continuous color. There is a large number of blue grid cells in the southeastern part of the country. Therefore, for southerly trajectories, the isobaric trajectory model calculates trajectories originating farther westward with longer trajectories than the three-dimensional, HY-SPLIT trajectory model. Additionally, there are more red grid cells over the western part of the continent. However, in general, the isobaric and HY-SPLIT trajectories are similar, which is encouraging and gives credibility to the isobaric trajectory analysis of this study.

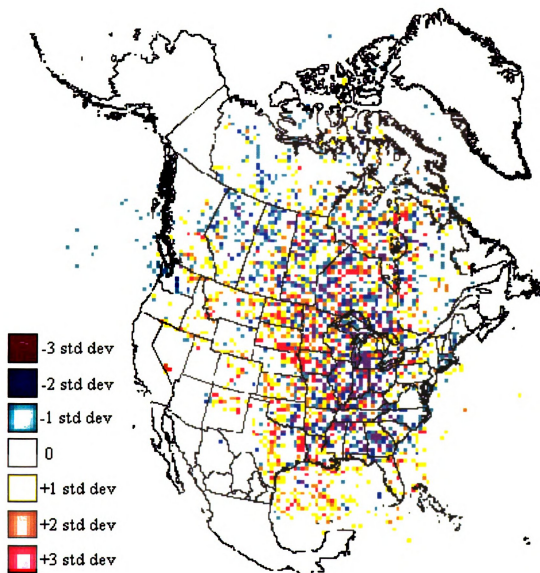


Figure 2.5. Results of the isobaric trajectory model and HY-SPLIT trajectory model comparison.

Figure

Figure

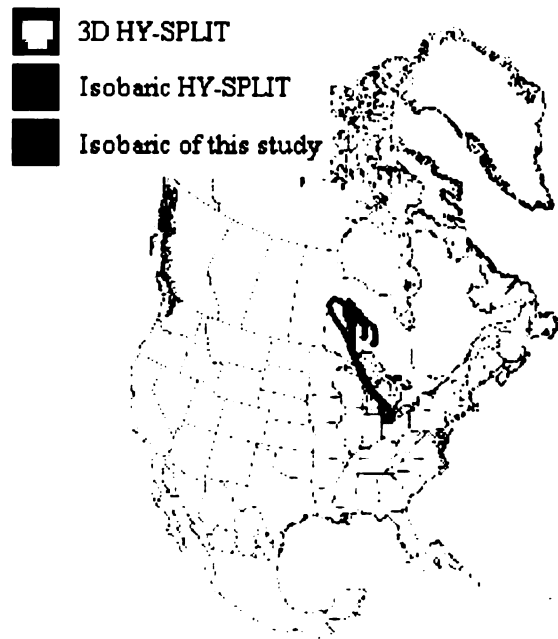


Figure 2.6. Isobaric and HY-SPLIT comparison for 0000 UTC July 1, 1999.

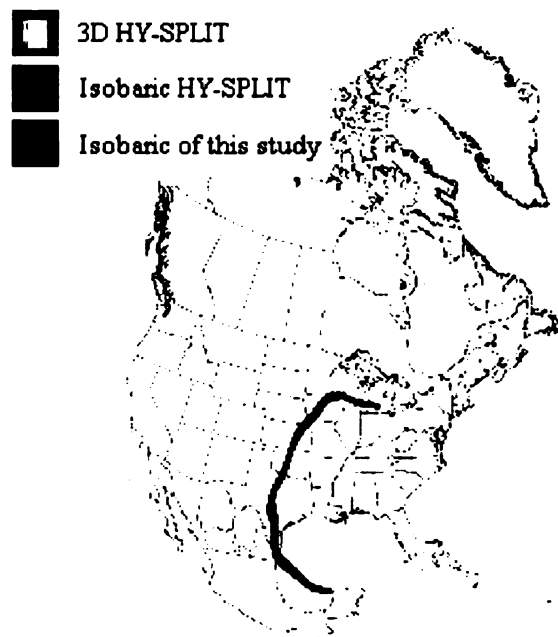


Figure 2.7. Isobaric and HY-SPLIT comparison for 0000 UTC August 1, 1999.

Figure 2

In a
were used to
Appendix A
1999, a total
distances a
for all time
in order to
distances a
positive va
west of the
distances g
are general

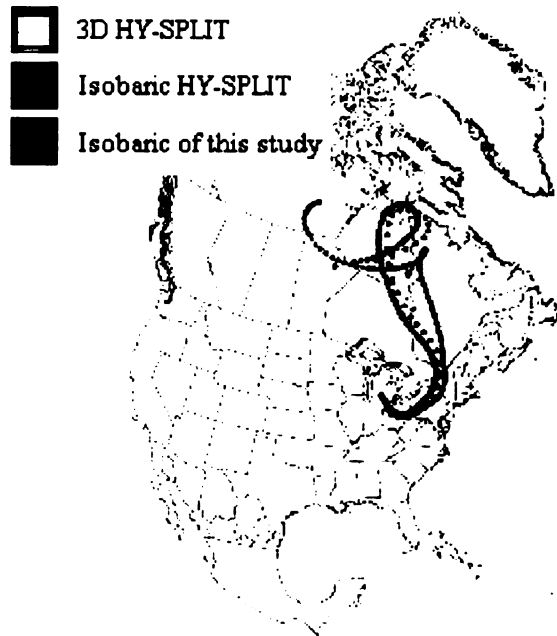


Figure 2.8. Isobaric and HY-SPLIT comparison for 0000 UTC September 1, 1999.

In an effort to quantify the isobaric and HY-SPLIT comparison, Equations 2.1-2.4 were used to solve for DIS_u and DIS_v for each of the 40 time steps of each trajectory (see Appendix A, section 8). Since the comparison is for one trajectory per day for the year of 1999, a total of 365 trajectories were compared. The average u , v , and hypotenuse distances are included in Table 2.3 for each time step. The final values are the average for all time steps. Table 2.4 is different in that it takes the sign of the values into account in order to display any possible bias in direction between the two models. The u distances are interesting in that they start out with negative values and then shift to positive values. This represents that the isobaric trajectories initially have a bias to the west of the HY-SPLIT trajectories, but then change to having a bias to the east. The v distances grow increasingly in the negative direction suggesting that isobaric trajectories are generally south of the HY-SPLIT trajectories.

Table 2.3. Average u, v, and hypotenuse distance in kilometers between the isobaric and HY-SPLIT model trajectory nodes at each of the 40 time steps.

Time Step	U distance	V distance	Hypotenuse
1	5.03	4.53	6.77
2	10.99	9.38	14.45
3	19.11	15.54	24.63
4	29.68	23.19	37.67
5	41.52	32.46	52.70
6	52.77	44.09	68.76
7	62.34	56.19	83.93
8	69.26	68.12	97.14
9	76.56	81.44	111.77
10	85.75	97.20	129.62
11	96.42	113.76	149.12
12	108.49	131.25	170.28
13	121.90	149.17	192.64
14	135.49	165.77	214.10
15	148.20	181.33	234.19
16	161.79	195.29	253.61
17	178.13	209.82	275.24
18	196.02	224.39	297.95
19	215.67	238.56	321.60
20	233.90	253.79	345.14
21	251.70	269.54	368.79
22	269.48	285.92	392.90
23	280.95	300.17	411.14
24	296.22	316.87	433.76
25	307.56	333.88	453.95
26	324.23	352.18	478.70
27	342.89	369.58	504.14
28	360.32	384.27	526.78
29	376.92	404.61	552.97
30	398.67	422.95	581.23
31	421.91	439.24	609.04
32	440.81	453.82	632.67
33	461.68	472.30	660.47
34	479.87	489.17	685.25
35	491.46	504.20	704.09
36	511.33	513.78	724.87
37	522.69	532.17	745.93
38	540.39	554.89	774.55
39	557.00	567.00	794.81
40	569.48	580.89	813.47
Average	251.81	266.55	366.68

Table 2.4. Average u, v, and hypotenuse distance in kilometers between the isobaric and HY-SPLIT model trajectory nodes at each of the 40 time steps. The sign is included to represent bias in direction.

Time Step	U distance	V distance	Hypotenuse
1	-3.68	-1.48	3.97
2	-8.75	-3.85	9.56
3	-15.13	-6.83	16.60
4	-22.33	-10.28	24.59
5	-29.21	-15.10	32.88
6	-34.87	-21.70	41.08
7	-38.72	-29.24	48.52
8	-40.63	-38.16	55.73
9	-41.31	-48.93	64.04
10	-41.75	-61.81	74.59
11	-41.69	-75.76	86.47
12	-40.59	-89.69	98.45
13	-38.76	-103.18	110.22
14	-35.89	-115.00	120.47
15	-32.05	-125.33	129.37
16	-27.72	-134.85	137.67
17	-23.20	-143.95	145.81
18	-18.89	-152.87	154.04
19	-13.28	-161.39	161.93
20	-6.27	-170.18	170.29
21	4.82	-178.04	178.11
22	16.76	-184.87	185.63
23	21.74	-188.86	190.11
24	31.74	-195.16	197.72
25	37.66	-202.37	205.85
26	46.71	-211.23	216.33
27	58.09	-220.31	227.84
28	75.85	-224.67	237.13
29	85.11	-233.44	248.47
30	103.65	-239.54	261.00
31	121.18	-246.45	274.63
32	131.08	-248.63	281.07
33	145.77	-255.06	293.78
34	151.80	-260.73	301.70
35	153.43	-264.89	306.12
36	163.28	-263.17	309.71
37	168.38	-271.33	319.33
38	178.72	-282.88	334.61
39	191.77	-274.10	334.52
40	189.81	-266.17	326.92
Average	35.86	-153.53	157.66

7. Atmospl

As s

indices. A

anomalies v

for each tel

(2001) exp

varimax re

The ampl

analysis.

a mean o

identified

teleconn

the CPC

-

different

between

be foun

in orde

CPC pr

7. Atmospheric Teleconnection Data

As discussed in Chapter 1, the CPC has calculated atmospheric teleconnection indices. A rotated principal components analysis of 700 hPa geopotential height anomalies was used to identify teleconnection patterns and to calculate monthly values for each teleconnection (Horel, 1981; Barnston and Livezey, 1987). The CPC website (2001) explains that only the top ten eigenvectors were retained for each month. A varimax rotation was conducted to isolate the ten strongest teleconnections by month. The amplitudes for each teleconnection were found using a least-squares regression analysis. The time series of amplitudes were standardized by month (i.e. the values have a mean of zero and a standard deviation of 1.0) (CPC, 2001). The CPC methodology identified 14 different teleconnections. Amplitude values are available for each teleconnection pattern back to 1950. The teleconnection indices were downloaded from the CPC website (CPC, 2003a).

The index for the SO is also available from the CPC, but is calculated using a different method. Traditionally, the index has been based on the difference in SLP between Tahiti and Darwin, Australia. Both anomaly and standardized SOI data sets can be found at the CPC website (CPC, 2003b). The study used the standardized SOI values in order to be consistent with the standardized teleconnection indices obtained from the CPC principle component analysis.

8. I

defin

neut

posit

orde

mon

(PN.

mon

seasc

sumr

FOR

com:

telec

infre

the p

8. Identifying Months of Strong Teleconnections

For each month during the 40-year study period, the teleconnection indices were defined as being in a strong positive phase (≥ 1.0), a strong negative phase (≤ -1.0), or neutral phase (> -1.0 and < 1.0). Months were then classified on the basis of co-existing positive, negative, and neutral teleconnections (see Appendix A, sections 10, 5, 12; the order of the sections refers to the order in which the programs were run). For example, a month may be categorized by a positive PNA, a neutral NAO, and a negative SOI (PNA+, NAO, SOI-). Twenty-seven teleconnection “combinations” were possible. All months of the same teleconnection combination were then grouped by the traditional seasonal categories: winter (December, January, February), spring (March, April, May), summer (June, July, August), and autumn (September, October, November). A FORTRAN program (see Appendix A, section 11) categorized each of the 27 combinations into the four seasonal categories making a potential of 108 possible teleconnection combinations to consider. However, some combinations occurred infrequently, so an arbitrary cutoff of three or more occurrences was used. As a result, the potential 108 combinations were reduced to 42, as shown in Table 2.5.

Table 2.3

TC #
1
2
3
4
5
6
7
8
9
10
11
12
13
14
15
16
17
18
19
20
21
22
23
24
25
26
27

Ras

seasonal tra

combination

number of

subset of th

the potentia

trajectory c

Table 2.5. The 27 possible teleconnection combinations and the number of monthly occurrences for each seasonal grouping.

TC #	PNA	NAO	SOI	Winter	Spring	Summer	Autumn
1	PNA+	NAO+	SOI+				
2	PNA+	NAO+	SOI		3		
3	PNA+	NAO	SOI+				
4	PNA	NAO+	SOI+	7			
5	PNA-	NAO-	SOI-				
6	PNA-	NAO-	SOI	6	4		
7	PNA-	NAO	SOI-				
8	PNA	NAO-	SOI-	5	3	7	
9	PNA+	NAO	SOI	5	8	3	8
10	PNA	NAO+	SOI	14	6	11	7
11	PNA	NAO	SOI+	12	9	7	14
12	PNA-	NAO	SOI	5	9		9
13	PNA	NAO-	SOI	4	15	8	7
14	PNA	NAO	SOI-	6	10	10	11
15	PNA+	NAO-	SOI-				
16	PNA-	NAO+	SOI-				
17	PNA-	NAO-	SOI+				
18	PNA-	NAO+	SOI+				
19	PNA+	NAO-	SOI+				
20	PNA+	NAO+	SOI-				
21	PNA	NAO+	SOI-	5	5	6	5
22	PNA	NAO-	SOI+				
23	PNA+	NAO	SOI-	7	6		
24	PNA-	NAO	SOI+				
25	PNA+	NAO-	SOI	5			3
26	PNA-	NAO+	SOI				
27	PNA	NAO	SOI	25	30	52	36

Raster-grid maps were then prepared to display the difference between the seasonal trajectory climatologies and trajectory patterns for each of the 42 teleconnection combinations. However, it was not appropriate to simply take the difference of the “raw” number of trajectory nodes per grid cell, because the teleconnection combinations are a subset of the total possible months (per season) during the study period. Consequently, the potential (or maximum) number of nodes per grid cell is much larger for the seasonal trajectory climatologies (calculated across all teleconnection combinations) than for the

indivi

seaso

equat

(2.11

(2.12

acros

each

area.

displ

stand

betw

Steps

imag

9. Te

precip

order

individual teleconnection combinations. To account for this, grid frequencies for both the seasonal climatologies and the teleconnection combinations were standardized using the equation below within a FORTRAN program (see Appendix A, section 13).

$$(2.11) \text{ Standardized Value} = (\text{ Number of nodes within grid cell } (x_i, y_i) \\ / \text{ Total number of nodes })$$

$$(2.12) \text{ Standardized Value} = \text{ Standardized Value} * 100,000$$

The total number of nodes was found by simply summing up the number nodes across all grid cells. Then, as shown in the equation above, the frequency of nodes in each grid cell (x_i, y_i) was divided by the total number of nodes across the entire analysis area. Since the quotient was very small, each value was multiplied by 100,000 for display purposes. Once all climatologies and teleconnection combinations were standardized, a FORTRAN program (see Appendix, section 9) obtained the difference between each teleconnection combination and its corresponding seasonal climatology. Steps b and c, described under section 5 of this chapter, were repeated to obtain the images for the teleconnection combination anomaly maps.

9. Temperature and Precipitation Data

Teleconnections have often been linked to local and regional temperature and precipitation anomalies (e.g., Leathers et al., 1991; Assel, 1992; Serreze et al., 1998). In order to help interpret the impact of changing trajectory patterns for different

telecomm

anomaly

W). By

circulat

Additio

anomaly

downlo

division

the term

the 196

Append

each tel

anomaly

were us

are incl

teleconnection combinations on the local climate, precipitation and temperature anomalies were calculated for the area surrounding the terminus point (42.5° N, 85.0° W). By considering local temperature, and precipitation, along with low-level circulation, source regions of heat and moisture can then be better understood. Additionally, the link between planetary-scale teleconnections and local-scale climate anomalies can be better elucidated.

Monthly temperature and precipitation data for local climate divisions were downloaded from the CDC website (CDC, 2003c). Data were extracted for climate division nine within lower Michigan (Figure 2.9), because this climate division includes the terminus point (42.5° N, 85.0° W). A temperature and precipitation climatology for the 1960-1999 study period was constructed for each season. A FORTRAN program (see Appendix A, section 14) then calculated the temperature and precipitation anomalies for each teleconnection combination. A one-sample t-test was used to test whether the anomaly values were statistically significant. Alpha (α) values equal to .05, .1, and .2 were used to display different levels of significance. The results of the one-sample t-test are included in Appendix C.

Figure 2.9.

10. Summ

Ch

precipitati

research s

all includ

trajectory



Figure 2.9. Climate division #9 within lower Michigan (from the National Climatic Data Center, 2003).

10. Summary

Chapter 2 described the wind, atmospheric teleconnection, temperature, and precipitation data used in the study. A discussion of the methods used to perform the research study was also presented. The FORTRAN programs used in the calculations are all included in Appendix A. The following chapters will present the results of the trajectory climatology and the teleconnection analysis.

1. Over

climato

perinsu

calcula

update

spatial

10 year

presen

Ohio (

this stu

of less

traject

map is

each in

19, 20

were se

the yea

termin

CHAPTER 3

CLIMATOLOGY OF AIR-PARCEL TRAJECTORIES

1. Overview

Chapter 3 presents the results of the climatology of air-parcel trajectories. The climatology is based on five-day back trajectories that terminate within the central lower peninsula of Michigan (42.5° N, 85.0° W). For a 40-year period, trajectories were calculated for the 925 hPa level. As mentioned previously, the climatology study is an update to the previous work of Waller (1999). However, the current study used a higher spatial and temporal resolution of input data. Also, the time period was increased from 10 years to 40 years to permit additional applications, such as the teleconnection study presented in the next chapter. Waller's study also used a terminus point in northwest Ohio (41.56° N, 84.09° W) and a study level of 850 hPa. However, the terminus point for this study is in lower Michigan (42.5° N, 85.0° W) and the level is 925 hPa. A difference of less than 1° latitude and longitude should result in little effect on the air-parcel trajectory patterns.

The monthly climatologies are shown below using two maps per month. The first map is a climatology that displays the total number of nodes for the 40-year period within each individual 50 km by 50 km grid cell. Six categories are used that correspond to 0-19, 20-34, 35-59, 60-99, 100-199, and 200 or more nodes per grid cell. The categories were selected based on natural breaks in the data that were appropriate for all months of the year. The grid cells with the highest numbers of nodes are always located near the terminus point (42.5° N, 85.0° W) with the number of nodes typically decreasing as the

distance

speeds a

aligned d

creating

is a path

W), and

subtrac

climate

cell ac

obtain

traject

month

month

conse

devia

and p

2. An

each

corrie

from

distance from the terminus point increases. Long paths of nodes reflect strong wind speeds and shorter paths reflect weak wind speeds. Large numbers of nodes are often aligned along a certain direction or multiple directions leading toward the terminus point creating what are subjectively referred to in this study as airflow “corridors.” A corridor is a path of high-node concentration extending toward the terminus point (42.5° N, 85.0° W), and illustrates where a large number of trajectories originated.

The second map is an anomaly display. The anomalies were calculated by subtracting the grid cell values for each month from the grid cell values of the annual climatology. The annual climatology was derived by adding the number of nodes by grid cell across all months. The total for each grid cell was then divided by 12 in order to obtain an annual average. The anomaly map for each month demonstrates how the trajectory pattern for the month differs from the annual average pattern. Unlike the monthly climatology maps, the anomaly maps do not use the same fixed categories for all months. Instead, the anomaly maps are displayed in terms of standard deviations. The consequent map categories are <-3, -3 to -2, -2 to -1, 1 to 2, 2 to 3, and >3 standard deviations from the annual average (negative categories are displayed as “cool” colors and positive categories are displayed as “warm” colors on the maps).

2. Annual Climatology

As just described, the annual climatology was calculated by adding the nodes for each grid cell across all months of the year and dividing by 12. Two primary airflow corridors are evident for the annual climatology (Figure 3.1). The first is a broad corridor from the northwest and the second corridor originates from the southwest. The

southwestern

region toward

Figure 3.
ground cell

3. January

The

airflow con

central Car

approxima

southwestern

point (42.5

southwesterly corridor is narrower and extends from Texas and the Gulf of Mexico region toward Michigan.

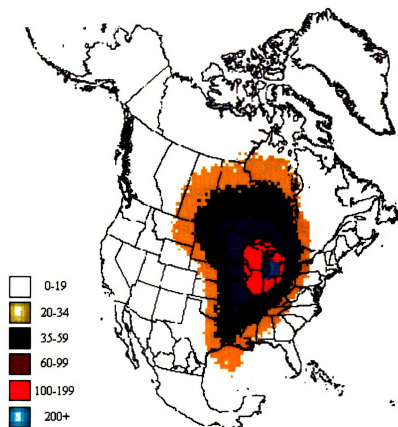


Figure 3.1. Annual climatology map. Number of trajectory nodes per 50 km by 50 km grid cell for the period 1960-1999. The trajectories are five-day back trajectories for the 925 hPa surface. Grid nodes were calculated at three-hour intervals.

3. January

The trajectory climatology plot for January (Figure 3.2) suggests that three airflow corridors are present: a broad, northwesterly corridor extending from north central Canada to the terminus point; a narrower, westerly corridor extending from approximately Utah and Idaho to the terminus point (42.5° N, 85.0° W); and a southwesterly corridor extending from approximately northern Louisiana to the terminus point (42.5° N, 85.0° W). The anomaly map for January indicates that the frequency of

trajecto

northw

during

Idaho

As dis

obser

winds

tend

also

patte

Mex

nort

surr

spee

sou

and

alt

to v

stu

Me

sou

trajectory nodes per grid cell is higher than the annual average values along the northwesterly and westerly corridors. The westerly corridor is an interesting feature during the winter season. An area of high-node density is located roughly at the Utah and Idaho border. This area reflects the elevated topography of the western United States. As discussed in Chapter 2, the NCEP/NCAR reanalysis data use the surface wind observations for atmospheric pressure levels located “below” the surface. Since the winds are relatively weak at the surface, the trajectories that reach the Rocky Mountains tend to “stall,” resulting in high-node densities.

In addition to the westerly and northwesterly corridors, a southwesterly corridor is also evident. However, during January the corridor is weaker than the annual average pattern and the trajectory origins remain inland rather than extending to the Gulf of Mexico. Another aspect of the climatology for January is the lack of trajectories to the north, east, and south. The anomaly map also shows large negative deviations surrounding Michigan, which is expected during the winter because of stronger wind speeds at this time of year. However, negative deviations also spread far to the north and south, which again suggests that Michigan is primarily under the influence of westerly and northwesterly airflow during January.

The January pattern depicted by Waller (1999) is similar to that presented here, although Waller’s study suggests somewhat more frequent easterly trajectories compared to this study. Also, the location of the southwesterly corridor differs between the two studies. This study shows that the southwesterly corridor originates from the Gulf of Mexico region, whereas Waller’s work depicts the corridor originating in the southwestern United States toward Baja California. In addition, this study found large-

fr

re

node frequencies over central Canada, whereas a northwesterly corridor is not as well defined in Waller's work.

Figure 3.2. January climatology (top) and anomaly (bottom) maps for the 925 hPa, isobaric back trajectories. The climatology map shows the total number of three-hour trajectory nodes per grid cell for the 1960-1999 study period. The colors represent the following categories: clear (0-19), tan (20-34), green (35-59), purple (60-99), red (100-199), and cyan (200 or more) nodes per grid cell. Anomalies were calculated by first differencing the monthly totals and the average annual value for each grid cell, and then expressing the differences as standard deviations. (See text for further details.) The “warm” colors on the anomaly map represent positive (1 to 2, 2 to 3, and >3) standard deviations from the mean and the “cool” colors represent negative (-1 to -2, -2 to -3, <-3) standard deviations from the mean.

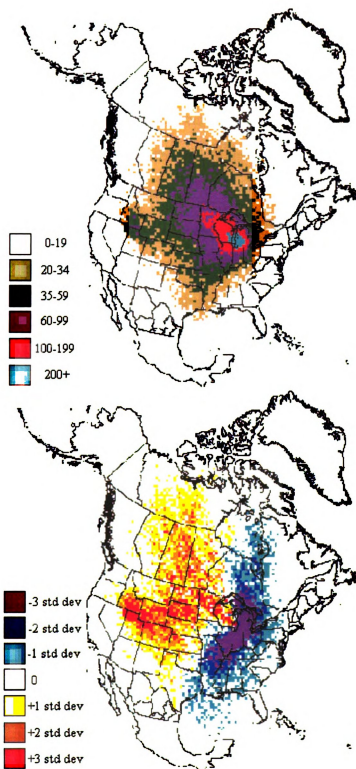


Figure 3.2. (see facing page for caption)

4. Feb

weste

mont

north

frequ

surpr

Janu

the s

origi

traje

a sh

comm

frequ

frequ

sou

4. February

The most obvious change between January and February is the weakening of the westerly corridor (Figure 3.3). However, other smaller differences between the two months are noticeable as well. The northwesterly corridor does not originate quite as far northwest in Canada as was the case for January. Instead, there is an increase in the frequency of trajectories originating from the north. Additionally, and somewhat surprisingly, southwesterly trajectories are even more infrequent in February than in January. The anomaly map strongly illustrates the lack of trajectories originating from the south. The westerly and northwesterly corridors still remain favorable for trajectory origination, but a weakening is beginning to take place. At this time, the frequency of trajectories from the north is still below average compared to the annual climatology, but a shift toward more frequent northerly airflow is beginning to become evident.

Waller's (1999) climatology for February is similar in that the northwesterly corridor was by far the strongest. However, Waller's study displayed an overall greater frequency of westerly trajectories, whereas this study displays a slightly greater frequency of southwesterly trajectories. In February, Waller (1999) found very few southerly trajectories.

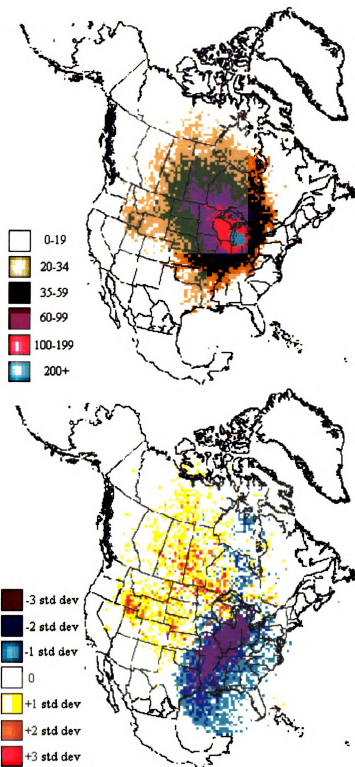


Figure 3.3. February climatology (top) and anomaly (bottom) maps for the 925 hPa, isobaric back trajectories. See caption to Figure 3.2 for further details.

5. Mar

March

western

original

Hudson

annual

trajectory

Waller

during

is prese

5. March

During March, a number of changes begin to take place. The anomaly map for March (Figure 3.4) illustrates the changes from the preceding winter months. The westerly and northwesterly corridors display negative deviations. Airflow continues to originate more from the north, with a large number of trajectories originate near the Hudson Bay region. Although the southwesterly corridor still remains weaker than the annual climatology, the corridor is beginning to show an increase in strength as trajectories originate throughout the Gulf of Mexico and the southeast United States. Waller (1999) also illustrated the increase in strength of a northerly, Hudson Bay corridor during March. In contrast, however, the strengthening of the southwesterly corridor that is present in this study was absent from Waller's study.

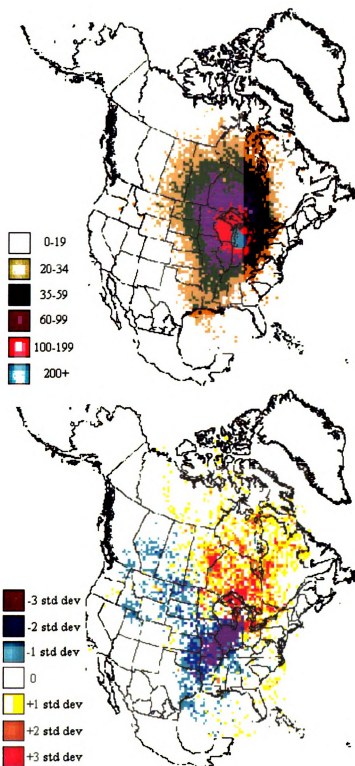


Figure 3.4. March climatology (top) and anomaly (bottom) maps for the 925 hPa, isobaric back trajectories. See caption to Figure 3.2 for further details.

6. Ap

year

north

defin

prev

betw

Me

devi

win

may

diff

Ap

6. April

The April climatology (Figure 3.5) displays the strongest northerly corridor of the year as trajectories originate far into the Hudson Bay region. The westerly and northwesterly corridors continue to weaken as the southwesterly corridor becomes more defined. However, the southwesterly corridor shifts slightly eastward compared to previous months. The anomaly map displays negative deviations spanning the area between Michigan and Texas. However, an increase in nodes throughout the Gulf of Mexico and the southeastern United States is evident. The presence of positive deviations in the Gulf region also suggests longer trajectories, and therefore, stronger wind speeds. The trajectory pattern for April suggests that Michigan receives the majority of its low-level airflow from either a northerly or southerly origin. This greatly differs from Waller's (1999) study since her study found the primary airflow pattern in April to be northwesterly rather than northerly and southerly.

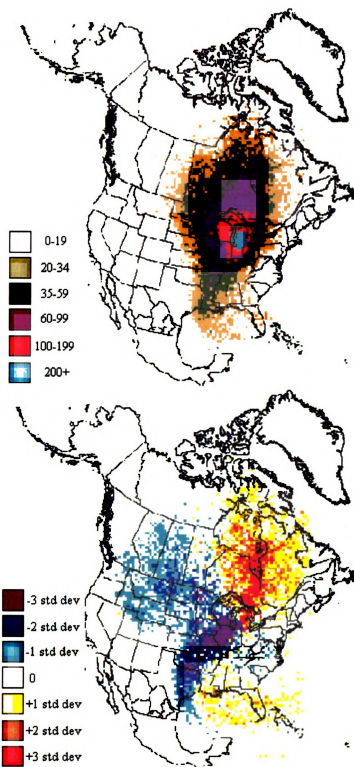


Figure 3.5. April climatology (top) and anomaly (bottom) maps for the 925 hPa, isobaric back trajectories. See caption to Figure 3.2 for further details.

7. May

The
trajectories
northerly
and includ
W). Dur
trajectories
strengthen
is evident
the western
eastward
continues
westerly a
year, near
nodes with
study and
suggested
west of th

7. May

The month of May (Figure 3.6) also is characterized by a large number of trajectories originating from the Hudson Bay area. However, the overall definition of the northerly corridor is not as organized as it was in April. The corridor spans a larger area and includes an increase in trajectories to the east of the terminus point (42.5° N, 85.0° W). During this month, the northwesterly corridor continues to weaken as more trajectories originate from the south. The anomaly map for May displays the strengthening of the southwesterly corridor. A continuous corridor of positive anomalies is evident from the Gulf of Mexico to Michigan. Negative anomalies are located along the western edge of the southwesterly corridor suggesting that the corridor has shifted eastward compared to the annual climatology. However, the southwesterly corridor continues to strengthen, as large numbers of nodes are located over the Gulf region. The westerly and northwesterly corridors remain weaker than average. Also, at this time of year, nearly the entire state of Michigan is highlighted by a large number of trajectory nodes within the state suggesting weaker wind speeds. The differences between this study and Waller's (1999) are similar for May as they were for April. Waller's study suggested a strong northwesterly corridor and an overall origination of trajectories to the west of the terminus point (42.5° N, 85.0° W).

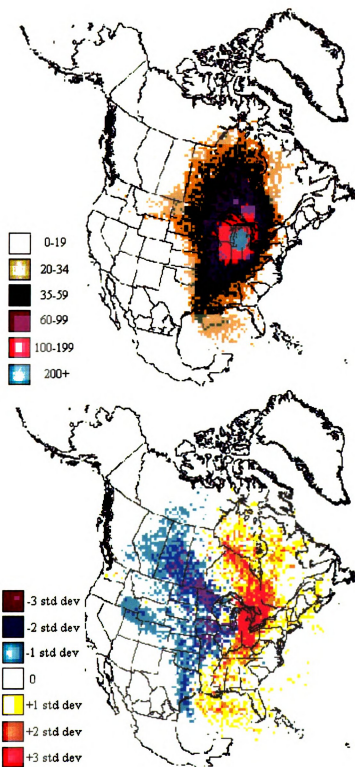


Figure 3.6. May climatology (top) and anomaly (bottom) maps for the 925 hPa, isobaric back trajectories. See caption to Figure 3.2 for further details.

8 June

In

terminus p

(Figure 3.1

defined as

westerly c

The most

from the C

that variat

she found

of a defin

8. June

In June, as well seen throughout the summer, high-node values are found near the terminus point (42.5° N, 85.0° W), reflecting weaker wind speeds at this time of year (Figure 3.7). The northerly corridor remains evident in June, although it is not as well defined as in previous months. Northwesterly airflow remains infrequent, but a small westerly corridor (best seen over North Dakota and Montana) is beginning to strengthen. The most important anomaly for June is a very defined southwesterly corridor that spans from the Gulf of Mexico to Michigan. The positive anomaly is very strong suggesting that variability in airflow is limited. Waller's (1999) study differs with this study in that she found a persistent northwesterly corridor during all summer months with an absence of a defined southwesterly corridor.

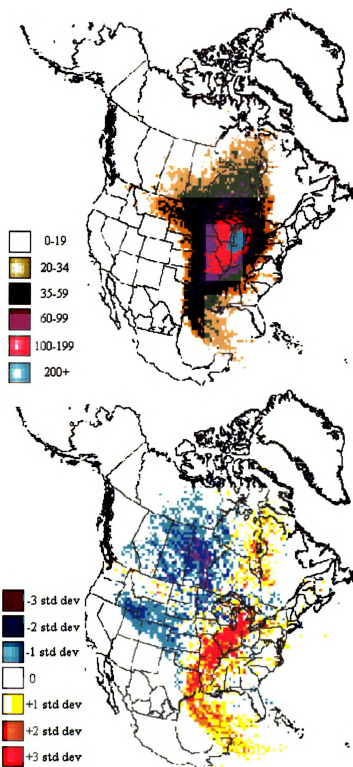


Figure 3.7. June climatology (top) and anomaly (bottom) maps for the 925 hPa, isobaric back trajectories. See caption to Figure 3.2 for further details.

9. Ju

mon

ong

few

Ba

Po

ov

ar

ne

9. July

The southwesterly corridor is strongest during July (Figure 3.8). The corridor is more defined and narrower than previous months with high-node concentrations now originating well into the Gulf of Mexico region. As a result, the anomaly map displays fewer trajectories originating in the southeastern United States. The northerly, Hudson Bay corridor is still quite evident and is actually slightly stronger than it was during June. Positive anomalies centered over Pennsylvania also suggest a short easterly corridor. The overall decline in the northwesterly corridor is still obvious, because negative anomalies are still widespread across the west and northwest region. However, the anomalies are not as strongly negative as they were in previous months.

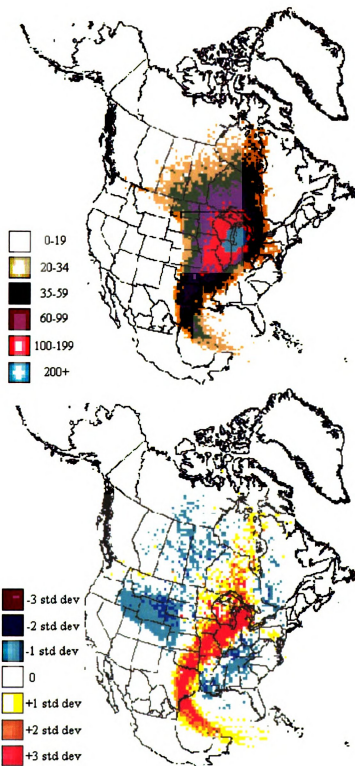


Figure 3.8. July climatology (top) and anomaly (bottom) maps for the 925 hPa, isobaric back trajectories. See caption to Figure 3.2 for further details.

of the

are

dec

and

con

to t

sug

10. August

The August climatology and anomaly maps (Figure 3.9) illustrate a high number of trajectory nodes located near the terminus point (42.5° N, 85.0° W). The trajectories are shorter suggesting that wind speeds are weakest during August. A broadening and decrease in the length of the southwesterly corridor is also noticeable. Small positive anomalies are still evident for the northerly corridor, but there is a definite weakening compared to previous months. The overall number of grid cells with negative anomalies to the west and northwest of the terminus point (42.5° N, 85.0° W) continues to decrease, suggesting the reintroduction of a northwesterly corridor.

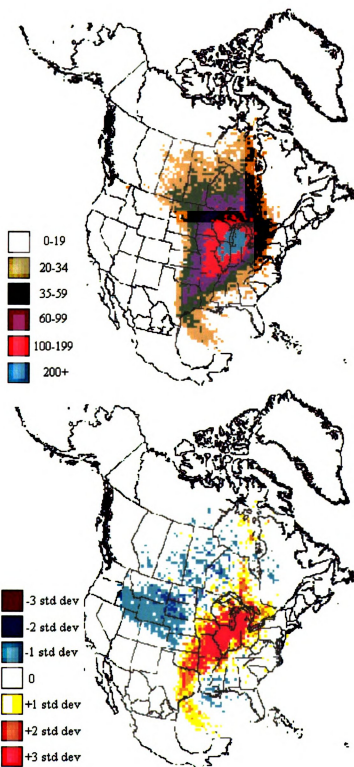


Figure 3.9. August climatology (top) and anomaly (bottom) maps for the 925 hPa, isobaric back trajectories. See caption to Figure 3.2 for further details.

11. September

The month of September (Figure 3.10) has some very different airflow patterns compared to August. Corridors from the north and the west are weak and the northerly corridor has diminished dramatically since August. A transition from a strong southwesterly corridor to a strong northwesterly corridor is clearly taking place. The southwesterly corridor is still prominent in September, but it has taken on very different characteristics from the previous summer months. Rather than being oriented southwesterly, the corridor has now shifted to a southerly orientation. The high-node frequencies that were once present in the Gulf of Mexico are now restricted to land. Additionally, the organization of the corridor has decreased. However, many more trajectories are originating over the southeastern United States. Although no corridor is clearly defined, an overall frequency of easterly trajectories is present as well. Another important change is that the once prominent northerly, Hudson Bay corridor has diminished, and the northwesterly corridor has strengthened. September is the only month where Waller's study (1999) suggested a southwesterly corridor; in contrast, the southwesterly corridor has diminished in this study. Additionally, in Waller's study, there was very little organization of any corridor during the months of September and October.

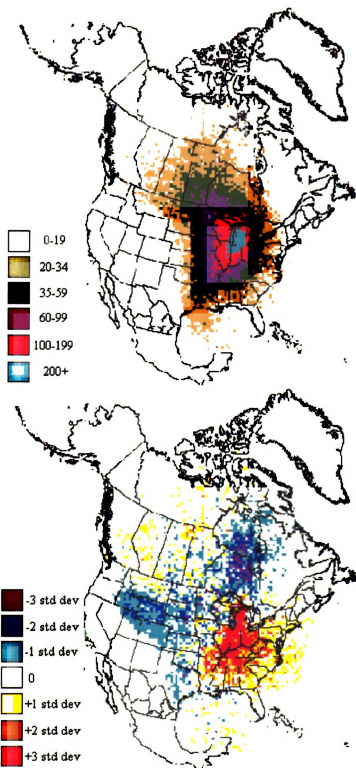


Figure 3.10. September climatology (top) and anomaly (bottom) maps for the 925 hPa, isobaric back trajectories. See caption to Figure 3.2 for further details.

12. October

During the month of October (Figure 3.11), the northwesterly corridor has strengthened and broadened. The northerly corridor is still relatively weak compared to previous months. However, an increase in strength of a westerly corridor has begun. The southwesterly corridor remains present displaying a similar pattern to that of September. High-node concentrations in the southeast United States remain evident. However, negative anomalies over the Gulf of Mexico now suggest that the lengths of the southerly trajectories are shorter than in previous months. Thus, those parcels traveling from the south will have less of a maritime influence than in previous months. One other important point for October is that the number of positive anomalies near the terminus point (42.5° N, 85.0° W) has declined. Overall, this suggests that wind speeds and trajectory lengths are increasing.

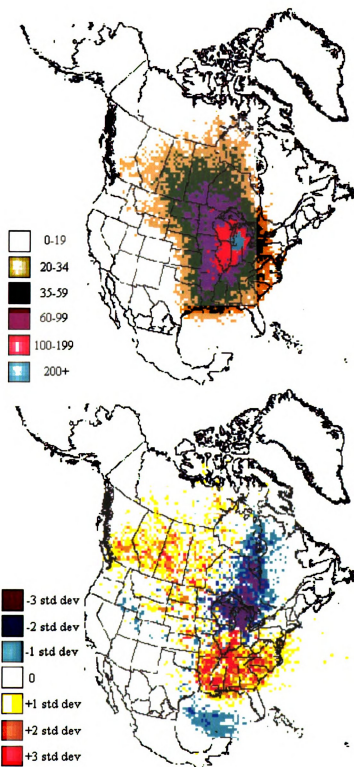


Figure 3.11. October climatology (top) and anomaly (bottom) maps for the 925 hPa, isobaric back trajectories. See caption to Figure 3.2 for further details.

and

is

no

pre

an

so

no

de

con

po

str

no

13. November

November (Figure 3.12) displays a strengthening of the northwesterly corridor and a weakening of the southwesterly corridor. During this month, the westerly corridor is continuing to strengthen as well, although it remains unclear whether or not separate northwesterly and westerly corridors are evident. The southwesterly corridor remains present, but the corridor is discontinuous. High-node values are located over Louisiana and the Gulf of Mexico, but not from Illinois to Michigan. This suggests that the southerly and southwesterly trajectories are long due to fast winds with few “intermediate nodes.” The number of “short” southerly and southwesterly trajectories appears to have decreased compared to previous months. The northerly, Hudson Bay corridor has also continued to weaken because large negative anomalies are evident north of the terminus point (42.5° N, 85.0° W). The past study by Waller (1999) also illustrated the strengthening of the northwesterly corridor. In addition, Waller’s study depicted a small northeasterly corridor while the southwesterly corridor remained absent in November.

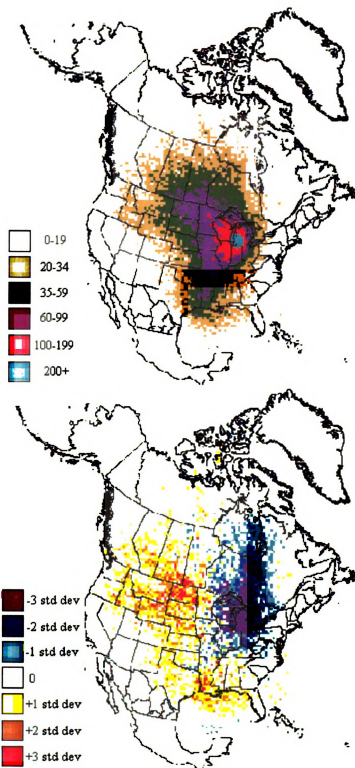


Figure 3.12. November climatology (top) and anomaly (bottom) maps for the 925 hPa, isobaric back trajectories. See caption to Figure 3.2 for further details.

14. December

The anomalies associated with December (Figure 3.13) are very well defined. The most important change in December is that there is now a clear separation between the strong westerly corridor and the northwesterly corridor. Strong positive anomalies are found west of the terminus point (42.5° N, 85.0° W). Negative anomalies continue to be present for the northerly corridor, to the east of the terminus point, and to the south of the terminus point as well. Compared to November, the northerly, Hudson Bay corridor displays an increase in strength, but is still not as dominant as the other strong corridors. Although still present, the southwesterly corridor is weaker compared to previous months. Waller's (1999) climatology for December is very similar to this study. However, compared to this study, the strong northwesterly corridor in Waller's study has a slightly more northerly orientation.

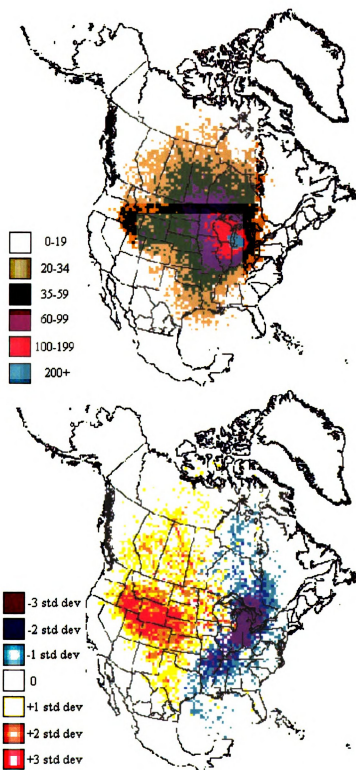


Figure 3.13. December climatology (top) and anomaly (bottom) maps for the 925 hPa, isobaric back trajectories. See caption to Figure 3.2 for further details.

15. Summary

Chapter 3 presented the results of a 40-year climatology of five-day back trajectories. An annual climatology was presented, as well as a climatology for each individual month. The trajectory climatology presented here for the terminus point (42.5° N, 85.0° W) has a well-defined annual cycle. The winter season is primarily associated with strong northwesterly and westerly airflow. The westerly airflow decreases in the spring as strong northerly, Hudson Bay airflow becomes evident and southwesterly airflow increases. Throughout summer, southwesterly airflow is very strong as the northerly airflow slowly weakens. During the autumn season, the southwesterly airflow begins to decrease as the northwesterly and westerly airflow becomes dominant once again. Chapter 3 also compared results of this trajectory climatology with a previous climatology by Waller (1999). The results of the two studies are generally similar with the main exception that a southwesterly corridor is absent from Waller's study, which is probably a result of the different data set, or the different terminus point location that she used. The next chapter will present the results of a teleconnection study that used these trajectory climatologies in an application of atmospheric teleconnection association with low-level airflow and local climate anomalies.

CHAPTER 4

RELATIONSHIP BETWEEN ATMOSPHERIC TELECONNECTIONS AND LOWER-TROPOSPHERIC AIRFLOW TRAJECTORIES

1. Overview

Chapter 4 describes the relationships between atmospheric teleconnections and lower-tropospheric back trajectories for central lower Michigan. Additionally, the differences in trajectory patterns for single and co-existing teleconnection combinations are related to deviations in seasonal-mean temperature and precipitation. The associations of atmospheric teleconnections with the climate of the lower peninsula of Michigan are studied in order to better understand the relationship between planetary-scale circulation and the regional-scale advection of heat and moisture from air-mass source regions.

As previously discussed, the NAO, PNA, and SO teleconnections were selected for this project because past literature has shown these indices to be the most influential for the Midwest (Wallace and Gutzler, 1981; Rogers, 1984; Leathers et al., 1991; Assel, 1992; Rohli and Rogers, 1993; Serreze et al., 1998; Changnon et al., 2000; Hu and Feng, 2001b). Monthly NAO, PNA, and SO indices obtained from the CPC were first categorized by their strength: strongly positive (≥ 1.0), strongly negative (≤ -1.0), or neutral (> -1.0 and < 1.0). Therefore, since the study uses three teleconnections with three categories for each, 27 teleconnection “combinations” are possible. Additionally, the effects of the 27 teleconnection combinations are studied seasonally, resulting in a potential of 108 teleconnection combinations. However, the 108 possible combinations

do not occur with equal frequency. Only those combinations that occurred three or more times during the 40-year study period were analyzed. A total of 42 teleconnection combinations met this criterion.

In the following discussion, the combinations will be referred to as TC1 through TC27 (e.g. TC1 is PNA+, NAO+, SOI+). The analysis steps can be summarized as follows. First, the previously calculated isobaric trajectories were sorted by teleconnection combination. Second, the plots of the frequency of trajectory nodes per grid cell were created for each teleconnection combination. Third, the frequency plots were standardized based on the total number of nodes across the analysis area (see Chapter 2, section 8 for a more detailed description of this process). Fourth, the same procedure was used to standardize the corresponding seasonal (i.e., winter, spring, summer, and autumn) climatology. Fifth, the standardized plots for the teleconnection combination and seasonal climatology were differenced. Sixth, the differences were plotted as standard deviations. As seen in the trajectory climatology results, the images often show patterns, or “corridors,” where anomalous low-level flow has taken place.

Many inferences can be drawn from the resulting images based on where an increase or decrease in airflow has taken place. However, it is inadequate to conclude that an increase in northerly (southerly) flow will always result in cooler (warmer)-than-normal temperatures in Michigan’s lower peninsula. Therefore, in order to understand the impact of changes in low-level airflow on local climate, seasonal temperature and precipitation anomalies were calculated. The temperature and precipitation data were gathered for climate division nine in central lower Michigan, where the terminus point for the trajectory calculations is located. The anomalies are the differences from the seasonal

temperature and precipitation means for the 40-year study period. These anomalies help researchers understand the advection of heat and/or moisture under different teleconnection combinations. The significance of the temperature and precipitation anomalies was tested using a one-sample t-test with alpha (α) levels of .05, .1, and .2. If the results are well defined between the teleconnection combinations and trajectories, and supported by significant temperature and precipitation anomalies, then these methodologies will be a good tool for improving medium to long-range climate forecasts for the Midwest region. Table 4.1 lists the temperature and precipitation anomalies for each teleconnection combination and Appendix C lists the results of the one-sample t-tests.

Table 4.1. Temperature (°C) and precipitation (mm) anomalies for the 27 teleconnection combinations by seasonal groupings.

TC #	Win Temp	Win Precip	Spr Temp	Spr Precip	Sum Temp	Sum Precip	Aut Temp	Aut Precip
1								
2			1.3	-1.5				
3								
4	1.7	17.8						
5								
6	-0.4	3.8	-2.4	2.5				
7								
8	-1.1	-6.6	-1.1	-3.8	-0.2	-13.5		
9	-1.8	-27.7	-0.2	-8.6	-0.2	-28.7	-1.4	-9.7
10	0.6	-4.1	0.3	-11.9	0.9	2.3	-0.7	-11.4
11	-0.4	5.8	-0.2	3.3	0.8	-2.3	0.4	3.0
12	-0.3	3.8	-0.4	3.0			1.0	15.0
13	0.8	13.0	-0.6	-6.1	-0.2	-11.4	-1.1	12.7
14	1.6	10.2	1.1	14.5	-0.2	6.9	0.1	-3.0
15								
16								
17								
18								
19								
20								
21	1.8	5.8	1.1	-8.1	-1.0	-6.6	0.8	-19.3
22								
23	2.9	-15.0	1.0	-4.1				
24								
25	-4.0	-20.1					0.3	2.3
26								
27	-0.2	0.0	0.2	-0.5	-0.1	1.3	-0.1	-4.1

2. TC2 (PNA+, NAO+, SOI)

TC2 occurred only three times during the study period with all occurrences during the spring months. Figure 4.1 illustrates a strong increase in trajectories within the southwesterly corridor and a moderate increase in the northerly, Hudson Bay corridor. Springtime westerly, northwesterly, and easterly airflow is less frequent for this teleconnection combination. The resulting temperature and precipitation anomalies are

1.3°C and -1.5 mm. The temperature anomaly is significant at the $\alpha = .05$ level, but precipitation is not significant for TC2. The temperature anomaly is consistent with the more frequent southwesterly airflow during this teleconnection combination. However, the insignificant precipitation anomaly is somewhat surprising, as southwesterly airflow would also be expected to transport more moisture into the study area. Previous literature indicates that a positive PNA is associated with cooler, drier conditions in the Midwest (Leathers et al., 1991; Rohli and Rogers, 1993), which agrees with the sign of the precipitation anomaly. However, a positive NAO is associated with warmer temperatures (Wallace and Gutzler, 1981; Rogers, 1984). This suggests a contradictory temperature projection for the Midwest under a positive NAO and positive PNA. The statistically significant warm anomaly found here suggests that a positive NAO may have a stronger association with local temperature than a positive PNA, at least for TC2.

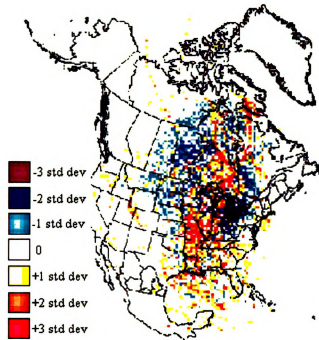


Figure 4.1. Deviation of trajectory frequencies during TC2 (PNA+, NAO+, SOI) in spring from the average springtime trajectory frequencies. The anomalies were calculated by first calculating the proportion of the total number of trajectory nodes (summed across all grid cells) that fell within each grid cell and then differencing the proportions for the springtime (March-May) occurrences of Teleconnection Combination #2 (TC2) from the proportional values for all spring seasons. The differences are plotted in terms of standard deviations around a mean difference of zero (see text for further details). The “warm” colors on the map indicate positive (1 to 2, 2 to 3, and >3) deviations from the mean and the “cool” colors represent negative (-1 to -2, -2 to -3, <-3) deviations from the mean.

3. TC4 (PNA, NAO+, SOI+)

TC4 occurred seven times during the winter months. Figure 4.2 shows much more frequent westerly and northwesterly trajectories with fewer northerly trajectories during this teleconnection combination. The lengths of the southerly trajectories are longer than average as indicated by the positive anomalies over the Gulf of Mexico. The consequent temperature and precipitation anomalies for this situation are 1.7°C (significant at $\alpha = .1$) and 17.8 mm (significant at $\alpha = .2$). Although a strong southwesterly corridor does not exist, the strong decrease in trajectories to the north of

the terminus point may be the explanation for the significantly warmer and wetter conditions under TC4. Also, the more frequent westerly trajectories would contribute to warmer temperatures compared to northerly trajectories. For winter, previous research has found positive values of the SOI (La Niña) to have a relationship with northwesterly airflow and cooler, wetter conditions in the Midwest (Changnon et al., 2000), whereas a positive NAO index value is associated with increased southerly airflow and warmer temperatures (Wallace and Gutzler, 1981; Rogers, 1984). The positive temperature anomalies for this teleconnection combination suggest that a positive NAO index has a stronger association with temperature in the Midwest than a positive SOI. However, the precipitation anomaly agrees with earlier studies of the SOI (Changnon et al. 2000).

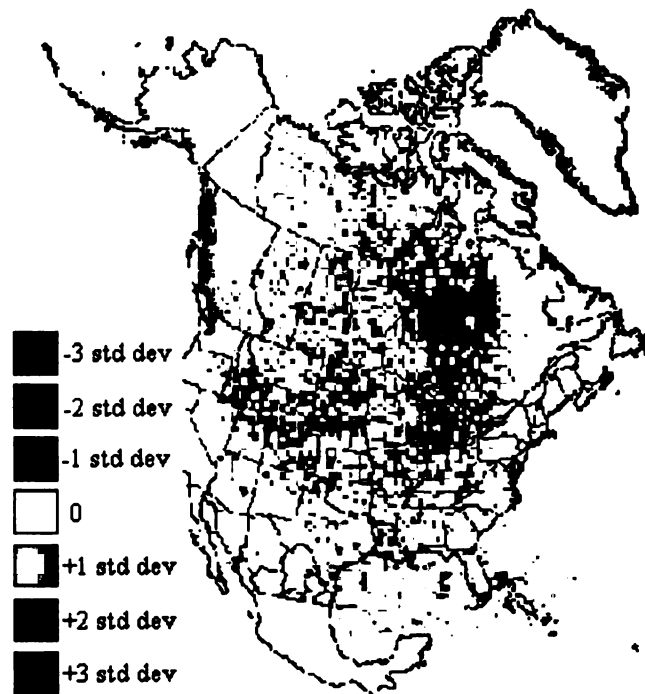


Figure 4.2. Deviation of trajectory frequencies during TC4 (PNA, NAO+, SOI+) in winter from the average wintertime trajectory frequencies. See caption to Figure 4.1 for further details.

4. TC6 (PNA-, NAO-, SOI)

TC6 occurred six times during the winter months, but this teleconnection pattern does not have any distinct airflow anomalies. The wintertime situation appears to be associated with an increase in northwesterly and southwesterly airflow, and a decrease in northerly and northeasterly airflow (Figure 4.3). The resulting temperature and precipitation anomalies are -0.4°C and 3.8 mm, neither of which is statistically significant. The fairly uniform airflow pattern fits with the insignificant temperature and precipitation anomalies. Past research describes a negative PNA to have an association with zonal flow and warmer temperatures (Leathers et al., 1991; Rohli and Rogers, 1993) and a negative NAO to have an association with increased northerly airflow and cooler temperatures within the Midwest (Wallace and Gutzler, 1981; Rogers, 1984). Thus, during winter, the airflow patterns associated with these phases of the two teleconnections are quite different. Figure 4.3 suggests that the combined influence of the teleconnection patterns results in small to moderate trajectory increases within the northwesterly and southwesterly corridors. Also, the previously identified temperature relationships are contradictory for the two teleconnection patterns, so it is not surprising that an insignificant temperature anomaly was found in this study. The negative PNA situation also suggests a possible association with increased precipitation (Leathers et al., 1991), which agrees with the anomaly of 3.8 mm; however, the anomaly is not significant.

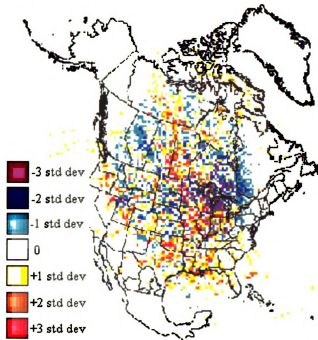


Figure 4.3. Deviation of trajectory frequencies during TC6 (PNA-, NAO-, SOI) in winter from the average wintertime trajectory frequencies. See caption to Figure 4.1 for further details.

TC6 also had four occurrences during the spring months. Even though the temperature and precipitation anomalies for the springtime situation (Figure 4.4) are of the same sign as the winter anomalies, the trajectory pattern is different. A decrease in southerly airflow is evident, but the trajectories are longer, suggesting faster wind speeds from the south. Increases in the northerly, northwesterly, and even northeasterly airflow are present. A large temperature anomaly of -2.4°C (significant at $\alpha = .05$) is the result from the increased northerly flow and decreased southerly flow. The precipitation anomaly of 2.5 mm is not significant. During spring, a negative PNA (westerly, warm) and negative NAO (northerly, cool) situation has a contradictory association with temperature in the Midwest. However, the results for the TC6 occurrences in spring suggest that the NAO association is stronger as indicated by the cool anomaly and

increased northerly flow. The association between a negative PNA and increased precipitation found elsewhere for the Midwest (Leathers et al., 1991), agrees with the sign of the precipitation anomaly found for the TC6 occurrences, although the value was not significant.

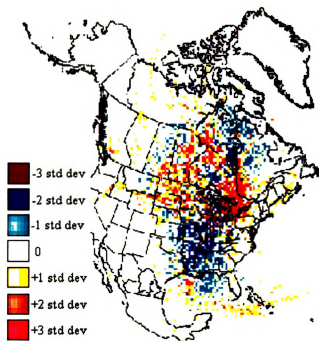


Figure 4.4. Deviation of trajectory frequencies during TC6 (PNA-, NAO-, SOI) in spring from the average springtime trajectory frequencies. See caption to Figure 4.1 for further details.

5. TC8 (PNA, NAO-, SOI-)

The TC8 situation occurred during all seasons except for autumn. Past events include: five winter occurrences, three spring occurrences, and seven summer occurrences. Although some differences in airflow are noticeable throughout the course of the seasons, the primary effect of TC8 is a decrease in southerly flow and an increase in northerly and northwesterly flow (Figures 4.5-4.7). Seasonal differences include a well-defined decrease in the frequency of westerly trajectories in winter, a pronounced

increase in northerly trajectories during spring, and a well-defined northwesterly corridor, but weaker northerly corridor in summer. The resulting temperature and precipitation anomalies are -1.1°C (significant at $\alpha = .2$) and -6.6 mm for winter, -1.1°C and -3.8 mm for spring, and -0.2°C and -13.5 mm (significant at $\alpha = .1$) for summer. Negative values of the SOI (El Niño) suggest zonal, upper-level airflow, warmer temperatures, and drier conditions during winter and spring, but cooler, drier conditions in summer (Changnon et al., 2000). A negative NAO is associated with increased northerly airflow and cooler temperatures for all seasons (Wallace and Gutzler, 1981; Rogers, 1984). The significant warm temperature anomaly found during winter is more consistent with the anomalies expected for a negative NAO situation than a negative SOI. Surprisingly, the temperature anomaly for spring is not significant and suggests that neither a negative NAO nor a negative SOI has a large association with local temperature during this time of year. However, the cool and dry anomalies for summer do agree with the SOI results from previous research.

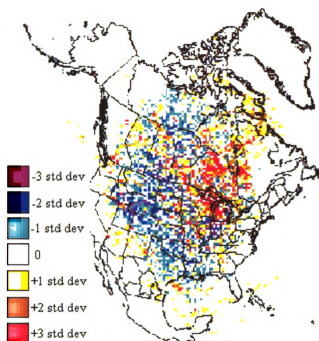


Figure 4.5. Deviation of trajectory frequencies during TC8 (PNA, NAO-, SOI-) in winter from the average wintertime trajectory frequencies. See caption to Figure 4.1 for further details.

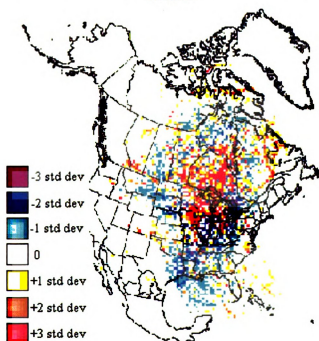


Figure 4.6. Deviation of trajectory frequencies during TC8 (PNA, NAO-, SOI-) in spring from the average springtime trajectory frequencies. See caption to Figure 4.1 for further details.

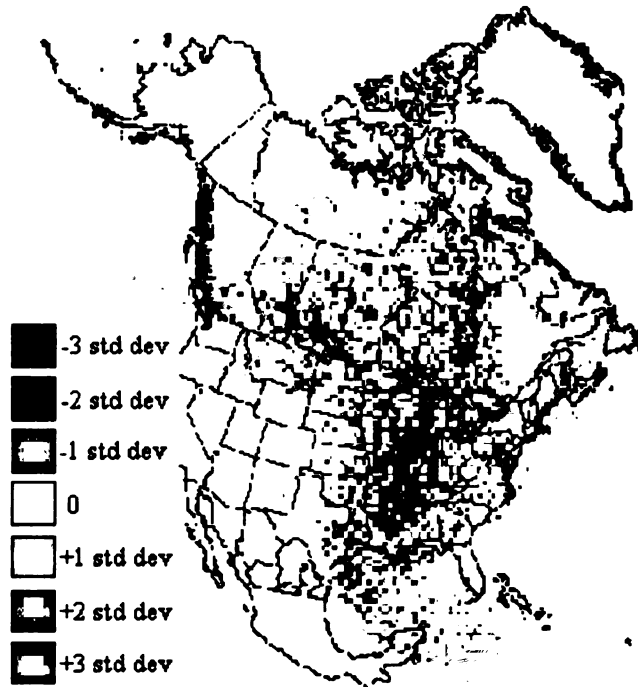


Figure 4.7. Deviation of trajectory frequencies during TC8 (PNA, NAO-, SOI-) in summer from the average summertime trajectory frequencies. See caption to Figure 4.1 for further details.

6. TC9 (PNA+, NAO, SOI)

TC9 occurred during all seasons: five occurrences in winter, eight occurrences in spring, three occurrences in summer, and eight occurrences in autumn. TC9 represents the anomalous strength of a single teleconnection (PNA+). The analysis performed by the CPC found the PNA to only be present 10 months (August-May) out of the year (CPC, 2002d). Therefore, the analysis shown below for TC9 occurrences in summer only includes events during August.

Even though the trajectory pattern differs throughout the year, a consistent increase of northerly trajectories and a decrease of southwesterly trajectories are present during all seasons. The winter (Figure 4.8) and autumn (Figure 4.11) seasons illustrate

this point well with more frequent-than-average northerly flow and decreased southerly flow. More frequent northerly flow is somewhat evident in spring (Figure 4.9) and summer (Figure 4.10), although the patterns are not as well defined during winter and autumn. The decrease in southwesterly airflow is particularly noticeable during summer and autumn. Also, an increased frequency of trajectories from the southeastern United States is evident in summer. The consequent temperature and precipitation anomalies for all seasons are -1.8°C (significant at $\alpha = .05$) and -27.7 mm (significant at $\alpha = .05$) for winter, -0.2°C and -8.6 mm for spring, -0.2°C and -28.7 mm for summer, and -1.4°C (significant at $\alpha = .05$) and -9.7 mm for autumn. The significant temperature and precipitation anomalies in winter and temperature anomaly in autumn correspond well to the seasonal airflow patterns for TC9, because increased northerly flow and decreased southwesterly flow should result in cooler, drier conditions. Additionally, previous research suggests that a positive PNA is associated with cooler, drier conditions over the Midwest and eastern United States, as a result of its associated ridge/trough pattern (Leathers et al., 1991; Rohli and Rogers, 1993).

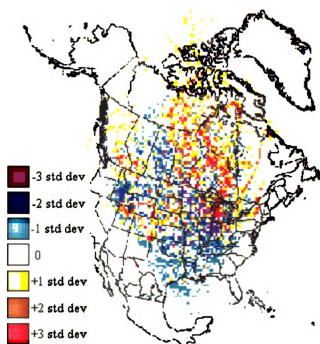


Figure 4.8. Deviation of trajectory frequencies during TC9 (PNA+, NAO, SOI) in winter from the average wintertime trajectory frequencies. See caption to Figure 4.1 for further details.

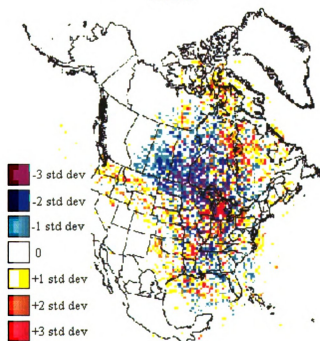


Figure 4.9. Deviation of trajectory frequencies during TC9 (PNA+, NAO, SOI) in spring from the average springtime trajectory frequencies. See caption to Figure 4.1 for further details.

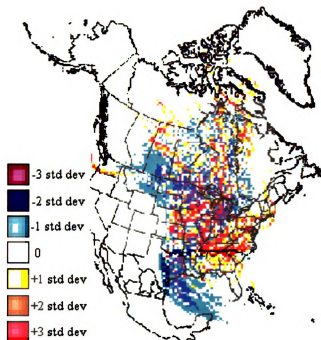


Figure 4.10. Deviation of trajectory frequencies during TC9 (PNA+, NAO, SOI) in summer from the average summertime trajectory frequencies. See caption to Figure 4.1 for further details.

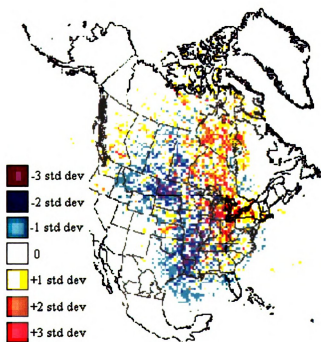


Figure 4.11. Deviation of trajectory frequencies during TC9 (PNA+, NAO, SOI) in autumn from the average autumn trajectory frequencies. See caption to Figure 4.1 for further details.

7. TC10 (PNA, NAO+, SOI)

TC10 is the positive phase of the NAO and has occurred during all seasons of the year. TC10 was most frequent in winter (14 times) and summer (11 times), compared to spring (6 times) and autumn (7 times). Winter (Figure 4.12) has a very diffuse pattern with a possibility of a stronger-than-normal southwesterly corridor. Spring (Figure 4.13) has the most clearly defined pattern with a well-defined southwesterly corridor.

Trajectories from the northwest also appear to be more frequent. Considerably fewer-than-average northerly trajectories are also evident. During summer (Figure 4.14), more easterly trajectories are present while there are fewer westerly trajectories. Also, large positive values over Michigan suggest weaker winds. Autumn (Figure 4.14) is marked by a decrease in trajectories from the south and southeast, a less-distinct decrease of trajectories from the northwest, and a modest increase in trajectories from the north and west. The resulting anomalies for temperature and precipitation include: 0.6°C and -4.1 mm for winter, 0.3°C and -11.9 mm (significant at $\alpha = .2$) for spring, 0.9°C (significant at $\alpha = .05$) and 2.3 mm for summer, and -0.7°C (significant at $\alpha = .1$) and -11.4 mm (significant at $\alpha = .2$) for autumn. Past literature suggests that a positive NAO is associated with warmer-than-normal temperatures over the eastern United States with no strong relationship to precipitation (Wallace and Gutzler, 1981; Rogers, 1984). The springtime precipitation anomaly can most likely be explained by the increased frequency of southerly trajectories. The warm summer anomaly may be due to generally weaker airflow and the fewer northwesterly trajectories for this teleconnection pattern. The

colder autumn temperatures correspond well with the less frequent southerly trajectories found on the trajectory map for autumn. The negative precipitation anomaly for autumn also agrees with the fact that fewer southerly trajectories exist.

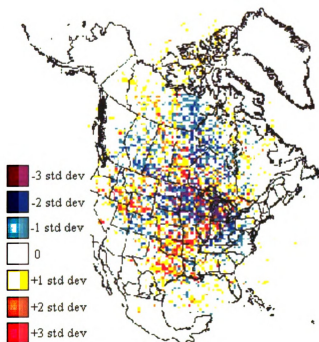


Figure 4.12. Deviation of trajectory frequencies during TC10 (PNA, NAO+, SOI) in winter from the average wintertime trajectory frequencies. See caption to Figure 4.1 for further details.

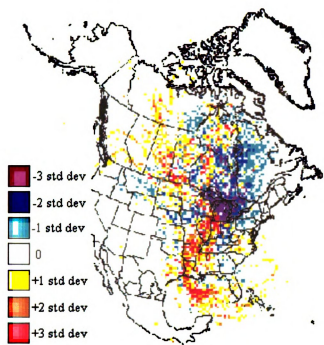


Figure 4.13. Deviation of trajectory frequencies during TC10 (PNA, NAO+, SOI) in spring from the average springtime trajectory frequencies. See caption to Figure 4.1 for further details.

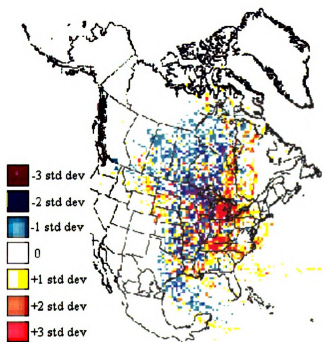


Figure 4.14. Deviation of trajectory frequencies during TC10 (PNA, NAO+, SOI) in summer from the average summertime trajectory frequencies. See caption to Figure 4.1 for further details.

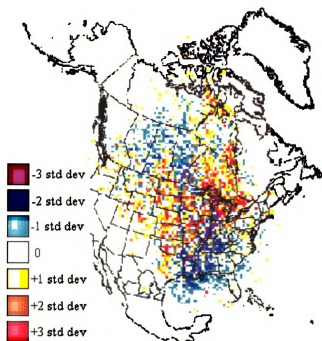


Figure 4.15. Deviation of trajectory frequencies during TC10 (PNA, NAO+, SOI) in autumn from the average autumn trajectory frequencies. See caption to Figure 4.1 for further details.

8. TC11 (PNA, NAO, SOI+)

TC11 (La Niña) occurred during all seasons with 12 occurrences in the winter months, 9 in the spring months, 7 in the summer months, and 14 in the autumn months. The winter (Figure 4.16) and spring (Figure 4.17) seasons display an increase in southwesterly flow, as well as northerly flow. Negative trajectory anomalies also surround the terminus point, which suggests faster wind speeds. Slightly cooler temperatures and higher-than-normal precipitation result with anomalies of -0.4°C and 5.8 mm for winter, and -0.2°C and 3.3 mm for spring, none of which are significant. Under TC11 (La Niña), there is typically a ridge over the western half of the continent and a trough over the eastern half (CPC, 2002c). During winter and spring, previous literature also suggests cooler and wetter conditions during the positive phase of the SO

(La Niña) (Changnon et al., 2000). Although the signs of the anomalies are in agreement with previous research, the insignificant values suggest little association between positive values of the SOI and temperature and precipitation during winter and spring in the Midwest, or at least the lower peninsula of Michigan.

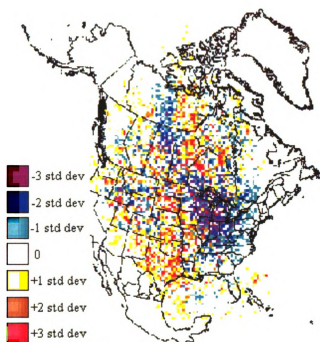


Figure 4.16. Deviation of trajectory frequencies during TC11 (PNA, NAO, SOI+) in winter from the average wintertime trajectory frequencies. See caption to Figure 4.1 for further details.

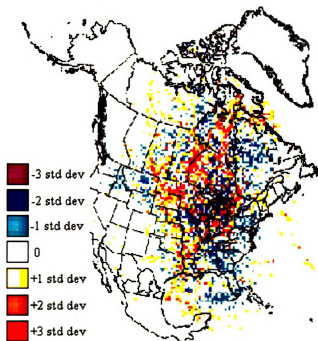


Figure 4.17. Deviation of trajectory frequencies during TC11 (PNA, NAO, SOI+) in spring from the average springtime trajectory frequencies. See caption to Figure 4.1 for further details.

During the summer (Figure 4.18) and autumn (Figure 4.19) seasons, there is a decrease in the frequency of trajectories within the northerly corridor while the southwesterly corridor remains strong. Additionally, an increase in trajectory frequency located over the southeastern United States is present during autumn. As expected under these airflow patterns, warm temperature anomalies are evident for both seasons, although the value is significant only for summer. The temperature and precipitation anomalies are 0.8°C (significant at $\alpha = .1$) and -2.3 mm summer and 0.4°C and 3.0 mm for autumn. During summer and autumn, a positive SOI value is associated with warmer, wetter conditions over the Midwest (Changnon et al., 2000). In this case, the signs of the temperature anomalies for both seasons, and the precipitation anomaly for autumn agree with previous research, although only the temperature anomaly for summer is significant.

The sign of the summer precipitation anomaly does not agree with the findings of previous authors, although the sign should be interpreted cautiously, if at all, as the precipitation anomaly is statistically insignificant. However, the statistically insignificant departures (with the exception of summer temperature) support Rogers's (1984) contention that the SO may not have as strong of a relationship with the climate of the Midwest as it does with the northwest and southeast portions of the North American continent.

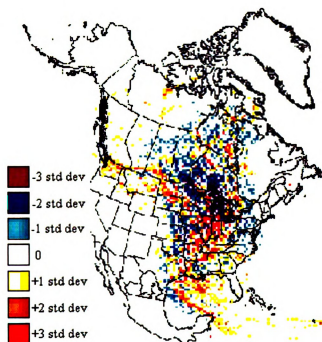


Figure 4.18. Deviation of trajectory frequencies during TC11 (PNA, NAO, SOI+) in summer from the average summertime trajectory frequencies. See caption to Figure 4.1 for further details.

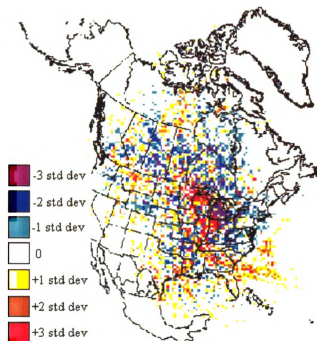


Figure 4.19. Deviation of trajectory frequencies during TC11 (PNA, NAO, SOI+) in autumn from the average autumn trajectory frequencies. See caption to Figure 4.1 for further details.

9. TC12 (PNA-, NAO, SOI)

TC12 occurred in all seasons, except summer, with five occurrences in the winter, nine in spring, and nine in autumn. The trajectory patterns for the TC12 seasons have some similarities, yet each is unique. In winter (Figure 4.20) there is an increase in node frequency to the west and southwest of the terminus point, but no defined corridor exists. Both the temperature and precipitation anomalies (-0.3°C and 3.8 mm) are insignificant. Spring (Figure 4.21) shows an increase in westerly and northwesterly node frequencies, but the temperature and precipitation anomalies of -0.4°C and 3.0 mm are also insignificant. During autumn (Figure 4.22), past research has shown a negative PNA to be related to zonal, upper-level airflow and increased precipitation into the Midwest (Leathers et al., 1991). This airflow pattern is confirmed by increased node frequencies

to the west and southwest of the terminus point for the autumn occurrences of TC12. The temperature and precipitation anomalies for autumn are 1.0°C (significant at $\alpha = .05$) and 15.0 mm. Previous literature suggests that a negative PNA is associated with warmer temperatures, and increased precipitation, which agrees with the results of this study for autumn (Wallace and Gutzler, 1981; Leathers et al., 1991).

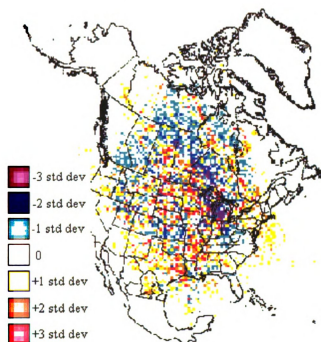


Figure 4.20. Deviation of trajectory frequencies during TC12 (PNA-, NAO, SOI) in winter from the average wintertime trajectory frequencies. See caption to Figure 4.1 for further details.

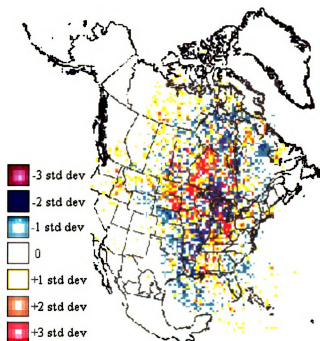


Figure 4.21. Deviation of trajectory frequencies during TC12 (PNA-, NAO, SOI) in spring from the average springtime trajectory frequencies. See caption to Figure 4.1 for further details.

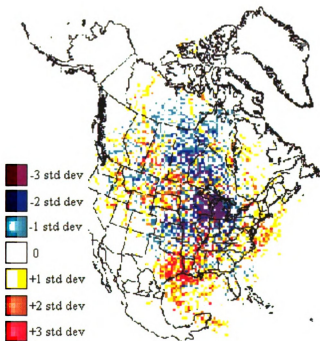


Figure 4.22. Deviation of trajectory frequencies during TC12 (PNA-, NAO, SOI) in autumn from the average autumn trajectory frequencies. See caption to Figure 4.1 for further details.

10. TC13 (PNA, NAO-, SOI)

TC13 has occurred during all seasons of the year. The number of events during the study period are: 4 occurrences during winter, 15 occurrences during spring, 8 occurrences during summer, and 7 occurrences during autumn. Compared to the mean trajectory patterns, the figures for all seasons generally show an increase in node frequency to the north/northwest of the terminus point and a decrease in node frequency to the south. This pattern is best defined in spring (Figure 4.24). The trajectory patterns alone suggest the possibility of cool and dry anomalies. Previous research also suggests that a negative NAO is associated with increased northerly upper-level airflow and cooler-than-normal temperatures (Wallace and Gutzler, 1981; Rogers, 1984). The temperature anomalies for spring (-0.6°C ; significant at $\alpha = .1$), and autumn (-1.1°C ; significant at $\alpha = .1$) are in agreement both with the decrease in southerly airflow seen on the trajectory plots and the previous research on teleconnection associations with the Midwest. In contrast, a significant positive temperature anomaly was found for winter (0.8°C ; significant at $\alpha = .2$) in spite of the well-defined increase in northerly trajectories evident on Figure 4.23. The temperature anomaly for summer (-0.2°C) was not significant, which is in line with the rather diffuse pattern seen in Figure 4.25. The only significant precipitation anomaly is the decrease found for summer (-11.4 mm ; significant at $\alpha = .2$), and can be explained by the somewhat less frequent southerly airflow during summer months with a negative NAO index value. The remaining precipitation

anomalies (13.0 mm for winter; -6.1 mm for spring, and 12.7 mm for autumn) were not significant.

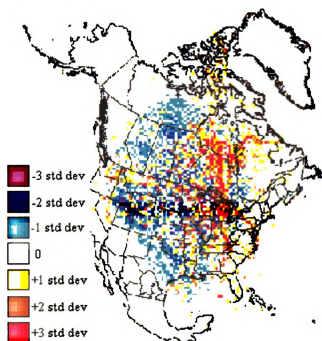


Figure 4.23. Deviation of trajectory frequencies during TC13 (PNA, NAO-, SOI) in winter from the average wintertime trajectory frequencies. See caption to Figure 4.1 for further details.

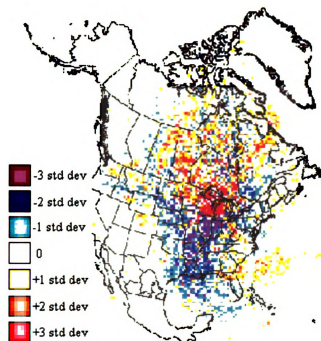


Figure 4.24. Deviation of trajectory frequencies during TC13 (PNA, NAO-, SOI) in spring from the average springtime trajectory frequencies. See caption to Figure 4.1 for further details.

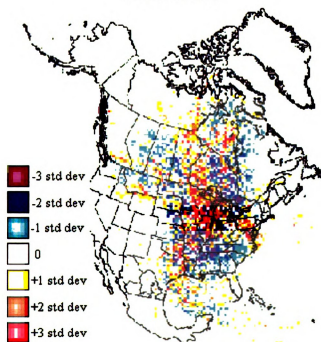


Figure 4.25. Deviation of trajectory frequencies during TC13 (PNA, NAO-, SOI) in summer from the average summertime trajectory frequencies. See caption to Figure 4.1 for further details.

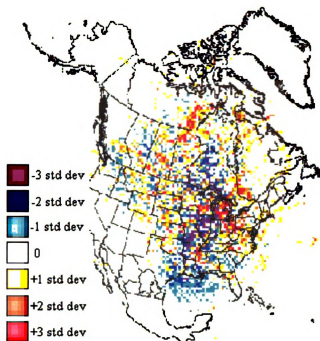


Figure 4.26. Deviation of trajectory frequencies during TC13 (PNA, NAO-, SOI) in autumn from the average autumn trajectory frequencies. See caption to Figure 4.1 for further details.

11. TC14 (PNA, NAO, SOI-)

TC14 is the negative phase of the SO (El Niño) and has occurred during all seasons. TC14 occurred 6 times during winter, 10 times during spring, 10 times during summer, and 11 times during autumn. The trajectory anomalies for TC14 differ greatly throughout the year. Winter (Figure 4.27) shows an increase in westerly and northwesterly trajectories, which surprisingly corresponds to anomalies of 1.6°C (significant at $\alpha = .1$) and 10.2 mm. Spring (Figure 4.28) displays an increase in node frequencies to the north and the south resulting in temperature and precipitation anomalies of 1.1°C (significant at $\alpha = .1$) and 14.5 mm (significant at $\alpha = .05$). Summer (Figure 4.29) shows an increase in both a defined northerly and southwesterly corridor,

with temperature and precipitation anomalies of -0.2°C and 6.9 mm (both are not significant). Lastly, autumn (Figure 4.30) primarily shows an increase in the northwesterly flow with statistically insignificant anomalies of 0.1°C and -3.0 mm.

Over the United States, El Niño is typically associated with zonal, upper-level airflow (Changnon et al., 2000), as depicted by the winter trajectory map. This situation is related to warmer temperatures and decreased precipitation in the winter and spring seasons (Changnon et al., 2000; CPC, 2002c). However, during summer and autumn, negative values of the SOI are associated with cooler, drier conditions (Changnon et al., 2000). The results of this study agree that TC14 (El Niño) is related to warmer temperatures in winter and spring, but they contradict the precipitation association since increased precipitation during winter and spring was found (although only the winter precipitation anomaly was significant). Temperature and precipitation anomalies during the summer and autumn months are insignificant. This result is not surprising for autumn, as grids cells with node frequencies above and below the seasonal average are fairly uniformly distributed across the study area. On the other hand, the lack of significant temperature and precipitation anomalies during summer is somewhat surprising given the increased frequency of southwesterly and northerly trajectories. Perhaps the opposing origins of these two primary airflow corridors contributed to the insignificant temperature and precipitation anomalies.

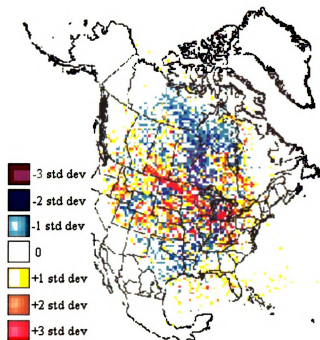


Figure 4.27. Deviation of trajectory frequencies during TC14 (PNA, NAO, SOI-) in winter from the average winter trajectory frequencies. See caption to Figure 4.1 for further details.

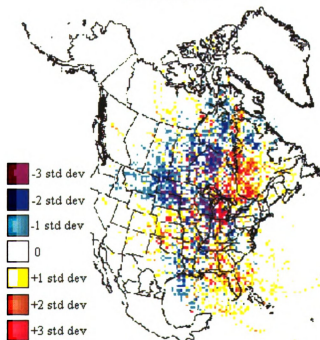


Figure 4.28. Deviation of trajectory frequencies during TC14 (PNA, NAO, SOI-) in spring from the average springtime trajectory frequencies. See caption to Figure 4.1 for further details.

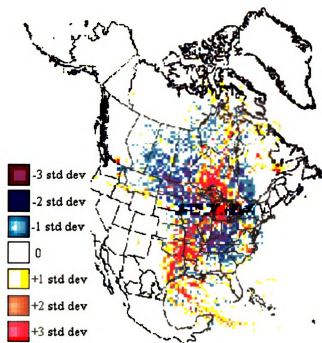


Figure 4.29. Deviation of trajectory frequencies during TC14 (PNA, NAO, SOI-) in summer from the average summertime trajectory frequencies. See caption to Figure 4.1 for further details.

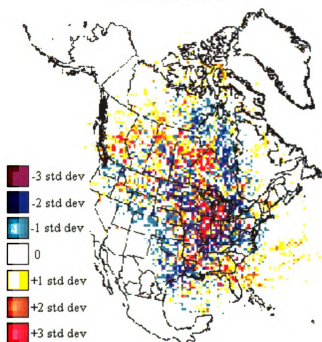


Figure 4.30. Deviation of trajectory frequencies during TC14 (PNA, NAO, SOI-) in autumn from the average autumn trajectory frequencies. See caption to Figure 4.1 for further details.

12. TC21 (PNA, NAO+, SOI-)

TC21 events were evenly distributed amongst the seasons with 5 occurrences during with winter, 5 during spring, 5 during autumn and 6 during summer. Interestingly, the trajectory patterns vary by season for this teleconnection combination, and the resulting temperature and precipitation anomalies are not consistent between months. Winter (Figure 4.31) is associated with a slight increase of trajectories from the northwest and south/southeast. The resulting temperature and precipitation anomalies are 1.8°C (significant at $\alpha = .2$) and 5.8 mm. Springtime (Figure 4.32) continues to demonstrate the strength of the northwesterly corridor and an overall increase in the frequency of westerly trajectories, while the northerly and southerly corridors have decreased numbers of trajectories. These patterns are considerably better defined for spring than for winter. The anomalies associated with spring during TC21 are 1.1°C (significant at $\alpha = .05$) and -8.1 mm. The warm anomaly is perhaps a result of the increased frequency of westerly trajectories and decreased frequency of northerly trajectories. This is in spite of the more frequent northwesterly trajectories and less frequent southerly trajectories, both of which would be expected to contribute to colder and drier than normal conditions. Past literature shows that a negative SOI (El Niño) in winter and spring is associated with zonal airflow, warmer-than-normal temperatures, and drier conditions within the Midwest (Changnon et al., 2000). Additionally, a positive NAO is associated with southerly upper-level airflow and warmer temperatures (Wallace and Gutzler, 1981; Rogers, 1984). The significant warm anomalies found here agree with previous findings, but are difficult to explain, especially in light of the decreased frequency of southerly trajectories during spring. The resulting anomalies for precipitation are both insignificant

and only in spring does the sign of the anomaly agree with the drier conditions suggested by previous literature.

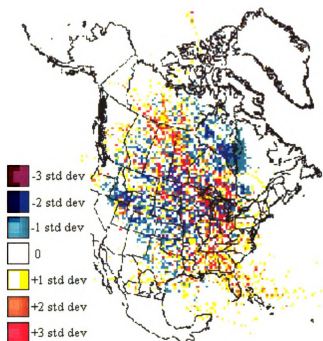


Figure 4.31. Deviation of trajectory frequencies during TC21 (PNA, NAO+, SOI-) in winter from the average wintertime trajectory frequencies. See caption to Figure 4.1 for further details.

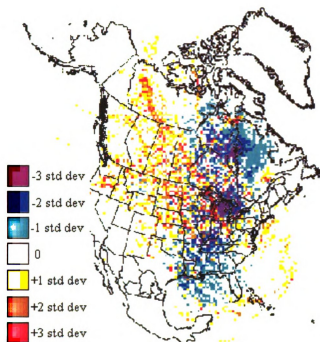


Figure 4.32. Deviation of trajectory frequencies during TC21 (PNA, NAO+, SOI-) in spring from the average springtime trajectory frequencies. See caption to Figure 4.1 for further details.

Summer (Figure 4.33) is associated with a more distinct change in the airflow. The southerly, northwesterly, and westerly corridors have decreased numbers of trajectories, but the northerly, Hudson Bay corridor strengthens. This situation would be expected to result in cooler and drier conditions in the Midwest. The resulting temperature and precipitation anomalies of -1.0°C (significant at $\alpha = .05$) and -6.6 mm (not significant) confirm the cooler conditions, but not the drier conditions, usually associated with this teleconnection combination. Another change is present in the autumn season (Figure 4.34). A northerly corridor remains evident, but a southerly/southwesterly corridor is also showing increased node frequencies. Under this airflow pattern, warmer temperatures and increased precipitation would probably be expected. The temperature anomaly is warmer than average at 0.8°C , but is not

significant. A precipitation anomaly of -19.3 mm is present; but it is also not significant. During summer and autumn of TC21, similar airflow patterns should be associated with the teleconnections as discussed for winter and spring. However, in the summer and autumn, previous research relates a negative SOI (El Niño) to cooler temperatures and drier conditions (Changnon et al., 2000), while a positive NAO is still related to warmer temperatures (Wallace and Gutzler, 1981; Rogers, 1984).

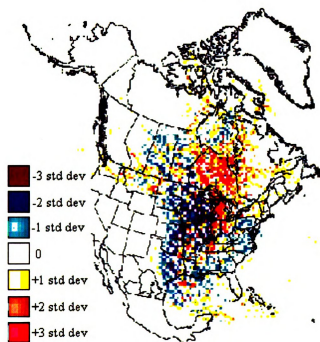


Figure 4.33. Deviation of trajectory frequencies during TC21 (PNA, NAO+, SOI-) in summer from the average summertime trajectory frequencies. See caption to Figure 4.1 for further details.

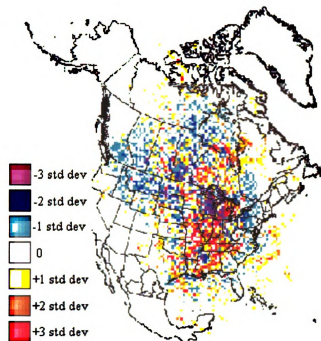


Figure 4.34. Deviation of trajectory frequencies during TC21 (PNA, NAO+, SOI-) in autumn from the average autumn trajectory frequencies. See caption to Figure 4.1 for further details.

13. TC23 (PNA+, NAO, SOI-)

TC23 has occurred seven times in the winter and six times in the spring. The winter (Figure 4.35) and spring (Figure 4.36) airflow patterns are quite similar, although the pattern for winter is more distinct. Both figures show an increase in trajectories along the northerly corridor, as well as some increased trajectories to the east of the terminus point, and, to a lesser extent, from the west. Negative node-frequency anomalies are located within the northwesterly corridor and in the Gulf of Mexico. Shorter trajectories from the south would suggest drier conditions, and fewer northwesterly trajectories would suggest warmer conditions. The resulting temperature and precipitation anomalies are 2.9°C (significant at $\alpha = .05$) and -15.0 mm (significant at $\alpha = .05$) for winter and

1.0°C (significant at $\alpha = .2$) and -4.1 mm for spring, confirm the prediction of warmer, drier conditions. The only exception is the insignificant (-4.1 mm) precipitation anomaly for spring. A positive phase of the PNA and negative phase of the SO (El Niño) is an unlikely pairing because a positive PNA is usually associated with increased ridging over the western part of the continent (Leathers et al., 1991; Rohli and Rogers, 1993), while a negative SO is associated with a weakening of the ridge, and therefore, associated with more zonal airflow (Changnon et al., 2000). Additionally, a positive PNA is related to cooler temperatures (Leathers et al., 1991; Rohli and Rogers, 1993) and a negative SOI is associated with warmer temperatures (Changnon et al., 2000), although both teleconnections are related to drier-than-normal conditions during winter and spring. For the TC23 a case in this study, the temperature pattern agrees more closely with that expected under a negative SOI.

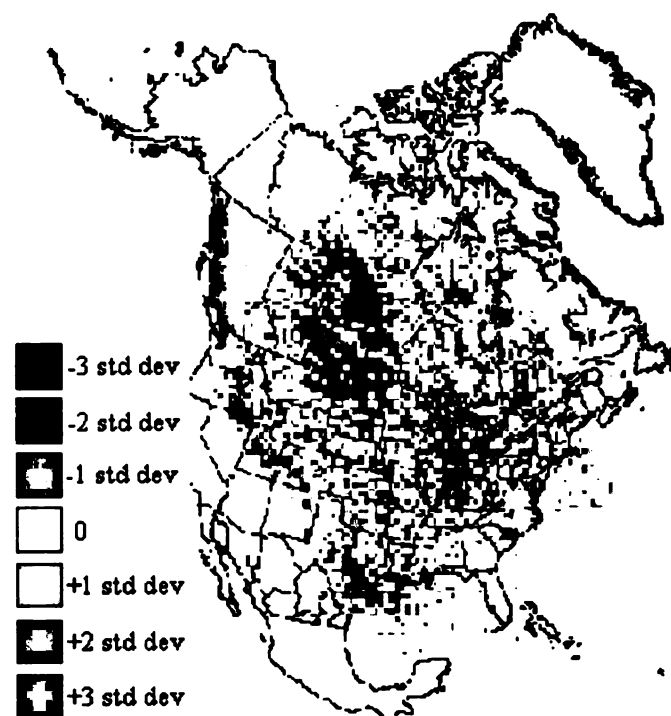


Figure 4.35. Deviation of trajectory frequencies during TC23 (PNA+, NAO, SOI-) in winter from the average wintertime trajectory frequencies. See caption to Figure 4.1 for further details.

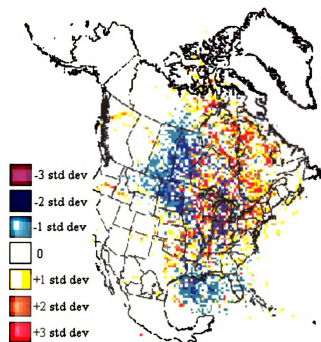


Figure 4.36. Deviation of trajectory frequencies during TC23 (PNA+, NAO-, SOI-) in spring from the average springtime trajectory frequencies. See caption to Figure 4.1 for further details.

14. TC25 (PNA+, NAO-, SOI)

In the past, TC25 occurred five times in winter and three times in autumn. Winter (Figure 4.37) shows an increased number of trajectories within the northwesterly corridor with a decreased number of trajectories within the southwesterly corridor. This airflow pattern would be expected to be associated with cooler temperatures and drier conditions. As expected, the anomalies are significant with a temperature anomaly of -4.0°C (significant at $\alpha = .05$) and a precipitation anomaly of -20.1 mm (significant at $\alpha = .1$). However, when TC25 occurs during the autumn months (Figure 4.38) the northwesterly airflow pattern is not as well defined. Therefore, the resulting anomalies in temperature

and precipitation are not as significant at 0.3°C and 2.3 mm. Previous literature states that both a positive PNA and a negative NAO are associated with cooler temperatures and drier conditions over the Midwest (Wallace and Gutzler, 1981; Rogers, 1984; Leathers et al., 1991; Rohli and Rogers, 1993). This is in agreement with the trajectories and anomaly patterns presented here for the winter months, but not for the autumn months.

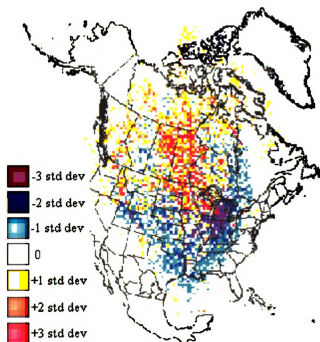


Figure 4.37. Deviation of trajectory frequencies during TC25 (PNA+, NAO-, SOI-) in winter from the average wintertime trajectory frequencies. See caption to Figure 4.1 for further details.

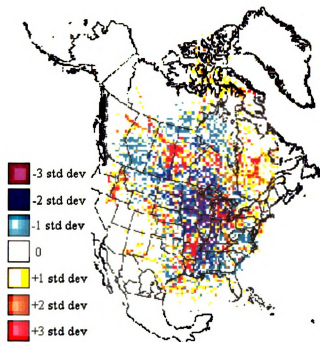


Figure 4.38. Deviation of trajectory frequencies during TC25 (PNA+, NAO-, SOI) in autumn from the average autumn trajectory frequencies. See caption to Figure 4.1 for further details.

15. TC27 (PNA, NAO, SOI)

TC27 is a general pattern where all three of the teleconnection indices are weak (> -1.0 and < 1.0), and is the most frequently occurring teleconnection combination. During the study period, TC27 occurred 25 times in winter, 30 times in spring, 52 times in summer, and 36 times in autumn. Although the following figures for TC27 do show some airflow patterns, it is important to understand that this teleconnection combination occurred much more frequently than the other combinations and that the colors on the figures are depicted by standard deviation. Therefore, the figures for TC27 have a much smaller standard deviation compared to the other combinations, so any minor airflow anomaly will appear more pronounced. As expected, the resulting temperature and

precipitation anomalies are very small and insignificant. The anomalies are -0.2°C and 0.0 mm for the winter, 0.2°C and -0.5 mm for the spring, -0.1°C and 1.3 mm for the summer, and -0.1°C and -4.1 mm for the autumn.

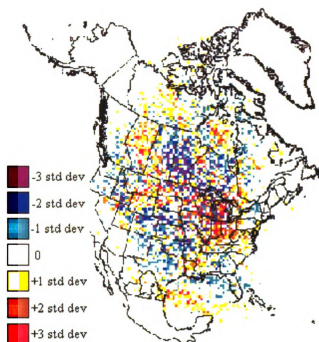


Figure 4.39. Deviation of trajectory frequencies during TC27 (PNA, NAO, SOI) in winter from the average wintertime trajectory frequencies. See caption to Figure 4.1 for further details.

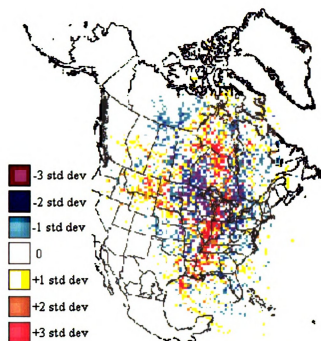


Figure 4.40. Deviation of trajectory frequencies during TC27 (PNA, NAO, SOI) in spring from the average springtime trajectory frequencies. See caption to Figure 4.1 for further details.

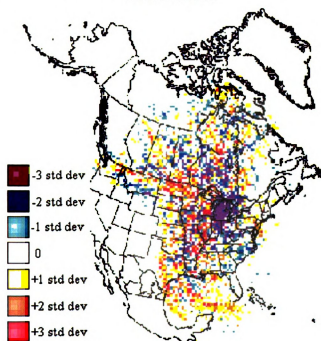


Figure 4.41. Deviation of trajectory frequencies during TC27 (PNA, NAO, SOI) in summer from the average summertime trajectory frequencies. See caption to Figure 4.1 for further details.

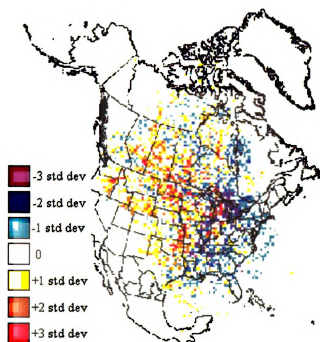


Figure 4.42. Deviation of trajectory frequencies during TC27 (PNA, NAO, SOI) in autumn from the average autumn trajectory frequencies. See caption to Figure 4.1 for further details.

16. Summary

Chapter 4 considered 27 teleconnection combinations and then analyzed each combination by season. Trajectories were plotted for the months of each combination in order to display the resulting low-level airflow anomalies. Associations were then discussed between the teleconnection combinations and seasonal airflow, temperature, and precipitation anomalies. A statistical, one-sample t-test was performed in order to determine the statistical significance of the temperature and precipitation anomalies. A discussion and summary of the teleconnection analyses will be presented in Chapter 5. Limitations in the study and suggested future work will also be discussed.

CHAPTER 5

DISCUSSION AND CONCLUSION

1. Overview

The research project presented here had two objectives: the first being the construction of a five-day back-trajectory climatology of a location in the lower peninsula of Michigan, and the second being an investigation of the associations between atmospheric teleconnections, low-level airflow, and local temperature and precipitation anomalies. Chapter 5 includes a discussion of the results, the limitations of the study, and suggestions for further research on the topics.

2. Discussion of the Research Questions

In Chapter 1, five research questions concerning the trajectory climatology and the association of atmospheric teleconnections with the climate of the lower peninsula of Michigan were presented. Each of the research questions will now be addressed and discussed based on the results found in this study and compared with the results of previous research.

(1) Based on an isobaric trajectory model using the NCEP/NCAR reanalysis wind data, what are the major airflow source regions and how do they vary by month?

The primary low-level sources of low-level airflow into lower Michigan throughout the year tend to be northwesterly and southwesterly. However, a distinct

annual pattern in the airflow is present. The winter season experiences more frequent westerly and northwesterly airflow. During spring, an increase in trajectories is located within a northerly corridor originating over the Hudson Bay region. The westerly and northwesterly corridors are weaker, showing a decreased number of trajectories during spring. As summer arrives, an overall increase in the southwesterly airflow is noticeable. A very distinct southwesterly corridor, which originates over the Gulf of Mexico, is present. Lastly, the autumn months are associated with another transition, as the southwesterly airflow decreases in frequency and the westerly and northwesterly airflow is more frequent once again.

(2) How does the trajectory climatology presented here differ from the climatology previously presented by Waller (1999), which used a different data source, a shorter time period, and a location in northwest Ohio (41.56° N, 84.09° W)?

One of the primary objectives of this study was to conduct an air-parcel trajectory climatology to improve the trajectory accuracy of Waller's (1999) previous study. Improvement was attempted in four ways. First, Waller's study used a data set from the NMC, whereas this study used a different, more recent data set from NCEP/NCAR in order to increase the spatial and temporal resolution. The NMC data have a spatial resolution of 381 km at 60° N (Jenne, 1975). However, the NCEP/NCAR reanalysis data have a spatial resolution of 2.5° by 2.5°, or approximately 277.5 km, if 111 km per degree latitude is assumed (Robinson et al., 1978; Dent, 1999). Second, the temporal resolution of the data sets was also different. The NMC data have a resolution of 12

hours, whereas the NCEP/NCAR reanalysis data have a resolution of six hours. Third, the NMC data include periods of “missing” data; however, the NCEP/NCAR reanalysis fields are model-derived so that no “missing” data are present. Lastly, a 40-year climatology of trajectories was conducted in this study, versus only a 10-year climatology in Waller’s (1999) study. Other differences in the two studies existed as well. For instance, a study location of 42.5° N and 85.0° W in lower Michigan was used in this study, but a study location of 41.56° N and 84.09° W in northwest Ohio was used in Waller’s (1999) climatology. Additionally, this study used a pressure level of 925 hPa, whereas Waller used the 850 hPa level.

The results of this study show some very distinct patterns in airflow. Some of the patterns match the results found in the previous work by Waller (1999), while other patterns found are quite different. During winter, Waller’s results agreed with those of this study, in that westerly and northwesterly airflow was the most dominant. However, the northwesterly corridor in her study often had a slightly more northerly orientation compared to this study. Additionally, her study did not depict the strong presence of a southwesterly corridor. Some southwesterly trajectories were present, but originated from the southwestern United States and Baja California rather than the Gulf of Mexico region.

Throughout the spring months, Waller (1999) showed an increased frequency of trajectories within a northerly, Hudson Bay corridor, which agreed with this study. In contrast, the increased number of southwesterly trajectories depicted during spring in this study was not evident in Waller’s study.

During all summer months, Waller's study varied substantially from this study in that she found a persistent northwesterly corridor with an absence of a defined southwesterly corridor. This study did show a large number of trajectories to the north and northwest of the terminus point (42.5° N, 85.0° W); however, the most noticeable airflow corridor was a southwesterly corridor originating from the Gulf of Mexico and spanning into lower Michigan.

Throughout autumn, the two studies were similar, both showing weak organization of the airflow corridors. Surprisingly, September was the only month where Waller's study (1999) suggested a southwesterly corridor, whereas the southwesterly corridor in this study began to diminish during that month. During autumn, both studies illustrated a strengthening of the northwesterly corridor.

(3) Does the low-level circulation, as depicted by back trajectories, differ from the mean circulation in the upper Midwest during months of strong, singly or co-existing teleconnection patterns?

Virtually no previous research has singled out and discussed the atmospheric teleconnection association with low-level airflow within the Midwest region of the United States. Some studies have presented temperature and precipitation associations or have discussed general airflow patterns across the United States (Wallace and Gutzler, 1981; Rogers, 1984; Leathers et al., 1991; Assel, 1992; Rohli and Rogers, 1993; Serreze et al., 1998; Changnon et al., 2000; Hu and Feng, 2001b). However, this study used an isobaric trajectory model to calculate the frequency and source regions of airflow

trajectories for the lower peninsula of Michigan in an effort to link the planetary-scale teleconnections to the local-scale climate anomalies of temperature and precipitation. Chapter 4 presented a number of teleconnection combinations and discussed the resulting airflow patterns associated with each. The results showed that the PNA, NAO, and SO teleconnections do have a relationship with the overall low-level circulation within the study region. Additionally, the low-level airflow patterns found here generally agree with the upper-level airflow results of previous literature. This suggests that teleconnection indices can be used in further work to forecast medium to long-range climate for the upper Midwest.

The current study strove to go beyond the work of previous research by considering “combinations” of co-existing, strong teleconnections. Previous literature on teleconnections has related single teleconnections to climate anomalies, but has not succeeded in going the additional step to consider the combined associations with multiple teleconnections. In this study, atmospheric teleconnection associations with airflow and climate anomalies were shown to differ under co-existing teleconnection combinations. Thus, this study has supported the idea that each of the teleconnection combinations needs to be considered when using teleconnections in future studies in order to more accurately understand any resulting perturbations in climate. Since three teleconnections were used, 27 combinations needed to be studied. Not all 27 combinations occurred frequently over the 40-year study period, but enough combinations were present to observe and compare the results of co-existing atmospheric teleconnections. For this study in lower Michigan, the overall airflow anomalies associated with the atmospheric teleconnections are as follows in Table 5.1:

Table 5.1. Summary of atmospheric teleconnection association with low-level airflow.

Teleconnection Combination	Code	Season	Distinctiveness of trajectory anomaly pattern (Subjectively determined based on spatial coherence of the grid cells with above or below average number of nodes)	Directions with more frequent trajectories compared to average seasonal pattern	Directions with less frequent trajectories compared to average seasonal pattern
PNA+, NAO+, SOI	TC2	spring	high	north, southwest	northwest, east
PNA, NAO+, SOI+	TC4	winter	high	west, northwest, southwest	north
PNA-, NAO-, SOI	TC6	winter	low	northwest, southwest	north, northeast
PNA-, NAO-, SOI	TC6	spring	medium	northwest, northeast	south, southwest
PNA, NAO-, SOI-	TC8	winter	medium	north	west, southwest
PNA, NAO-, SOI-	TC8	spring	medium	north	south, west
PNA, NAO-, SOI-	TC8	summer	medium	northwest	south
PNA+, NAO, SOI	TC9	winter	medium	north	southwest, west
PNA+, NAO, SOI	TC9	spring	medium		northwest
PNA+, NAO, SOI	TC9	summer	medium	southeast (shorter trajectories)	southwest, west
PNA+, NAO, SOI	TC9	autumn	high	north	southwest, west
PNA, NAO+, SOI	TC10	winter	low	southwest	
PNA, NAO+, SOI	TC10	spring	high	southwest, northwest	north
PNA, NAO+, SOI	TC10	summer	medium	southeast, northeast (shorter trajectories)	northwest, southwest
PNA, NAO+, SOI	TC10	autumn	medium	north, west	south, southeast, northwest
PNA, NAO, SOI+	TC11	winter	medium	southwest, north (longer trajectories)	southeast, east

Table 5.1 (cont'd).

PNA, NAO, SOI+	TC11	spring	medium	north, northwest, southwest	southeast
PNA, NAO, SOI+	TC11	summer	medium	southwest	northwest
PNA, NAO, SOI+	TC11	autumn	low	southeast	north, northeast
PNA-, NAO, SOI	TC12	winter	low	west, southwest	
PNA-, NAO, SOI	TC12	spring	low	northwest	southwest
PNA-, NAO, SOI	TC12	autumn	medium	southwest	north
PNA, NAO-, SOI	TC13	winter	medium	north, southeast	west, northwest, southwest
PNA, NAO-, SOI	TC13	spring	high	north, northwest	south, southwest
PNA, NAO-, SOI	TC13	summer	low	northwest	southeast, south
PNA, NAO-, SOI	TC13	autumn	low	northwest, north	south
PNA, NAO, SOI-	TC14	winter	medium	west	southwest, north
PNA, NAO, SOI-	TC14	spring	medium	northeast, southeast	west, northwest
PNA, NAO, SOI-	TC14	summer	high	southwest, north	northwest, southeast
PNA, NAO, SOI-	TC14	autumn	low	northwest	
PNA, NAO+, SOI-	TC21	winter	low	southeast, south, northwest	west
PNA, NAO+, SOI-	TC21	spring	high	northwest, west	north, south
PNA, NAO+, SOI-	TC21	summer	high	north	southwest, south
PNA, NAO+, SOI-	TC21	autumn	medium	south, north	west
PNA+, NAO, SOI-	TC23	winter	high	north, east	northwest
PNA+, NAO, SOI-	TC23	spring	medium	north, east	northwest
PNA+, NAO-, SOI	TC25	winter	high	northwest	southwest, west
PNA+, NAO-, SOI	TC25	autumn	low		
PNA, NAO, SOI	TC27	winter	low		
PNA, NAO, SOI	TC27	spring	low		
PNA, NAO, SOI	TC27	summer	low		
PNA, NAO, SOI	TC27	autumn	low		

Of the 42 seasonal teleconnection combinations with three or more monthly occurrences, 10 had very “distinct” (high) airflow anomalies, 18 had “moderately distinct” (medium) airflow anomalies, and 14 had “diffuse” (low) patterns. Of the 10

combinations with distinct airflow patterns, four were single teleconnections and six were co-existing teleconnection combinations. All but one (SOI- in summer) were associated with either a significant temperature or precipitation anomaly. Thus, teleconnections (occurring singly or co-existing) associated with distinct airflow patterns have considerable utility in medium and long-range weather forecasting. Additionally, four combinations were associated with a statistically significant cold anomaly and four were associated with a statistically significant warm anomaly, while three were associated with a significant dry anomaly and one was associated with a significant wet anomaly. Therefore, teleconnection combinations with distinct airflow anomaly patterns have a greater probability to be associated with temperature anomalies than precipitation anomalies. Teleconnection combinations with distinct airflow anomaly patterns are also have a greater probability to be associated with a dry anomaly than a wet anomaly, while there is an equal likelihood of a warm or cold temperature anomaly. The two distinct airflow anomaly patterns that did not have significant temperature anomalies were characterized by increases in trajectories from generally “opposite” or opposing directions (e.g., northwest and southwest for TC10 in spring). As a result, the study area would be influenced by contrasting air masses resulting in a near zero temperature anomaly. However, there probably is considerable daily temperature variability (or day-to-day temperature swings) during TC10 in spring and TC14 in summer. Lastly, the 10 combinations with distinct airflow patterns are approximately equally distributed across seasons, which is a useful point for medium and long-range predictions.

Of the 18 teleconnection combinations with “moderately distinct” airflow anomalies, 12 had a significant temperature or precipitation anomaly. Therefore,

teleconnection patterns with “moderately distinct” patterns also have potential for medium and long-range predictions. Warm anomalies are more likely to be associated with “moderately distinct” airflow anomaly patterns; only four of the teleconnection combinations had negative (cold) temperature anomalies whereas seven had positive (warm) temperature anomalies. Additionally, there were three dry anomalies, while only one wet anomaly. Of the 18 teleconnection combinations with “moderately distinct” airflow anomalies, 13 were single teleconnection patterns and five were co-existing (two or more) strong teleconnections. Also, there were somewhat more occurrences in spring and winter: spring (6), winter (5), summer (4), and autumn (3).

Diffuse airflow anomaly patterns are not expected to be associated with as many significant temperature and precipitation anomalies, since no defined, anomalous airflow is present. In general, this was true, but there were three exceptions: TC13 summer, TC13 autumn, and TC21 winter. Furthermore, most of the teleconnection combinations with diffuse trajectory patterns were single teleconnections rather than co-existing teleconnection combinations.

(4) During months of anomalous circulation associated with teleconnections, can relationships be drawn between the trajectory patterns and trajectory frequencies with local-scale climate, as depicted by temperature and precipitation anomalies?

As discussed in Chapter 2, one method to test the significance of the temperature and precipitation anomalies is by the use of a statistical, one-sample t-test. The test is simply a way to give a value to how much a particular anomaly deviates from the

expected mean of the 40-year climatology for that particular season. Alpha (α) values of .05, .1, and .2 were used to demonstrate three levels of significance. Typically, studies use values of .05 and .1. However, in some cases where the samples are small, it is permissible to use a lower significance criterion such as .2. The significance of the temperature and precipitation anomalies is particularly important to this study because to demonstrate a strong association of the atmospheric teleconnections with climate anomalies, a statistically significant result is crucial. For many of the teleconnection combinations, the sign of the temperature and precipitation anomalies corresponded to what was expected based on earlier teleconnection analyses for the Midwest. However, the statistically significant associations provide further support that the relationship could be causal. Table 5.2 displays all teleconnection combinations and the corresponding seasons that have statistically significant temperature and/or precipitation anomalies.

Table 5.2. Statistically significant temperature (°C) and precipitation (mm) anomalies for the 27 teleconnection combinations by seasonal groupings (where: *** is significant at $\alpha = .05$; ** is significant at $\alpha = .1$; and * is significant at $\alpha = .2$).

TC #	Win Temp	Win Precip	Spr Temp	Spr Precip	Sum Temp	Sum Precip	Aut Temp	Aut Precip
1								
2			warm***					
3								
4	warm**	wet*						
5								
6			cold***					
7								
8	cold*					dry**		
9	cold***	dry***					cold***	
10				dry*	warm***		cold**	dry*
11					warm**			
12							warm*	
13	warm*		cold**			dry*	cold**	
14	warm**		warm**	wet***				
15								
16								
17								
18								
19								
20								
21	warm*		warm***		cold***			
22								
23	warm***	dry***	warm*					
24								
25	cold***	dry**						
26								
27								

Table 5.2 shows that a large number of the climate anomalies were significant. In fact, out of the 42 seasonal teleconnection combinations studied, 21 out of 42 had a significant temperature anomaly, while nine out of 42 had significant precipitation anomalies. This supports previous research on teleconnections, because associations with

temperature have been strong while associations with precipitation have been weak (Wallace and Gutzler, 1981; Rogers, 1984; Leathers et al., 1991; Assel, 1992; Serreze et al., 1998). In addition, it is important to consider whether the sign of any of the temperature and/or precipitation anomalies shown in Table 5.2 differ from what would be expected given the findings of previous studies. As an example, was there ever a significantly cold anomaly during a positive NAO when temperatures are expected to be warmer than normal? Out of the 21 significant temperature anomalies, only two were significant of the opposite sign. For precipitation, one out of the nine was significant of the opposite sign. The occurrences include: summer temperature for TC10, winter temperature for TC13, and spring precipitation for TC14. Since these occurrences were infrequent, it is reassuring that the majority of significant anomalies were in support of what was expected.

The results of this study show that although the relationships between temperature and precipitation relationships and the PNA, NAO, and SO teleconnections patterns are often strong, but not always the case. Twenty-four of the single or co-existing teleconnection combinations had significant temperature and/or precipitation anomalies, while 18 of the single or co-existing teleconnections that occurred at least three times during the study period did not have significant temperature or precipitation anomalies. Thus, not all teleconnection combinations are likely to be important in medium and long-range forecasting. The temperature and precipitation associations with the atmospheric teleconnections are summarized in Table 5.3.

Table 5.3. Summary of atmospheric teleconnection association with temperature and precipitation anomalies.

Teleconnection Combination	Code	Season	Temperature Anomaly (only significant anomalies alpha=.20 or smaller)	Precipitation anomaly (significant only, alpha =.20 or smaller)
PNA+, NAO+, SOI	TC2	spring	warm	
PNA, NAO+, SOI+	TC4	winter	warm	wet
PNA-, NAO-, SOI	TC6	winter		
PNA-, NAO-, SOI	TC6	spring	cold	
PNA, NAO-, SOI-	TC8	winter	cold	
PNA, NAO-, SOI-	TC8	spring		
PNA, NAO-, SOI-	TC8	summer		dry
PNA+, NAO, SOI	TC9	winter	cold	dry
PNA+, NAO, SOI	TC9	spring		
PNA+, NAO, SOI	TC9	summer		
PNA+, NAO, SOI	TC9	autumn	cold	
PNA, NAO+, SOI	TC10	winter		
PNA, NAO+, SOI	TC10	spring		dry
PNA, NAO+, SOI	TC10	summer	warm	
PNA, NAO+, SOI	TC10	autumn	cold	dry
PNA, NAO, SOI+	TC11	winter		
PNA, NAO, SOI+	TC11	spring		
PNA, NAO, SOI+	TC11	summer	warm	
PNA, NAO, SOI+	TC11	autumn		
PNA-, NAO, SOI	TC12	winter		
PNA-, NAO, SOI	TC12	spring		
PNA-, NAO, SOI	TC12	autumn	warm	
PNA, NAO-, SOI	TC13	winter	warm	
PNA, NAO-, SOI	TC13	spring	cold	
PNA, NAO-, SOI	TC13	summer		dry
PNA, NAO-, SOI	TC13	autumn	cold	
PNA, NAO, SOI-	TC14	winter	warm	
PNA, NAO, SOI-	TC14	spring	warm	wet
PNA, NAO, SOI-	TC14	summer		
PNA, NAO, SOI-	TC14	autumn		
PNA, NAO+, SOI-	TC21	winter	warm	
PNA, NAO+, SOI-	TC21	spring	warm	
PNA, NAO+, SOI-	TC21	summer	cold	
PNA, NAO+, SOI-	TC21	autumn		
PNA+, NAO, SOI-	TC23	winter	warm	dry
PNA+, NAO, SOI-	TC23	spring	warm	
PNA+, NAO-, SOI	TC25	winter	cold	dry
PNA+, NAO-, SOI	TC25	autumn		
PNA, NAO, SOI	TC27	winter		
PNA, NAO, SOI	TC27	spring		
PNA, NAO, SOI	TC27	summer		
PNA, NAO, SOI	TC27	autumn		

Some reoccurring patterns with the co-existing teleconnections are evident. Nine of the 15 co-existing teleconnection combinations had a significant temperature or precipitation anomaly. All but two (TC23 winter and TC23 spring) of the co-existing teleconnection combinations included either a strong positive or strong negative NAO. Additionally, all but five of the combinations (TC2 spring, TC6 winter, TC6 spring, TC25 winter, TC25 autumn) included either a strong positive or strong negative SOI. The NAO tends to present a stronger relationship with temperature than it does with precipitation. Furthermore, under circumstances when the NAO and another teleconnection suggested the same temperature prediction, a statistically significant temperature anomaly would usually result. Ironically, when the NAO was present during neutral phases of the PNA and SO, the resulting temperature anomalies were not as statistically significant.

As previous research has demonstrated, it is also important to consider atmospheric teleconnections singly. A positive PNA occurred in all seasons of the year, and was associated with trajectory anomaly patterns that had moderately distinct to distinct airflow anomalies. However, only in winter and autumn were the temperature anomalies significant. Both were cold anomalies associated with an increased frequency of low-level northerly trajectories and decreased frequency of low-level southerly and southwesterly trajectories. In winter, a positive PNA is also associated with a dry anomaly, which also makes sense given the smaller number of southwesterly trajectories and larger number of northerly trajectories.

A negative PNA occurred in all seasons except summer, but the trajectory anomaly patterns were not as distinct as they were for a positive PNA pattern. In autumn, the negative PNA was associated with a significantly warm temperature anomaly, which corresponds well with the more frequent trajectories from the southwest.

A positive NAO occurred in all seasons. All seasons, except winter, had a significant temperature or precipitation anomaly. Also, a positive NAO in spring and autumn is associated with dry conditions. Interestingly, in summer, a positive NAO is associated with more frequent southerly trajectories and a warm anomaly, and in autumn associated with more frequent northerly trajectories and a cold anomaly. This result indicates that a teleconnection can be associated with different low-level airflow patterns (and different temperature anomalies) in different seasons.

A negative NAO also occurred in all seasons. All seasons had a significant temperature or precipitation anomaly, even if the trajectory anomaly pattern was not distinct. Again, there were contrasting patterns depending on the season. In winter, there was a warm anomaly (north, southeasterly trajectories), whereas in spring and autumn, there was a cold anomaly (north, northwesterly trajectories). The dry anomaly in summer may be a response to increased northwesterly trajectories. Overall, the results suggest that the relationship between the NAO and low-level airflow, temperature, and precipitation in the lower peninsula of Michigan is complex.

Positive values for the SOI occurred in all seasons. Despite moderately distinct airflow anomaly patterns in winter, spring, and summer, a significantly warm temperature anomaly occurred only in summer.

A negative SOI is associated with increased westerly trajectories and a warm anomaly in winter. Increased easterly trajectories along with warm and wet anomalies existed in spring. In summer, there was increased airflow from opposing directions, which may have led to considerable variation in temperature and moisture during this season.

(5) Does the association of single or co-existing teleconnections with airflow trajectories and local-scale temperature and precipitation vary by season?

By taking the 27 teleconnection combinations and grouping them by season, 108 possible teleconnection situations could be studied. However, not all 108 situations occurred. In fact, only 42 were present three or more months during a particular season throughout the 40-year study period. Additionally, not all combinations occurred in all seasons. The patterns can be seen from Table 2.5 in Chapter 2. Some combinations occurred in only one season, some occurred in all seasons, and some occurred in a combination of seasons. The resulting airflow, temperature, and precipitation anomalies were not always consistent across the seasons of a particular teleconnection combination. As a result, researchers should consider a small time scale, of a season or less, when suggesting relationships about atmospheric teleconnections and climate.

As stated previously, the associations of the teleconnections with the temperature anomalies are stronger than the associations with the precipitation anomalies. Table 5.2 shows this well by the distribution of the statistically significant anomalies. A seasonal pattern is evident for both the temperature and precipitation anomalies, with significant

anomalies more likely to occur in winter and spring. In terms of significant temperature anomalies, eight teleconnection combinations had significant anomalies in winter, six in spring, three in summer, and four in autumn. In terms of significant precipitation anomalies, four teleconnection combinations had significant anomalies in winter, two in spring, two in summer, and one in autumn. Previous literature has also suggested that the associations of teleconnections with climate are strongest during the cooler seasons (Rogers, 1984, 1985; Leathers et al., 1991; Hastenrath and Greischar, 2001). Seasonal differences in the frequency of the teleconnection combinations were also evident. Table 2.5 from Chapter 2 shows many more neutral teleconnection values (TC27) during the summer (52 occurrences) compared to winter (25 occurrences). The disparity suggests that the teleconnections are more likely to have stronger values during the cooler months than in the warmer months of the year.

3. Limitations of the Study

As with any scientific study, some shortcomings of the research need to be addressed. The first area of concern is the possible issue in using the NCEP/NCAR reanalysis data. Even though the reanalysis fields have a higher spatial and temporal data resolution than the NWS rawinsonde observations, the reanalysis data are model-derived, and are therefore, not exactly “real” data that have been measured. However, as discussed in Chapter 2, because the reanalysis wind fields are Type A variables, they are heavily dependent on the NWS observations. Consequently, the reanalysis fields also reflect any erroneous data that may be present within the NWS rawinsonde observations. Research is currently underway to find and discuss the errors within the rawinsonde wind

observations, but has yet to be published in the refereed literature (see Van Ravensway et al., 2003; Winkler, 2004 for preliminary discussions).

An additional area of concern includes the data resolution. Despite the fact that this study has increased both the spatial and temporal resolution of the air-parcel trajectory model compared to the earlier study conducted by Waller (1999), there is concern whether this resolution is sufficient. The NCEP/NCAR reanalysis fields still only have a temporal resolution of six hours. Therefore, when the isobaric trajectory model used in this study calculated the three-hour nodes, some interpolation was required. Any further interpolation to a finer temporal scale more than likely would have increased, rather than decreased, trajectory error. Vertical resolution is also an issue because this study was limited only to the 925 hPa level. Even though this level is a good representation for the low-level airflow within the study area, low-level airflow is obviously not limited only to the 925 hPa level. Additional trajectory analyses could have been carried out for other pressure levels. However, this also shows the data resolution limits of the NCEP/NCAR reanalysis fields because data are only available at the 1000, 925, 850, 700, 500, 400, 300, 250, 200, 150, 100, 70, 50, 30, 20, 10, and 3 hPa levels. Another resolution issue is the number of study locations. The study used a single location in lower Michigan (42.5° N, 85.0° W) because of the time-consuming analysis. The inclusion of additional study points could be beneficial to represent the airflow for other areas and capture possible regional associations with teleconnections.

Other limiting issues in this study involve the use of the atmospheric teleconnections. Due to the large number of possible “combinations,” only the three most previously studied teleconnections were considered (NAO, PNA, and SO).

However, according to the CPC, even without considering the SO, at least 14 different teleconnections exist within the Northern Hemisphere. In order to obtain a more thorough representation of the teleconnection associations with airflow, temperature, and precipitation anomalies, all teleconnections need to be considered. Furthermore, only one data set for the SO was used in this study. Various methods of measuring the SO indices exist and can also be used in place of the traditional Tahiti-Darwin SOI.

Atmospheric teleconnection data from the CPC are limiting in that they were not collected or analyzed prior to 1950. Despite the fact that this study used a longer study period than many previous studies, still, only a 40-year period was used (1960-1999). As a result, some teleconnection combinations occurred very infrequently, and therefore, the one-sample t-tests were often based on small sample sizes. Larger sample sizes would lend increased support to the relationships between the atmospheric teleconnections and the temperature and precipitation anomalies.

4. Future Work

Lastly, it is important to keep in mind that even though this study has built on previous work and strove to suggest associations of atmospheric teleconnections with low-level airflow and climate anomalies of lower Michigan, it is difficult to assume direct relationships with teleconnections. The teleconnections are very important planetary-scale weather phenomena. On the other hand, surface temperature and precipitation anomalies are measured at a local scale. At the current time in teleconnection research, a linkage or association is usually drawn between planetary-scale circulation and the local-scale climate. However, synoptic and mesoscale phenomena also affect local climate,

and in turn the large-scale circulation influences circulation as the synoptic and meso scales. The 925 hPa trajectories presented here represent one attempt to better understand the linkages between teleconnection patterns, synoptic and mesoscale circulations and local climate. Future work needs to continue to explore these linkages at a range of scales in order to improve our understanding of atmospheric circulation and to improve medium to long-range climate forecasting. By addressing the limitations discussed in the previous section, an increased understanding of the teleconnection associations can be achieved. Additionally, as researchers gain a better grasp of how atmospheric teleconnections behave, improved predictions of their occurrence and impacts will hopefully be possible.

APPENDIX A: FORTRAN PROGRAMS

1. Readgeneral.f

The readgeneral.f program was downloaded from the Climate Diagnostics Center (CDC, 2003b). The netCDF and udunits libraries needed to be installed onto the UNIX machine to be able to compile the program. Once the proper directories were included in the program, the program was then compiled. The addition of -ludunits and -lnetcdf to the compile command is necessary for the program to compile.

g77 readgeneral.f -o readgeneral -ludunits -lnetcdf

2. Merge.f

```

program merge
cccccccccc1cccccccccc2cccccccccc3cccccccccc4cccccccccc5cccccccccc6cccccccccc7c
c      Written July 2002 By: Ryan P. Shadbolt
c      Last Revision September 2002 By: Ryan P. Shadbolt
c      Send questions to: shadbolt@msu.edu
c
c      The Department of Geography at Michigan State University
c
c      This program is ran after the completion of running the programs
c      "readu.f" and "readv.f", which are versions of "readgeneral.f".
c      The two resulting files from running those two programs can be
c      combined by the use of this program.  The user will be asked to
c      input the desired year and the program assumes that the files for
c      this year already exist.  The output will be dispensed to 12
c      different files.  Data exists for the 925, 850, and 700mb levels
c      and each of these levels has time intervals of 00z, 06z, 12z, and
c      18z corresponding to them.  The file names will have the
c      following names:
c
c      /wind/wlllyyttt.dat
c
c      where lll is the level, yy is the year, and ttt is the time.
cccccccccc1cccccccccc2cccccccccc3cccccccccc4cccccccccc5cccccccccc6cccccccccc7c
c      implicit none
c      character(2) cyr
c      real rlat,rlon,uwnd,vwnd
c      integer a,b,c,d,i,j,year,month,day,time,ilev,irec,iunit,iyr,ntime
c      integer lpyrs(10)

```

```

data lpyrs /96,92,88,84,80,76,72,68,64,60/
c
c Ask the user for the desired year.
c
100 write(*,*)' Enter the year that will be used (59-99): '
    read(*,*)iyr
    if(iyr.lt.59 .or. iyr.gt.99)then
        goto 100
    else
        write(cyr,'(i2)')iyr
    endif
c
c Open the input files.
c
    open(10,file='uwnd'//cyr//'.dat')
    open(11,file='vwnd'//cyr//'.dat')
c
c Open the output files.
c
    open(16,file='/data/shadbolt/wind/1925/w925'//cyr//'00z.dat',
&      recl=12,form='formatted',access='direct')
    open(17,file='/data/shadbolt/wind/1925/w925'//cyr//'06z.dat',
&      recl=12,form='formatted',access='direct')
    open(18,file='/data/shadbolt/wind/1925/w925'//cyr//'12z.dat',
&      recl=12,form='formatted',access='direct')
    open(19,file='/data/shadbolt/wind/1925/w925'//cyr//'18z.dat',
&      recl=12,form='formatted',access='direct')
    open(20,file='/data/shadbolt/wind/1850/w850'//cyr//'00z.dat',
&      recl=12,form='formatted',access='direct')
    open(21,file='/data/shadbolt/wind/1850/w850'//cyr//'06z.dat',
&      recl=12,form='formatted',access='direct')
    open(22,file='/data/shadbolt/wind/1850/w850'//cyr//'12z.dat',
&      recl=12,form='formatted',access='direct')
    open(23,file='/data/shadbolt/wind/1850/w850'//cyr//'18z.dat',
&      recl=12,form='formatted',access='direct')
    open(24,file='/data/shadbolt/wind/1700/w700'//cyr//'00z.dat',
&      recl=12,form='formatted',access='direct')
    open(25,file='/data/shadbolt/wind/1700/w700'//cyr//'06z.dat',
&      recl=12,form='formatted',access='direct')
    open(26,file='/data/shadbolt/wind/1700/w700'//cyr//'12z.dat',
&      recl=12,form='formatted',access='direct')
    open(27,file='/data/shadbolt/wind/1700/w700'//cyr//'18z.dat',
&      recl=12,form='formatted',access='direct')
c
c Check if the desired year is a leap year.
c
do a=1,10
    if(iyr.eq.lpyrs(a))then
        ntime=1464
        exit
    else
        ntime=1460
    endif
enddo
c
c Initialize to the first output file.
c

```

```

iunit=16
C
C Loop through the levels 925, 850, and 700mb
C
do b=1,3
    irec=0
C
C Loop through the time periods for the entire year. Read
C the data from the input files and write them out to the
C new output files.
C
do c=1,ntime
    read(10,*), ilev,month,day,time,uwnd
    read(11,*), vwnd
    if(time.eq.0)then
        irec=irec+1
        write(iunit,'(i2)',rec=irec)month
        irec=irec+1
        write(iunit,'(i2)',rec=irec)day
        irec=irec+1
        write(iunit,'(2(f6.1))',rec=irec)uwnd,vwnd
C
C Loop through the 00z gridpoints.
C
do d=2,1085
    read(10,*), ilev,month,day,time,uwnd
    read(11,*), vwnd
    irec=irec+1
    write(iunit,'(2(f6.1))',rec=irec)uwnd,vwnd
enddo
iunit=iunit+1
elseif(time.eq.6)then
    irec=irec-1086
    write(iunit,'(i2)',rec=irec)month
    irec=irec+1
    write(iunit,'(i2)',rec=irec)day
    irec=irec+1
    write(iunit,'(2(f6.1))',rec=irec)uwnd,vwnd
C
C Loop through the 06z gridpoints.
C
do d=2,1085
    read(10,*), ilev,month,day,time,uwnd
    read(11,*), vwnd
    irec=irec+1
    write(iunit,'(2(f6.1))',rec=irec)uwnd,vwnd
enddo
iunit=iunit+1
elseif(time.eq.12)then
    irec=irec-1086
    write(iunit,'(i2)',rec=irec)month
    irec=irec+1
    write(iunit,'(i2)',rec=irec)day
    irec=irec+1
    write(iunit,'(2(f6.1))',rec=irec)uwnd,vwnd
C
C Loop through the 12z gridpoints.

```

```

c
      do d=2,1085
        read(10,*), ilev,month,day,time,uwnd
        read(11,*), vwnd
        irec=irec+1
        write(iunit,'(2(f6.1))',rec=irec)uwnd,vwnd
      enddo
      iunit=iunit+1
    else
      irec=irec-1086
      write(iunit,'(i2)',rec=irec)month
      irec=irec+1
      write(iunit,'(i2)',rec=irec)day
      irec=irec+1
      write(iunit,'(2(f6.1))',rec=irec)uwnd,vwnd
c
c      Loop through the 18z gridpoints.
c
      do d=2,1085
        read(10,*), ilev,month,day,time,uwnd
        read(11,*), vwnd
        irec=irec+1
        write(iunit,'(2(f6.1))',rec=irec)uwnd,vwnd
      enddo
      iunit=iunit-3
    endif
  enddo
  close(iunit)
  close(iunit+1)
  close(iunit+2)
  close(iunit+3)
  iunit=iunit+4
enddo

999  stop
     end program merge

```

3. Getbktr.f

```

      program getbktr
cccccccccccccccccccc2cccccccccccccccccccccccc4cccccccccccccccccccccccc6cccccccccccccccccccc7c
c      Written July 2002 By: Ryan P. Shadbolt
c      Last Revision March 2003 By: Ryan P. Shadbolt
c      Send questions to: shadbolt@msu.edu
c
c      Original algorithm and source code by: Eleanor A. Waller
c
c      The Geography Department of Michigan State University
c
c      This program is designed to get the 5-day back trajectories
c      from the u and v wind data at the 925, 850, or 700mb level. The
c      data is collected from the NCEP reanalysis data. The programs
c      "readu.f" and "readv.f" must first be ran to get the correct
c      u and v data sets. "Merge.f" will then be ran to merge the

```



```

data x1(10)          /' -30hr'/
data x1(11)          /' -33hr'/
data x1(12)          /' -36hr'/
data x1(13)          /' -39hr'/
data x1(14)          /' -42hr'/
data x1(15)          /' -45hr'/
data x1(16)          /' -48hr'/
data x1(17)          /' -51hr'/
data x1(18)          /' -54hr'/
data x1(19)          /' -57hr'/
data x1(20)          /' -60hr'/
data x1(21)          /' -63hr'/
data x1(22)          /' -66hr'/
data x1(23)          /' -69hr'/
data x1(24)          /' -72hr'/
data x1(25)          /' -75hr'/
data x1(26)          /' -78hr'/
data x1(27)          /' -81hr'/
data x1(28)          /' -84hr'/
data x1(29)          /' -87hr'/
data x1(30)          /' -90hr'/
data x1(31)          /' -93hr'/
data x1(32)          /' -96hr'/
data x1(33)          /' -99hr'/
data x1(34)          /' -102hr'/
data x1(35)          /' -105hr'/
data x1(36)          /' -108hr'/
data x1(37)          /' -111hr'/
data x1(38)          /' -114hr'/
data x1(39)          /' -117hr'/
data x1(40)          /' -120hr'/

c
c   Set parameters to missing to indicate that this is the first pass
c   and all input parameters need to be specified.
c
1   iyr=imiss
    imnth=imiss
    ng=imiss
    nt=imiss
    nlev=imiss

c
c   Get the latitude and longitude locations for each of the
c   1085 gridpoints. The grid used is 10N-85N and 60W-145W.
c
    call conijll(npts,rlt,rln)

c
c   Determine which year the user is interested in.
c
10  if(iyr.eq.imiss)then
      write(*,*)'Enter year (60-99): '
      read(*,*)iyr
      if(iyr.lt.60 .or. iyr.gt.99)then
          iyr=imiss
          goto 10
      endif
      write(cyr,'(i2)')iyr
  endif

```

```

C
C      Determine which month the user is interested in.
C
11      if(imnth.eq.imiss)then
           write(*,*)'Enter month (1-12): '
           read(*,*)imnth
           if(imnth.lt.1 .or. imnth.gt.12)then
               imnth=imiss
               goto 11
           endif
       endif

C
C      Determine the starting point(s) for the back-trajectories.
C
12      if(ng.eq.imiss)then
           write(*,*)'Enter the desired number of back-trajectory'
           write(*,1001)ngmax
1001      format(' starting gridpoints (1-',i1,'): ')
           read(*,*)ng
           if(ng.lt.1 .or. ng.gt.ngmax)then
               ng=imiss
               goto 12
           endif
           do i=1,ng
13              write(*,1002)i
1002          format(' Enter gridpoint #',i1,': ')
              read(*,*)ngpts(i)
              if(ngpts(i).lt.1 .or. ngpts(i).gt.npts) goto 13
              rlatst(i)=rlt(ngpts(i))
              rlonst(i)=rln(ngpts(i))
           enddo
       endif

C
C      Determine the number of 3-hour time steps (Example=40).
C
14      if(nt.eq.imiss)then
           write(*,1003)ntmax
1003      format(' Enter the number of 3-hour time steps (1-',i2,'):')
           read(*,*)nt
           if(nt.lt.1 .or. nt.gt.ntmax)then
               nt=imiss
               goto 14
           endif
           write(cnt, '(i2.2)')nt
       endif

C
C      Determine which level will be used (925, 850, or 700mb).
C
15      if(nlev.eq.imiss)then
           write(*,*)'Enter desired level (1=925, 2=850, 3=700):'
           read(*,*)nlev
           if(nlev.lt.1 .or. nlev.gt.3)then
               nlev=imiss
               goto 15
           endif
       endif

```

```

c      Open the 4 times daily u and v wind component files for the
c      specified year and level.  If January is the specified month,
c      then the previous year's files will also need to be opened to
c      use December.
c      iunit=10 is 00z      iunit=15 is 06z
c      iunit=20 is 12z      iunit=25 is 18z
c      iunit=30,35,40,45 are the same files for the previous year.
c
      if(nlev.eq.1)then
        inname(1)='/data/shadbolt/wind/1925/w925'//cyr//'00z.dat'
        inname(2)='/data/shadbolt/wind/1925/w925'//cyr//'06z.dat'
        inname(3)='/data/shadbolt/wind/1925/w925'//cyr//'12z.dat'
        inname(4)='/data/shadbolt/wind/1925/w925'//cyr//'18z.dat'
        if(imnth.eq.1)then
          write(cmyr,'(i2)')iyr-1
          inname(5)='/data/shadbolt/wind/1925/w925'//cmyr//'00z.dat'
          inname(6)='/data/shadbolt/wind/1925/w925'//cmyr//'06z.dat'
          inname(7)='/data/shadbolt/wind/1925/w925'//cmyr//'12z.dat'
          inname(8)='/data/shadbolt/wind/1925/w925'//cmyr//'18z.dat'
          open(30,file=inname(5),recl=12,form='formatted',
&            access='direct')
          open(35,file=inname(6),recl=12,form='formatted',
&            access='direct')
          open(40,file=inname(7),recl=12,form='formatted',
&            access='direct')
          open(45,file=inname(8),recl=12,form='formatted',
&            access='direct')
        endif
      elseif(nlev.eq.2)then
        inname(1)='/data/shadbolt/wind/1850/w850'//cyr//'00z.dat'
        inname(2)='/data/shadbolt/wind/1850/w850'//cyr//'06z.dat'
        inname(3)='/data/shadbolt/wind/1850/w850'//cyr//'12z.dat'
        inname(4)='/data/shadbolt/wind/1850/w850'//cyr//'18z.dat'
        if(imnth.eq.1)then
          write(cmyr,'(i2)')iyr-1
          inname(5)='/data/shadbolt/wind/1850/w850'//cmyr//'00z.dat'
          inname(6)='/data/shadbolt/wind/1850/w850'//cmyr//'06z.dat'
          inname(7)='/data/shadbolt/wind/1850/w850'//cmyr//'12z.dat'
          inname(8)='/data/shadbolt/wind/1850/w850'//cmyr//'18z.dat'
          open(30,file=inname(5),recl=12,form='formatted',
&            access='direct')
          open(35,file=inname(6),recl=12,form='formatted',
&            access='direct')
          open(40,file=inname(7),recl=12,form='formatted',
&            access='direct')
          open(45,file=inname(8),recl=12,form='formatted',
&            access='direct')
        endif
      elseif(nlev.eq.3)then
        inname(1)='/data/shadbolt/wind/1700/w700'//cyr//'00z.dat'
        inname(2)='/data/shadbolt/wind/1700/w700'//cyr//'06z.dat'
        inname(3)='/data/shadbolt/wind/1700/w700'//cyr//'12z.dat'
        inname(4)='/data/shadbolt/wind/1700/w700'//cyr//'18z.dat'
        if(imnth.eq.1)then
          write(cmyr,'(i2)')iyr-1
          inname(5)='/data/shadbolt/wind/1700/w700'//cmyr//'00z.dat'
          inname(6)='/data/shadbolt/wind/1700/w700'//cmyr//'06z.dat'

```

```

        inname(7)='/data/shadbolt/wind/1700/w700'//cmyr//'12z.dat'
        inname(8)='/data/shadbolt/wind/1700/w700'//cmyr//'18z.dat'
        open(30,file=inname(5),recl=12,form='formatted',
&         access='direct')
        open(35,file=inname(6),recl=12,form='formatted',
&         access='direct')
        open(40,file=inname(7),recl=12,form='formatted',
&         access='direct')
        open(45,file=inname(8),recl=12,form='formatted',
&         access='direct')
    endif
endif
open(10,file=inname(1),recl=12,form='formatted',access='direct')
open(15,file=inname(2),recl=12,form='formatted',access='direct')
open(20,file=inname(3),recl=12,form='formatted',access='direct')
open(25,file=inname(4),recl=12,form='formatted',access='direct')
c
c      Initialize variables for the first pass.
c
    iunit=25
    istat=0
    irec=0
    do j=1,ngmax
        nback(j)=0
        do k=1,nposs
            iday(j,k)=0
            itime(j,k)=0
            do m=1,ntmax
                rlat(j,k,m)=rmiss
                rlon(j,k,m)=rmiss
            enddo
        enddo
    enddo
100    imyrrec=0
c
c      The first pass will use the 00z (10) file, followed by the
c      06z (15), 12z (20), and the 18z (25) file of the same day.
c      After that, the 00z of the next day will be used. This process
c      will continue until the end of the specified year has been
c      reached.
c
    if(iunit.eq.25)then
        iunit=10
        ihr=0
    elseif(iunit.eq.10)then
        iunit=15
        irec=irec-(npts+2)
        ihr=6
    elseif(iunit.eq.15)then
        iunit=20
        irec=irec-(npts+2)
        ihr=12
    elseif(iunit.eq.20)then
        iunit=25
        irec=irec-(npts+2)
        ihr=18
    endif

```

```

C
C      Begin to read in records for an entire day, beginning with the
C      record to identify the month.  If we have started a new month
C      with this record or hit and end of file, then go to 400 and
C      write out the data from the previous month.  Come back to 200
C      when finished writing out the data to start the next month.
C
      irec=irec+1
      read(iunit,'(i2)',rec=irec,iostat=istat)imo
      if(istat.ne.0) goto 400
      if(imo.gt.imnth) goto 400
C
C      Read the day record.
C
200      irec=irec+1
      read(iunit,'(i2)',rec=irec)idy
C
C      Loop through the 1085 u and v grid for this day.
C
      do i=1,npts
        irec=irec+1
C
C        Is this the desired month?
C        If so, find the starting gridpoint(s) and read u and v.
C
        if(imo.eq.imnth)then
          do j=1,ng
            if(i.eq.ngpts(j))then
              read(iunit,'(2(f6.1))',rec=irec)u(1),v(1)
C
C              Start the -3hr back-trajectory.
C
              if(nback(j).lt.nposs)then
                nback(j)=nback(j)+1
              else
                write(*,*)'WARNING: ARRAY OVERFLOW IN BACK.'
                goto 400
              endif
C
C              Save the data for the starting gridpoint.
C
              iday(j,nback(j))=idy
              itime(j,nback(j))=ihr
              iunitx=iunit
              ntime=0
              nhr=ihr
              ndy=idy
              nmo=imo
              alat=rlatst(j)
              alon=rlonst(j)
              irecl=irec
C
C              Begin the loop of -3hr back-trajectory points.
C
300              ntime=ntime+1
C
C              Calculate the date/time of each location.  If

```

```

c      time equals 0, we must go to the previous day at
c      21z. If day equals 0, we must go to the previous
c      month at 21z. If month equals 2, we must check whether
c      or not this February is a leap year. If month equals
c      0, go to the December of the previous year at 21z.
c      This year must also be checked for leap year status.
c      If none of these criteria pertain to this time, then we
c      will simply go back an additional 3hrs for this next
c      trajectory node calculation.
c
      if(nhr.eq.0) then
        nhr=21
        ndy=ndy-1
        if(ndy.eq.0) then
          nmo=nmo-1
          ndy=ndays(nmo+1)
          if(nmo.eq.2) then
            do ii=1,10
              if(iyr.eq.ilpyrs(ii)) ndy=ndy+1
            enddo
          endif
          if(nmo.eq.0) then
            nmo=12
            iunitx=iunitx+20
            do ii=1,10
              if(iyr-1.eq.ilpyrs(ii)) then
                imyrrec=(366*(npts+2))-(npts-i)
                exit
              else
                imyrrec=(365*(npts+2))-(npts-i)
              endif
            enddo
          endif
        endif
        if(nmo.eq.12 .and. ndy.ne.31) imyrrec=imyrrec-(npts+2)
      else
        nhr=nhr-3
      endif
c
c      Save starting u, v, lat, and lon.
c
      uorig=u(1)
      vorig=v(1)
      alato=alat
      alono=alon
c
c      Calculate estimated -3hr location (lat,lon) from
c      u and v. U and v are converted to km/hour to do this.
c
      ukmphr=(uorig*3600.)/1000.
      vkmphr=(vorig*3600.)/1000.
      ukmm3=ukmphr*3.
      vkmm3=vkmphr*3.
      alat=alato-(vkmm3/rkmpdgt)
      alatr=alat*radpdeg
      deglon=cos(alatr)*rkmpdgt
      alon=alono+(ukmm3/deglon)

```

```

C
C      Check to see if alat and alon are outside of the domain
C      10N-85N and 60W-145W.  If they are, set the record
C      number to the correct value and go back to 100.
C
      if(alat.lt.10. .or. alat.gt.85. .or. alon.lt.60 .or.
&      alon.gt.145.)then
          irec=irec+(npts-i)
          goto 100
      endif

C
C      Find the four surrounding gridpoints for the -3hr
C      location.
C
      call conllij(alat,alon,xi,xj,igpts)

C
C      Save current unit and record numbers.
C
      iunito=iunitx
      ireco=irecl

C
C      Find u and v at the four surrounding -3hr gridpoints.
C
      call calcwind(iunitx,i,irecl,nhr,ndy,igpts,xi,xj,
&      npts,imyrrec,u,v)

C
C      Calculate average of starting u and v and interpolated
C      u and v to achieve a new u and v value.
C
      u(1)=(u(1)+uorig)/2.
      v(1)=(v(1)+vorig)/2.

C
C      Recalculate estimated -3hr location (lat,lon) from
C      u and v. U and v are converted to km/hour to do this.
C
      ukmphr=(u(1)*3600.)/1000.
      vkmphr=(v(1)*3600.)/1000.
      ukmm3=ukmphr*3.
      vkmm3=vkmphr*3.
      alat=alato-(vkmm3/rkmpdgt)
      alatr=alat*radpdeg
      deglon=cos(alatr)*rkmpdgt
      alon=alono+(ukmm3/deglon)
      rlat(j,nback(j),ntime)=alat
      rlon(j,nback(j),ntime)=alon

C
C      Find the new four surrounding gridpoints for the
C      -3hr location.
C
      call conllij(alat,alon,xi,xj,igpts)

C
C      Find u and v at the four new surrounding -3hr gridpoints.
C
      iunitx=iunito
      irecl=ireco
      call calcwind(iunitx,i,irecl,nhr,ndy,igpts,xi,xj,
&      npts,imyrrec,u,v)

```

```

C
C          Go back and find the next -3hr location, if necessary.
C
C          if(ntime.lt.nt) goto 300
C          endif
C          enddo
C          endif
C        enddo
C
C      If this is the 00z time, go back and look at the 06z time for
C      the same day.  If it is the 06z time, go back and look at the
C      12z time.  If this is the 12z time, go back and look at the 18z
C      time.  If this is the 18z time, go back and look at the 00z time
C      for the next day.
C
C      goto 100
C
C      Write out the back-trajectory data for the specified month.
C
400  if(nlev.eq.1)then
C      write(clvl,'(i3)')925
C    elseif(nlev.eq.2)then
C      write(clvl,'(i3)')850
C    elseif(nlev.eq.3)then
C      write(clvl,'(i3)')700
C    endif
C    ichrcnt=3
C
C      Each starting gridpoint will have a separate file of back-
C      trajectory analysis.
C
C      do j=1,ng
C
C        Open the .txt (as 50) and .doc (as 55) output files.
C
C        write(cgrdpt,'(i4.4)')ngpts(j)
C        outnam(1)='/data/shadbolt/back/'//month(imnth)//'/1'
C      &      //clvl(1:ichrcnt)//'/b'//cyr//cgrdpt//cnt//'.txt'
C        outnam(2)='/data/shadbolt/back/'//month(imnth)//'/1'
C      &      //clvl(1:ichrcnt)//'/b'//cyr//cgrdpt//cnt//'.doc'
C        open(50,file=outnam(1),recl=200,form='formatted',
C      &      access='sequential')
C        open(55,file=outnam(2),recl=120,form='formatted',
C      &      access='sequential')
C
C      Write titles and headings in the .doc file.
C
C      write(55,1004)months(imnth),cyr,clvl
1004  format(a8,' 19',a2,1x,a4,'MB',/)
C      write(55,1005)ngpts(j),rlatst(j),-rlonst(j)
1005  format('Starting gridpoint: ',i4.4,3x,'(',f4.1,
C      &      ' latitude, ',f6.1,' longitude)')
C      write(55,'(/,9x,10(a1))')(x1(m),m=1,nt)
C
C      Loop through the back-trajectories and write out lat,lon
C      coordinates to both files.
C

```

```

do k=1,nback(j)
  do m=1,nt
    if(rlat(j,k,m).ne.rmiss .and. rlon(j,k,m).ne.rmiss)then
      write(50,1006)rlat(j,k,m),-rlon(j,k,m)
1006      format(f5.2,',',f7.2)
    endif
  enddo
  write(55,1007)iday(j,k),month(imnth),itime(j,k),'Z',
    &      (rlat(j,k,m),-rlon(j,k,m),m=1,nt)
1007      format(i2.2,a3,i2.2,a1,2x,10(f6.2,f8.2))
c
c      Reinitialize the array elements.
c
    iday(j,k)=0
    itime(j,k)=0
    do m=1,nt
      rlat(j,k,m)=rmiss
      rlon(j,k,m)=rmiss
    enddo
  enddo
  nback(j)=0
  close(50)
  close(55)
enddo

if(istat.ne.0)then
c
c      End of file or error. Close files and ask for another year.
c
    close(10)
    close(15)
    close(20)
    close(25)
    close(30)
    close(35)
    close(40)
    close(45)
c
c      Determine if user would like to do analysis for another year.
c
    write(*,*)'Would youlike to specify new criteria? (y/n)'
    read(*,'(a)')answer
    if(answer.eq.'Y' .or. answer.eq.'y')then
      goto 1
    else
      goto 999
    endif
  else
c
c      Status is normal; go back and continue on to the next month.
c
    imnth=imnth+1
    goto 200
  endif

999  stop
end program getbktr

```

```

      subroutine conij11(npts,rlt,rln)
cccccccc1cccccccc2cccccccc3cccccccc4cccccccc5cccccccc6cccccccc7c
c      This subroutine converts the i=3,33 and j=87,121 points of
c      each gridpoint to the lat/lon positions (10N-85N, 60W-145W).
c      Point 3,87 is 85N,145W and point 33,121 is 10N,60W. Intervals
c      are every 2.5 degrees.
cccccccc1cccccccc2cccccccc3cccccccc4cccccccc5cccccccc6cccccccc7c
      real x,y,rlt(npts),rln(npts)
      integer i,j,k

      k=1
      x=85.
      do i=3,33
        y=145.
        do j=87,121
          rlt(k)=x
          rln(k)=y
          y=y-2.5
          k=k+1
        enddo
        x=x-2.5
      enddo

      return
    end subroutine conij11

      subroutine conllij(alat,alon,xi,xj,igpts)
cccccccc1cccccccc2cccccccc3cccccccc4cccccccc5cccccccc6cccccccc7c
c      This subroutine converts the lat/lon points of the four
c      surrounding gridpoints to the 1-1085 gridpoint number and
c      returns xi, and xj (the 3-33, 87-121 gridpoint number) of the
c      trajectory location. Xi and xj are based on a simple linear
c      equation of the 3-33, 87-121 grid and the lat/lon grid where
c      -.4 is the slope and 37. and 145. are the y-intercepts. Igpts(1)
c      is the bottom left, igpts(2) is the top left, igpts(3) is the top
c      right and igpts(4) is the bottom right.
cccccccc1cccccccc2cccccccc3cccccccc4cccccccc5cccccccc6cccccccc7c
      integer a,b,n,z,igpts(4)
      real x,y

      z=0
      x=85.
      do a=3,33
        y=145.
        do b=87,121
          z=z+1
          if(alat.ge.x .and. alon.ge.y)then
            igpts(1)=z-1
            igpts(2)=z-36
            igpts(3)=z-35
            igpts(4)=z
            goto 500
          else
            y=y-2.5
          endif
        enddo
      enddo

```

```

        x=x-2.5
    enddo
500  xi=(-.4)*alat)+37.
    xj=(-.4)*alon)+145.

    return
end subroutine conllij

subroutine calcwind(iunitx,i,irecl,nhr,ndy,igpts,xi,xj,npts,
&                    imyrrec,u,v)
ccccccccclcccccccccc2cccccccccc3cccccccccc4cccccccccc5cccccccccc6cccccccccc7c
c    This subroutine is used to find the wind values of the four
c    surrounding gridpoints and then uses them to calculate u(1) and
c    v(1), which are the u and v values of the new -3hr trajectory
c    point. If the current time is 03z, 09z, 15z, or 21z, an
c    interpolation will be used to calculate the wind values at those
c    times.
ccccccccclcccccccccc2cccccccccc3cccccccccc4cccccccccc5cccccccccc6cccccccccc7c
    integer k,irecx,igpts(4)
    real p,q,u(4),v(4)
    real u00(4),v00(4),u06(4),v06(4),u12(4),v12(4),u18(4),v18(4)

    if(iunitx.eq.10)then
        if(nhr.eq.21)then
            do k=1,4
                irecx=irecl+(igpts(k)-i)
                read(iunitx,'(2(f6.1))',rec=irecx)u00(k),v00(k)
            enddo
            iunitx=25
            irecl=irecl-(npts+2)
            do k=1,4
                irecx=irecl+(igpts(k)-i)
                read(iunitx,'(2(f6.1))',rec=irecx)u18(k),v18(k)
            enddo
            iunitx=10
        elseif(nhr.eq.18)then
            iunitx=25
            do k=1,4
                irecx=irecl+(igpts(k)-i)
                read(iunitx,'(2(f6.1))',rec=irecx)u18(k),v18(k)
            enddo
        endif
    elseif(iunitx.eq.15)then
        if(nhr.eq.3)then
            do k=1,4
                irecx=irecl+(igpts(k)-i)
                read(iunitx,'(2(f6.1))',rec=irecx)u06(k),v06(k)
            enddo
            iunitx=10
            do k=1,4
                irecx=irecl+(igpts(k)-i)
                read(iunitx,'(2(f6.1))',rec=irecx)u00(k),v00(k)
            enddo
            iunitx=15
        elseif(nhr.eq.0)then
            iunitx=10
            do k=1,4

```

```

        irecx=irecl+(igpts(k)-i)
        read(iunitx,'(2(f6.1))',rec=irecx)u00(k),v00(k)
    enddo
endif
elseif(iunitx.eq.20)then
    if(nhr.eq.9)then
        do k=1,4
            irecx=irecl+(igpts(k)-i)
            read(iunitx,'(2(f6.1))',rec=irecx)u12(k),v12(k)
        enddo
        iunitx=15
        do k=1,4
            irecx=irecl+(igpts(k)-i)
            read(iunitx,'(2(f6.1))',rec=irecx)u06(k),v06(k)
        enddo
        iunitx=20
    elseif(nhr.eq.6)then
        iunitx=15
        do k=1,4
            irecx=irecl+(igpts(k)-i)
            read(iunitx,'(2(f6.1))',rec=irecx)u06(k),v06(k)
        enddo
    endif
elseif(iunitx.eq.25)then
    if(nhr.eq.15)then
        do k=1,4
            irecx=irecl+(igpts(k)-i)
            read(iunitx,'(2(f6.1))',rec=irecx)u18(k),v18(k)
        enddo
        iunitx=20
        do k=1,4
            irecx=irecl+(igpts(k)-i)
            read(iunitx,'(2(f6.1))',rec=irecx)u12(k),v12(k)
        enddo
        iunitx=25
    elseif(nhr.eq.12)then
        iunitx=20
        do k=1,4
            irecx=irecl+(igpts(k)-i)
            read(iunitx,'(2(f6.1))',rec=irecx)u12(k),v12(k)
        enddo
    endif
endif

```

c
c
c
c

This is used if we are calculating for early January.
We will need December from the previous year to do this.

```

elseif(iunitx.eq.30)then
    if(nhr.eq.21)then
        do k=1,4
            if(ndy.eq.31)then
                iunitx=10
                irecx=irecl+(igpts(k)-i)
                read(iunitx,'(2(f6.1))',rec=irecx)u00(k),v00(k)
            else
                irecl=(imyrrec+(npts+2))
                irecx=irecl+(igpts(k)-i)
                read(iunitx,'(2(f6.1))',rec=irecx)u00(k),v00(k)
            endif
        enddo
    endif
endif

```

```

        endif
    enddo
    iunitx=45
    irecl=imyrrec
    do k=1,4
        irecx=irecl+(igpts(k)-i)
        read(iunitx,'(2(f6.1))',rec=irecx)u18(k),v18(k)
    enddo
    iunitx=30
elseif(nhr.eq.18)then
    iunitx=45
    irecl=imyrrec
    do k=1,4
        irecx=irecl+(igpts(k)-i)
        read(iunitx,'(2(f6.1))',rec=irecx)u18(k),v18(k)
    enddo
endif
elseif(iunitx.eq.35)then
    irecl=imyrrec
    if(nhr.eq.3)then
        do k=1,4
            irecx=irecl+(igpts(k)-i)
            read(iunitx,'(2(f6.1))',rec=irecx)u06(k),v06(k)
            iunitx=35
        enddo
        iunitx=30
        do k=1,4
            irecx=irecl+(igpts(k)-i)
            read(iunitx,'(2(f6.1))',rec=irecx)u00(k),v00(k)
        enddo
        iunitx=35
    elseif(nhr.eq.0)then
        iunitx=30
        do k=1,4
            irecx=irecl+(igpts(k)-i)
            read(iunitx,'(2(f6.1))',rec=irecx)u00(k),v00(k)
        enddo
    endif
elseif(iunitx.eq.40)then
    irecl=imyrrec
    if(nhr.eq.9)then
        do k=1,4
            irecx=irecl+(igpts(k)-i)
            read(iunitx,'(2(f6.1))',rec=irecx)u12(k),v12(k)
        enddo
        iunitx=35
        do k=1,4
            irecx=irecl+(igpts(k)-i)
            read(iunitx,'(2(f6.1))',rec=irecx)u06(k),v06(k)
        enddo
        iunitx=40
    elseif(nhr.eq.6)then
        iunitx=35
        do k=1,4
            irecx=irecl+(igpts(k)-i)
            read(iunitx,'(2(f6.1))',rec=irecx)u06(k),v06(k)
        enddo
    enddo

```

```

endif
elseif(iunitx.eq.45)then
  irecl=imyrrec
  if(nhr.eq.15)then
    do k=1,4
      irecx=irecl+(igpts(k)-i)
      read(iunitx,'(2(f6.1))',rec=irecx)u18(k),v18(k)
    enddo
    iunitx=40
    do k=1,4
      irecx=irecl+(igpts(k)-i)
      read(iunitx,'(2(f6.1))',rec=irecx)u12(k),v12(k)
    enddo
    iunitx=45
  elseif(nhr.eq.12)then
    iunitx=40
    do k=1,4
      irecx=irecl+(igpts(k)-i)
      read(iunitx,'(2(f6.1))',rec=irecx)u12(k),v12(k)
    enddo
  endif
endif

if(nhr.eq.0)then
  do k=1,4
    u(k)=u00(k)
    v(k)=v00(k)
  enddo
elseif(nhr.eq.3)then
  do k=1,4
    u(k)=(u00(k)+u06(k))/2.
    v(k)=(v00(k)+v06(k))/2.
  enddo
elseif(nhr.eq.6)then
  do k=1,4
    u(k)=u06(k)
    v(k)=v06(k)
  enddo
elseif(nhr.eq.9)then
  do k=1,4
    u(k)=(u06(k)+u12(k))/2.
    v(k)=(v06(k)+v12(k))/2.
  enddo
elseif(nhr.eq.12)then
  do k=1,4
    u(k)=u12(k)
    v(k)=v12(k)
  enddo
elseif(nhr.eq.15)then
  do k=1,4
    u(k)=(u12(k)+u18(k))/2.
    v(k)=(v12(k)+v18(k))/2.
  enddo
elseif(nhr.eq.18)then
  do k=1,4
    u(k)=u18(k)
    v(k)=v18(k)
  enddo

```

```

        enddo
    elseif(nhr.eq.21)then
        do k=1,4
            u(k)=(u18(k)+u00(k))/2.
            v(k)=(v18(k)+v00(k))/2.
        enddo
    endif
c
c    Use a bi-linear interpolation using the 4 nearest
c    gridpoints to compute u and v.
c
    p=xi-aint(xi)
    q=xj-aint(xj)

    u(1)=u(1)*p*(1.-q)
&    +u(2)*(1.-p)*(1.-q)
&    +u(3)*(1.-p)*q
&    +u(4)*p*q

    v(1)=v(1)*p*(1.-q)
&    +v(2)*(1.-p)*(1.-q)
&    +v(3)*(1.-p)*q
&    +v(4)*p*q

    return
end subroutine calcwind

```

4. Combine.f

```

    program combine
cccccccccc1cccccccccc2cccccccccc3cccccccccc4cccccccccc5cccccccccc6cccccccccc7c
c    Written October 2002 By: Ryan P. Shadbolt
c    Last Revision March 2003 By: Ryan P. Shadbolt
c    Send questions to: shadbolt@msu.edu
c
c    The Department of Geography at Michigan State University
c
c    This program combines the .txt output files from getbktr.f for a
c    month for all 40 years at a certain level.
c
c    Example: All Januarys from 1960-1999 at 850mb
c
c    Files will be located in the following directory:
c    /data/shadbolt/back/mmml/llll/lllcombine.txt where
c    mmm is the month, and lll is the level.
cccccccccc1cccccccccc2cccccccccc3cccccccccc4cccccccccc5cccccccccc6cccccccccc7c
    implicit none
    integer month,year,endyear,lev,istat
    real lat,lon
    character(2) cyear
    character(3) cleve,months(12)
    data months /'jan','feb','mar','apr','may','jun','jul','aug',
&              'sep','oct','nov','dec'/

```

```

c
c   Ask for month and level to be combined.
c
1   write(*,*)'Enter the month to be combined (1-12):'
    read(*,*)month
    if(month.lt.1 .or. month.gt.12) goto 1
2   write(*,*)'Enter the beginning year (60-99):'
    read(*,*)year
    if(year.lt.60 .or. year.gt.99) goto 2
3   write(*,*)'Enter the ending year (' ,year,'-99):'
    read(*,*)endyear
    if(endyear.lt.year .or. endyear.gt.99) goto 3
4   write(*,*)'Enter the level in mb (925, 850, or 700):'
    read(*,*)lev
    if(lev.ne.925 .and. lev.ne.850 .and. lev.ne.700) goto 4
    write(clev,'(i3)')lev
c
c   Initialization.
c
    istat=0
c
c   Open output file.
c
    open(10,file='/data/shadbolt/back/'//months(month)//'/1'
&///clev///'/'//clev//'combine.txt')
    write(10,1000)'lat,lon'
1000 format(a7)
5   write(cyear,'(i2)')year
c
c   Open current input file.
c
    open(11,file='/data/shadbolt/back/'//months(month)//'/1'
&///clev///'b'//cyear//'062040.txt')
c
c   Read the lat and lon values and write them out to output file.
c   If end of file, go to next year.  If the end of years is
c   reached, end the program.
c
do
    read(11,'(f5.2,1x,f7.2)',iostat=istat)lat,lon
    if(istat.ne.0)then
        close(11)
        if(year.eq.endyear)then
            close(10)
            goto 999
        else
            year=year+1
            goto 5
        endif
    else
        write(10,1001)lat,lon
1001 format(f5.2,',',f7.2)
        endif
    enddo
999 stop
end program combine

```

5. Count.f

```
      program count
cccccccccc1cccccccccc2cccccccccc3cccccccccc4cccccccccc5cccccccccc6cccccccccc7c
c      Written October 2002 By: Ryan P. Shadbolt
c      Last Revision April 2003 By: Ryan P. Shadbolt
c      Send questions to: shadbolt@msu.edu
c
c      The Geography Department of Michigan State University
c
c      This program is used to count up how many trajectory points land
c      in each grid cell. The grid is composed of 150 columns and 160
c      rows with a 50000m X 50000m dimension. The results of this
c      program will ultimately be the results for the final climatology
c      grids for display within the GIS.
cccccccccc1cccccccccc2cccccccccc3cccccccccc4cccccccccc5cccccccccc6cccccccccc7c
      implicit none
      integer i,j,istat,month,lev,countarray(160,150)
      real x,y,ulx,uly,lrx,lry
      character(3) months(12),clev
      data months/'jan','feb','mar','apr','may','jun','jul','aug',
&                'sep','oct','nov','dec'/

c
c      Ask the user for the month.
c
10    write(*,*)'Enter the month (1-12): '
      read(*,*)month
      if(month.lt.1 .or. month.gt.12) goto 10
c
c      Ask the user for the level.
c
20    write(*,*)'Enter the level in mb (925, 850, or 700): '
      read(*,*)lev
      if(lev.ne.925 .and. lev.ne.850 .and. lev.ne.700) goto 20
      write(clev,'(i3)')lev
c
c      Open the input and output files.
c
      open(10,file='/data/shadbolt/925files/'//months(month)//clev//
&'.txt')
      open(20,file='/data/shadbolt/925files/'//months(month)//clev//
&'.asc')
c
copen(10,file='/data/shadbolt/teleconnections/mamimages/lambert/lam
c      &am925gp2.txt')
c
copen(20,file='/data/shadbolt/teleconnections/mamimages/lambert/lam
c      &am925gp2.asc')
c
c      Initializations.
c
      istat=0
```

```

do i=1,160
  do j=1,150
    countarray(i,j)=0
  enddo
enddo

c
c Read through the trajectory file. Once the end of file is
c reached, go to the next grid cell and then check that. Keep
c going until the entire 160X150 grid has been checked.
c
do
  read(10,*,iostat=istat)x,y
  if(istat.ne.0) goto 40

c
c Loop through the 160X150 grid and check to see if each
c trajectory point falls within a grid cell. If it does, the
c grid cell array called "countarray" will be incremented.
c Otherwise, the array is left at 0.
c

  uly=5000000.
  lry=4950000.
  do i=1,160
    ulx=-4850000.
    lrx=-4800000.
    do j=1,150
      if(x.ge.ulx .and. x.lt.lrx .and. y.le.uly .and.
&      y.gt.lry)then
        countarray(i,j)=countarray(i,j)+1
        goto 30
      else
        ulx=ulx+50000.
        lrx=lrx+50000.
      endif
    enddo
    uly=uly-50000.
    lry=lry-50000.
  enddo
30 enddo

c
c Write out the output from the countarray.
c
40 do i=1,160
  write(20,1000)(countarray(i,j),j=1,150)
1000 format(149(i4,', '),i4)
  enddo
  close(10)
  close(20)

999 stop
end program count

```

6. Readhysplit.f

```

program readhysplit

```

```

cccccccc1cccccccc2cccccccc3cccccccc4cccccccc5cccccccc6cccccccc7c
c      Written March 2003 By: Ryan P. Shadbolt
c      Last Revision March 2003 By: Ryan P. Shadbolt
c
c      This was used to read the hysplit output files and extract
c      the lat/lon data and then combine the daily data into one
c      monthly file. The monthly files will later be combined
c      by use of the "cat" command at the UNIX prompt.
cccccccc1cccccccc2cccccccc3cccccccc4cccccccc5cccccccc6cccccccc7c
implicit none
integer endday,ndays(12),imonth,k,j,i,unit
real lat,lon
character(3) cmonth,month(12)
character(2) cmth
data ndays /31,28,31,30,31,30,31,31,30,31,30,31/
data month/'jan','feb','mar','apr','may','jun','jul','aug','sep',
&'oct','nov','dec'/

open(10,file='hysplit13d99.txt')
write(*,*)'Please enter the month (1-12): '
read(*,*)imonth
100 do i=1,12
    if(i.eq.imonth)then
        endday=ndays(i)
        write(cmonth,'(a3)')month(i)
        write(cmth,'(i2)')imonth
        exit
    endif
enddo
open(11,file=' '//cmonth//'3d99' '//cmth//'0199.txt')
open(12,file=' '//cmonth//'3d99' '//cmth//'0299.txt')
open(13,file=' '//cmonth//'3d99' '//cmth//'0399.txt')
open(14,file=' '//cmonth//'3d99' '//cmth//'0499.txt')
open(15,file=' '//cmonth//'3d99' '//cmth//'0599.txt')
open(16,file=' '//cmonth//'3d99' '//cmth//'0699.txt')
open(17,file=' '//cmonth//'3d99' '//cmth//'0799.txt')
open(18,file=' '//cmonth//'3d99' '//cmth//'0899.txt')
open(19,file=' '//cmonth//'3d99' '//cmth//'0999.txt')
open(20,file=' '//cmonth//'3d99' '//cmth//'1099.txt')
open(21,file=' '//cmonth//'3d99' '//cmth//'1199.txt')
open(22,file=' '//cmonth//'3d99' '//cmth//'1299.txt')
open(23,file=' '//cmonth//'3d99' '//cmth//'1399.txt')
open(24,file=' '//cmonth//'3d99' '//cmth//'1499.txt')
open(25,file=' '//cmonth//'3d99' '//cmth//'1599.txt')
open(26,file=' '//cmonth//'3d99' '//cmth//'1699.txt')
open(27,file=' '//cmonth//'3d99' '//cmth//'1799.txt')
open(28,file=' '//cmonth//'3d99' '//cmth//'1899.txt')
open(29,file=' '//cmonth//'3d99' '//cmth//'1999.txt')
open(30,file=' '//cmonth//'3d99' '//cmth//'2099.txt')
open(31,file=' '//cmonth//'3d99' '//cmth//'2199.txt')
open(32,file=' '//cmonth//'3d99' '//cmth//'2299.txt')
open(33,file=' '//cmonth//'3d99' '//cmth//'2399.txt')
open(34,file=' '//cmonth//'3d99' '//cmth//'2499.txt')
open(35,file=' '//cmonth//'3d99' '//cmth//'2599.txt')
open(36,file=' '//cmonth//'3d99' '//cmth//'2699.txt')
open(37,file=' '//cmonth//'3d99' '//cmth//'2799.txt')
open(38,file=' '//cmonth//'3d99' '//cmth//'2899.txt')

```

```

open(39,file=' '//cmonth//'3d99' '//cmth//'2999.txt')
open(40,file=' '//cmonth//'3d99' '//cmth//'3099.txt')
open(41,file=' '//cmonth//'3d99' '//cmth//'3199.txt')
if(imonth.eq.1) write(10,*) 'lat,lon'
unit=11
do j=1,endday
  read(unit,'(5x)')
  read(unit,'(37x)')
  read(unit,'(37x)')
  read(unit,'(37x)')
  read(unit,'(18x)')
  read(unit,'(47x)')
  read(unit,'(13x)')
  k=4
  do i=1,121
    read(unit,'(58x,f6.3,f8.3,16x)') lat,lon
    if(i.eq.k)then
      write(10,1000) lat,lon
      k=k+3
    endif
  enddo
  close(unit)
  unit=unit+1
enddo
if(imonth.le.11)then
  imonth=imonth+1
  goto 100
else
  close(10)
endif
1000 format(f6.3,', ',f8.3)
end program readhysplit

```

7. Boundary.f

```

program boundary
cccccccccccccccccccc2cccccccccc3cccccccccc4cccccccccc5cccccccccc6cccccccccc7c
c   Written March 2003 By: Ryan P. Shadbolt
c   Last Revision March 2003 By: Ryan P. Shadbolt
c
c   This program was used to extract only the hysplit data
c   points that were within the study domain of 10N-85N and
c   60W-145W.
cccccccccccccccccccc2cccccccccc3cccccccccc4cccccccccc5cccccccccc6cccccccccc7c
  implicit none
  integer i
  real lat,lon

  open(10,file='hysplit3d99.txt')
  open(11,file='hysplit3d99new.txt')
  write(11,*) 'lat,lon'
  do i=1,14600
    read(10,1000) lat,lon
    if(lat.ge.10 .and. lat.le.85 .and. lon.ge.-145.

```

```

&      .and. lon.le.-60.)then
      write(11,1000)lat,lon
    endif
  enddo
close(10)
close(11)
1000 format(f6.3,',',f8.3)
end program boundary

```

8. Hysplitcheck.f

```

      program hysplitcheck
cccccccccc1cccccccccc2cccccccccc3cccccccccc4cccccccccc5cccccccccc6cccccccccc7c
c      Written October 2003 By: Ryan P. Shadbolt
c      Last Revision November 2003 By: Ryan P. Shadbolt
c
c      This program quantifies the difference between the isobaric model
c      used in this study to the HY-SPLIT model. Difference in the u
c      and v distance is taken for each trajectory node for each day of
c      the year for 1999 at 00z for a sample of 365 trajectories.
cccccccccc1cccccccccc2cccccccccc3cccccccccc4cccccccccc5cccccccccc6cccccccccc7c
      implicit none
      integer j,k,istat,hstat
      real ilat,ilon,hlat,hlon,templat,deglon,radpdeg,rkmpdeg,count1
      real totaldisu(40),totaldisv(40),avgdisu(40),avgdisv(40)
      real disu(40),disv(40),totaldisu1,totaldisv1,avgdisu1,avgdisv1
      real count(40),distance1,distance(40)
      parameter (radpdeg=0.01745329,rkmpdeg=111.)

      open(30,file='/data/shadbolt/hysplit/distance.txt')

      do j=1,40
        count(j)=0.
        totaldisu(j)=0.
        totaldisv(j)=0.
        avgdisu(j)=0.
        avgdisv(j)=0.
        distance(j)=0.
      enddo
      open(10,file='/data/shadbolt/hysplit/hysplitdiffmine.txt')
      open(20,file='/data/shadbolt/hysplit/hysplitdiff3d.txt')
      istat=0
      hstat=0
      j=0
      k=0
      totaldisu1=0.
      totaldisv1=0.
      avgdisu1=0.
      avgdisv1=0.
      count1=0.
      read(10,*)
      read(20,*)
100  read(10,1000,iostat=istat)ilat,ilon
      if(istat.ne.0) goto 200

```

```

if(ilat.eq.99.99 .and. ilon.eq.9999.99)then
  do
    if(hlat.eq.99.999 .and. hlon.eq.9999.999) exit
    read(20,1001)hlat,hlon
    if(hstat.ne.0) goto 200
  enddo
  j=0
  goto 100
endif
read(20,1001,iostat=hstat)hlat,hlon
if(hstat.ne.0) goto 200
if(hlat.eq.99.999 .and. hlon.eq.9999.999)then
  do
    if(ilat.eq.99.99 .and. ilon.eq.9999.99) exit
    read(10,1000)ilat,ilon
    if(istat.ne.0) goto 200
  enddo
  j=0
  goto 100
endif
j=j+1
ilon=abs(ilon)
hlon=abs(hlon)
disv(j)=-1.*(rkmpdeg*(hlat-ilat))
templat=hlat*radpdeg
deglon=cos(templat)*rkmpdeg
disu(j)=deglon*(hlon-ilon)
totaldisu(j)=totaldisu(j)+abs(disu(j))
totaldisv(j)=totaldisv(j)+abs(disv(j))
count(j)=count(j)+1.
k=k+1
goto 100
200 close(10)
close(20)

do j=1,40
  avgdisu(j)=totaldisu(j)/count(j)
  avgdisv(j)=totaldisv(j)/count(j)
  distance(j)=SQRT(avgdisu(j)**2.+avgdisv(j)**2.)
  totaldisu1=totaldisu1+totaldisu(j)
  totaldisv1=totaldisv1+totaldisv(j)
  count1=count1+count(j)
  write(30,1002)j,avgdisu(j),avgdisv(j),distance(j)
enddo

write(30,*)
avgdisu1=totaldisu1/count1
avgdisv1=totaldisv1/count1
distance1=SQRT(avgdisu1**2.+avgdisv1**2.)
write(30,1002)j,avgdisu1,avgdisv1,distance1
close(30)

1000 format(f5.2,1x,f7.2)
1001 format(f6.3,1x,f8.3)
1002 format(i2,',',f7.2,',',f7.2,',',f7.2)

end program hysplitcheck

```

9. Anomaly.f

```

program anomaly
cccccccccc1cccccccccc2cccccccccc3cccccccccc4cccccccccc5cccccccccc6cccccccccc7c
c      Written October 2002 By: Ryan P. Shadbolt
c      Last Revision April 2003 By: Ryan P. Shadbolt
c
c      This program takes the difference between two arrays and then
c      puts those values into a new array.
cccccccccc1cccccccccc2cccccccccc3cccccccccc4cccccccccc5cccccccccc6cccccccccc7c
      implicit none
      integer unit,i,j,k
      real array1(150),array2(150)
      real difference(150,160)

      open(1,file='/data/shadbolt/hysplit/lahysplit3d99.asc')
      open(2,file='/data/shadbolt/hysplit/lahysplitmine.asc')
      open(3,file='/data/shadbolt/hysplit/lahysplitdiff.asc')
c      open(1,file='/data/shadbolt/teleconnections/mamimages/
c      &standmam925.asc')
c      open(2,file='/data/shadbolt/teleconnections/mamimages/
c      &standmamgp2.asc')
c      open(3,file='/data/shadbolt/teleconnections/mamimages/
c      &mamgp2anom.asc')
      do i=1,160
        do j=1,150
          difference(j,i)=0
        enddo
      enddo
      do j=1,160
c      read(1,'(149(i4,1x),i4)')(array1(k),k=1,150)
c      read(2,'(149(i4,1x),i4)')(array2(k),k=1,150)
        read(1,'(149(f5.1,1x),f5.1)')(array1(k),k=1,150)
        read(2,'(149(f5.1,1x),f5.1)')(array2(k),k=1,150)
        do k=1,150
          difference(k,j)=array2(k)-array1(k)
        enddo
        write(3,1001)(difference(k,j),k=1,150)
c1001  format(149(i4,','),i4)
1001   format(149(f5.1,','),f5.1)
      enddo
      close(1)
      close(2)
      close(3)

999   stop
      end program anomaly

```

10. Teleextract.f

program teleextract

```

cccccccc1cccccccc2cccccccc3cccccccc4cccccccc5cccccccc6cccccccc7c
c      Written December 2002 By: Ryan P. Shadbolt
c      Last Revision December 2002 By: Ryan P. Shadbolt
c      Michigan State University Dept of Geography
c
c      This program is designed to extract particular teleconnection
c      combinations from the CPC's data set. The PNA, NAO and SOI.
cccccccc1cccccccc2cccccccc3cccccccc4cccccccc5cccccccc6cccccccc7c
implicit none
integer i,j,k,month,year,iunit,count(27)
real nao,wp,ep,pna,soianom,soistan
character(40) header

open(unit=10,file='TeleDataSet.csv')
open(unit=11,file='group1.dat')
open(unit=12,file='group2.dat')
open(unit=13,file='group3.dat')
open(unit=14,file='group4.dat')
open(unit=15,file='group5.dat')
open(unit=16,file='group6.dat')
open(unit=17,file='group7.dat')
open(unit=18,file='group8.dat')
open(unit=19,file='group9.dat')
open(unit=20,file='group10.dat')
open(unit=21,file='group11.dat')
open(unit=22,file='group12.dat')
open(unit=23,file='group13.dat')
open(unit=24,file='group14.dat')
open(unit=25,file='group15.dat')
open(unit=26,file='group16.dat')
open(unit=27,file='group17.dat')
open(unit=28,file='group18.dat')
open(unit=29,file='group19.dat')
open(unit=30,file='group20.dat')
open(unit=31,file='group21.dat')
open(unit=32,file='group22.dat')
open(unit=33,file='group23.dat')
open(unit=34,file='group24.dat')
open(unit=35,file='group25.dat')
open(unit=36,file='group26.dat')
open(unit=37,file='group27.dat')
do i=1,27
  count(i)=0
enddo
read(10,'(a40)')header

c
c      Read through the 40 years of data 1960-1999.
c
do i=1960,1999

c
c      Read through the 12 months of each year.
c
do j=1,12
  read(10,*)year,month,nao,wp,ep,pna,soianom,soistan

c
c      If the values are set to missing (-9.9), change the value to
c      zero for easier use.

```

```

c      if(pna.eq.-9.9) pna=0.0
      if(nao.eq.-9.9) nao=0.0
      if(soistan.eq.-9.9) soistan=0.0
c
c      Start checking for teleconnection combinations of PNA, NAO,
c      and SOI. There are 27 possible combinations.
c
      if(pna.ge.1. .and. nao.ge.1. .and. soistan.ge.1.)then
        k=1
        count(k)=count(k)+1
        iunit=k+10
        write(iunit,200)year,month,pna,nao,soistan
      elseif(pna.ge.1. .and. nao.ge.1. .and. soistan.lt.1.
&        .and. soistan.gt.-1.)then
        k=2
        count(k)=count(k)+1
        iunit=k+10
        write(iunit,200)year,month,pna,nao,soistan
      elseif(pna.ge.1. .and. nao.lt.1. .and. nao.gt.-1.
&        .and. soistan.ge.1.)then
        k=3
        count(k)=count(k)+1
        iunit=k+10
        write(iunit,200)year,month,pna,nao,soistan
      elseif(pna.lt.1. .and. pna.gt.-1. .and. nao.ge.1.
&        .and. soistan.ge.1.)then
        k=4
        count(k)=count(k)+1
        iunit=k+10
        write(iunit,200)year,month,pna,nao,soistan
      elseif(pna.le.-1 .and. nao.le.-1. .and. soistan.le.-1.)then
        k=5
        count(k)=count(k)+1
        iunit=k+10
        write(iunit,200)year,month,pna,nao,soistan
      elseif(pna.le.-1 .and. nao.le.-1. .and. soistan.lt.1.
&        .and. soistan.gt.-1.)then
        k=6
        count(k)=count(k)+1
        iunit=k+10
        write(iunit,200)year,month,pna,nao,soistan
      elseif(pna.le.-1 .and. nao.lt.1. .and. nao.gt.-1.
&        .and. soistan.le.-1)then
        k=7
        count(k)=count(k)+1
        iunit=k+10
        write(iunit,200)year,month,pna,nao,soistan
      elseif(pna.lt.1. .and. pna.gt.-1. .and. nao.le.-1
&        .and. soistan.le.-1.)then
        k=8
        count(k)=count(k)+1
        iunit=k+10
        write(iunit,200)year,month,pna,nao,soistan
      elseif(pna.ge.1. .and. nao.lt.1. .and. nao.gt.-1.
&        .and. soistan.lt.1 .and. soistan.gt.-1)then
        k=9

```

```

        count(k)=count(k)+1
        iunit=k+10
        write(iunit,200)year,month,pna,nao,soistan
elseif(pna.lt.1. .and. pna.gt.-1. .and. nao.ge.1.
&      .and. soistan.lt.1 .and. soistan.gt.-1.)then
        k=10
        count(k)=count(k)+1
        iunit=k+10
        write(iunit,200)year,month,pna,nao,soistan
elseif(pna.lt.1. .and. pna.gt.-1. .and. nao.lt.1.
&      .and. nao.gt.-1. .and. soistan.ge.1.)then
        k=11
        count(k)=count(k)+1
        iunit=k+10
        write(iunit,200)year,month,pna,nao,soistan
elseif(pna.le.-1. .and. nao.lt.1. .and. nao.gt.-1.
&      .and. soistan.lt.1. .and. soistan.gt.-1.)then
        k=12
        count(k)=count(k)+1
        iunit=k+10
        write(iunit,200)year,month,pna,nao,soistan
elseif(pna.lt.1. .and. pna.gt.-1. .and. nao.le.-1.
&      .and. soistan.lt.1. .and. soistan.gt.-1.)then
        k=13
        count(k)=count(k)+1
        iunit=k+10
        write(iunit,200)year,month,pna,nao,soistan
elseif(pna.lt.1. .and. pna.gt.-1. .and. nao.lt.1.
&      .and. nao.gt.-1. .and. soistan.le.-1)then
        k=14
        count(k)=count(k)+1
        iunit=k+10
        write(iunit,200)year,month,pna,nao,soistan
elseif(pna.ge.1. .and. nao.le.-1. .and. soistan.le.-1.)then
        k=15
        count(k)=count(k)+1
        iunit=k+10
        write(iunit,200)year,month,pna,nao,soistan
elseif(pna.le.-1. .and. nao.ge.1. .and. soistan.le.-1.)then
        k=16
        count(k)=count(k)+1
        iunit=k+10
        write(iunit,200)year,month,pna,nao,soistan
elseif(pna.le.-1. .and. nao.ge.1. .and. soistan.ge.1.)then
        k=17
        count(k)=count(k)+1
        iunit=k+10
        write(iunit,200)year,month,pna,nao,soistan
elseif(pna.le.-1. .and. nao.ge.1. .and. soistan.ge.1.)then
        k=18
        count(k)=count(k)+1
        iunit=k+10
        write(iunit,200)year,month,pna,nao,soistan
elseif(pna.ge.1. .and. nao.le.-1. .and. soistan.ge.1.)then
        k=19
        count(k)=count(k)+1
        iunit=k+10

```

```

        write(iunit,200)year,month,pna,nao,soistan
    elseif(pna.ge.1. .and. nao.ge.1. .and. soistan.le.-1)then
        k=20
        count(k)=count(k)+1
        iunit=k+10
        write(iunit,200)year,month,pna,nao,soistan
    elseif(pna.lt.1. .and. pna.gt.-1. .and. nao.ge.1.
&      .and. soistan.le.-1.)then
        k=21
        count(k)=count(k)+1
        iunit=k+10
        write(iunit,200)year,month,pna,nao,soistan
    elseif(pna.lt.1. .and. pna.gt.-1. .and. nao.le.-1.
&      .and. soistan.ge.1.)then
        k=22
        count(k)=count(k)+1
        iunit=k+10
        write(iunit,200)year,month,pna,nao,soistan
    elseif(pna.ge.1. .and. nao.lt.1. .and. nao.gt.-1.
&      .and. soistan.le.-1.)then
        k=23
        count(k)=count(k)+1
        iunit=k+10
        write(iunit,200)year,month,pna,nao,soistan
    elseif(pna.le.-1. .and. nao.lt.1. .and. nao.gt.-1.
&      .and. soistan.ge.1.)then
        k=24
        count(k)=count(k)+1
        iunit=k+10
        write(iunit,200)year,month,pna,nao,soistan
    elseif(pna.ge.1. .and. nao.le.-1. .and. soistan.lt.1.
&      .and. soistan.gt.-1.)then
        k=25
        count(k)=count(k)+1
        iunit=k+10
        write(iunit,200)year,month,pna,nao,soistan
    elseif(pna.le.-1. .and. nao.ge.1. .and. soistan.lt.1.
&      .and. soistan.gt.-1.)then
        k=26
        count(k)=count(k)+1
        iunit=k+10
        write(iunit,200)year,month,pna,nao,soistan
    else
        k=27
        count(k)=count(k)+1
        iunit=k+10
        write(iunit,200)year,month,pna,nao,soistan
    endif
enddo
enddo
do i=1,27
    write(*,*)count(i)
enddo
do i=10,37
    close(i)
enddo
200 format(i4,1x,i2,3(1x,f4.1))

```

```

999  stop
      end program teleextract

```

11. Teleconnections.f

```

      program teleconnections
cccccccccc1cccccccccc2cccccccccc3cccccccccc4cccccccccc5cccccccccc6cccccccccc7c
c      Written February 2003 By: Ryan P. Shadbolt
c      Last Revision April 2003 By: Ryan P. Shadbolt
c
c      This program was used to combine the groups of teleconnection
c      combinations into the proper monthly intervals of DJF, MAM, JJA,
c      and SON.
cccccccccc1cccccccccc2cccccccccc3cccccccccc4cccccccccc5cccccccccc6cccccccccc7c
      implicit none
      integer i, istat, nstat, imonth
      real lat, lon
      character(2) year
      character(3) cmonth, month(12)
      data month / 'jan', 'feb', 'mar', 'apr', 'may', 'jun', 'jul', 'aug',
&                'sep', 'oct', 'nov', 'dec' /

      open(10, file='/data/shadbolt/teleconnections/group26.dat')
      open(20, file='/data/shadbolt/teleconnections/DJF925group26.txt')
      open(30, file='/data/shadbolt/teleconnections/MAM925group26.txt')
      open(40, file='/data/shadbolt/teleconnections/JJA925group26.txt')
      open(50, file='/data/shadbolt/teleconnections/SON925group26.txt')
      write(20, *) 'lat, lon'
      write(30, *) 'lat, lon'
      write(40, *) 'lat, lon'
      write(50, *) 'lat, lon'
      istat=0
      do
        read(10, '(2x,a2,1x,i2)', iostat=istat) year, imonth
        if(istat.ne.0) goto 999
        do i=1,12
          if(i.eq.imonth) then
            cmonth=month(i)
            exit
          endif
        enddo
        write(*, *) year, imonth, cmonth
        nstat=0
        open(60, file='/data/shadbolt/back/'//cmonth//'/1925/b'
&                '//year//'062040.txt')
        do
          read(60, '(f5.2,1x,f7.2)', iostat=nstat) lat, lon
          if(nstat.ne.0) then
            close(60)
            goto 888
          else
            if(imonth.eq.12 .or. imonth.eq.1 .or. imonth.eq.2) then
              write(20,1000) lat, lon
            elseif(imonth.eq.3 .or. imonth.eq.4 .or. imonth.eq.5) then

```

```

        write(30,1000)lat,lon
        elseif(imonth.eq.6 .or. imonth.eq.7 .or. imonth.eq.8)then
            write(40,1000)lat,lon
        elseif(imonth.eq.9.or. imonth.eq.10 .or. imonth.eq.11)then
            write(50,1000)lat,lon
        endif
    endif
enddo
888 enddo

999 close(10)
    close(20)
    close(30)
    close(40)
    close(50)

1000 format(f5.2,',',f7.2)

    end program teleconnections

```

12. Divide.f

```

    program divide
cccccccc1cccccccc2cccccccc3cccccccc4cccccccc5cccccccc6cccccccc7c
c    Written March 2003 By: Ryan P. Shadbolt
c    Last Revision March 2003 By: Ryan P. Shadbolt
c
c    This program is used to combine monthly combinations together.
c    Example DJF, MAM, JJA, SON
cccccccc1cccccccc2cccccccc3cccccccc4cccccccc5cccccccc6cccccccc7c
    implicit none
    integer unit,i,j,k,newarray1(150,160),array(150)
    integer newarray2(150,160),newarray3(150,160)
    integer newarray4(150,160)
    real DJFcombine(150,160),MAMcombine(150,160),JJACombine(150,160)
    real SONcombine(150,160)

    open(1,file='/data/shadbolt/925files/jan925.asc')
    open(2,file='/data/shadbolt/925files/feb925.asc')
    open(3,file='/data/shadbolt/925files/mar925.asc')
    open(4,file='/data/shadbolt/925files/apr925.asc')
    open(5,file='/data/shadbolt/925files/may925.asc')
    open(6,file='/data/shadbolt/925files/jun925.asc')
    open(7,file='/data/shadbolt/925files/jul925.asc')
    open(8,file='/data/shadbolt/925files/aug925.asc')
    open(9,file='/data/shadbolt/925files/sep925.asc')
    open(10,file='/data/shadbolt/925files/oct925.asc')
    open(11,file='/data/shadbolt/925files/nov925.asc')
    open(12,file='/data/shadbolt/925files/dec925.asc')
    open(13,file='DJFcombine925.asc')
    open(14,file='MAMcombine925.asc')
    open(15,file='JJACombine925.asc')
    open(16,file='SONcombine925.asc')
    do i=1,160

```

```

        do j=1,150
            DJFcombine(j,i)=0
            MAMcombine(j,i)=0
            JJAcombine(j,i)=0
            SONcombine(j,i)=0
        enddo
    enddo
    unit=1
    do i=1,12
        do j=1,160
            read(unit, '(149(i4,1x),i4)')(array(k),k=1,150)
            do k=1,150
                if(i.eq.12 .or. i.eq.1 .or. i.eq.2)then
                    DJFcombine(k,j)=DJFcombine(k,j)+array(k)
                elseif(i.eq.3 .or. i.eq.4 .or. i.eq.5)then
                    MAMcombine(k,j)=MAMcombine(k,j)+array(k)
                elseif(i.eq.6 .or. i.eq.7 .or. i.eq.8)then
                    JJAcombine(k,j)=JJAcombine(k,j)+array(k)
                elseif(i.eq.9 .or. i.eq.10 .or. i.eq.11)then
                    SONcombine(k,j)=SONcombine(k,j)+array(k)
                endif
            enddo
        enddo
        close(unit)
        unit=unit+1
    enddo
    do i=1,160
        do j=1,150
            newarray1(j,i)=int(DJFcombine(j,i))
            newarray2(j,i)=int(MAMcombine(j,i))
            newarray3(j,i)=int(JJAcombine(j,i))
            newarray4(j,i)=int(SONcombine(j,i))
        enddo
    enddo
    do i=1,160
        write(13,1000)(newarray1(k,i),k=1,150)
        write(14,1000)(newarray2(k,i),k=1,150)
        write(15,1000)(newarray3(k,i),k=1,150)
        write(16,1000)(newarray4(k,i),k=1,150)
    enddo

1000  format(149(i5,', '),i5)
999   stop
      end program divide

```

13. Standardize.f

```

      program standardize
cccccccccc1cccccccccc2cccccccccc3cccccccccc4cccccccccc5cccccccccc6cccccccccc7c
c      Written March 2003 By: Ryan P. Shadbolt
c      Last Revision April 2003 By: Ryan P. Shadbolt
c
c      This program is used to take the difference of the standardized
c      trajectory files, so that the anomaly images can be made for each

```

```

c      teleconnection combination during each of the monthly intervals
c      of DJF, MAM, JJA, SON.
cccccccc1cccccccc2cccccccc3cccccccc4cccccccc5cccccccc6cccccccc7c
      implicit none
      integer i,j,array1(150,160)
      real total,constant,array2(150,160),array3(150,160)

open(10,file='/data/shadbolt/teleconnections/mamimages/lambert/lam
      &am925gp2.asc')

open(20,file='/data/shadbolt/teleconnections/mamimages/standmamgp2
      &.asc')
c      open(10,file='/data/shadbolt/teleconnections/jjaimages/
c      &JJAcombine925.asc')
c      open(20,file='/data/shadbolt/teleconnections/jjaimages/
c      &standjja925.asc')
      total=14441.
      constant=100000.
      do j=1,160
        read(10,'(149(i4,1x),i4)')(array1(i,j),i=1,150)
c      read(10,'(149(i5,1x),i5)')(array1(i,j),i=1,150)
        do i=1,150
          array2(i,j)=real(array1(i,j))
          array3(i,j)=(array2(i,j)/total)*constant
        enddo
        write(20,1000)(array3(i,j),i=1,150)
      enddo

      close(10)
      close(20)

c1000  format(149(f4.1,','),f4.1)
1000   format(149(f5.1,','),f5.1)
999    stop
      end program standardize

```

14. Temp_precip.f

```

      program temp_precip
cccccccc1cccccccc2cccccccc3cccccccc4cccccccc5cccccccc6cccccccc7c
c      Written July 2003 By: Ryan P. Shadbolt
c      Last Revision August 2003 By: Ryan P. Shadbolt
c
c      This program is used to compare teleconnection combinations to
c      temperature and precip anomalies within the climate division #9
c      within Michigan's lower peninsula.
cccccccc1cccccccc2cccccccc3cccccccc4cccccccc5cccccccc6cccccccc7c
      implicit none
      character(1) number1
      character(2) number2
      integer a,i,j,k,imiss,year,year1,year2,month,istat
      real temp(12),precip(12),djfcount,mamcount,jjacount,soncount
      real rmiss,djftemp,djfp precip,mamtemp,mamprecip,jjatemp,jjaprecip
      parameter (imiss=-999,rmiss=-999.)

```

```

do i=1,27
  if(i.le.9)then
    write(number1,'(i1)')i
    open(10,file='/data/shadbolt/teleconnections/group'
&      //number1//'.dat')
    open(40,file='/data/shadbolt/teleconnections/group'
&      //number1//'.djf.txt')
    open(50,file='/data/shadbolt/teleconnections/group'
&      //number1//'.mam.txt')
    open(60,file='/data/shadbolt/teleconnections/group'
&      //number1//'.jja.txt')
    open(70,file='/data/shadbolt/teleconnections/group'
&      //number1//'.son.txt')
  else
    write(number2,'(i2)')i
    open(10,file='/data/shadbolt/teleconnections/group'
&      //number2//'.dat')
    open(40,file='/data/shadbolt/teleconnections/group'
&      //number2//'.djf.txt')
    open(50,file='/data/shadbolt/teleconnections/group'
&      //number2//'.mam.txt')
    open(60,file='/data/shadbolt/teleconnections/group'
&      //number2//'.jja.txt')
    open(70,file='/data/shadbolt/teleconnections/group'
&      //number2//'.son.txt')
  endif
  istat=0
100  read(10,1000,iostat=istat)year,month
  if(istat.ne.0) goto 400
  open(20,file='/data/shadbolt/teleconnections/temp.txt')
  open(30,file='/data/shadbolt/teleconnections/precip.txt')
200  read(20,1001)year1,(temp(a),a=1,12)
  read(30,1002)year2,(precip(a),a=1,12)
  if(year.eq.year1 .and. year.eq.year2)then
    if(month.eq.12. .or. month.eq.1 .or. month.eq.2)then
      write(40,1003)year1,temp(month),precip(month)
    elseif(month.eq.3. .or. month.eq.4 .or. month.eq.5)then
      write(50,1003)year1,temp(month),precip(month)
    elseif(month.eq.6. .or. month.eq.7 .or. month.eq.8)then
      write(60,1003)year1,temp(month),precip(month)
    elseif(month.eq.9. .or. month.eq.10 .or. month.eq.11)then
      write(70,1003)year1,temp(month),precip(month)
    endif
  else
    goto 200
  endif
  close(20)
  close(30)
300  goto 100
400  close(10)
  close(20)
  close(30)
  close(40)
  close(50)
  close(60)
  close(70)

```

```
        enddo  
1000  format(i4,1x,i2)  
1001  format(i13,12(f13.1))  
1002  format(i13,12(f13.2))  
1003  format(i13,f13.1,f13.2)  
      end program temp_precip
```

APPENDIX B: GIS COMMANDS

1. Projecting the Back-Trajectory Files

```
Arc: project cover <oldfilename> <newfilename>
Project: input
Project: projection geographic
Project: units dd
Project: parameters
Project: output
Project: projection lambert_azimuth
Project: units meters
Project: parameters
radius of the sphere of reference [ 0.00000 ]:
longitude of center of projection [ 0 0 0.000 ]: -85 00 00
latitude of center of projection [ 0 0 0.000 ]: 42 30 00
false easting (meters) [ 0.00000 ]:
false northing (meters) [ 0.00000 ]:
Project: end
```

2. Projecting the Raster Grids

The raster grids were projected within ERDAS Imagine by the following tasks: go to the “Image Info” option and select “edit and change map model.” Within this option, the boundary units and map projection were manually changed to their desired values. In this study, the boundary for the upper left corner had new coordinates of (-4850000 m, 5000000 m) and the boundary of the lower right corner had new coordinates of (2600000 m, -2950000 m). The projection was then changed to a Lambert-Azimuthal Equal-Area projection. The image was then saved and reopened to use the file with the new projection coordinates.

3. Trajectory Node Locations in Meters

The location in meters for each trajectory node needed to be obtained. This was done by opening each vector file within ERDAS Imagine and then selecting the “vector attributes” option where the node values were listed in meters. The files were very large, so storage space was an issue. Within ERDAS Imagine, the files were imported as ASCII to raster format using the “import” option and selecting “ASCII.” By following the steps in section 2, the file was re-projected. The file was then saved as a raster file and reopened as a pseudo-color image. Once the image was displayed, by selecting “raster attributes,” the colors of specified trajectory node densities were changed for an easier-to-read display.

APPENDIX C: T-TEST RESULTS

1. TC2 (PNA+, NAO+, SOI) Spring

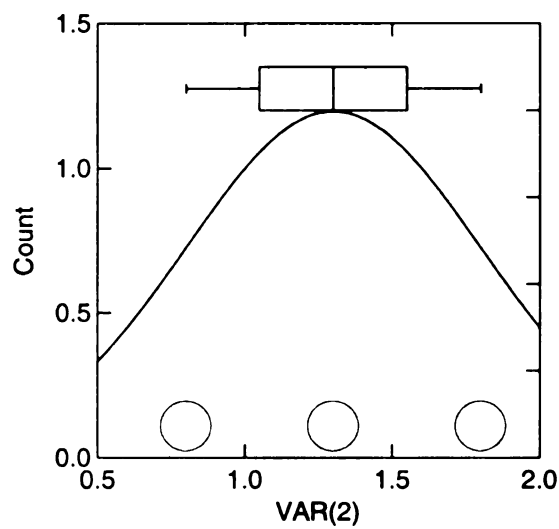


Figure C.1. One-sample t test of temperature with 3 cases; Mean = 1.3, SD = 0.5, Prob = 0.0

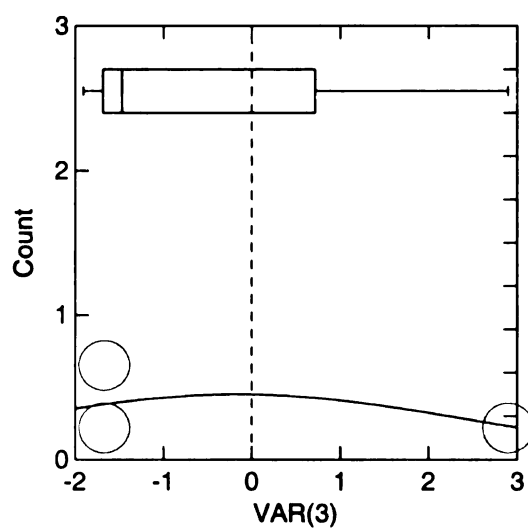


Figure C.2. One-sample t test of precipitation with 3 cases; Mean = -2.0, SD = 27.0, Prob = 0.9

2. TC4 (PNA, NAO+, SOI+) Winter

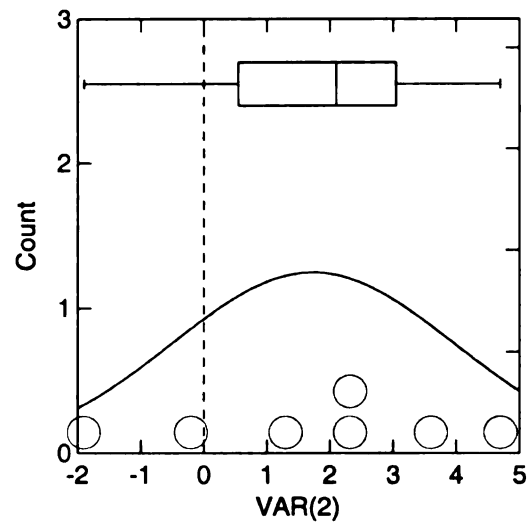


Figure C.3. One-sample t test of temperature with 7 cases; Mean = 1.7, SD = 2.2, Prob = 0.1

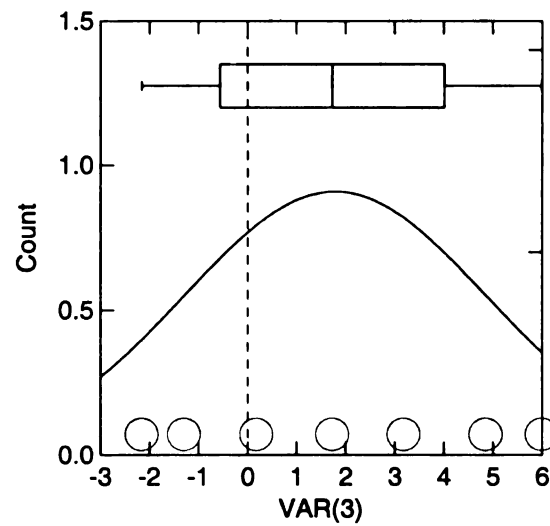


Figure C.4. One-sample t test of precipitation with 7 cases; Mean = 18.0, SD = 31.0, Prob = 0.2

3. TC6 (PNA-, NAO-, SOI) Winter

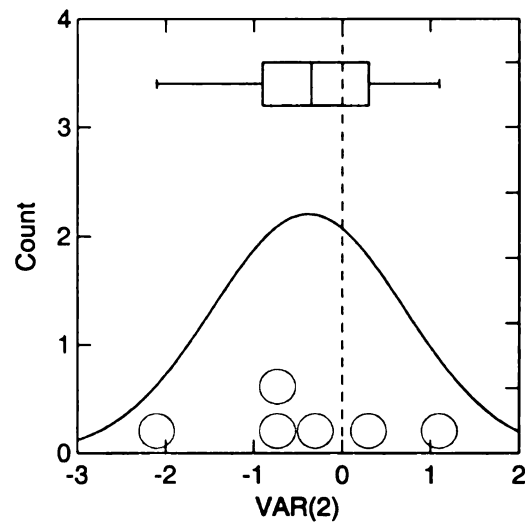


Figure C.5. One-sample t test of temperature with 6 cases; Mean = -0.4, SD = 1.1, Prob = 0.4

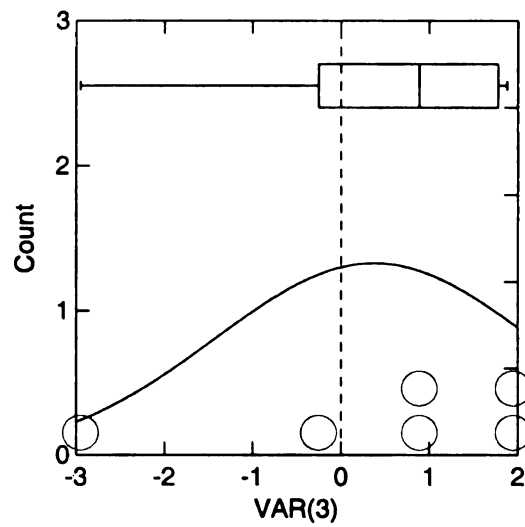


Figure C.6. One-sample t test of precipitation with 6 cases; Mean = 4.0, SD = 18.0, Prob = 0.6

4. TC6 (PNA-, NAO-, SOI) Spring

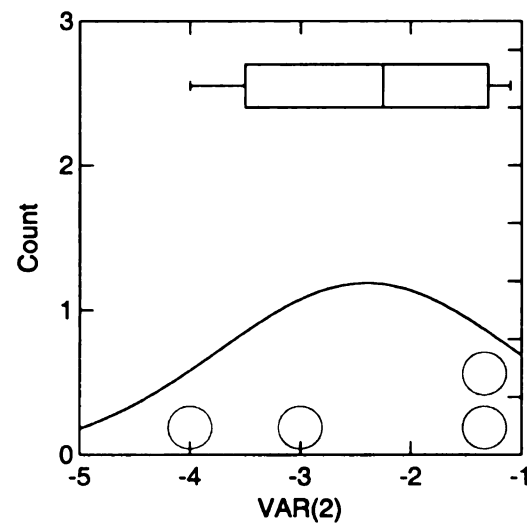


Figure C.7. One-sample t test of temperature with 4 cases; Mean = -2.4, SD = 1.3, Prob = 0.0

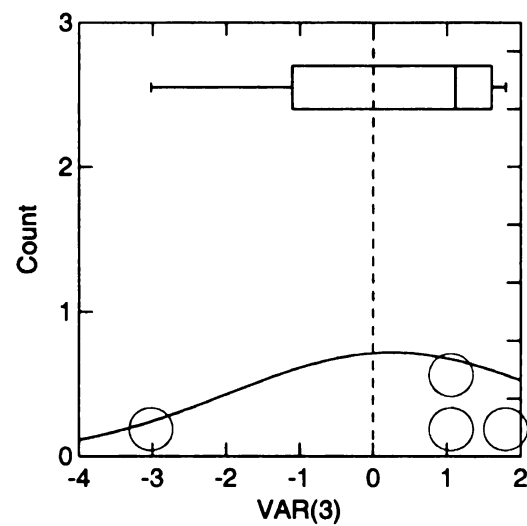


Figure C.8. One-sample t test of precipitation with 4 cases; Mean = 3.0, SD = 22.0, Prob = 0.8

5. TC8 (PNA, NAO-, SOI-) Winter

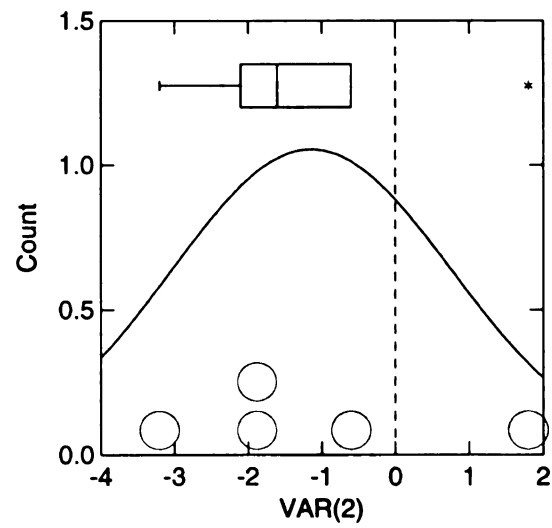


Figure C.9. One-sample t test of temperature with 5 cases; Mean = -1.1, SD = 2.9, Prob = 0.2

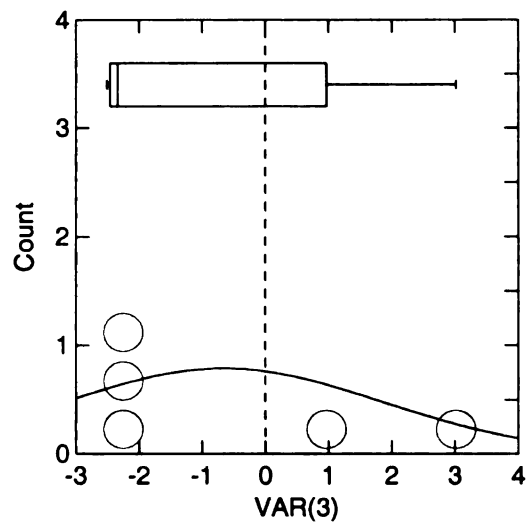


Figure C.10. One-sample t test of precipitation with 5 cases; Mean = -7.0, SD = 25.0, Prob = 0.6

6. TC8 (PNA, NAO-, SOI-) Spring

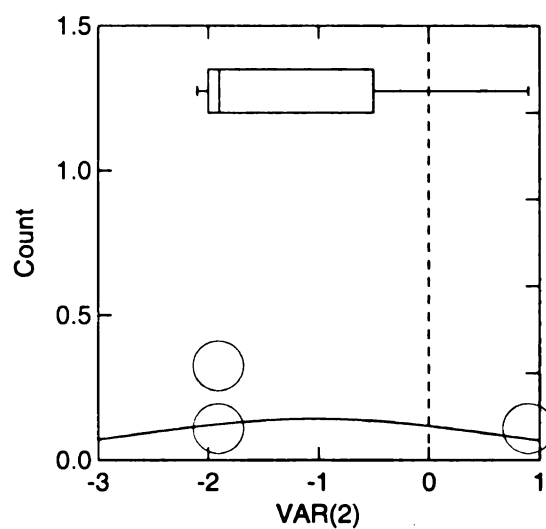


Figure C.11. One-sample t test of temperature with 3 cases; Mean = -1.0, SD = 1.7, Prob = 0.4

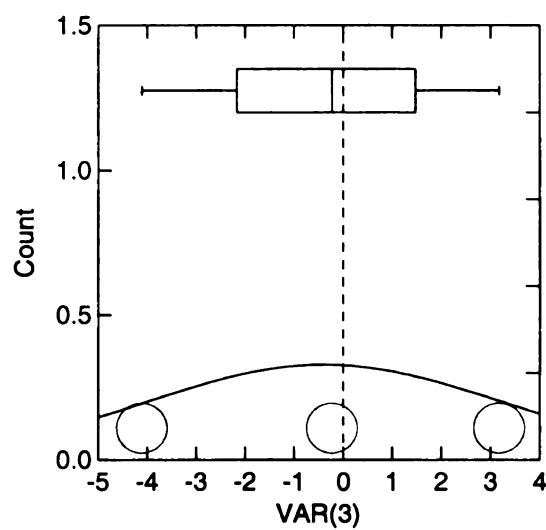


Figure C.12. One-sample t test of precipitation with 3 cases; Mean = -4.0, SD = 36.0, Prob = 0.9

7. TC8 (PNA, NAO-, SOI-) Summer

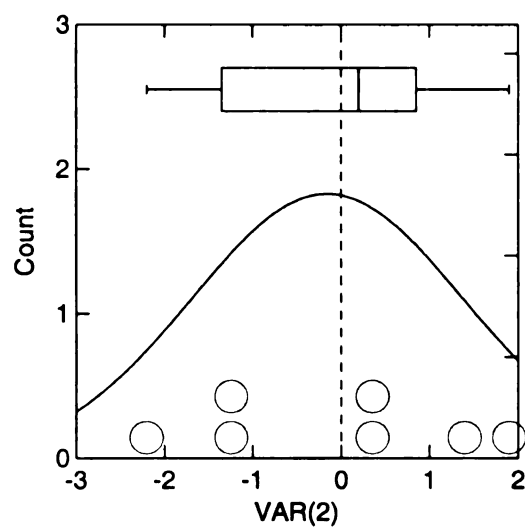


Figure C.13. One-sample t test of temperature with 7 cases; Mean = -0.2, SD = 1.5, Prob = 0.8

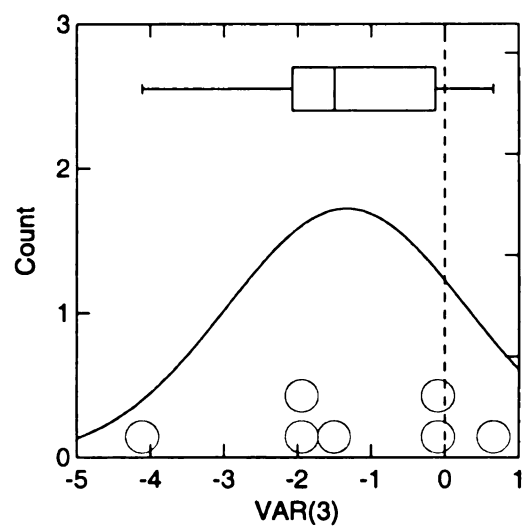


Figure C.14. One-sample t test of precipitation with 7 cases; Mean = -13.0, SD = 16.0, Prob = 0.1

8. TC9 (PNA+, NAO, SOI) Winter

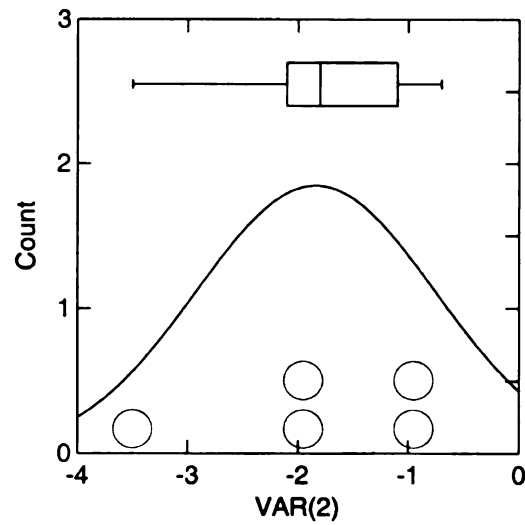


Figure C.15. One-sample t test of temperature with 5 cases; Mean = -1.8, SD = 1.1, Prob = 0.0

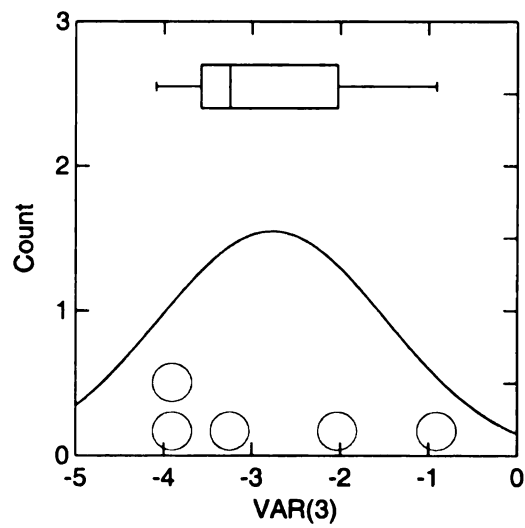


Figure C.16. One-sample t test of precipitation with 5 cases; Mean = -28.0, SD = 13.0, Prob = 0.0

9. TC9 (PNA+, NAO, SOI) Spring

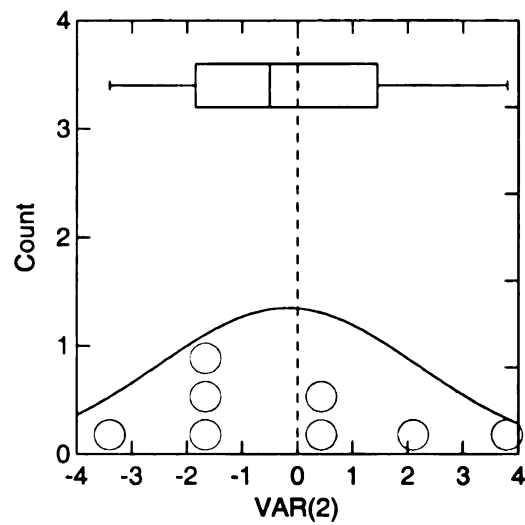


Figure C.17. One-sample t test of temperature with 8 cases; Mean = -0.2, SD = 2.4, Prob = 0.8

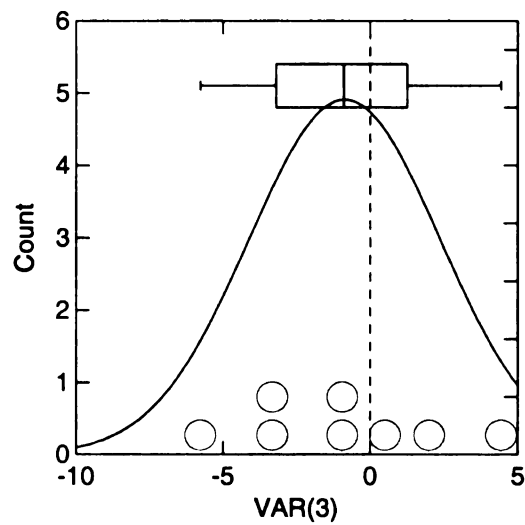


Figure C.18. One-sample t test of precipitation with 8 cases; Mean = -9.0, SD = 33.0, Prob = 0.5

10. TC9 (PNA+, NAO, SOI) Summer

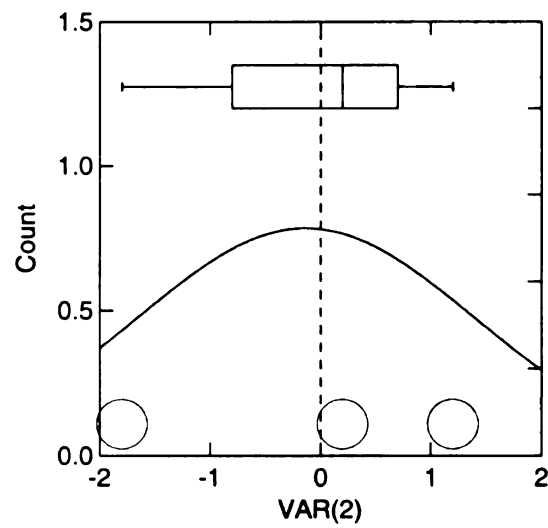


Figure C.19. One-sample t test of temperature with 3 cases; Mean = -0.1, SD = 1.5, Prob = 0.9

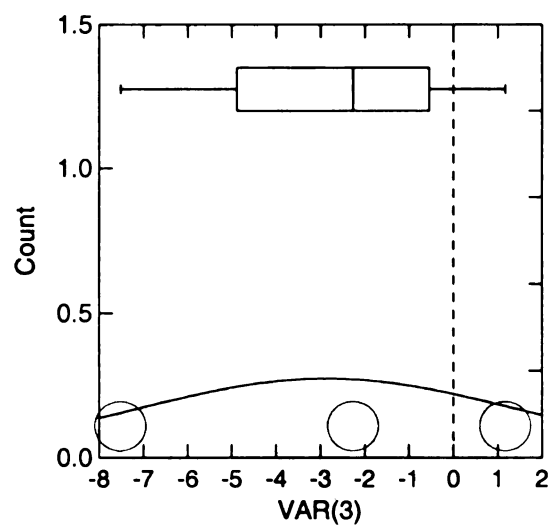


Figure C.20. One-sample t test of precipitation with 3 cases; Mean = -29.0, SD = 44.0, Prob = 0.4

11. TC9 (PNA+, NAO, SOI) Autumn

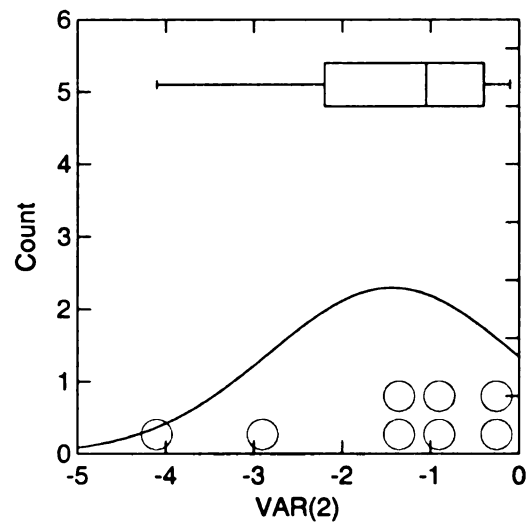


Figure C.21. One-sample t test of temperature with 8 cases; Mean = -1.4, SD = 1.4, Prob = 0.0

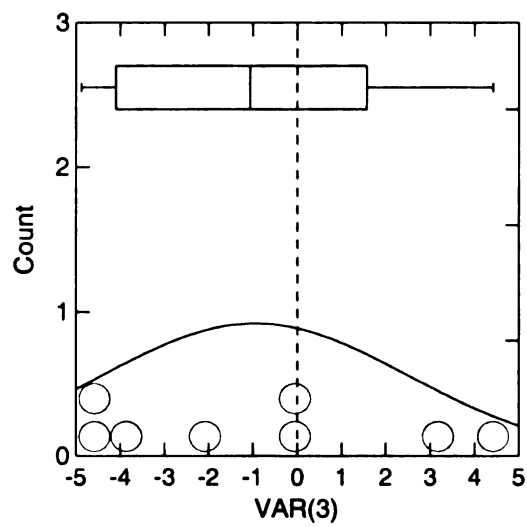


Figure C.22. One-sample t test of precipitation with 8 cases; Mean = -10.0, SD = 35.0, Prob = 0.5

12. TC10 (PNA, NAO+, SOI) Winter

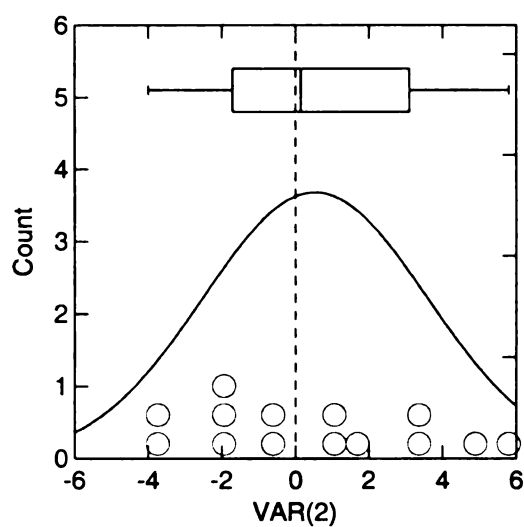


Figure C.23. One-sample t test of temperature with 14 cases; Mean = 0.5, SD = 3.0, Prob = 0.5

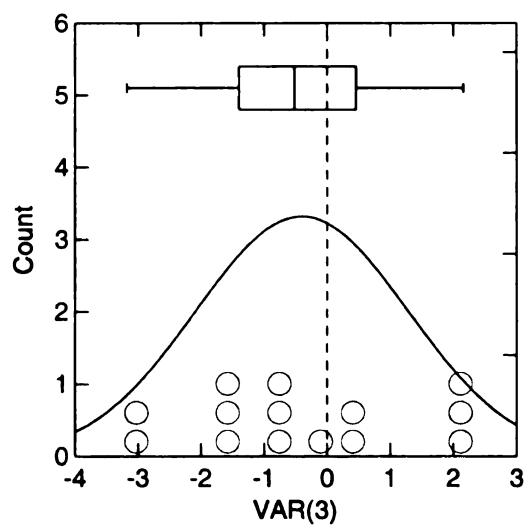


Figure C.24. One-sample t test of precipitation with 14 cases; Mean = -4.0, SD = 17.0, Prob = 0.4

13. TC10 (PNA, NAO+, SOI) Spring

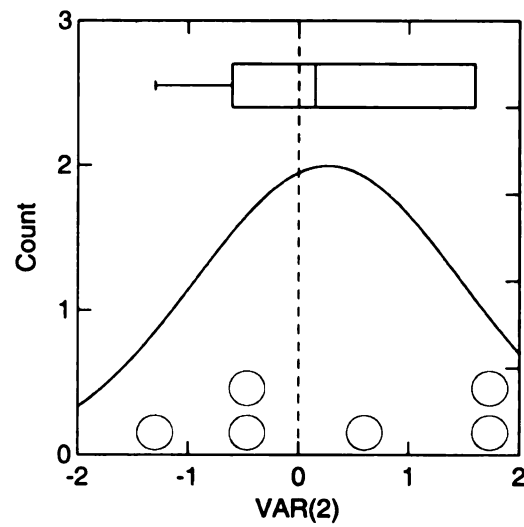


Figure C.25. One-sample t test of temperature with 6 cases; Mean = 0.3, SD = 1.2, Prob = 0.6

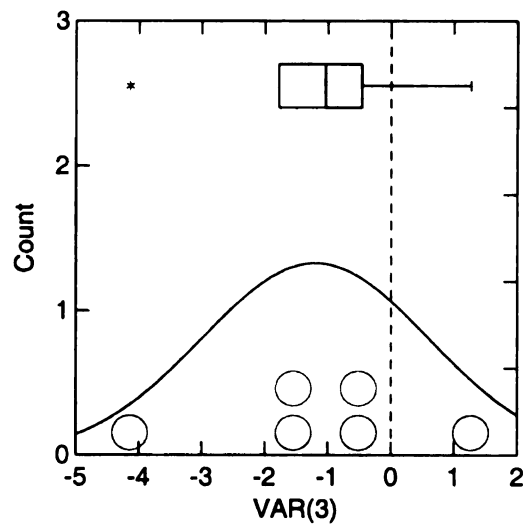


Figure C.26. One-sample t test of precipitation with 6 cases; Mean = -12.0, SD = 18.0, Prob = 0.2

14. TC10 (PNA, NAO+, SOI) Summer

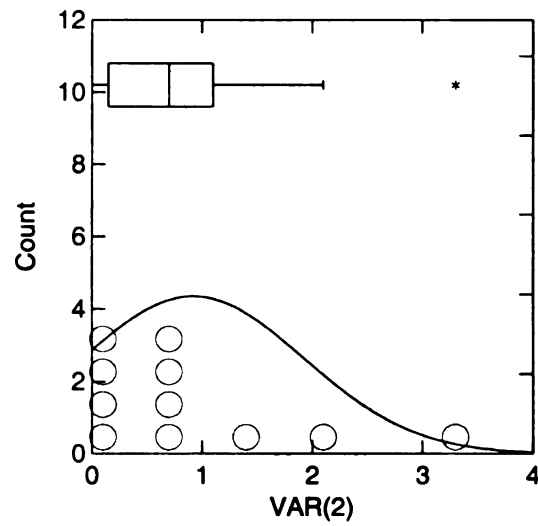


Figure C.27. One-sample t test of temperature with 11 cases; Mean = 0.9, SD = 1.0, Prob = 0.0

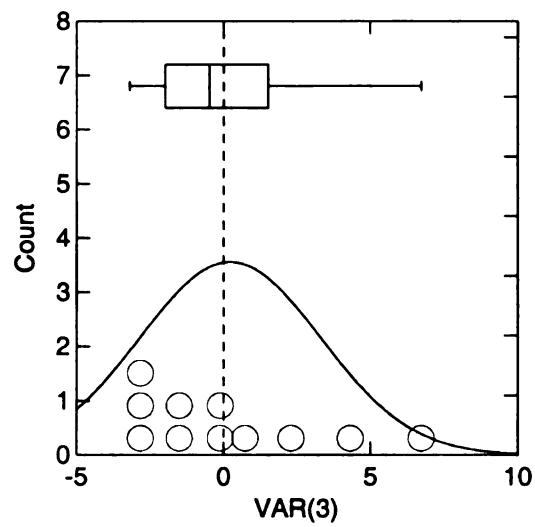


Figure C.28. One-sample t test of precipitation with 11 cases; Mean = 2.0, SD = 31.0, Prob = 0.8

15. TC10 (PNA, NAO+, SOI) Autumn

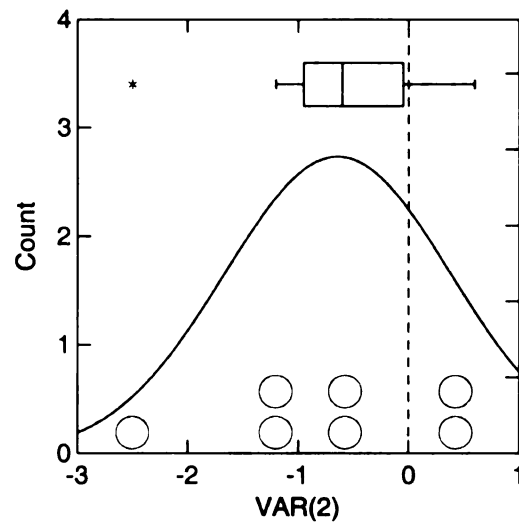


Figure C.29. One-sample t test of temperature with 7 cases; Mean = -0.6, SD = 1.0, Prob = 0.1

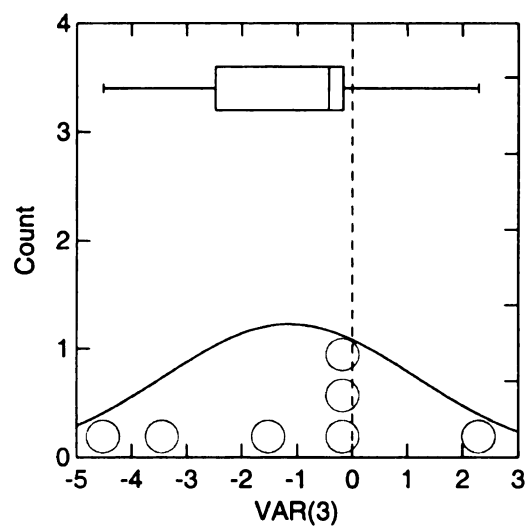


Figure C.30. One-sample t test of precipitation with 7 cases; Mean = -11.0, SD = 23.0, Prob = 0.2

16. TC11 (PNA, NAO, SOI+) Winter

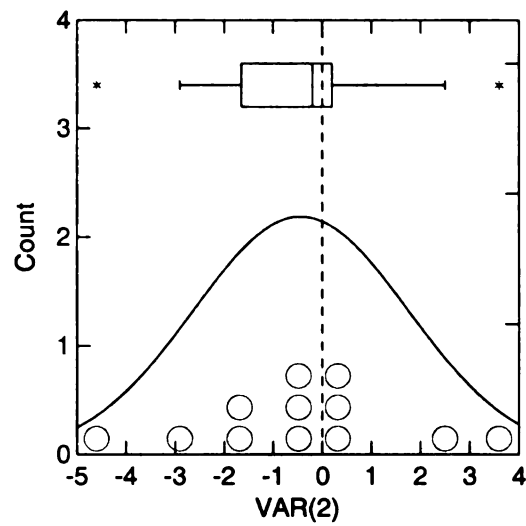


Figure C.31. One-sample t test of temperature with 12 cases; Mean = -0.4, SD = 2.2, Prob = 0.5

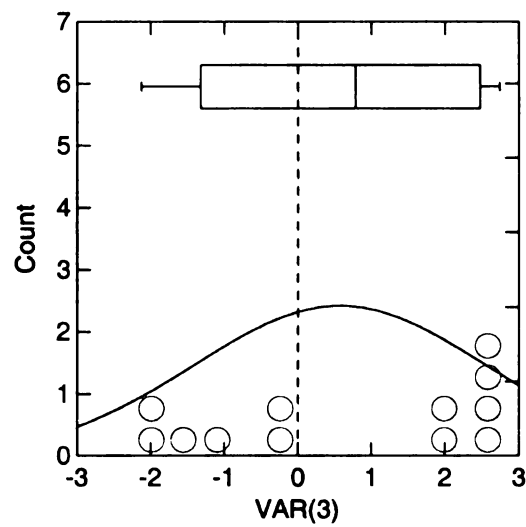


Figure C.32. One-sample t test of precipitation with 12 cases; Mean = 6.0, SD = 20.0, Prob = 0.3

17. TC11 (PNA, NAO, SOI+) Spring

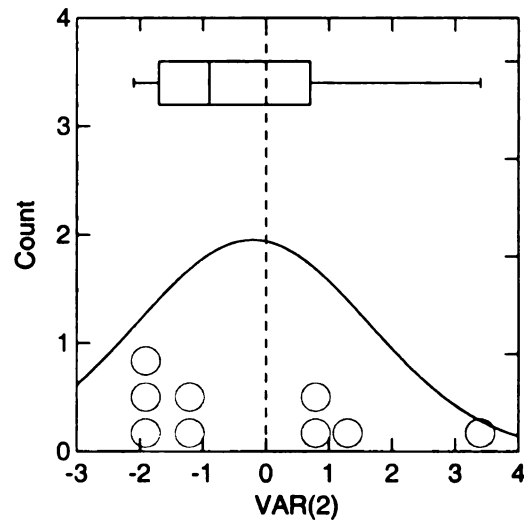


Figure C.33. One-sample t test of temperature with 9 cases; Mean = -0.2, SD = 1.8, Prob = 0.7

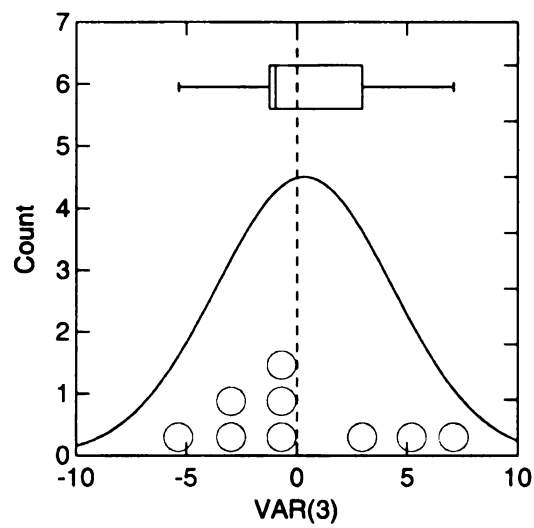


Figure C.34. One-sample t test of precipitation with 9 cases; Mean = 3.0, SD = 40.0, Prob = 0.8

18. TC11 (PNA, NAO, SOI+) Summer

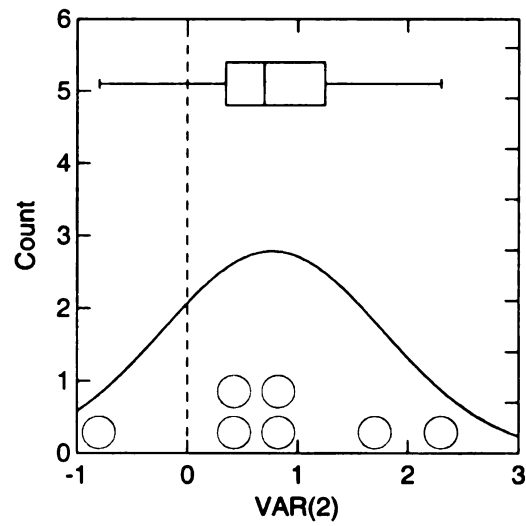


Figure C.35. One-sample t test of temperature with 7 cases; Mean = 0.8, SD = 1.0, Prob = 0.1

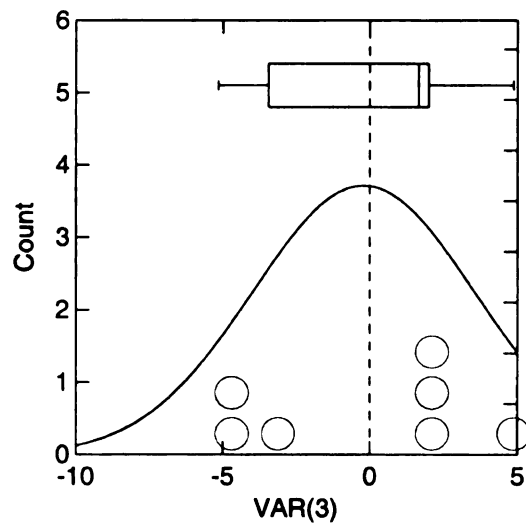


Figure C.36. One-sample t test of precipitation with 7 cases; Mean = -2.0, SD = 38.0, Prob = 0.9

19. TC11 (PNA, NAO, SOI+) Autumn

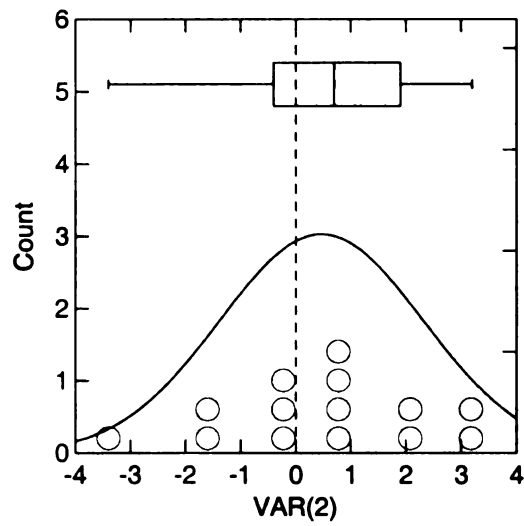


Figure C.37. One-sample t test of temperature with 14 cases; Mean = 0.5, SD = 1.8, Prob = 0.4

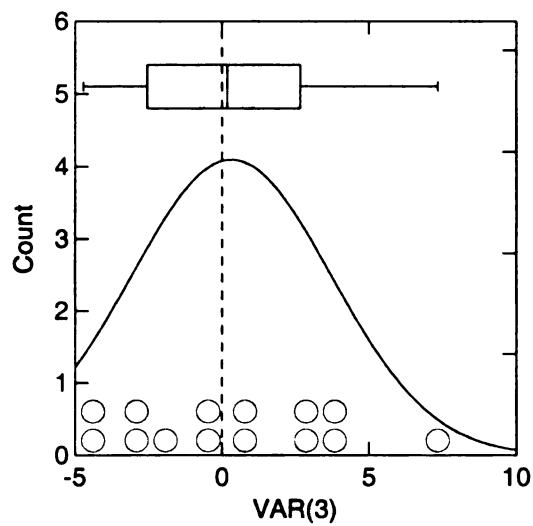


Figure C.38. One-sample t test of precipitation with 14 cases; Mean = 3.0, SD = 34.0, Prob = 0.7

20. TC12 (PNA-, NAO, SOI) Winter

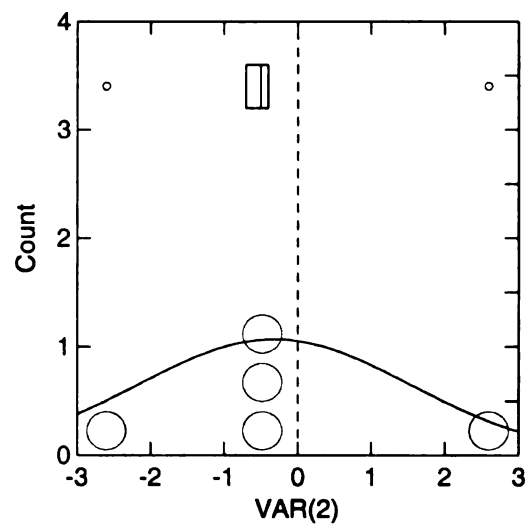


Figure C.39. One-sample t test of temperature with 5 cases; Mean = -0.3, SD = 1.9, Prob = 0.7

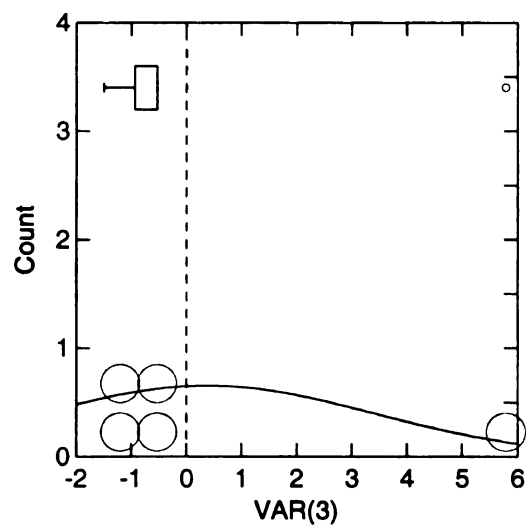


Figure C.40. One-sample t test of precipitation with 5 cases; Mean = 4.0, SD = 30.0, Prob = 0.8

21. TC12 (PNA-, NAO, SOI) Spring

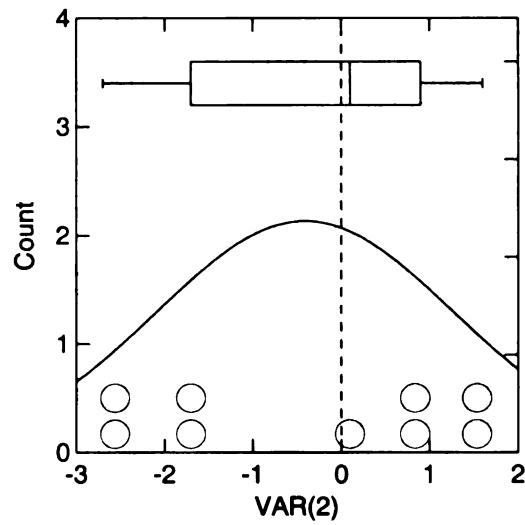


Figure C.41. One-sample t test of temperature with 9 cases; Mean = -0.4, SD = 1.7, Prob = 0.5

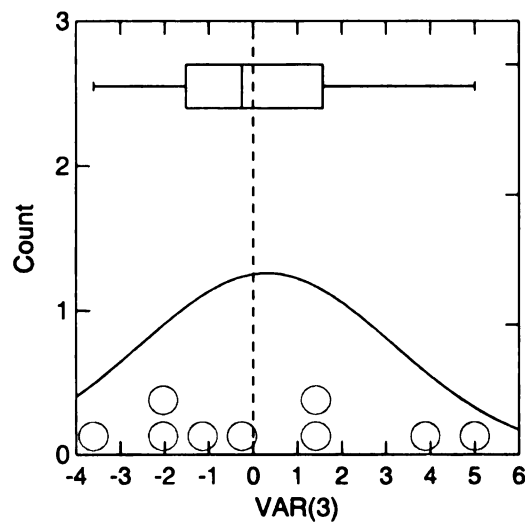


Figure C.42. One-sample t test of precipitation with 9 cases; Mean = 3.0, SD = 29.0, Prob = 0.8

22. TC12 (PNA-, NAO, SOI) Autumn

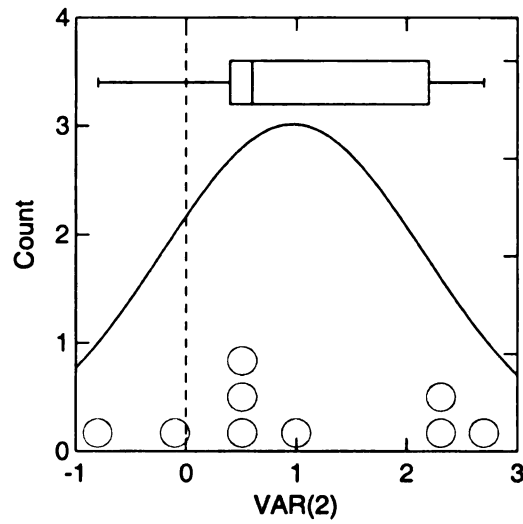


Figure C.43. One-sample t test of temperature with 9 cases; Mean = 1.0, SD = 1.2, Prob = 0.0

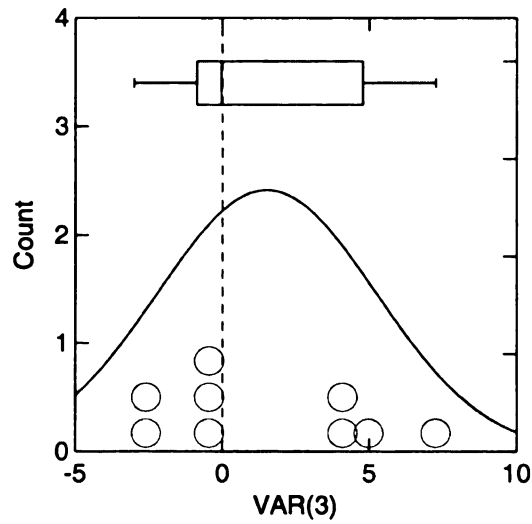


Figure C.44. One-sample t test of precipitation with 9 cases; Mean = 15.0, SD = 37.0, Prob = 0.3

23. TC13 (PNA, NAO-, SOI) Winter

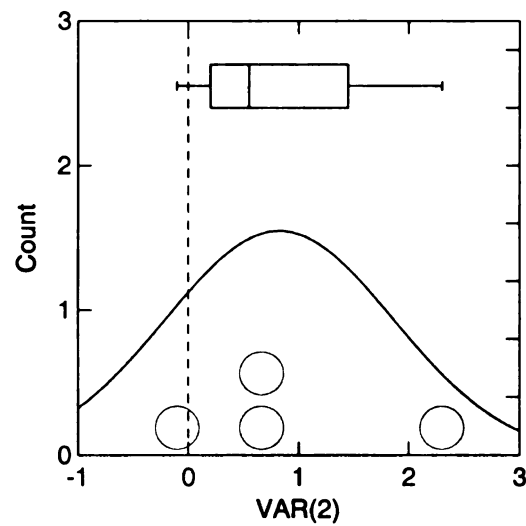


Figure C.45. One-sample t test of temperature with 4 cases; Mean = 0.8, SD = 1.0, Prob = 0.2

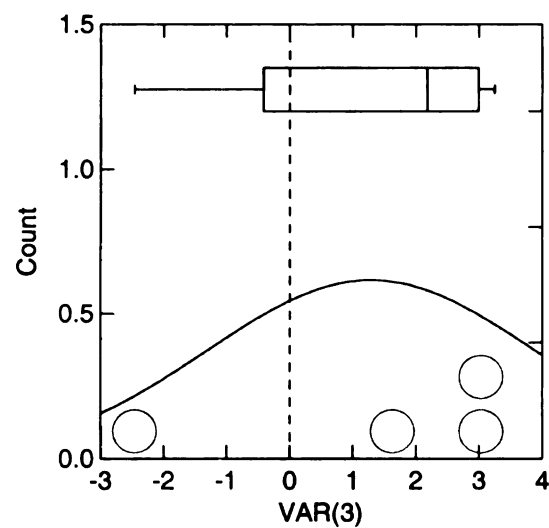


Figure C.46. One-sample t test of precipitation with 4 cases; Mean = 13.0, SD = 26.0, Prob = 0.4

24. TC13 (PNA, NAO-, SOI) Spring

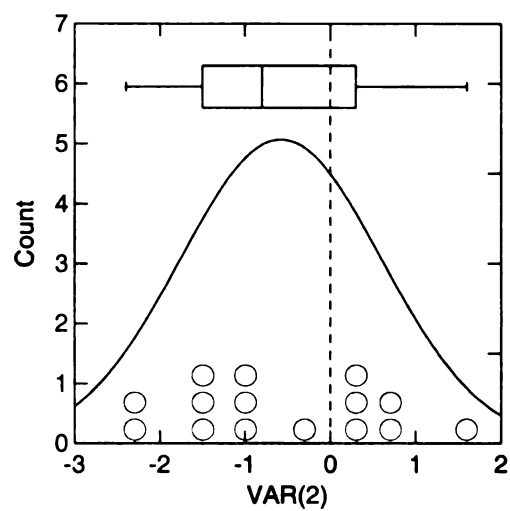


Figure C.47. One-sample t test of temperature with 15 cases; Mean = -0.6, SD = 1.2, Prob = 0.1

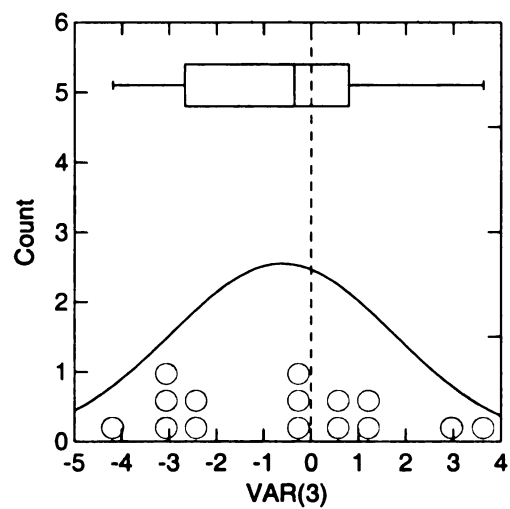


Figure C.48. One-sample t test of precipitation with 15 cases; Mean = -6.0, SD = 23.0, Prob = 0.3

25. TC13 (PNA, NAO-, SOI) Summer

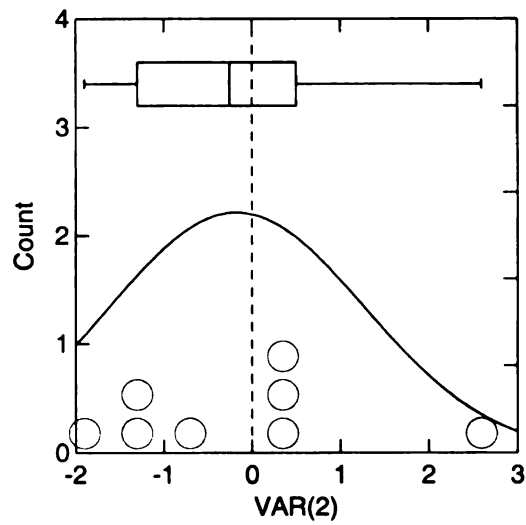


Figure C.49. One-sample t test of temperature with 8 cases; Mean = -0.2, SD = 1.4, Prob = 0.7

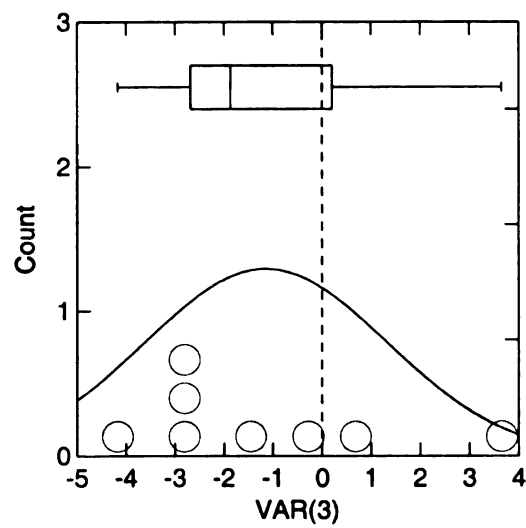


Figure C.50. One-sample t test of precipitation with 8 cases; Mean = -11.0, SD = 25.0, Prob = 0.2

26. TC13 (PNA, NAO-, SOI) Autumn

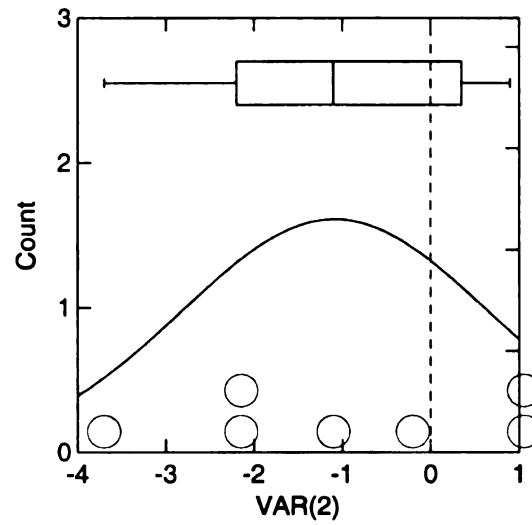


Figure C.51. One-sample t test of temperature with 7 cases; Mean = -1.1, SD = 1.7, Prob = 0.1

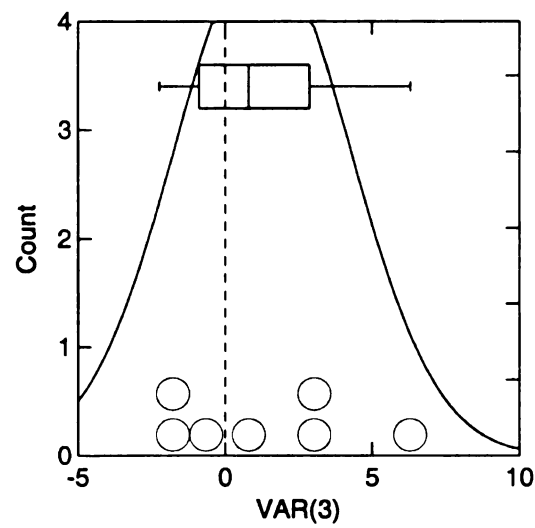


Figure C.52. One-sample t test of precipitation with 7 cases; Mean = 13.0, SD = 30.0, Prob = 0.3

27. TC14 (PNA, NAO, SOI-) Winter

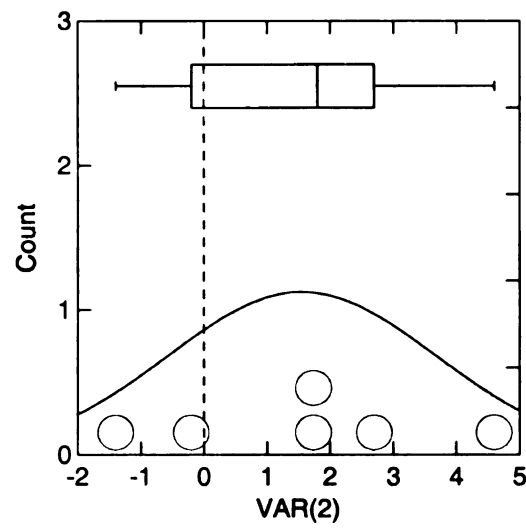


Figure C.53. One-sample t test of temperature with 6 cases; Mean = 1.6, SD = 2.1, Prob = 0.1

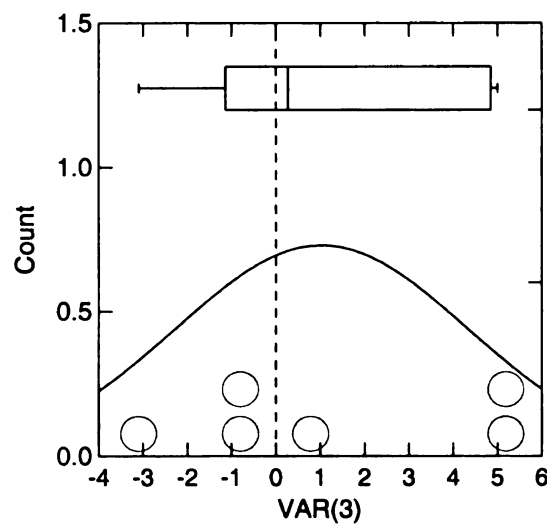


Figure C.54. One-sample t test of precipitation with 6 cases; Mean = 10.0, SD = 33.0, Prob = 0.5

28. TC14 (PNA, NAO, SOI-) Spring

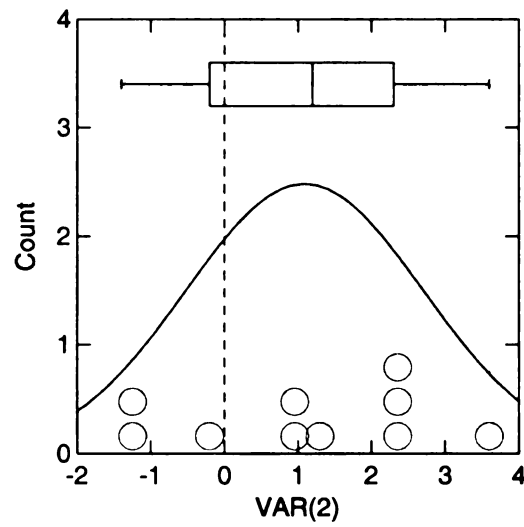


Figure C.55. One-sample t test of temperature with 10 cases; Mean = 1.1, SD = 1.6, Prob = 0.1

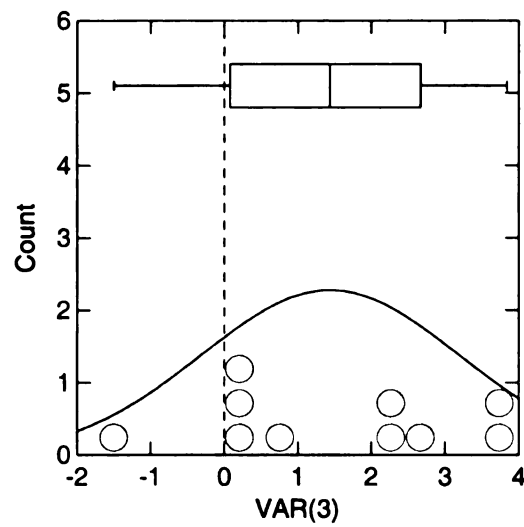


Figure C.56. One-sample t test of precipitation with 10 cases; Mean = 14.0, SD = 18.0, Prob = 0.0

29. TC14 (PNA, NAO, SOI-) Summer

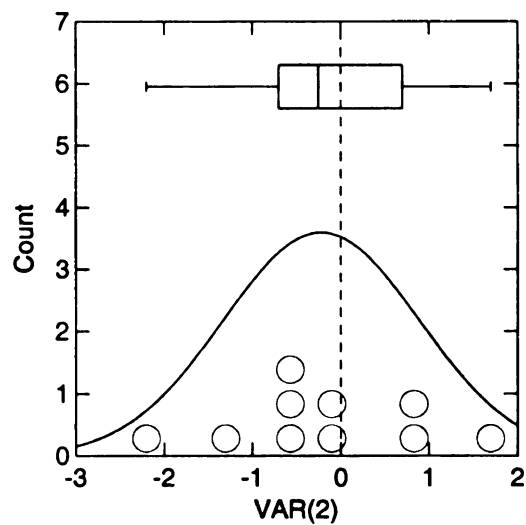


Figure C.57. One-sample t test of temperature with 10 cases; Mean = -0.2, SD = 1.1, Prob = 0.5

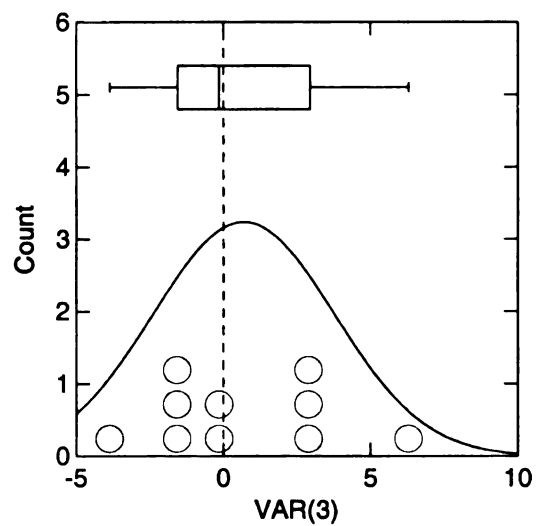


Figure C.58. One-sample t test of precipitation with 10 cases; Mean = 7.0, SD = 31.0, Prob = 0.5

30. TC14 (PNA, NAO, SOI-) Autumn

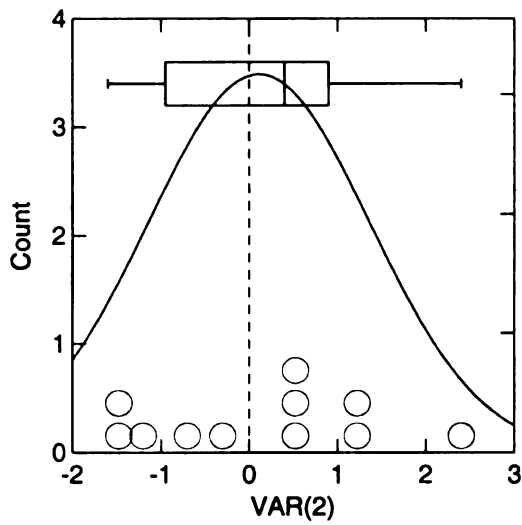


Figure C.59. One-sample t test of temperature with 11 cases; Mean = 0.1, SD = 1.3, Prob = 0.8

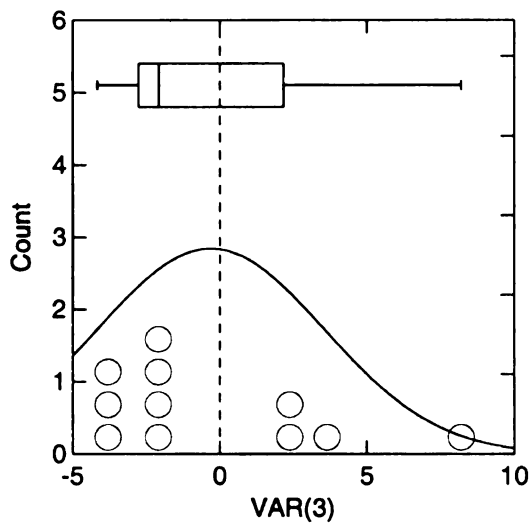


Figure C.60. One-sample t test of precipitation with 11 cases; Mean = -3.0, SD = 39.0, Prob = 0.8

31. TC21 (PNA, NAO+, SOI-) Winter

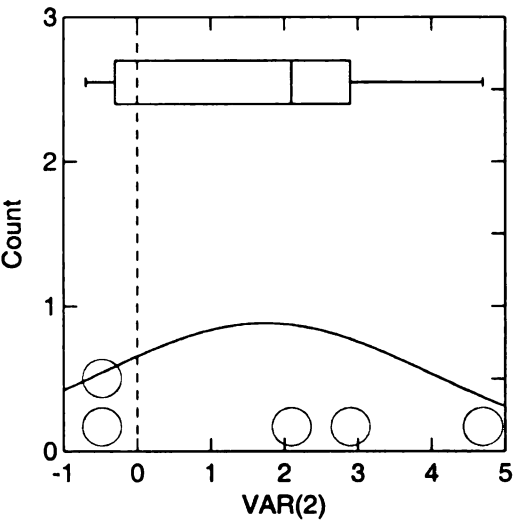


Figure C.61. One-sample t test of temperature with 5 cases; Mean = 1.7, SD = 2.3, Prob = 0.2

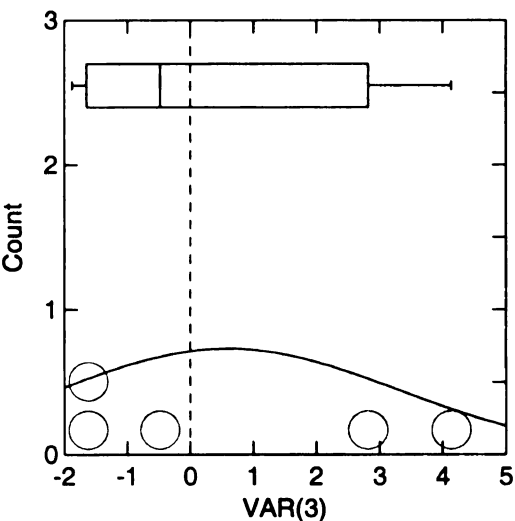


Figure C.62. One-sample t test of precipitation with 5 cases; Mean = 6.0, SD = 27.0, Prob = 0.7

32. TC21 (PNA, NAO+, SOI-) Spring

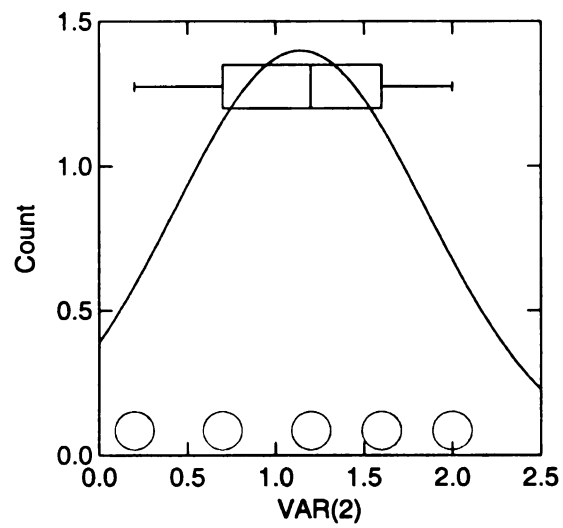


Figure C.63. One-sample t test of temperature with 5 cases; Mean = 1.1, SD = 0.7, Prob = 0.0

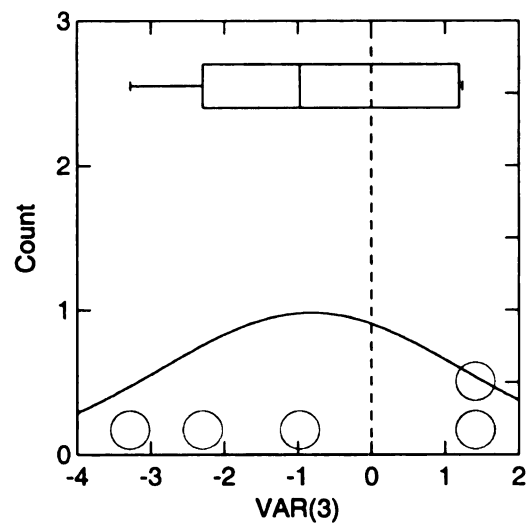


Figure C.64. One-sample t test of precipitation with 5 cases; Mean = -8.0, SD = 20.0, Prob = 0.4

33. TC21 (PNA, NAO+, SOI-) Summer

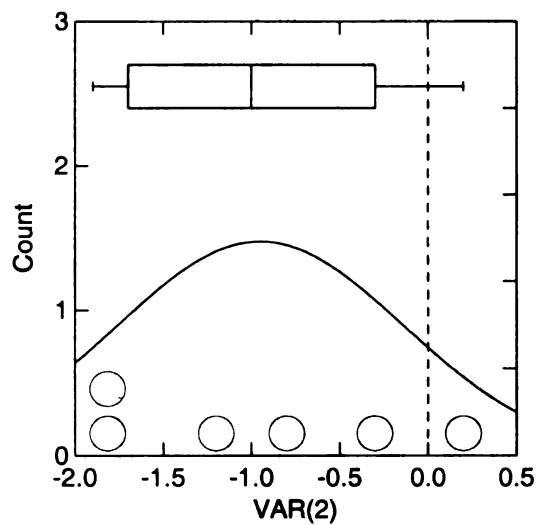


Figure C.65. One-sample t test of temperature with 6 cases; Mean = -1.0, SD = 0.8, Prob = 0.0

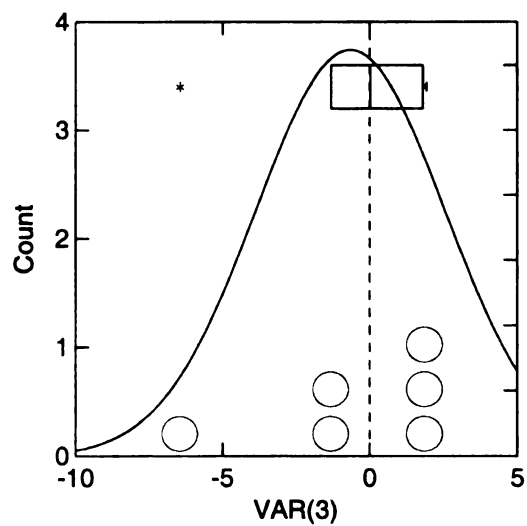


Figure C.66. One-sample t test of precipitation with 6 cases; Mean = -7.0, SD = 32.0, Prob = 0.6

34. TC21 (PNA, NAO+, SOI-) Autumn

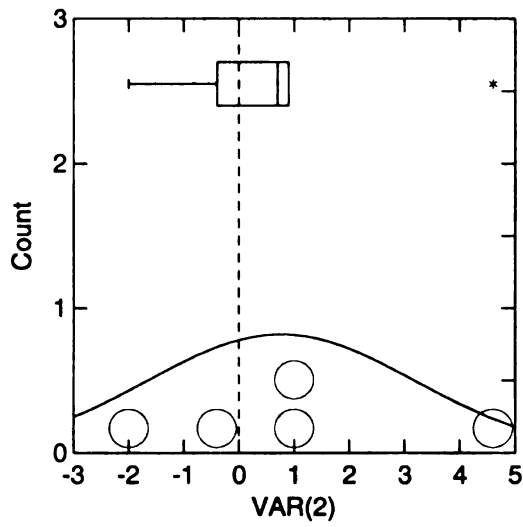


Figure C.67. One-sample t test of temperature with 5 cases; Mean = 0.8, SD = 2.4, Prob = 0.5

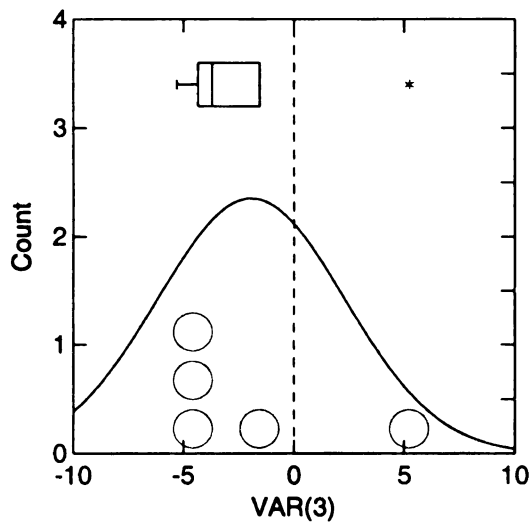


Figure C.68. One-sample t test of precipitation with 5 cases; Mean = -19.0, SD = 42.0, Prob = 0.4

35. TC23 (PNA+, NAO, SOI-) Winter

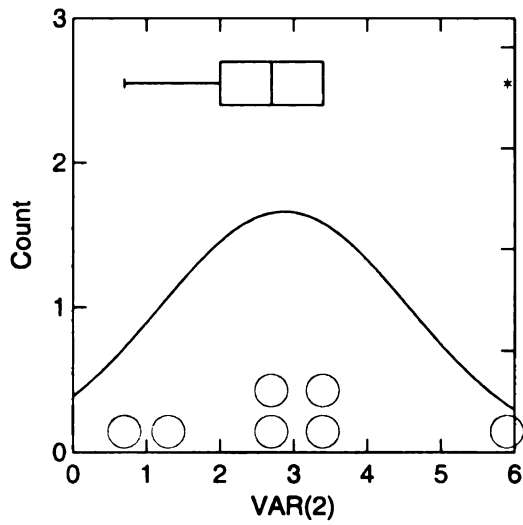


Figure C.69. One-sample t test of temperature with 7 cases; Mean = 2.9, SD = 1.7, Prob = 0.0

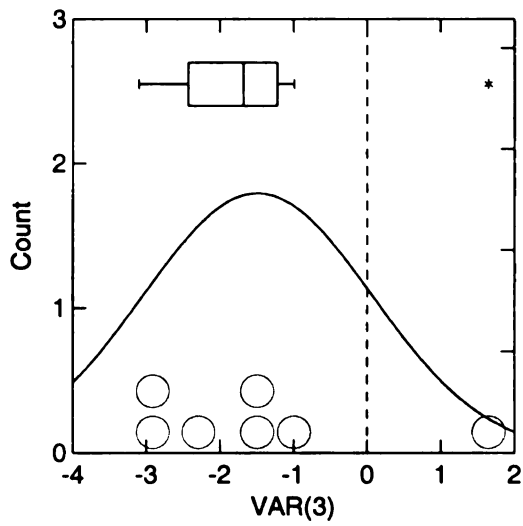


Figure C.70. One-sample t test of precipitation with 7 cases; Mean = -15.0, SD = 16.0, Prob = 0.0

36. TC23 (PNA+, NAO, SOI-) Spring

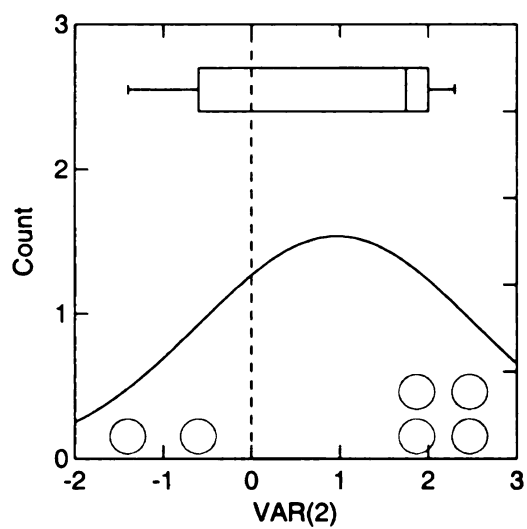


Figure C.71. One-sample t test of temperature with 6 cases; Mean = 1.0, SD = 1.6, Prob = 0.2

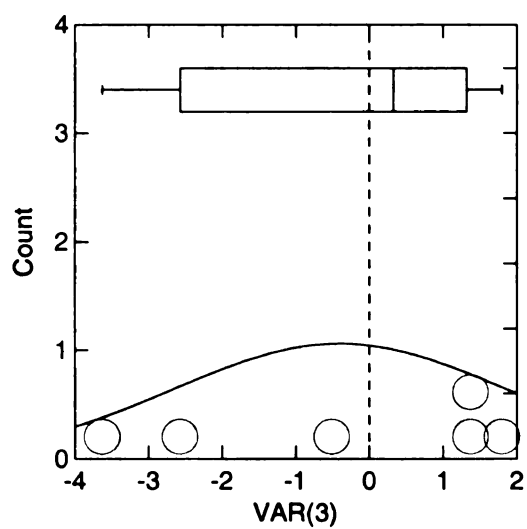


Figure C.72. One-sample t test of precipitation with 6 cases; Mean = -4.0, SD = 23.0, Prob = 0.7

37. TC25 (PNA+, NAO-, SOI) Winter

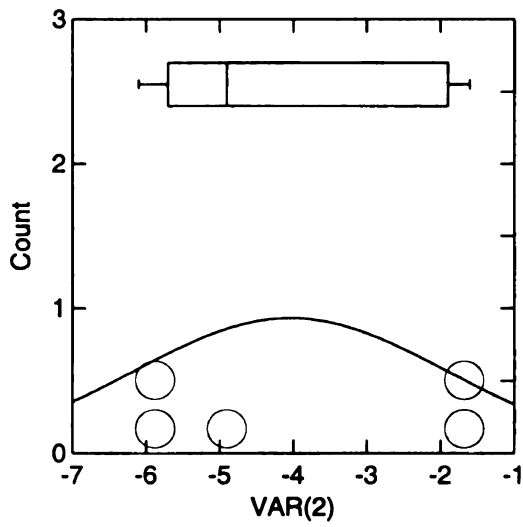


Figure C.73. One-sample t test of temperature with 5 cases; Mean = -4.0, SD = 2.1, Prob = 0.0

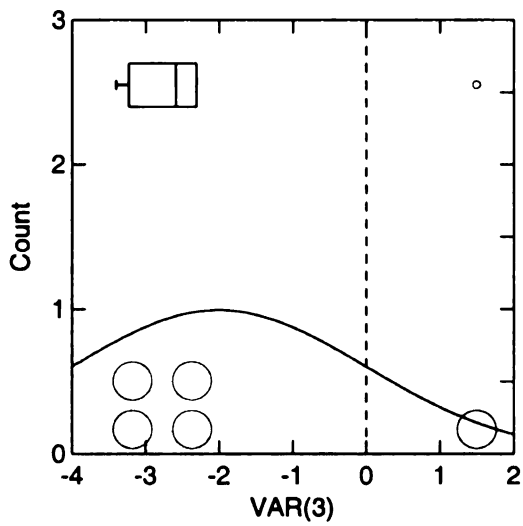


Figure C.74. One-sample t test of precipitation with 5 cases; Mean = -20.0, SD = 20.0, Prob = 0.1

38. TC25 (PNA+, NAO-, SOI) Autumn

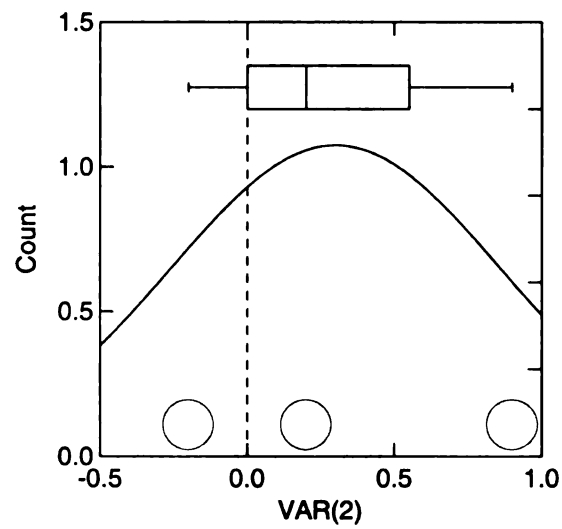


Figure C.75. One-sample t test of temperature with 3 cases; Mean = 0.3, SD = 0.6, Prob = 0.4

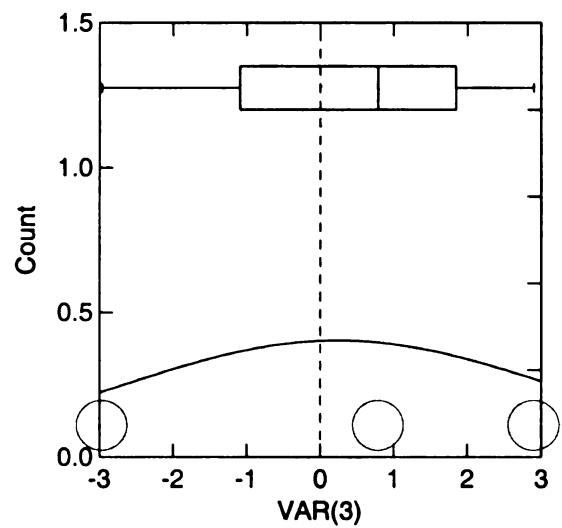


Figure C.76. One-sample t test of precipitation with 3 cases; Mean = 2.0, SD = 30.0, Prob = 0.9

39. TC27 (PNA, NAO, SOI) Winter

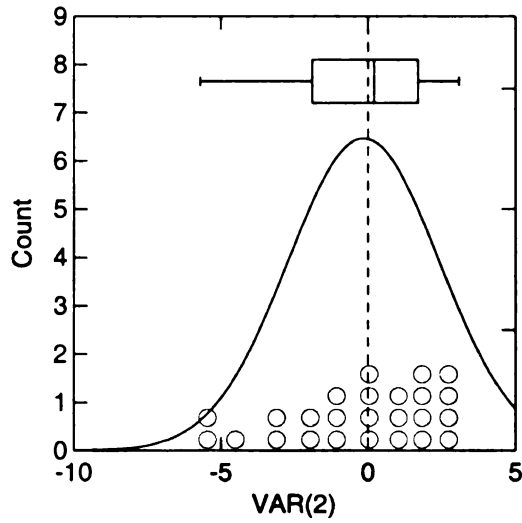


Figure C.77. One-sample t test of temperature with 25 cases; Mean = -0.2, SD = 2.6, Prob = 0.8

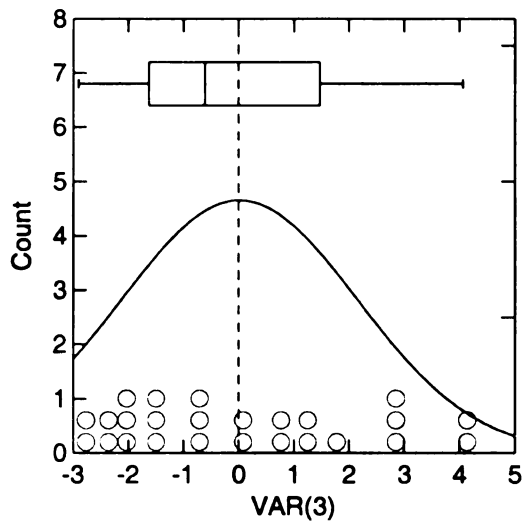


Figure C.78. One-sample t test of precipitation with 25 cases; Mean = 0.0, SD = 2.1, Prob = 1.0

40. TC27 (PNA, NAO, SOI) Spring

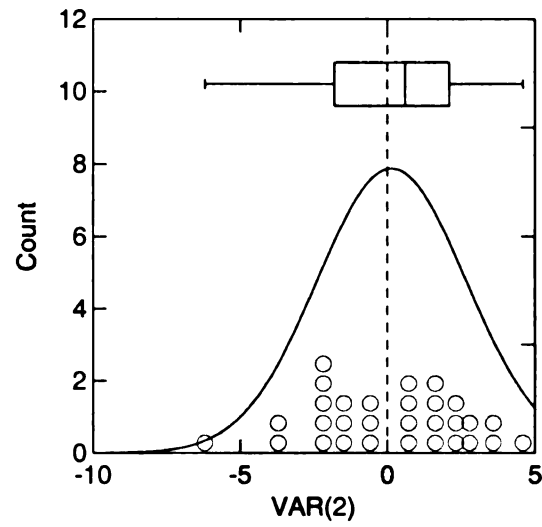


Figure C.79. One-sample t test of temperature with 30 cases; Mean = 0.1, SD = 2.5, Prob = 0.8

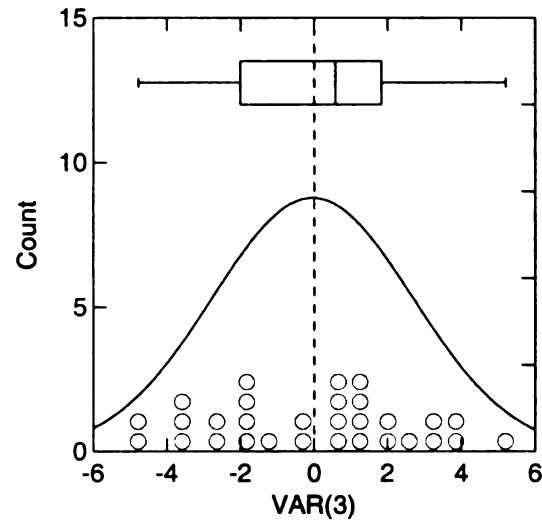


Figure C.80. One-sample t test of precipitation with 30 cases; Mean = -0.0, SD = 27.0, Prob = 0.9

41. TC27 (PNA, NAO, SOI) Summer

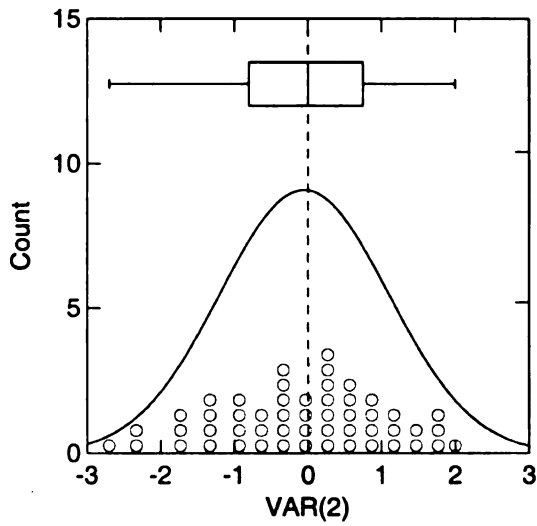


Figure C.81. One-sample t test of temperature with 52 cases; Mean = -0.0, SD = 1.1, Prob = 0.8

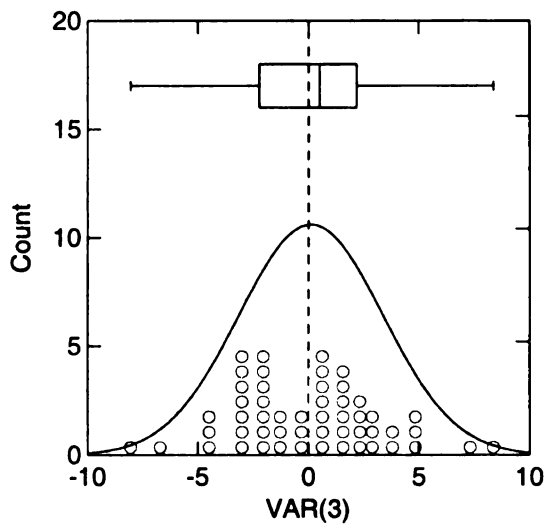


Figure C.82. One-sample t test of precipitation with 52 cases; Mean = 1.0, SD = 33.0, Prob = 0.8

42. TC27 (PNA, NAO, SOI) Autumn

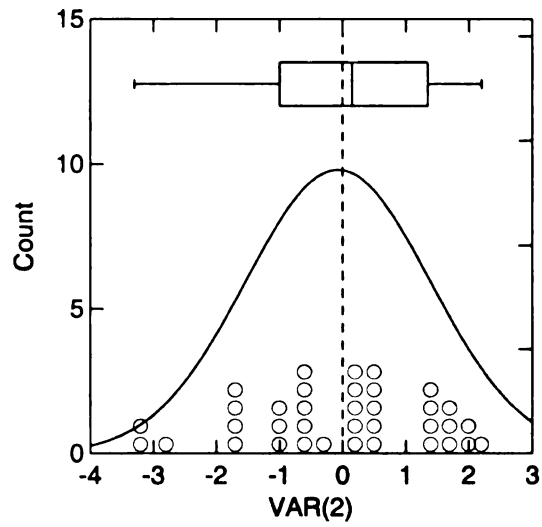


Figure C.83. One-sample t test of temperature with 36 cases; Mean = -0.1, SD = 1.5, Prob = 0.8

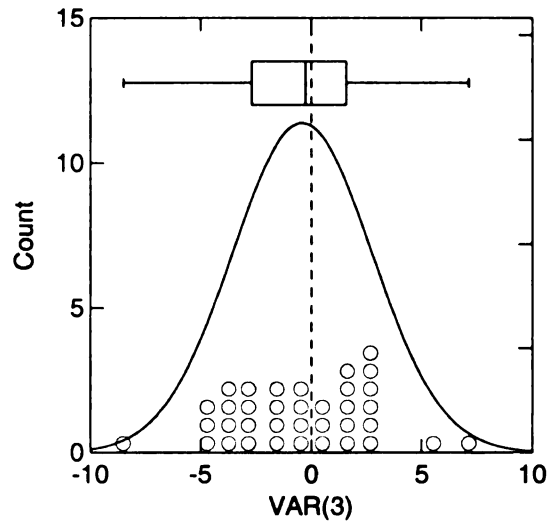


Figure C.84. One-sample t test of precipitation with 36 cases; Mean = -4.0, SD = 32.0, Prob = 0.4

BIBLIOGRAPHY

- American Meteorological Society (2000) *Glossary of Meteorology*, 2nd ed., American Meteorological Society.
- Ångström, A. (1935) Teleconnections of climate changes in present time. *Geografiska Annaler*, vol. 17, 242-258.
- Assel, R. A. (1992) Great lakes winter-weather 700-hPa PNA teleconnections. *Monthly Weather Review*, vol. 120, 2156-2163.
- Austin, J., Tuck, A. F. (1985) The calculation of stratospheric air parcel trajectories using satellite data. *Quarterly Journal of the Royal Meteorological Society*, vol. 111, 279-307.
- Barnston, A. G., Livezey, R. E. (1987) Classification, seasonality and persistence of low-frequency atmospheric circulation patterns. *Monthly Weather Review*, vol. 115, 1083-1126.
- Barry, R. G., Carleton, A. M. (2001) *Synoptic and Dynamic Climatology*, Routledge.
- Bates, G. T., Hoerling, M. P., Kumar, A. (2001) Central U.S. springtime precipitation extremes: teleconnections and relationships with sea surface temperature. *Journal of Climate*, vol. 14, 3751-3766.
- Baumann, K., Stohl, A. (1997) Validation of a long-range trajectory model using gas balloon tracks from the Gordon Bennett Cup 95. *Journal of Applied Meteorology*, vol. 36, 711-720.
- Bell, G. D., Janowiak, J. E. (1995) Atmospheric circulation associated with the Midwest floods of 1993. *Bulletin of the American Meteorological Society*, vol. 76(5), 681-695.
- Bjerknes, J. (1969) Atmospheric teleconnections from the equatorial Pacific. *Monthly Weather Review*, vol. 97, 162-172.
- Bradbury, J. A., Keim, B. D., Wake, C. P. (2003) The influence of regional storm tracking and teleconnections on winter precipitation in the northeastern United States. *Annals of the Association of American Geographers*, vol. 93(3), 544-556.
- Changnon, S. A., Hilberg, S. D., Kunkel, K. E. (2000) El Niño 1997-1998 in the Midwest. *Midwestern Regional Climate Center*, Champaign, IL.
- Clark, T. L., Cohn, R. D. (1990) The Across North America Tracer Experiment (ANATEX) model evaluation study. EPA-600/3-90-051, U.S. Environmental Protection Agency, Research Triangle Park, NC.

Clarke, J. F., Clark, T. L., Ching, J. K. S., Haagensohn, P. L., Husar, R. B., Patterson, D. E. (1983) Assessment of model simulation of long-distance transport. *Atmospheric Environment*, vol. 17, 2449-2462.

Climate Diagnostics Center. (2003a) The National Centers for Environmental Prediction (NCEP) and the National Center for Atmospheric Research (NCAR) reanalysis data. <<ftp://ftp.cdc.noaa.gov/Datasets/ncep.reanalysis/pressure/>>.

Climate Diagnostics Center. (2003b) Readgeneral.f. <<http://climserv.lmd.polytechnique.fr/soft/utilitaires/ncep/cdc/>>.

Climate Diagnostics Center. (2003c) Create a monthly or seasonal time series of climate variables. <<http://www.cdc.noaa.gov/Timeseries/>>.

Climate Prediction Center. (2001) Northern Hemisphere teleconnection patterns. <<http://www.cpc.noaa.gov/data/teledoc/telecontents.html>>.

Climate Prediction Center. (2002a) North Atlantic Oscillation (NAO). <<http://www.cpc.noaa.gov/data/teledoc/naomap.gif>>.

Climate Prediction Center. (2002b) Pacific/North American Pattern (PNA). <<http://www.cpc.noaa.gov/data/teledoc/pnamap.gif>>.

Climate Prediction Center. (2002c) El Niño and La Niña - related winter features over North America. <http://www.cpc.noaa.gov/products/analysis_monitoring/ensocycle/nawinter.html>.

Climate Prediction Center. (2002d) Pacific/North American (PNA). <<http://www.cpc.noaa.gov/data/teledoc/pna.html>>.

Climate Prediction Center. (2003a) Standardized Northern Hemisphere teleconnection indices. <ftp://ftp.ncep.noaa.gov/pub/cpc/wd52dg/data/indices/tele_index.nh>.

Climate Prediction Center. (2003b) Stand Tahiti - Stand Darwin sea level pressure. <<ftp://ftp.ncep.noaa.gov/pub/cpc/wd52dg/data/indices/soi>>.

Committee on Extension to the Standard Atmosphere (1962) U.S. Standard Atmosphere. NASA, U.S. Air Force, and U.S. Weather Bureau. Washington D.C.

Danielsen, E. F. (1961) Trajectories: isobaric, isentropic, and actual. *Journal of Meteorology*, vol. 18, 479-486.

Dent, B. D. (1999) *Cartography: Thematic Map Design*, 5th ed., The McGraw-Hill Companies Inc.

Digital Chart of the World Server. (1992) Penn State University Libraries.
<<http://www.maproom.psu.edu/dcw/>>.

Dole, R. M. (1986) Persistent anomalies of the extratropical Northern Hemisphere wintertime circulation structure. *Monthly Weather Review*, vol. 114, 178-207.

Doty, K. G., Perkey, D. J. (1993) Sensitivity of trajectory calculations to the temporal frequency of wind data. *Monthly Weather Review*, vol. 121, 387-401.

Draxler, R. R. (1996) Trajectory optimization for balloon flight planning. *Weather Forecast*, vol. 11, 111-114.

Draxler, R. R. (1999) HYSPLIT_4 User's Guide. *NOAA Technical Memorandum ERL ARL-230*, June, 33 pp.

Draxler, R. R., Hess, G. D. (1998a) Description of the HYSPLIT_4 modeling system. *NOAA Technical Memorandum ERL ARL-224*, August, 24 pp.

Draxler, R. R., Hess, G. D. (1998b) An overview of the HY-SPLIT_4 modeling system for trajectories, dispersion, and deposition. *Australian Meteorological Magazine*, vol. 47, 295-308.

Djurić, D. (1961) On the accuracy of air trajectory computations. *Journal of Meteorology*, vol. 18, 597-605.

Eliassen A. (1978) The OECD study of long-range transport of air pollutants. Long-range transport modeling. *Atmospheric Environment*, vol. 12, 479-487.

Esbensen, S. K. (1984) A comparison of intermonthly and interannual teleconnections in the 700 mb geopotential height field during the Northern Hemisphere winter. *Monthly Weather Review*, vol. 112, 2016-2032.

Gislason, K. B., Prahm, L. P. (1983) Sensitivity study of air trajectory long-range transport modeling. *Atmospheric Environment*, vol. 17, 2463-2472.

Gray, W. M., Sheaffer, J. D. (1991) El Niño and QBO influences on tropical cyclone activity. In: M. H. Glantz et al., eds, *Teleconnections Linking Worldwide Climate Anomalies*. Cambridge University Press. 257-284.

Haagenson, P. L., Kuo, Y., Caldwell, G. A. (1985) A relationship between acid precipitation and three-dimensional transport associated with synoptic scale cyclones. *Journal of Climate and Applied Meteorology*, vol. 24, 967-976.

Haagenson, P. L., Kuo, Y., Skumanich, M. (1987) Tracer verification of trajectory models. *Journal of Climate and Applied Meteorology*, vol. 26, 410-426.

Hastenrath, S., Greischar, L. (2001) The North Atlantic Oscillation in the NCEP-NCAR Reanalysis. *Journal of Climate*, vol. 14, 2404-2413.

Hildebrandsson, H. H. (1897) Quelques recherches sur les centres d'action de l'Atmosphère. *Kungl. Svenska Vetenskaps-Akademiens Handlingar*, vol. 29(3), 2-11.

Hoecker, W. H. (1977) Accuracy of various techniques for estimating boundary-layer trajectories. *Journal of Applied Meteorology*, vol. 16, 374-383.

Horel, J. D. (1981) A rotated principal component analysis of the interannual variability of the Northern Hemisphere 500mb height field. *Monthly Weather Review*, vol. 109, 2080-2092.

Hu, Q., Feng, S. (2001a) Variations of teleconnections of ENSO and interannual variation in summer rainfall in the central United States. *Journal of Climate*, vol. 14, 2469-2480.

Hu, Q., Feng, S. (2001b) Climatic role of the southerly flow from the Gulf of Mexico in interannual variations in summer rainfall in the central United States. *Journal of Climate*, vol. 14, 3156-3171.

Jenne, R. L. (1975) Data sets for meteorological research. *NCAR Tech. Note NCAR-TN/IA-111*, 194 pp.

Jenne, R. (2001) Reanalysis: The observations and analysis. *Large Scale Observations: a SEARCH workshop*, November 27-29, 2001, Seattle, WA.
<<http://www.epic.noaa.gov/SEARCH/obs/workshop>>.

Kahl, J. D., Samson, P. J. (1986) Uncertainty in trajectory calculations due to low-resolution meteorological data. *Journal of Applied Meteorology*, vol. 25, 1816-1831.

Kahl, J. D., Samson, P. J. (1988) Trajectory sensitivity to rawinsonde data resolution. *Atmospheric Environment*, vol. 22(7), 1291-1299.

Kalnay, E., Kanamitsu, M., Kistler, R., Collins, W., Deaven, D., Gandin, L., Iredell, M., Saha, S., White, G., Woolen, J., Zhu, Y., Chelliah, M., Ebisuzaki, W., Higgins, W., Janowiak, J., Mo, K. C., Ropelewski, C., Wang, J., Leetmaa, A., Reynolds, R., Jenne, R., Joseph, D. (1996) The NCEP/NCAR 40-year reanalysis project. *Bulletin of the American Meteorological Society*, vol. 77(3), 437-471.

Kistler, R., Kalnay, E., Collins, W., Saha, S., White, G., Woolen, J., Chelliah, M., Ebisuzaki, W., Kanamitsu, M., Kousky, V., van den Dool, H., Jenne, R., Fiorino, M. (2001) The NCEP-NCAR 50-year reanalysis: Monthly means CD-ROM and documentation. *Bulletin of the American Meteorological Society*, vol. 82(2), 247-267.

- Kunkel, K. E., Angel, J. R. (1999) Relationship of ENSO to snowfall and related cyclone activity in the contiguous United States. *Journal of Geophysical Research*, vol. 104(D16), 19425-19434.
- Kuo, Y., Skumanich, M., Haagenson, P. L., Chang, J. S. (1985) The accuracy of trajectory models as revealed by the observing system simulation experiments. *Monthly Weather Review*, vol. 113(11), 1852-1867.
- Leathers, D. J., Yarnal, B., Palecki, M. A. (1991) The Pacific/North American teleconnection pattern and United States climate. Part I: Regional temperature and precipitation associations. *Journal of Climate*, vol. 4, 517-528.
- Lee, T.-Y., Park, S.-W., Kim, S.-B. (1997) Dependence of trajectory accuracy on the spatial and temporal densities of wind data. *Tellus*, vol. 49B, 199-215.
- Lorenz, E. N. (1951) Seasonal and irregular variations of the Northern Hemisphere sea level pressure profile. *Journal of Meteorology*, vol. 8, 52-59.
- McGinnis, D. L. (2001) "Teleconnection combination and variability." *The Association of American Geographers Annual Meeting*. New York, NY. March 2, 2001.
- Merrill, J. T. (1994) Isentropic airflow probability analysis. *Journal of Geophysical Research*, vol. 99(D12), 25881-25889.
- Mo, K. C., Livezey, R. E., (1986) Tropical-extratropical geopotential height teleconnections during the Northern Hemisphere winter. *Monthly Weather Review*, vol. 114, 2488-2515.
- National Climatic Data Center. (2003) Climate divisions for Michigan. <<http://www.ncdc.noaa.gov/img/onlineprod/drought/mi.gif>>.
- National Oceanic and Atmospheric Administration (NOAA) Air Resources Laboratory. (2003) NOAA ARL HYSPLIT Model. <<http://www.arl.noaa.gov/ready/hysplit4.html>>.
- Pack, D. H., Ferber, G. L., Heffter, J. L., Telegadas, K., Angell, J. K., Hoecker, W. H., Machta, L. (1977) Meteorology of long-range transport. *Atmospheric Environment*, vol. 12, 425-444.
- Portis, D. H., Walsh, J. E., Hamly, M. E., Lamb, P. J. (2001) Seasonality of the North Atlantic Oscillation. *Journal of Climate*, vol. 14, 2069-2078.
- Robinson, A. H., Sale, R., Morrison, J. (1978) *Elements of Cartography*, 4th ed., John Wiley & Sons, New York.

- Rogers, J. C. (1984) The association between the North Atlantic oscillation and the Southern Oscillation in the Northern Hemisphere. *Monthly Weather Review*, vol. 112, 1999-2015.
- Rogers, J. C. (1985) Atmospheric circulation changes associated with the warming over North Atlantic in the 1920s. *Journal of Climate and Applied Meteorology*, vol. 24, 1303-1310.
- Rogers, J. C. (1990) Patterns of low-frequency monthly sea level pressure variability (1899-1986) and associated wave cyclone frequencies. *Journal of Climate*, vol. 3(12), 1364-1379.
- Rohli, R. V., Rogers, J. C. (1993) Atmospheric teleconnections and citrus freezes in the southern United States. *Physical Geography*, vol. 14(1), 1-15.
- Rolph, G. D., Draxler, R. R., de Pena, R. G. (1992) Modeling sulfur concentrations and depositions in the United States during ANATEX. *Atmospheric Environment*, vol. 26A(1), 73-93.
- Saxena, V. K., Durkee, P. A., Menon, S., Anderson, J., Burns, K. L., Nielsen, K. E. (1996) Physico-chemical measurements to investigate regional cloud-climate feedback mechanisms. *Atmospheric Environment*, vol. 30(10/11) 1573-1579.
- Scott, R. W., Achtemeier, G. L. (1987) Estimating pathways of migrating insects carried in atmospheric winds. *Environmental Entomology*, vol. 16(6), 1244-1254.
- Serreze, M. C., Clark, M. P., McGinnis, D. L. (1998) Characteristics of snowfall over the eastern half of the United States and relationships with principle modes of low-frequency atmospheric variability. *Journal of Climate*, vol. 11, 234-250.
- Stein, A. F., Lamb, D. (2000) The sensitivity of sulfur wet deposition to atmospheric oxidants. *Atmospheric Environment*, vol. 34, 1681-1690.
- Stein, A. F., Lamb, D., Draxler, R. R. (2000) Incorporation of detailed chemistry into a three-dimensional Lagrangian-Eulerian hybrid model: application to regional tropospheric ozone. *Atmospheric Environment*, vol. 34(2000), 4361-4372.
- Stohl, A. (2001) A 1-year Lagrangian "climatology" of airstreams in the Northern Hemisphere troposphere and lowermost stratosphere. *Journal of Geophysical Research*, vol. 106(D7), 7263-7279.
- Stohl, A., Haimberger, L., Scheele, M. P., Wernli, H. (2001) An intercomparison of results from three trajectory models. *Meteorological Applications*, vol. 8, 127-135.

Stohl, A., Seibert, P. (1998) Accuracy of trajectories as determined from the conservations of meteorological tracers. *Quarterly Journal of the Royal Meteorological Society*, vol. 124, 1465-1484.

Stohl, A., Wotawa, G., Seibert, P., Kromp-Kolb, H. (1995) Interpolation errors in wind fields as a function of spatial and temporal resolution and their impact on different types of kinematic trajectories. *Journal of Applied Meteorology*, vol. 34, 2149-2165.

Trenberth, K. E., Caron, J. M. (2000) The southern oscillation revisited: sea-level pressures, surface temperatures, and precipitation. *Journal of Climate*, vol. 13, 4358-4365.

Trenberth, K. E., Hurrell, J. W. (1994) Decadal atmosphere-ocean variations in the Pacific. *Climate Dynamics*, vol. 9, 303-319.

Van Ravensway, J., Winkler, J. A., Shadbolt, R. P., Walters, C. K. (2003) "A Preliminary Assessment of the Quality of Upper-Air Wind Observations." *Meeting of the East Lakes and West Lakes Divisions of the Association of American Geographers*. Kalamazoo, MI. October 18, 2003.

Visbeck, M. H., Hurrell, J. W., Polvani, L., Cullen, H. M. (2001) The North Atlantic Oscillation: past, present, and future. *Proceedings of the National Academy of Sciences of the United States of America (PNAS)*, vol. 98(23), 12876-12877.

Walker, G. T. (1924) Correlation in seasonal variations of weather. IX. A further study of world weather. *Memoirs of the Indian Meteorological Department*, vol. 24, 275-332.

Walker, G. T., Bliss, E. W. (1932) World Weather V. *Memoirs of the Royal Meteorological Society*, vol. 44, 53-84.

Wallace, J. M., Gutzler, D. S. (1981) Teleconnections in the geopotential height field during the Northern Hemisphere winter. *Monthly Weather Review*, vol. 109, 784-812.

Wallace, J. M., Hobbs, P. V. (1977) *Atmospheric Science: An introductory survey*. Academic Press, New York and London.

Waller, E. A. (1999) An air mass climatology for northwest Ohio based on airflow trajectories. Master's Thesis, Department of Geography, Michigan State University, East Lansing, MI.

Wendland, W. M., Bryson, R. A. (1981) Northern Hemisphere airstream regions. *Monthly Weather Review*, vol. 109, 255-270.

Winkler, J. A. (2004) The impact of technology upon in situ atmospheric observations and climate science. In: S.D. Brunn, S.L. Cutter, and J.W. Harrington, eds, *Geography and Technology*. Kluwer Academic Publishers. 461-490.